2016

New archaeological research at Liang Bua on the island of Flores: implications for the extinction of Homo floresiensis and the arrival of Homo sapiens in eastern Indonesia

Thomas Sutikna

University of Wollongong

New archaeological research at Liang Bua on the island of Flores: implications for the extinction of *Homo floresiensis* and the arrival of *Homo sapiens* in eastern Indonesia

A thesis submitted in fulfilment of the requirements for the award of the degree

Doctor of Philosophy

from

University of Wollongong

By
Thomas Sutikna

Centre for Archaeological Science
School of Earth and Environmental Sciences
2016

CERTIFICATION

I, Thomas Sutikna, declare that this thesis, submitted in fulfilment of the requirements for the award of Doctor of Philosophy, in the School of Earth and Environmental Sciences, University of Wollongong, is wholly my own work unless otherwise referenced or acknowledged. The document has not been submitted for qualifications at any academic institution.

Thomas Sutikna
March 30, 2016

STATEMENT OF AUTHORSHIP

The journal article submissions that comprise Chapters 2, 3 and 4 of this thesis were chosen under an agreement between Thomas Sutikna and the principal supervisor, Professor Richard G. Roberts. All of these journal articles are primarily based on archaeological research that was done by the PhD candidate, Thomas Sutikna, prior to and during his enrolment at the University of Wollongong. As co-director of ongoing archaeological research at Liang Bua, Thomas Sutikna has supervised all of the excavations: in 2001–2004 with M.J. Morwood, R.P. Soejono and R.G. Roberts; 2007–2009 with M.J. Morwood and Wahyu Saptomo; and 2010–present with M.W. Tocheri, Wahyu Saptomo and Jatmiko. All of these co-directors have contributed in various ways to the overall direction of the Liang Bua research. From 2001 to the present, Thomas Sutikna has been responsible for the direction of all field work components, including selecting the areas for excavation and the methods used, managing all excavated findings and the interpretation of all field data, as well as leading the stratigraphic analyses and chronological interpretations of the Liang Bua sequence. Thomas Sutikna is the lead author of all journal article submissions in this thesis, he wrote the initial drafts and coordinated all input from the co-authors. The journal articles included in this thesis are as follows:

Chapter 2 – Sutikna, T., Tocheri, M.W., Morwood, M.J., Saptomo, E.W., Jatmiko, Due Awe, R., Wasisto, S., Westaway, K.E., Aubert, M., Li, B., Zhao, J-x., Storey, M., Alloway, B.V., Morley, M.W., Meijer, H.J.M., van den Bergh, G.D., Grün, R., Dosseto, A., Brumm, A., Jungers, W.L., Roberts, R.G., 2016. Revised stratigraphy and chronology for *Homo floresiensis* at Liang Bua in Indonesia. *Nature* 532, 366–369.

Chapter 3 – Sutikna, T., Tocheri, M.W., Jatmiko, Saptomo, E.W., Due Awe, R., Roberts, R.G., in preparation. Radiocarbon dating of charcoal from Liang Bua (Flores, Indonesia) reveals significant new insights into the depositional history of the cave over the last 50,000 years.

Chapter 4 – Sutikna, T., Tocheri, M.W., Faith, J.T., Jatmiko, Due Awe, R., Meijer, H.J.M., Saptomo, E.W., Jungers, W.L., Roberts, R.G., in preparation. The spatio-temporal distribution of archaeological finds at Liang Bua suggests modern humans arrived on Flores by ~46 thousand years ago.

Thomas Sutikna
PhD Candidate
March 2016

Prof. Richard G. Roberts
Principal Supervisor
March 2016

ABSTRACT

The discovery in 2003 of the partial skeleton of a diminutive and primitive hominin species, *Homo floresiensis*, has generated wide interest and scientific debate. These remains were found buried in cave sediments at the site of Liang Bua on the island of Flores, eastern Indonesia, in association with stone artefacts and the remains of other extinct endemic fauna, such as pygmy *Stegodon*, marabou stork and vulture. A major reason that *H. floresiensis* has stirred such controversy is because the associated deposits were dated to between about 95 and 12 thousand calendar years (ka) ago. These ages implied that *H. floresiensis* survived on Flores long after modern humans (*H. sapiens*) had arrived in Australia by about 50 ka ago, thus posing a challenge to prevailing notions of modern human dispersals and human evolution in Southeast Asia and Australasia.

The research conducted for this thesis is aimed at addressing several unresolved questions arising from the original investigations at Liang Bua. A series of new excavations were conducted at Liang Bua between 2007 and 2014 to shed further light on the history of site formation and the hominin skeletal and cultural remains preserved within the cave deposits. The stratigraphic, chronological, archaeological and faunal evidence gleaned from these excavations is described and analysed in this thesis, and this information is integrated with that obtained in 2001–2004 to culminate in a new interpretation of the time of *H. floresiensis* extinction and *H. sapiens* arrival at Liang Bua.

A reassessment of the Liang Bua stratigraphy reveals that all known skeletal remains of *H. floresiensis* are preserved in a large pedestal of remnant deposit, almost 4 m in thickness, which has been truncated by erosion. The erosional surface slopes steeply downward from the rear of the cave to the front, and was not recognised as a stratigraphic unconformity during the original excavations. The existence of this unconformity, and its proximity to the holotype specimen of *H. floresiensis* (LB1), raises serious questions about the accuracy of previous interpretations of the age of the *H. floresiensis* remains and the associated fauna and archaeology.

Dating of *H. floresiensis* bones and the pedestal deposits containing them reveals that all skeletal remains of this species are between about 100 and 60 ka in age, while stone artefacts attributable to *H. floresiensis* range from about 190 to 50 ka. The new chronology does not support the previous age estimate for LB1 – about 18 ka – or the time of last appearance of *H. floresiensis*, for which a date as recent as 12 ka was claimed. It remains an open question, however, as to whether *H. floresiensis* survived

after 50 ka, potentially encountering modern humans on Flores or other hominins dispersing through Island Southeast Asia.

A further aim of this research is to refine and extend our understanding of when modern humans first reached Flores, and to compare the palaeoecology and behaviour of *H. floresiensis* and *H. sapiens* by examining the associated faunal and cultural remains. Previous work at Liang Bua suggested modern humans first arrived ~11 ka ago. However, two isolated human teeth that most likely represent *H. sapiens* were recovered during new excavations from deposits now dated to about 46 ka, and other evidence for modern human activities is contained in deposits dated here to between about 41 ka and after. A significant shift is observed in the choice of raw material used to make stone artefacts, from volcanic-based rock (silicified tuff) in the *H. floresiensis* levels to limestone-based rock (chert) in the modern human levels. A major shift is also observed in the composition of the faunal assemblages, reflecting changes in palaeoecology and hominin behaviour. The arrival of *H. sapiens* on Flores about 46 ka ago is consistent with archaeological evidence for the modern human colonisation of Australia and is among the oldest ages for modern humans in Island Southeast Asia. It is also conspicuously close to the probable time of extinction of *H. floresiensis* and the associated endemic fauna (*Stegodon*, giant marabou stork and vulture) at Liang Bua, about 50 ka ago.

The preservation of remains of two hominin species in direct association with behavioural and faunal evidence makes Liang Bua one of the most important archaeological sites in Island Southeast Asia and Australasia, as well as Asia more broadly. The existence of *H. floresiensis* on Flores before 50 ka provides additional evidence that at least one premodern human species had successfully crossed the Wallace Line long before *H. sapiens* arrived in the region. Without the direct association of hominin skeletal remains and stone artefacts, therefore, careful consideration must be given to which species was responsible for the manufacture of artefacts at other sites across Island Southeast Asia and Australasia. Furthermore, given the current dearth of knowledge about the timing and geographic spread of modern humans across this region before 40 ka ago, the new chronological interpretations of *H. floresiensis* disappearance and *H. sapiens* arrival at Liang Bua pose some intriguing questions – such as whether the two species interacted with each other or with other hominins dispersing through the region. Future research at Liang Bua and other sites in Island Southeast Asia have considerable potential to provide answers.

ACKNOWLEDGEMENTS

From the beginning of my involvement in archaeological research at Liang Bua (Flores, Indonesia) until the writing of this thesis, I have received invaluable support from colleagues, friends and institutions. Without their generous support and encouragement, I would not have been able to accomplish my studies.

I would like to thank the University of Wollongong for the support of a postgraduate scholarship and the Australian Research Council for additional funding through a Discovery Project to Professor Michael J. Morwood (DP0770234). Special thanks to Dr Tony Djubiantono and Dr Bambang Sulisyanto (former Directors of ARKENAS), Dr I Made Geria (current Director of ARKENAS) and Dr Valentinus N. Sene (Head of the Cultural and Tourism Department at Ruteng) for their support of my archaeological research at Liang Bua.

I would like to express my sincere gratitude to my supervisors, Professor Richard G. Roberts and Dr Matthew W. Tocheri. I have admired your insightful feedback and thoughtful discussions over the years, whether in the field at Liang Bua or elsewhere. Thank you for your professional supervision that greatly improved the quality of my thesis.

Special thanks to my friends Wahyu Saptomo, Jatmiko, Wasisto, Matthew Tocheri, Kira Westaway, William Jungers and the local villagers from Teras, Golo Manuk and Bere for over a decade of wonderful, but sometimes stressful, times during our archaeological research at Liang Bua. These memories will stay with me for the rest of my life.

My sincere thanks also to the members of the University of Wollongong's Centre for Archaeological Science: Richard 'Bert' Roberts, Zenobia Jacobs, Richard Fullagar, Gert van den Bergh, Kat Szabó, Bo Li, Mike Morley and Paul Goldberg. I am also grateful to Adam Brumm, Maxime Aubert, Hanneke Meijer, Grace Veatch, Tony Dosseto, Terry Lachlan, Priyanto Hadi and Bambang Budi Utomo. Thank you for your time and support, which has greatly aided my research.

I am also grateful to the members of Perhimpunan Pelajar Indonesia Australia, the Wollongong Indonesian Badminton Group and the Wollongong–Indonesia Community for their social and spiritual encouragement during my studies and time in Australia.

My sincerest gratitude to my family: my mother Mrs Siswapranata, my daughter Stefanie Anindita Waraningtyas, my sister Ch. Nanik Meiyani and my brother F.X. Suparno; thank you for your patience and for always being there when I needed you.

Finally, I would like to dedicate my thesis to my late father Ambrosius Siswapranata and my colleagues and friends who have passed away: Professor Mike Morwood, Professor Raden Pandji Soejono and Rokus Due Awe.

Table of contents

TITLE PAGE..... i
CERTIFICATION..... iii
STATEMENT OF AUTHORSHIP..... iv
ABSTRACT..... v
ACKNOWLEDGEMENTS..... vii
TABLE OF CONTENTS..... ix
LIST OF FIGURES..... xiii
LIST OF TABLES..... xxii

Chapter 1 – Introduction..... 1
1.1 Study site..... 1
1.2 Island Southeast Asia – archaeological and palaeoanthropological context... 7
1.3 The research aims and structure of the thesis..... 14

Chapter 2 – Revised stratigraphy and chronology for Liang Bua..... 18
2.1 Preface..... 18
2.2 Revised stratigraphy and chronology for *Homo floresiensis* at Liang Bua in Indonesia..... 20
Acknowledgements..... 27
Author contributions..... 28
Author information..... 28
2.3 Figures..... 29
2.4 Methods..... 32
2.4.1 Archaeological excavation..... 32
2.4.2 Electron microprobe analysis of volcanic glass..... 32
2.4.3 Infrared stimulated luminescence (IRSL) dating of feldspar grains..... 33
2.4.4 Thermoluminescence (TL) dating of quartz grains..... 35
2.4.5 Uranium-series ($^{234}U/^{230}Th$) dating of bones..... 37
2.4.6 Uranium-series ($^{234}U/^{230}Th$) dating of speleothems..... 38
2.4.7 Argon-argon ($^{40}Ar/^{39}Ar$) dating of hornblende crystals..... 39
2.4.8 Radiocarbon (^{14}C) dating of charcoal..... 41
2.5 Extended Data figures..... 43
2.6 Supplementary information section 2.1..... 56

2.6.1 Supplementary discussion – Tephra deposits at Liang Bua…… 56
2.6.2 Supplementary table 2.1 – Major element composition of glass shards at Liang Bua…….. 59
2.7 Supplementary information section 2.2……. 60
2.7.1 Supplementary discussion – Luminescence dating of feldspar and quartz grains…… 60
Infrared stimulated luminescence (IRSL)...……..60
Thermoluminescence (TL)……....65
2.7.2 Supplementary table 2.2 – Dose rate data for IRSL and TL samples…...68
2.7.3 Supplementary table 2.3 – Equivalent doses and ages for IRSL and TL samples…….69
2.8 Supplementary information section 2.3……71
2.8.1 Supplementary table 2.4 – Laser-ablation uranium-series dating of hominin bones…….. 71
2.8.2 Supplementary table 2.5 – Laser-ablation uranium-series dating of *Stegodon* bones……75
2.9 Supplementary information section 2.4……83
2.9.1 Supplementary table 2.6 – Uranium-series dating of speleothems……...83
2.10 Supplementary information section 2.5……...84
2.10.1 Supplementary table 2.7 – $^{40}Ar/^{39}Ar$ dating of tephra T1……...84
2.11 Supplementary information section 2.6……...85
2.11.1 Supplementary table 2.8 – Radiocarbon (^{14}C) dating of charcoal…….. 85

Chapter 3 – Radiocarbon dating of charcoal samples from Liang Bua..... 86
3.1 Preface……..... 86
Radiocarbon dating of charcoal from Liang Bua (Flores, Indonesia) reveals significant new insights into the depositional history of the cave over the last 50,000 years……..... 88
Abstract……..89
3.2 Introduction 89
3.3 Methods……. 93
3.4 Results……... 96
3.4.1 Recalibration of published ^{14}C ages for Liang Bua……. 96
3.4.2 Discovery of deposits dating to between about 41 and 25 ka…….. 97

Sector XXIV…….. 97
Sector XXVII……100
3.4.3 Dating of the Holocene sediments and tephras T7 and T8…… 102
Sector XXVI……..102
Sector XVI……... 104
Sector XIX……... 106
Sectors IV and XI…….....107
3.5 Discussion…….....110
3.5.1 Implications for the Late Pleistocene history of sedimentation at Liang Bua after 50 ka...…….....111
3.5.2 Refinement of the chronology of the terminal Pleistocene and Holocene deposits…….. 113
3.6 Conclusions……..... 117

Chapter 4 – The spatio-temporal distribution of archaeological finds at Liang Bua…….... 119
4.1 Preface……. 119
The spatio-temporal distribution of archaeological finds at Liang Bua suggests modern humans arrived on Flores by ~46 thousand years ago..... 122
Abstract..... 123
4.2 Introduction……..... 123
4.2.1 Previous studies……..... 124
4.2.2 Research objectives……..... 131
4.3 Materials and methods……..... 131
4.3.1 Stratigraphic units……..... 131
4.3.2 Faunal assemblage……..... 133
4.3.3 Stone artefact assemblage……..... 135
4.4 Results……..... 136
4.4.1 Faunal assemblage…….. 136
4.4.2 Stone artefact assemblage……... 149
4.5 Implications for palaeoecology and human behaviour……..... 157
4.6 Conclusions……...167

Chapter 5 – Synthesis of findings, broader implications and directions for future research..... 170

5.1 Synthesis and implications of the new research at Liang Bua……..... 170

5.2 Future research directions..... 177

REFERENCES……... 181

APPENDIX A Background to the excavation strategy at Liang Bua since 2001..... 197

List of figures (and extended data figures for Chapter 2)

Figure 1.1 Location of Liang Bua. **a.** The location of Liang Bua on Flores within the Indonesian archipelago; **b.** Liang Bua located at the foothills of Golo Tando; **c.** Liang Bua as viewed from the outside where the cave mouth faces to the northeast. (Photos: © Liang Bua Team). 2

Figure 1.2 Modern human burials with Neolithic grave goods recovered by Verhoeven when he excavated Liang Bua in 1965 (redrawn from Verhoeven's sketch in 1965) 3

Figure 1.3 Plan of Liang Bua with excavated Sectors. The excavations in 2001–2003 included Sectors I, III, IV and VII, which had been excavated previously by Soejono 4

Figure 1.4 Neolithic and Palaeometalic burials from Soejono's excavations at Liang Bua between 1978 and 1989. **a.** Modern human burial with grave goods recovered in Sector X; **b.** Grave goods, including fine pottery, found in association with a second burial in Sector X; **c.** Bronze axe recovered with a modern human burial in Sector II (see also Fig. 1.5). (Photos: ©ARKENAS) 5

Figure 1.5 Palaeometalic (left) and Neolithic (right) modern human burials with associated grave goods from Soejono's 1978 excavation of Sector II at Liang Bua. (Redrawn from Soejono, 1978) 6

Figure 1.6 Map of Island Southeast Asia and Australasia showing Sundaland, Wallacea and Sahuland. Late Pleistocene archaeological sites and possible routes for modern human dispersal are also indicated (modified from Birdsell, 1977; Bird *et al.*, 2005; O'Connor, 2007) 9

Figure 2.1 Site location. **a**, Location of Flores within Indonesia. **b**, Location of Liang Bua on Flores. **c**, Site plan of Sectors discussed in the text (the 2001–2004 and 2007–2014 excavations are shaded red and blue, respectively). The remaining cave floor sediments are shaded white, while the areas shaded brown are exposed rocks, stalagmites and other surfaces covered in speleothems 29

Figure 2.2 Composite stratigraphic section of deposits at Liang Bua, with approximate ages. The deposits accumulated above a fluvial conglomerate and are capped by recent sediments (both shown in grey). Skeletal remains of *Homo floresiensis* occur in deposits stratigraphically beneath a sequence of eight volcanic tephras (T1–T8), separated by calcitic speleothems (blue) and fine-grained clastic sediments (green). As the thickness, grain size and slope angle of each unit vary considerably within the cave, only the approximate relative thicknesses of the units discussed in the text are shown; the minimum

depth of this composite section would exceed 15 m. See Fig. 2.3 and Extended Data fig. 2.5a for three-dimensional representations of the stratigraphy. Also indicated are units with concentrations of rounded, gravel-size clasts of igneous rock (red) or irregularly shaped, eroded fragments of T1, T2 and T3 (orange), and units with signs of bioturbation (upper parts of T3 and T7). The photograph shows T1–T5 and interstratified sediments that conformably overlie the H. floresiensis-bearing deposits (south baulk of Sector XXI) 30

Figure 2.3 Stratigraphy of excavated Sectors near the eastern wall of the cave. Multiple specimens of *Homo floresiensis* (LB1, LB4, LB6 and LB8) were recovered previously (Brown *et al*., 2004; Morwood *et al*., 2004, 2005; Falk *et al*., 2005; Larson *et al*., 2007; Tocheri *et al*., 2007; Jungers *et al*., 2009; Morwood and Jungers, 2009; Kaifu *et al*., 2011; Orr *et al*., 2013) from sediments now recognised to directly underlie a sequence of five tephras (T1–T5) and interstratified deposits. Together, these remnant deposits form a pedestal, the top of which is dated to ~46 kyr cal. BP (charcoal sample denoted by the red star at ~2 m depth in Sector XXIII). The overlying section – separated here by a white band and dotted lines for emphasis – represents deposits (including three additional tephras, T6–T8) that rest uncomformably on the steeply sloping erosional surface of the pedestal. The green stars in Sector VII mark the respective locations (from top to bottom) of the charcoal samples dated to approximately 13.0, 18.5, 18.1, 19.0 and 19.2 kyr cal. BP, which were used erroneously (Morwood *et al*., 2004, 2005; Roberts et al., 2009) to infer the latest occurrences of *H. floresiensis* 31

Extended data figure 2.1 Stratigraphy of the excavated area near the eastern cave wall at eight stages of depositional history, with approximate ages indicated. Each panel (**a–h**) shows the remnant deposits exposed in the 2 m-wide baulks of the following Sectors (from left to right): north VII, east VII, XI and XXIII, south XXIII and XXI, west XXI, XV and XVI, and north XVI. The pedestal deposits shown in **b–d** were truncated by one or more phases of erosion that resulted in an erosional surface (i.e., an unconformity) that slopes steeply down towards the cave mouth (see also Supplementary information video 2.1). The black arrows relate to the accompanying text in each panel. The maximum depth excavated was 10.75 m in Sector VII (e.g., the left two panels in **h**) 43

Extended data figure 2.2 Deposits containing the remains of *Homo floresiensis*. These deposits (**A**) consist of multiple layers of fine-grained sediment interspersed with layers of weathered limestone and loose gravel, and are directly overlain by two tephras (**T1** and **T2**). **a**, South baulk of Sector XV, near the eastern cave wall. **b**, West baulk of Sector XV, also showing the uncomformably overlying deposits (**B**). **c** and **d**, North and east baulks of Sector XIX, near the cave centre 44

Extended data figure 2.3 The volcaniclastic deposits at Liang Bua. **a,** Photograph of tephras T6–T8 (north baulk of Sector XVI). **b**, Photograph of tephras T1–T5 (south baulk of Sector XXI). **c**, Bivariate plot of FeO and CaO concentrations (expressed as weight %), acquired by electron microprobe analysis of glass shards from T1 (n = 6), T3 (n = 4), T5 (n = 10) and T7 (n = 15), as well as the Youngest Toba Tuff (YTT, n = 207, ± 1σ) from northern Sumatra. **d**, Bivariate plot of FeO and K_2O concentrations (symbols as in **c**). **e**, Bivariate plot of SiO_2 and $Na_2O + K_2O$ concentrations (symbols as in **c**). **f**, Isotope correlation (inverse isochron) plot for hornblende crystals from T1. The error ellipses represent individual analyses (n = 28). The ellipse on the far right-hand side was omitted from the $^{40}Ar/^{39}Ar$ age determination of 79 ± 12 kyr (at 1σ) 45

Extended data figure 2.4 Erosional surface of the pedestal in the west baulks of Sectors XV and XVI. The dashed line marks the steeply sloping boundary between remnant deposits (**T2**, **T1** and the underlying *Homo floresiensis*-bearing sediments) that comprise part of the pedestal (**A**) and the much younger deposits (**B**) that unconformably overlie the contact. **a**, Photograph taken at an upward angle showing the sedimentary differences between the deposits above and below the erosional boundary. **b**, Illustration of the erosional surface and underlying deposits shown in **a**..... 46

Extended data figure 2.5 Erosional surface of the pedestal near the eastern wall of the cave. **a**, Illustration of the erosional surface and the locations of LB1, LB4, LB6 and LB8 below the boundary (see also Fig. 2.3). The deposits that unconformably overlie the pedestal are shown in the south and west baulks. The stippled cube outlines the photographed area (in Sector XV) shown in **b** and **c**. Both photographs taken from above, with north towards the bottom of the page 47

Extended data figure 2.6 Locations of sediment samples dated in this study and TL data for quartz grains from Liang Bua. **a**, Stratigraphy of the excavated area near the eastern cave wall (Sector baulks as in Extended Data fig. 2.1) with TL samples indicated by red circles, IRSL samples by blue circles and the $^{40}Ar/^{39}Ar$ sample by a yellow square. Also shown are the TL and IRSL sample codes and the locations of hominin remains LB1 and LB6. **b**, Representative isothermal (260 °C) TL decay curves for the natural (black line) and test dose (grey line) signals from sample LB08-15-3. **c** and **d**, Regenerated TL dose-response curves for one pair of Aliquots A and B of sample LB08-15-3, respectively; the equivalent dose (D_e) is estimated by projecting the natural signal (red square) on to the dose-response curve fitted to the regenerated signals (blue diamonds). **e**, Radial plot (Galbraith *et al.*, 1999; Galbraith and Roberts, 2012) of D_e values for Aliquot A (n = 12) of sample LB08-15-3; the

grey band is centered on the weighted mean D_e calculated using the central age model. **f**, Radial plot of the corresponding D_e values for Aliquot B (n = 12) of the same sample. The grey band is centered on the central age model estimate, with the two high-D_e outliers omitted. The red line intersects the right-hand axis at the D_e calculated by fitting the minimum age model (Galbraith *et al*., 1999; Galbraith and Roberts, 2012) to all 12 values. **g** and **h**, Radial plots of D_e values for Aliquots A and B of sample LB12-23-1(symbols as in **e** and **f**) 48

Extended data figure 2.7 IRSL data and potassium (K) concentrations for feldspar grains from Liang Bua. **a**, Representative IRSL (50 °C) and multiple elevated temperature (100–250 °C) post-infrared IRSL (pIRIR) decay curves for a single aliquot of sample LB12-OSL1. **b**, IRSL (50 °C) and pIRIR (290 °C) decay curves for a different aliquot of LB12-OSL1. **c**, Regenerated pIRIR (290 °C) dose-response curve for the aliquot shown in **b**; the equivalent dose (D_e) is estimated by projecting the natural signal (red square) on to the dose-response curve fitted to the regenerated signals (blue diamonds). **d–j**, Radial plots of IRSL ages (corrected for residual dose and anomalous fading) for single aliquots of each sample: **d**, LB12-OSL1; **e**, LB12-OSL2; **f**, LB12-OSL3; **g**, LB12-OSL4; **h**, LB12-OSL5; **i**, LB12-OSL6; and **j**, LB12-OSL7. IRSL ages were also obtained for single grains of samples LB12-OSL3 and LB12-OSL4, and are shown as open triangles in plots **f** and **g**. The grey bands in each plot are centered on the weighted mean ages calculated using the central age model. **k** and **l**, Radial plots of IRSL ages (corrected as for **d–j**) for samples LBS7-40a and LBS7-42a, respectively; single aliquots are shown as filled circles and single grains as open triangles. The upper and lower red lines intersect the right-hand axis at the maximum and minimum single-grain ages, respectively. **m**, Distribution of pIRIR intensities from 28 individual grains of feldspar from sample LB12-OSL3 that had been given a regenerative dose of 80 Gy. The relative contribution of each grain to the total (cumulative) pIRIR light sum is plotted as a function of K concentration (measured by wavelength-dispersive X-ray spectroscopy); note the reversed scale on the *x*-axis. **n**, Cumulative pIRIR light sum for the same 28 grains as shown in **m**, plotted as a function of grains ranked by K concentration (which decreases from left to right)..... 50

Extended data figure 2.8 Laser-ablation uranium-series analyses of hominin bone fragments from various Sectors and spits (depth intervals), and their modelled ages. **a**, Modern human femur (132A/LB/27D/03) from Sector IV, spit 27 (265–275 cm). **b**, *Homo floresiensis* ulna (LB1/52) from Sector XI, spit 58A (575–585 cm). **c**, *H. floresiensis* ulna (LB2/1) from Sector IV, spit 42D (415–425 cm). **d**, *H. floresiensis* ulna (LB6/3) from Sector XI, spit 51 (505–515 cm). Each laser spot is 265 μm in diameter and the age errors are at 2σ 52

Extended data figure 2.9 Laser-ablation uranium-series analyses of bone fragments of *Stegodon florensis insularis* from various spits (depth intervals) in Sector XI, and their modelled ages. **a**, U-s-01/LB/XI/32/04, spit 32 (315–325 cm). **b**, U-s-02/LB/XI/45/04, spit 45 (445–455 cm). **c**, U-s-03/LB/XI/47/04, spit 47 (465–475 cm). **d**, U-s-04/LB/XI/49/04, spit 49 (485–495 cm). **e**, U-s-05/LB/XI/51/04, spit 51 (505–515 cm). **f**, U-s-06/LB/XI/52/04, spit 52 (515–525 cm). **g**, U-s-07/LB/XI/65/04, spit 65 (645–655 cm). **h**, U-s-08/LB/XI/65B/04, spit 65B (645–655 cm). Each laser spot is 265 μm in diameter and the age errors are at 2σ 53

Extended data figure 2.10 Deposits stratigraphically above the unconformity in Sector XVI and displaced slab of deposit in Sector XXII. **a**, The north baulk (~2 m wide) of Sector XVI. **b**, Excavated floors (white arrow points north) of spits 61–63 (615–635 cm depth); the field of view is ~1.6 m in width. The stippled box in **a** indicates the floor of spit 63 in **b**, where fragments of T1 (+) are visible in spit 63, and fragments of T3 (*) and T1 are concentrated in the band just above the label for spit 61. Eroded fragments (between about 1 cm and 60 cm in size) of T1, T2 and T3 have been consistently recovered from deposits unconformably overlying the erosional surface of the pedestal, indicating reworking of the pedestal deposits before ~13 kyr cal. BP. **c**, Photograph of the west baulk and parts of the south and north baulks (at left and right, respectively) of Sector XXII showing a displaced slab of deposit that contains intact portions of the uppermost part of T3 (arrow) and the overlying layers, up to and including the flowstone (fs) that caps T5. The stratigraphic position of the slab beneath T7 and T8 indicates that it broke away from its original location, slightly to the south, and slid down the steeply sloping erosional surface prior to ~13 kyr cal. BP. Also shown are the *Homo floresiensis*-bearing deposits (**A**) and the unconformably overlying deposits (**B**), which include eroded fragments of T1 (+), T2 (#) and T3 (*). **d**, Illustration of the west baulk of Sector XXII, as shown in **c** 54

Figure 3.1 Composite section of the Liang Bua depositional sequence, showing the tephras and other key stratigraphic markers with approximate ages. The modern soil and basal sediments are shaded grey at the top and bottom of the section, respectively. Note the gap in the section between 46 and 20 ka, constrained by flowstone directly overlying T5 and the charcoal sample dated by ^{14}C to ~46 ka cal BP. 91

Figure 3.2 Site plan of Liang Bua and excavated Sectors. Sectors from which charcoal has been dated by ^{14}C are shaded: yellow, ages reported by Roberts *et al*. (2009); green, ages reported in Chapter 2 of this thesis (Sutikna *et al*., 2016); blue, ages reported in this study. The remaining cave floor sediments are shaded white, while the areas shaded gray are exposed rocks, stalagmites and other surfaces covered in speleothems..... 93

Figure 3.3 Stratigraphic profile of the western baulks of Sectors XXIV (at left) and XXVII (at right). The locations of the dated charcoal samples are shown projected on to the west wall as green circles with their median calibrated ^{14}C ages (in ka). Colours are used to illustrate the spatial extent of each stratigraphic layer, with clasts of limestone and gravel shown in dark grey. Black arrows indicate a combustion feature (a hearth). Red arrows indicate the termination of T3 in Sector XXIV and tephras T3, T4 and T5 are indicated in the right margin. 101

Figure 3.4 Stratigraphic profile of the western baulks of Sectors XV, XVI and XXVI (left, middle and right panels, respectively). The locations of the dated charcoal samples are shown projected on to the west wall as green circles with their median calibrated ^{14}C ages (in ka). Tephras T1, T2, T3, T7 and T8 are also indicated..... 103

Figure 3.5 Linear regression fit to the ^{14}C ages (circles) from the Holocene sequence in Sector XXVI. The fitted line is defined as $y = 33.89x - 2200$, with $R^2 = 0.989$..... 104

Figure 3.6 Linear regression analyses of the ^{14}C ages (circles) from the Holocene sequence in Sector XVI. The fitted lines are as follows: all samples (black), $y = 37.83x - 1589.2$, $R^2 = 0.970$; southern half (orange), $y = 44.29x - 2261.1$, $R^2 = 0.956$; northern half (grey), $y = 37.41x - 1722.7$, $R^2 = 0.999$ 106

Figure 3.7 Stratigraphic profile of the eastern baulks of Sectors IV and XIX (left and right panels, respectively). Note that there is 50 cm of unexcavated deposit between the two baulks and that the orientation of Sector IV is at an angle relative to Sector XIX (see Fig. 3.2). The locations of dated charcoal samples are shown projected on to the east wall as green circles with their median calibrated ^{14}C ages (in ka). Tephras T1, T2, T3, T5, T7 and T8 are also indicated..... 108

Figure 3.8 Linear regression fit to the ^{14}C ages (circles) from the Holocene sequence in Sector IV. The fitted line is defined as $y = 28.65x - 625.97$, with $R^2 = 0.996$..... 109

Figure 3.9 Linear regression analysis of the ^{14}C ages (circles) from the Holocene sequence in Sector XI. The fitted line is defined as $y = 44.04x - 1661.44$, with $R^2 = 0.985$..... 110

Figure 3.10 Linear regression analysis of the ^{14}C ages by depth for the Holocene and terminal Pleistocene deposits in Sectors aligned south to north as follows: XI (blue), XVI south (orange), XVI south (grey) and XXVI (red). Sector IV (yellow) lies further to the west (Fig. 3.2). ANCOVA results indicate that the regression slopes of Sectors XI and XVI south are significantly different from the others ($p < 0.05$), essentially tracking the

stratigraphic observations that the deposits slope downward towards the north. The regression slopes of Sectors XVI north, XXVI and IV are not significantly different from each other 115

Figure 3.11 Composite section of the Liang Bua depositional sequence, showing the tephras and other key stratigraphic markers with approximate ages. The modern soil and basal sediments are shaded grey at the top and bottom of the section, respectively. Note that the previous gap between 46 and 20 ka (Fig. 3.1) now contains sediments dated to this interval in Sectors XXIV and XXVII as a result of this study. The depositional age of T8 is now more tightly constrained to ~12 ka, based on new ^{14}C ages for charcoal samples collected from immediately below and above this tephra. 116

Figure 4.1 Site location and plan: **a**, Location of Flores island within the Indonesian archipelago; **b**, Location of Liang Bua on Flores island; **c**, Liang Bua plan and Sectors discussed in the text 125

Figure 4.2 Composite stratigraphy at Liang Bua with approximate ages and units/subunits based on Sutikna *et al*. (2016). The modern soil and basal sediments are shaded grey at the top and bottom of the section, respectively. Eight identified tephras (T1–T8) define the eight main units/subunits used in this chapter (Units 1A–8C). The data shown for the fauna and stone artefacts are based on samples obtained during the 2001–2004 excavations. Based on this revised stratigraphy and chronology, the vertical blue lines show the known faunal presence (Morwood and Jungers, 2009; van den Bergh *et al*., 2009; Meijer *et al*., 2013) and the raw material preferred by hominins for stone artefacts (Moore *et al*., 2009). The dotted vertical lines indicate presumed presence of *H. floresiensis* based on stone artefacts (Sutikna *et al*., 2016). Question marks highlight new uncertainties raised by the results of previous publications, in combination with the revised stratigraphic and chronological framework for the site. 126

Figure 4.3 Chord distance (CD) values (dimensionless) for the faunal assemblages across successive pairs of assigned depositional units at Liang Bua. The tephras are denoted as T1–T8. CD values close to zero indicate no change between units, while higher values indicate more change 137

Figure 4.4 Unweighted pair group method with arithmetic mean (UPGMA) cluster analysis of stratigraphic units at Liang Bua. The dendrogram is based on a similarity index (dimensionless) calculated using the matrix of all pairwise chord distances between units. Deeper branches between units indicate less similarity in faunal structure (e.g., Unit 1B compared with all other units) 138

Figure 4.5 Taxonomic evenness throughout the stratigraphic sequence, determined using the Shannon evenness index. Approximate 95% confidence intervals for the index of each unit were estimated using the bootstrap procedure

(9999 resamples with replacement) provided in PAST, version 3 (Hammer, 2015). Greater evenness is indicated by higher index values. Note the significant differences between the indices of assemblages of Units 1A–2 compared to Units 4–8C 139

Figure 4.6 Correspondence analysis of faunal taxa abundances within stratigraphic units. Axes 1 and 2 explain 70.7% and 21.3% of the variance, respectively. Unit symbols: >50 ka, squares; 50 to 12 ka, diamonds (with unit containing T7 and T8 denoted in grey); 12 ka to present, circles 140

Figure 4.7 Relative frequencies (calculated as % vertebrate NISP) of rat by stratigraphic unit at Liang Bua. There is a consistent decrease in rat abundance from Units 2 to 8B. The *x*-axis ranges between 0 and 100% 142

Figure 4.8 Relative frequencies (calculated as % vertebrate NISP) of stegodont by stratigraphic unit at Liang Bua. *Stegodon* remains from Units 4–6 and 8A may be reworked from Units 1A–2 (see text for discussion). Note the *x*-axis ranges between 0 and 10% 142

Figure 4.9 Relative frequencies (calculated as % vertebrate NISP) of frog by stratigraphic unit at Liang Bua. Frog remains are most abundant in the Holocene units (8A–8C). Note the *x*-axis ranges between 0 and 25% 143

Figure 4.10 Relative frequencies (calculated as % vertebrate NISP) of snake by stratigraphic unit at Liang Bua. Note the *x*-axis ranges between 0 and 5% 143

Figure 4.11 Relative frequencies (calculated as % vertebrate NISP) of megabat by stratigraphic unit at Liang Bua. The largest abundances are observed above tephra T3, in Units 4–8C. Note the *x*-axis ranges between 0 and 10% 144

Figure 4.12 Relative frequencies (calculated as % vertebrate NISP) of microbat by stratigraphic unit at Liang Bua. As with the megabat, the highest abundances occur in Units 4–8C. Note the *x*-axis ranges between 0 and 25% 144

Figure 4.13 Relative frequencies (calculated as % total faunal NISP) of aquatic invertebrate by stratigraphic unit at Liang Bua. By far the largest abundances are in Units 8B and 8C. Note the *x*-axis ranges between 0 and 20% 145

Figure 4.14 Relative frequencies (calculated as % total faunal NISP) of terrestrial invertebrate by stratigraphic unit at Liang Bua. Note the *x*-axis ranges between 0 and 20% 145

Figure 4.15 Relative frequencies (calculated as % vertebrate NISP) of introduced large mammal by stratigraphic unit at Liang Bua. These only occur in Units 8A–8C. Note the *x*-axis ranges between 0 and 10% 146

Figure 4.16 Chord distance (CD) values for the faunal assemblages across successive pairs of assigned depositional units at Liang Bua, assuming *Stegodon* and stork/vulture are extinct in Units 4 and above. The tephras are denoted as T1–T8. CD values close to zero indicate no change between units, while higher values indicate more change..... 147

Figure 4.17 Correspondence analysis of faunal taxa abundances within stratigraphic units, assuming *Stegodon* and stork/vulture are extinct in Units 4 and above. Axes 1 and 2 explain 70.0% and 21.9% of the variance, respectively. Unit symbols as in Fig. 4.6. Note that in comparison with Fig. 4.6, axis 2 is inverted; this is solely a statistical artefact and otherwise both plots are essentially identical 148

Figure 4.18 Unweighted pair group method with arithmetic mean (UPGMA) cluster analysis of stratigraphic units at Liang Bua, assuming *Stegodon* and stork/ vulture are extinct in Units 4 and above. The dendrogram is based on a similarity index (dimensionless) calculated using the matrix of all pairwise chord distances between units. Deeper branches between units indicate less similarity in faunal structure (e.g., Units 1A–2 are more similar to each other than any of them are to Units 4–8A)..... 149

Figure 4.19 Chord distance (CD) values for raw material abundances across successive pairs of assigned depositional units at Liang Bua. The tephras are denoted as T1–T8. CD values close to zero indicate no change between units, while higher values indicate more change..... 150

Figure 4.20 Unweighted pair group method with arithmetic mean (UPGMA) cluster analysis of raw material abundance by stratigraphic unit at Liang Bua. The dendrogram is based on a similarity index (dimensionless) calculated using the matrix of all pairwise chord distances between units. Deeper branches between units indicate less similarity in raw material used (e.g., Units 1A–2 are more similar to each other than any of them are to Units 4–8C)..... 151

Figure 4.21 Raw material evenness throughout the stratigraphic sequence, determined using the Shannon evenness index. Approximate 95% confidence intervals for the index of each unit were estimated using the bootstrap procedure (9999 resamples with replacement) provided in PAST, version 3 (Hammer, 2015). Greater evenness is indicated by higher index values. Note the significant differences between the indices of assemblages of Unit 1B compared to Units 4–8C..... 152

Figure 4.22 Correspondence analysis of raw material abundances within stratigraphic units. Axes 1 and 2 explain 76.7% and 17.3% of the variance, respectively. Unit symbols as in Fig. 4.6. Variance along Axis 1 is mainly explained by the abundances of chert and silicified tuff..... 154

Figure 4.23 Relative frequencies (calculated as % raw material NISP) of silicified tuff by stratigraphic unit at Liang Bua. The largest abundances are in Units 1A–2. The *x*-axis ranges between 0 and 100% 154

Figure 4.24 Relative frequencies (calculated as % raw material NISP) of chert by stratigraphic unit at Liang Bua. Chert is most abundant in Units 4–8C. As with Fig. 4.23, the *x*-axis ranges between 0 and 100% 155

Figure 4.25 Relative frequencies (calculated as % raw material NISP) of chalcedony by stratigraphic unit at Liang Bua. Note the *x*-axis ranges between 0 and 25% 155

Figure 4.26 Relative frequencies (calculated as % raw material NISP) of quartz by stratigraphic unit at Liang Bua. Note the *x*-axis ranges between 0 and 25%... 156

Figure 4.27 Relative frequencies (calculated as % raw material NISP) of jasper by stratigraphic unit at Liang Bua. Note the *x*-axis ranges between 0 and 25%... 156

Figure 4.28 Relative frequencies (calculated as % raw material NISP) of silicified limestone by stratigraphic unit at Liang Bua. Note the *x*-axis ranges between 0 and 25%..... 157

Figure 4.29 Relative frequencies (calculated as % vertebrate NISP) of varanid by stratigraphic unit at Liang Bua. Note the *x*-axis ranges between 0 and 5%..... 159

Figure 4.30 Relative frequencies (calculated as % vertebrate NISP) of stork/ vulture by stratigraphic unit at Liang Bua. Note the *x*-axis ranges between 0 and 1%..... 159

Figure 4.31 The left maxillary 3rd premolar (**a**, centre) and right mandibular 2nd molar (**b**, centre) from Unit 4 at Liang Bua. In **a**, the right (mirrored) and left maxillary 3rd premolars of LB1 are shown at left and right, respectively (modified from Kaifu *et al*., 2015). In **b**, the left (mirrored) and right mandibular 1st–3rd molars of LB1 are shown at the far left and second from left, respectively, and the left (mirrored) and right mandibular 1st–3rd molars of LB6 are shown at the far right and second from right, respectively (modified from Kaifu *et al*., 2015). Note the difference in shape and absolute and relative cusp size between the teeth of *H. floresiensis* and the two teeth from Unit 4 (1 cm scale shown) 162

Figure 4.32 Mesiodistal (MD) lengths and buccolingual (BL) widths of maxillary 3rd premolars from *H. floresiensis* (LB1) (Brown *et al*., 2004; Kaifu *et al*., 2015), modern humans (*N* = 502) (Voisin *et al*., 2012) and Unit 4 at Liang Bua (~46 ka cal. BP, shown by the filled circle). The dotted line is the linear regression for the dataset of modern human premolars 163

Figure 4.33 Mesiodistal (MD) lengths and buccolingual (BL) widths of mandibular 2nd molars from *H. floresiensis* (LB1 and LB6) (Brown *et al*., 2004; Kaifu *et al*., 2015), modern humans (*N* = 502) (Voisin *et al*., 2012), modern humans (*N* = 1181) (Brown and Maeda, 2009) and Unit 4 at Liang Bua (~46 ka cal. BP, shown by the filled circle). The dotted line is the linear regression for the dataset of modern human molars 164

Figure 4.34 Relative frequencies (calculated as % vertebrate NISP) of fish by stratigraphic unit at Liang Bua. Note the *x*-axis ranges between 0 and 5% 165

Figure 4.35 Composite stratigraphy at Liang Bua with approximate ages and units/subunits based on Sutikna *et al*. (2016). Same as Fig. 4.2, but updated with a summary of the results of this study. Note the many areas where significant questions have been answered. The dotted vertical lines indicate presumed presence of *H. floresiensis* based on stone artefacts, and possible extensions to the time ranges of some other fauna..... 169

Figure 5.1 Map of Island Southeast Asia and Australasia showing Sundaland, Wallacea and Sahuland. Late Pleistocene archaeological sites and possible routes for modern human dispersal are also indicated. The yellow circle highlights the new evidence for modern humans at Liang Bua ~46 ka ago presented in this thesis (modified from Birdsell, 1977; Bird *et al*., 2005; O'Connor, 2007) 174

Figure A.1 Volcanic ashes recognised in the 2001–2003 excavations. **a.** North baulk of Sector IV. **b.** West baulk of Sector VII. Numbers denote the following: **1** = upper 'white tuff' (now Tephra 8 or T8), **2** = lower 'white tuff' (now Tephra 7 or T7), **3** = fragments 'black tuff' (with yellow lines in **a**, now Tephra 3 or T3). (Photos: © Liang Bua Team)..... 198

Figure A.2 The discovery of *Homo floresiensis*. **a.** The moment when the partial skeleton of *Homo floresiensis* was unearthed in a fragile condition. **b.** Preparation for preserving the bones before they were lifted. Yellow arrow shows a small block of 'black tuff' ~1 m above the skeleton (see Fig. A.1b). (Photos: © Liang Bua Team) 199

Figure A.3 Black tuff and white tuff in Sector XI. **a.** South baulk of Sector XI exposed black tuff (there is no white tuff in the south baulk). **b.** West baulk of Sector XI shows that the white tuff extended southward underneath the black tuff (this photo was taken in 2008 during excavation of Sector XV). White arrows indicate white tuff and black arrows indicate black tuff. (Photos: © Liang Bua Team) 200

Figure A.4 Black tuff in Sector XII. **a.** The entire black tuff exposed at ~2 m depth in Sector XII (there is no white tuff in this Sector). **b.** North baulk of Sector

XII, showing the black tuff is as thick as in Sector XI. (Photos: © Liang Bua Team) 201

Figure A.5 Exposure of the black tuff in Sector XV. **a.** The upper part of the black tuff (T3) extends ~70 cm (in the middle) from the south baulk to the north (photo taken from the top). **b.** Black tuff overlain by pinkish volcanic ash (now Tephra 5 or T5) and flowstones. Numbers denote the following: **1** = flowstone, **2** = T5, **3** = T3, **4** = limestone block, **5** = broken fallen stalactites. (Photos: © Liang Bua Team) 203

Figure A.6 Contact boundaries between the black and white tuffs in Sector XV. **a.** Photo taken from the top, south to north. **b.** Photo taken from the top, west to east. Numbers denote the following: **1** = upper white tuff (T8), **2** = lower white tuff (T7), **3** = black tuff (T3). White dashed lines indicate the termination of the white tuff and yellow dashed lines indicate the border between Sectors XI and XV. Red arrows indicate huge limestone boulder. (Photos: © Liang Bua Team) 204

Figure A.7 White tuff in the small cavity beneath the black tuff. **a.** The black tuff rested on a huge limestone boulder in the south baulk of Sector XV. **b.** In the southeast corner of Sector XV, the distal 'tail' of white tuff and other younger sediments had filled the cavity beneath the black tuff (see also Fig. A.3b). Numbers denote the following: **1** = upper white tuff (T8), **2** = limestone block, **3** = black tuff (T3), **4** = pinkish volcanic ash (T5). The yellow dashed circle indicates the cavity and the red arrows indicate the thin flowstone covering it. Yellow arrows indicate the distal tail of white tuff. (Photos: © Liang Bua Team)..... 205

Figure A.8 Erosional surface of the black tuff. **a.** As exposed in the west baulk of Sector XVII. **b.** As exposed in the east baulk of Sector XIX. The yellow dashed lines indicate the erosional surface of the black tuff as well as the contact boundaries with much younger deposits. Numbers denote the following: **1** = flowstone, **2** = pinkish volcanic ash (T5), **3** = black tuff (T3). White arrow indicates T4. (Photos: © Liang Bua Team)..... 205

List of tables

Table 3.1 Recalibration of published ^{14}C ages for charcoal samples from Liang Bua 96

Table 3.2 New ^{14}C ages for charcoal samples from Sectors XXIV and XXVII 98

Table 3.3 New ^{14}C ages for charcoal samples from Sector XXVI..... 99

Table 3.4 New ^{14}C ages for charcoal samples from Sector XVI..... 99

Table 3.5 New ^{14}C ages for charcoal samples from Sector XIX..... 107

Table 4.1 Summary of the Liang Bua assemblages examined in this study 133

Table 4.2 Number of identified specimens (NISP) by stratigraphic unit and taxon ... 135

Table 4.3 Number of identified specimens (NISP) by stratigraphic unit and raw material (excluding debitage)..... 136

CHAPTER 1

Introduction

1.1 Study site

The study site for this thesis is Liang Bua, a large limestone cave on the Indonesian island of Flores, one of many oceanic islands (together known as Wallacea) that occur between the Asian and Australian continental shelves. Located in the western part of Flores in the Manggarai Regency (one of eight government districts on the island), Liang Bua lies at an altitude of about 592 m above sea level with a latitude and longitude of 08° 31' 50.4" S and 120° 26' 36.9" E, respectively. The name of the cave derives from the local Manggarai language (part of the Austronesian linguistic family) and means 'cold cave' ('Liang' meaning cave and 'Bua' meaning cold). The cave is situated at the base of Golo Tando ('Golo' meaning hill) around 200 m south of the confluence of two perennial rivers, the Wae Racang and Wae Mulu ('Wae' meaning river), and is about 14 km northwest of Ruteng, the capital city of the Manggarai Regency (Fig. 1.1).

Archaeological research at Liang Bua began in 1950 when Theodorus Lambertus Verhoeven, a Dutch Catholic priest based at the Mataloko Seminary in the Ngada Regency of central Flores, visited the cave for the first time (Verhoeven, 1952). Traveling across western Flores with two other Catholic missionary priests, Wilhelmus van Bekkum and Adriaan Mommersteeg, Verhoeven collected surface finds from the cave floor at Liang Bua and several other sites (Verhoeven, 1952).

Fifteen years later, Verhoeven returned to Liang Bua and, during a short field season between late June and early July 1965, he excavated an area near the western

cave wall, where he discovered six modern human burials (Fig. 1.2 and 1.3) (Soejono, 1978).

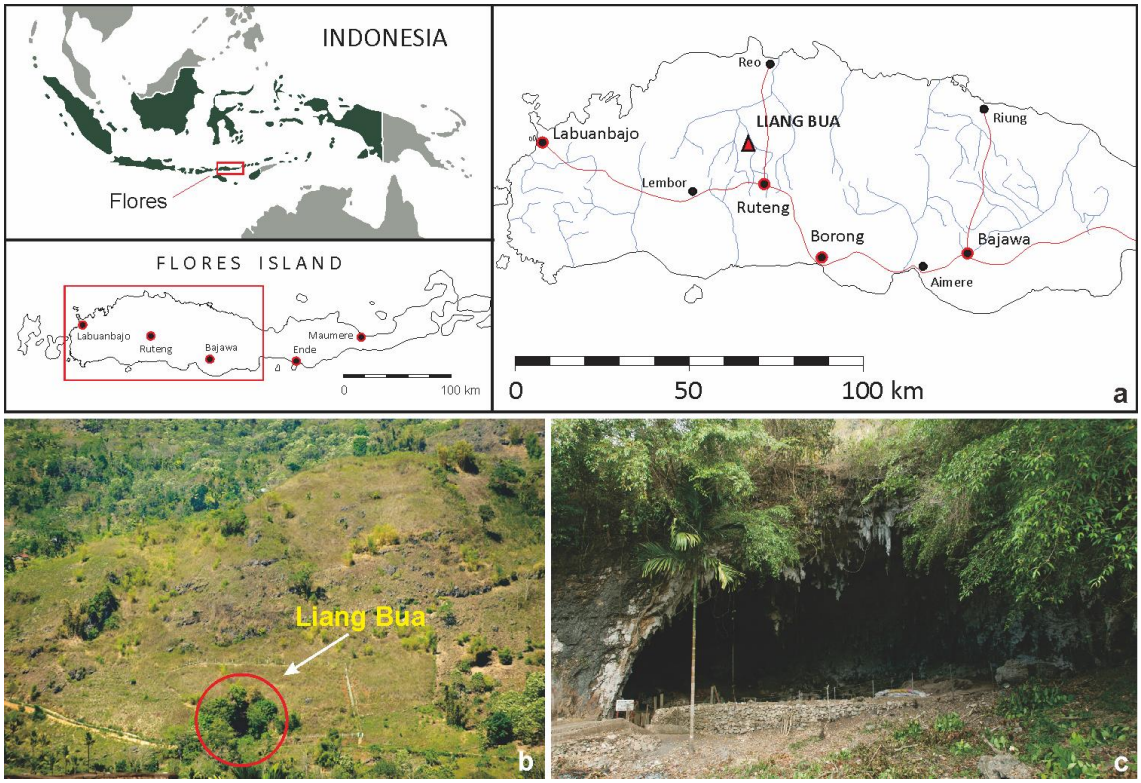

Figure 1.1 Location of Liang Bua. **a.** The location of Liang Bua on Flores within the Indonesian archipelago; **b.** Liang Bua located at the foothills of Golo Tando; **c.** Liang Bua as viewed from the outside where the cave mouth faces to the northeast. (Photos: © Liang Bua Team).

Each of these burials was accompanied by Neolithic grave goods, such as pottery, stone adzes and pig tusks, at about 1 m depth. Parts of a child's cranium (possibly from the Mesolithic) were also recovered at about 2 m depth. The artefacts and faunal remains recovered from Verhoeven's excavations are stored at various places, including the Naturalis Museum of Natural History (Leiden, Netherlands), the Blikon Blewut Museum (Maumere, east Flores) and Pusat Penelitian Arkeologi Nasional (Jakarta, Indonesia). The modern human skeletal remains were brought to the University of Airlangga (Surabaya, Jawa Timur) in the late 1960s, but mostly only cranial and dental material from five of the individuals remain (Delta Bayu Murti, 2011).

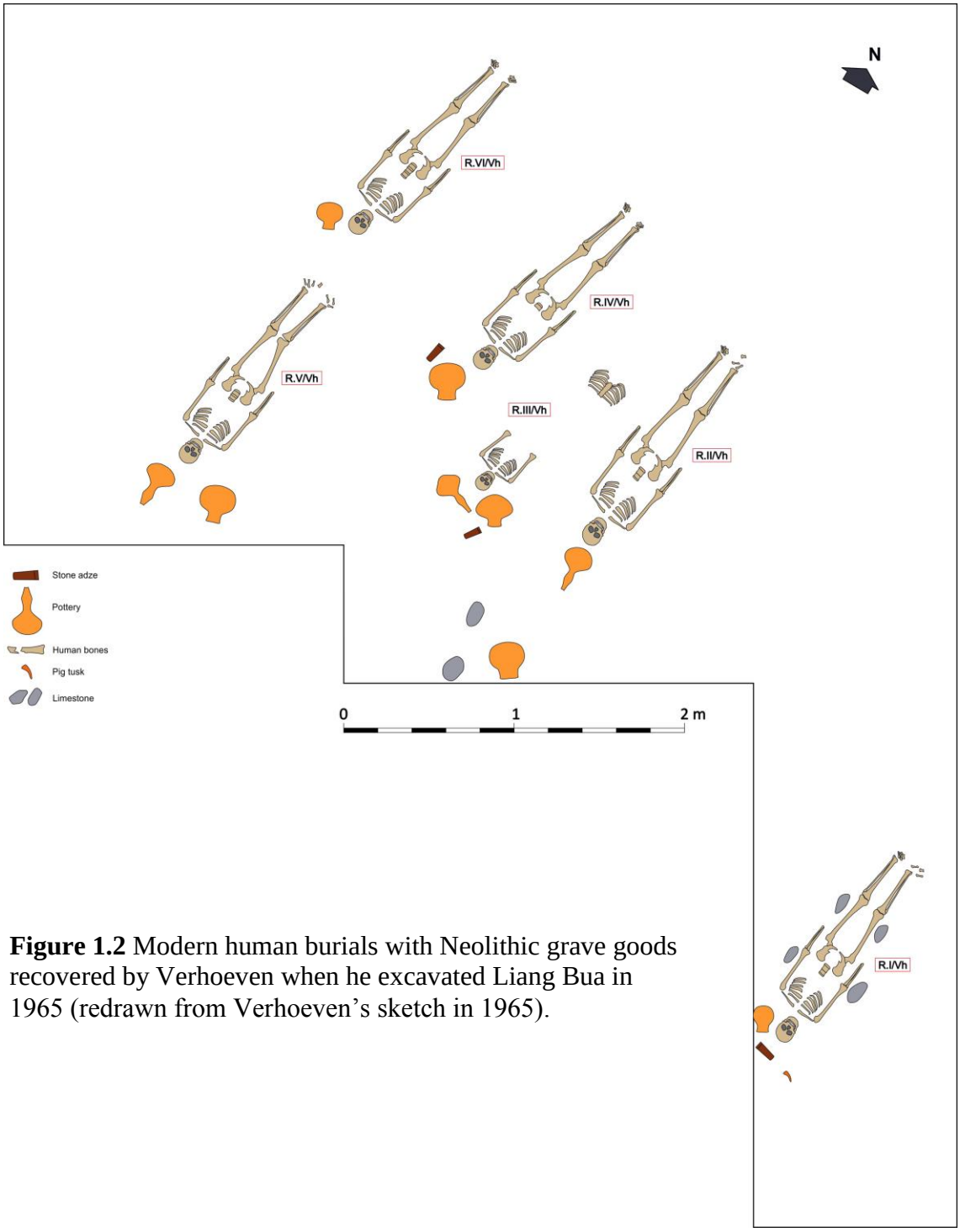

Figure 1.2 Modern human burials with Neolithic grave goods recovered by Verhoeven when he excavated Liang Bua in 1965 (redrawn from Verhoeven's sketch in 1965).

Thirteen years after Verhoeven's initial excavation, archaeological research at Liang Bua commenced again led by Professor Raden P. Soejono from Pusat Penelitian Arkeologi Nasional (which translates as the National Research Centre for Archaeology, and is hereafter referred to as Arkeologi Nasional or ARKENAS). Between 1978 and 1989, Soejono and his team excavated ten areas (referred to as Sectors) during the

course of seven different seasons (Soejono, 1978, 1981; Kosasih, 1985; Jatmiko, 1989). Four of these Sectors (I–IV) were 3 x 3 metres in plan area while the remaining six were 2 x 2 metres in area (V–X) (Fig. 1.3). These excavations typically reached a maximum depth of 1–2 m, except for Sectors VII and IV, which reached depths of 2.75 and 3.15 m, respectively.

Figure 1.3 Plan of Liang Bua with excavated Sectors. The excavations in 2001–2003 included Sectors I, III, IV and VII, which had been excavated previously by Soejono.

Charcoal recovered in 1989 from the lowest excavated spit of Sector IV yielded a radiocarbon (^{14}C) age range (95% confidence interval) of 12.8–10.0 thousand calibrated ^{14}C years before present (ka cal. BP, where the 'present' is defined by convention as

A.D. 1950). Other charcoal, sampled previously from higher in the sequence, ranged up until 450 cal. years BP in age (Roberts *et al*., 2009). Stone artefacts, faunal remains (vertebrate and invertebrate) and pottery, as well as nine additional modern human burials, were recovered, but almost all of this material remains unpublished. Most of the human burials were recovered from ~1 m depth and are characteristic of the Neolithic period, with associated grave goods similar to those recovered by Verhoeven (e.g., pottery and rectangular stone adzes) (Fig. 1.4) (Soejono, 1978, 1981; Kosasih, 1985; Jatmiko, 1989; Delta Bayu Murti, 2011). One of the skeletons was recovered closer to the cave surface (~50 cm depth), along with a bronze axe indicating that it likely derives from the Paleometalic period (Fig. 1.5). Characteristics of this bronze axe are unique in that both lateral sides were folded such that it formed a channel to insert a shaft. Due to its unique form, this bronze axe has been assumed to represent a pre-socketed axe in the early metal age and it is the only one that has yet been found in Indonesia. All nine of the modern human skeletons recovered during the 1978–1989 excavations were taken to Professor Teuku Jacob at Gadjah Mada University in Jogjakarta immediately upon returning from the field. Only a few descriptions or analyses of these burials exist (Delta Bayu Murti, 2011).

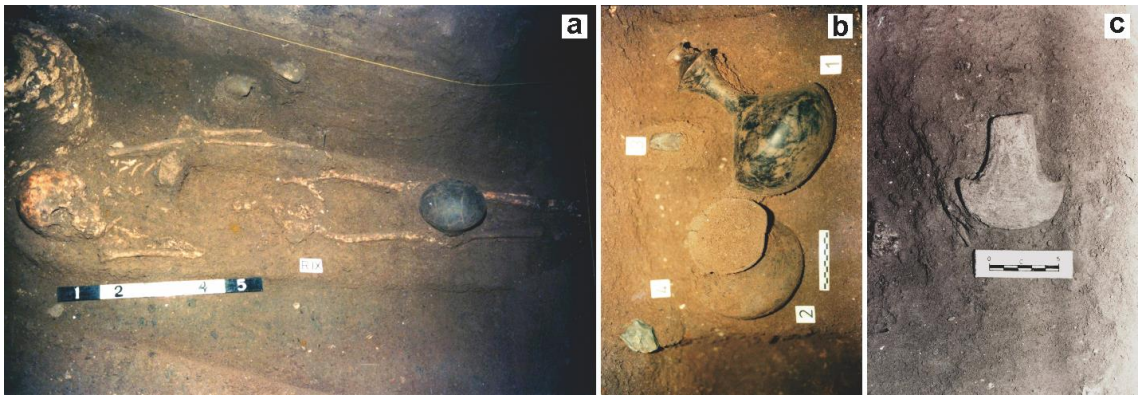

Figure 1.4 Neolithic and Palaeometalic burials from Soejono's excavations at Liang Bua between 1978 and 1989. **a.** Modern human burial with grave goods recovered in Sector X; **b.** Grave goods, including fine pottery, found in association with a second burial in Sector X; **c.** Bronze axe recovered with a modern human burial in Sector II (see also Fig. 1.5). (Photos: ©ARKENAS)

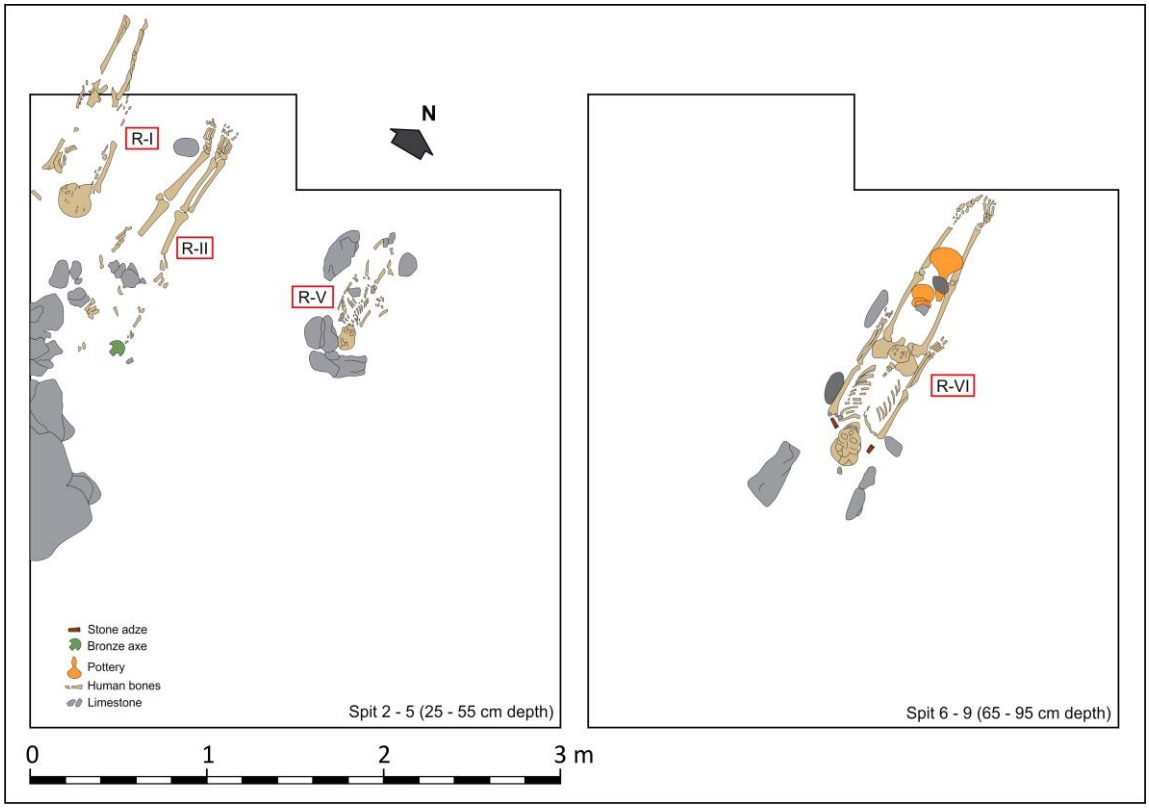

Figure 1.5 Palaeometalic (left) and Neolithic (right) modern human burials with associated grave goods from Soejono's 1978 excavation of Sector II at Liang Bua. (Redrawn from Soejono, 1978)

In 2004, Liang Bua became a world-famous archaeological site, when it was announced that the remains of a new fossil human species, *Homo floresiensis*, had been discovered ~6 m deep within its sediments (Brown *et al*., 2004; Morwood *et al*., 2004). This surprising discovery provided evidence that at least one premodern human species had successfully crossed the Wallace Line – and likely long before *Homo sapiens* (modern humans) had even evolved in Africa (White *et al*., 2003; McDougall *et al*., 2005) if the stone tools found in central Flores and dated to around 800–900 ka had been made by this hominin species (Morwood *et al*., 1998).

However, the unexpectedly recent age estimates for *H. floresiensis* at Liang Bua raised many interesting questions that still remain unanswered to this day. The holotype (LB1) and remains of other individuals were dated to ~18 ka cal. BP and 13–11 ka cal.

BP, respectively, while remains from the cave centre were dated to ~74 ka ago (Morwood et al., 2004, 2005; Roberts et al., 2009). These relatively young ages suggested the possibility of 30–40 millennia of potential overlap with modern humans, who were present elsewhere in Island Southeast Asia as early as ~50 ka ago, but evidence of modern humans on Flores prior to ~11 ka cal. BP was conspicuously lacking (Morwood *et al*., 2004). The following section provides a brief overview of the archaeological evidence for early modern human dispersals through Island Southeast Asia, so that the discoveries at Liang Bua can be placed in a broader regional context. The chapter concludes with the research aims of this thesis and an outline of its structure.

1.2 Island Southeast Asia – archaeological and palaeoanthropological context

When and how modern humans dispersed through Island Southeast Asia is a longstanding research problem. Archaeological evidence suggests that modern humans first reached Sahul (the collective landmass of Pleistocene Australia, New Guinea and the Aru islands) by at least 47–48 ka ago (Allen and O'Connell, 2014; O'Connell and Allen, 2015) and probably as early as 50–60 ka ago (Roberts *et al*., 1990, 1994, 1998; Turney *et al*., 2001; Bowler *et al*., 2003; Clarkson *et al*., 2015; Hiscock, 2015; Saltré *et al*., 2016). The genomic sequence of an Aboriginal Australian from the early 20th century suggests that the first modern humans to arrive in Sahul were the direct ancestors of the living Aboriginal inhabitants of Australia and New Guinea (Rasmussen *et al*., 2011). Moreover, these ancestral populations derive from an early wave of modern humans that probably left Africa between 62 and 75 ka ago (Rasmussen *et al*., 2011). These results have been recently extended by analysis of Aboriginal Australian Y chromosomes that suggests the divergence – and hence, a minimum date for modern

human arrival in Australia – from other modern human Y chromosomal DNA ~54 ka ago (Bergström *et al*., 2016). The concordance of these archaeological and genetic data from Australia suggests that modern humans must have been in Island Southeast Asia sometime between 62–75 and ~50 ka ago, but corroborative evidence in the region itself has remained elusive.

Birdsell (1977) proposed several possible dispersal routes through Island Southeast Asia for the modern human colonisation of Sahul (Fig. 1.6). Northern routes would have likely begun from southeast Borneo and included narrow sea crossings to Sulawesi and then Sula. From there, these modern humans (and their descendants) would have dispersed to Obi, Halmahera and/or Gebe and then on to the bird's head of Papua (western New Guinea) or, alternatively, directly to Buru, Seram and then Misool or passing through Kei to the Aru islands. Southern routes would have involved dispersal through the Lesser Sunda Islands, including (from west to east) Lombok, Sumbawa, Flores, Timor and then either directly to Australia by passing through Rote or continuing east to Babar, Tanimbar and then to the Aru islands.

Bird *et al*. (2005) suggested that an open savanna may have stretched along a narrow landbridge from peninsular Malaysia and Sumatra (Bangka-Belitung islands) to the north coast of Java whenever sea levels were ~40 m or more below modern levels (e.g., during Pleistocene glacial periods). This 'savanna corridor' presumably would have enabled modern humans to expand widely throughout the Sunda shelf and set the stage for subsequent dispersals, most likely along the Lesser Sunda Islands to Sahul, as the dense forests of Borneo may have acted as a barrier for further dispersals along the northern routes during glacial periods (Bird *et al*., 2005).

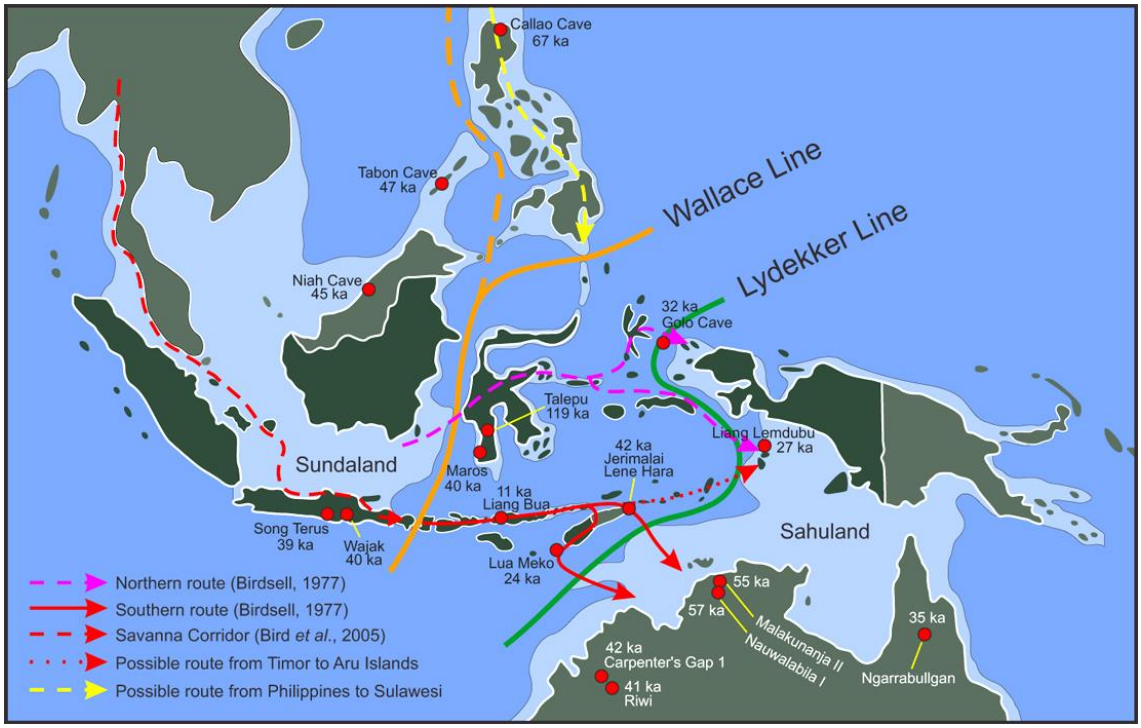

Figure 1.6 Map of Island Southeast Asia and Australasia showing Sundaland, Wallacea and Sahuland. Late Pleistocene archaeological sites and possible routes for modern human dispersal are also indicated (modified from Birdsell, 1977; Bird *et al*., 2005; O'Connor, 2007).

The relative shorter distances and inter-visibility between islands are criteria often cited in support of a southern route (Birdsell, 1977; O'Connor, 2007) but similar criteria have also been used to support a northern route (O'Connell and Allen, 2015). Regardless of which route or routes were involved in this prehistoric migration, the end result implies that these modern human populations had significant maritime and navigational skills, as well as the ability to adapt quickly to new environments and ecosystems (O'Connor, 2015). The earliest evidence of modern humans in the Lesser Sundas is ~42 ka cal. BP from Jerimalai shelter and Lene Hara on the eastern part of the island of Timor (O'Connor *et al*., 2011; O'Connor, 2015). Jerimalai is especially important because it also preserves the most compelling evidence to date that these early modern humans were highly competent mariners capable of capturing pelagic species of fish, such as tuna (O'Connor *et al*., 2011; O'Connor, 2015). Most of the

pelagic fish remains recovered at Jerimalai in sediments dated to between ~42 and 38 ka cal. BP are small in size, suggesting immature fish were typically targeted, probably using nets rather than angling (O'Connor *et al*., 2011). Direct evidence of technology related to fishing remains to be discovered in this early occupation phase at Jerimalai, but two fishhooks made of shell are present at the site in deposits dated to ~23–16 and ~11 ka cal. BP, respectively (O'Connor *et al*., 2011). A ~11 ka cal. BP fishhook has also been recovered from the nearby site of Lene Hare (O'Connor and Veth, 2005). Older cultural deposits are also present at Lene Hare, including a fine-grained red chert flake dated to ~42 ka cal. BP, based on ^{14}C ages for two marine shells recovered in association with the artefact (O'Connor *et al*., 2010). Although some temporal gaps remain in the Lene Hare stratigraphic sequence (e.g., the two intervals of 28–22 and 21–11 ka cal. BP), O'Connor *et al*. (2010) suggest these may reflect inadequate sampling of the deposits rather than periods in which modern humans abandoned the site. If their suggestion is correct, then Lene Hare provides a strong case for reasonably continuous modern human presence on the doorstep of Sahul from ~42 ka cal. BP onward (O'Connor *et al*., 2010).

Beyond these two sites in East Timor, there is only one other area in Wallacea that currently preserves compelling evidence of early modern human behaviour as early as ~40 ka ago. This is the Maros karst region of southwestern Sulawesi, where cave sites preserve rock art dated by uranium-series methods to more than 17.4 ka ago (Aubert *et al*., 2014). Hand stencils are the oldest documented motifs at these sites, with minimum ages of ~39.9 and ~39.4 ka from Leang Timpuseng and Leang Jarie, respectively (Aubert *et al*., 2014) and these ages are similar to those reported for the oldest rock art in Europe (Pike *et al*., 2012). These Sulawesi results build on the earlier and influential

work of Ian Glover, who excavated many sites on the island and elsewhere in Wallacea during the 1970s and 1980s (Glover, 1976, 1977, 1981).

One of the Sulawesi sites excavated by Glover that contains Late Pleistocene deposits was Leang Burung 2, a rockshelter also located in the Maros region (Glover, 1981). The deposits excavated in 1975 were dated to between 31 and 19 ka BP (uncalibrated ^{14}C years) on the basis of five ^{14}C ages for shells of a freshwater gastropod *Brotia perfecta* (now *Tylomelania perfecta*) (Glover, 1981). Recovered stone artefacts were mostly small flakes and debitage primarily made of chert (94%). However, large macroblade points with facetted platforms were also found and several flakes showed indication of silica gloss, possibly the result of processing plant materials. A fragment of an ochre pellet was also found with traces of abrasion, which may have been used to produce the ochre pigment for the hand stencils and other motifs on the walls (Glover, 1981). Although the excavation reached a maximum depth of 3.6 m, Glover did not encounter bedrock and archaeological finds were present at the base of the excavated trenches. New and ongoing excavations at Leang Burung 2 may find further, and perhaps older, evidence of modern human behaviour on Sulawesi during the Late Pleistocene (Brumm, 2012).

Several other sites in Wallacea provide a record of modern human activities during the Late Pleistocene from about ~30 ka onward, such as Leang Sakapao 1 in South Sulawesi (Bulbeck *et al*., 2004), Daeo Cave 2 in Morotai island (Bellwood *et al*., 1998), Golo Cave in Gebe island (Bellwood *et al*., 1998; Szabó *et al*., 2007), Leang Lembudu in the Aru islands (O'Connor *et al*., 2006), and Pia Hudale and Lua Meko on Rote island (Mahirta, 2009). Since the current ages for these sites are considerably younger than those from Sahul, however, their relevance to earlier modern human dispersals through the region is limited. Moreover, several new fossil discoveries made

in Sundaland during the past few years are much older than any found in Wallacea, such as the 67 ka metatarsal of an unidentified hominin in the Philippines (Mijares *et al*., 2010) and the remains of modern humans in Laos and southern China dated by uranium-series methods to more than ~63 and ~80 ka, respectively (Demeter *et al*., 2012; Liu *et al*., 2015).

Situated close to the eastern extent of the Sunda shelf on the island of Borneo, Niah Cave is a key site in Island Southeast Asia that preserves unequivocal modern human skeletal material associated with complex behavioural evidence dating back more than 40 millennia (Barker *et al*., 2007; Barker, 2013). Although the provenance and age of the 'Deep Skull' – a modern human cranium discovered at Niah Cave in 1958 and initially dated to ~40 ka (Harrison, 1959; Brothwell, 1960) – was questioned for decades, recent chronometric summaries suggest that it has a minimum age of ~37 ka, based on direct U-series dating of two small fragments of skull (Barker *et al*., 2007, 2013; Reynolds *et al*., 2013). U-series ages for bone are commonly interpreted as minimum estimates, due to the open-system geochemical behavior of bone (Grün *et al*., 2014), so these ages are consistent with the calibrated ^{14}C ages of 38,985–41,043 and 39,676–41,503 cal. BP (OxA-15126 and OxA-V-2076-16, respectively) obtained on two archived samples of charcoal collected from Harrison's excavation (Barker *et al*., 2007, 2013; Higham *et al*., 2009; Reynolds *et al*., 2013). In addition, there is evidence of human activity at the site that precedes the Deep Skull and its surrounding sediments, extending to around 50 ka ago (Barker *et al*., 2007; Higham *et al*., 2009; Reynolds *et al*., 2013). Whether this activity is the result of modern human behaviour or that of some other hominin species is not yet certain, but the behavioural evidence is similar to that found in the sediments dated to less than 45 ka (Barker *et al*., 2007, 2013; Barton *et al*., 2013).

Also situated near the edge of the Sunda shelf is the site of Wajak in East Java. Modern human remains from this site have been dated by 'open system' uranium-series methods to at least 36.5 ± 3.2 ka for a femoral shaft and at least ~40 ka for two cranial fragments (Storm *et al*., 2013). On the eastern side of Wallacea, Sahul's earliest known human remains are those discovered at Lake Mungo in southeastern Australia, where the burial sediments have been dated using optically stimulated luminescence (OSL) methods to ~40 ka (Bowler *et al*., 2003). On both sides of Wallacea, therefore, there is fossil evidence for modern human remains dating to at least 40 ka ago, and artefacts to ~50 ka ago or earlier.

The apparent survival of *H. floresiensis* at Liang Bua until 18 ka cal. BP or later thus required a more cautious approach be taken to interpreting the archaeological evidence in Island Southeast Asia, in particular, and Southeast Asia and Australasia more broadly. In the absence of directly associated hominin skeletal remains, assemblages of stone artefacts and other evidence of hominin behaviour require careful consideration as to whether they are the handiwork of modern humans or another hominin species (Trinkaus, 2005; Barker *et al*., 2007; O'Connor, 2007).

The need for caution has been reinforced by further enigmatic discoveries, such as the genetic sequence of the Denisovan hominin lineage (Krause *et al*., 2010; Reich *et al*., 2010), the 67 ka hominin metatarsal from Callao Cave in the Philippines (Mijares *et al*., 2010) and the recovery of stone artefacts older than ~120 ka at Talepu in Sulawesi (van den Bergh *et al*., 2016). The late survival of premodern hominins at Liang Bua therefore represents a chronological conundrum that is challenging to reconcile with our current, sketchy knowledge of early modern humans in Island Southeast Asia and Australasia prior to ~40 ka ago (O'Connor *et al*., 2010).

1.3 The research aims and structure of the thesis

Archaeology is concerned with the study of physical evidence to reconstruct evolutionary changes, past behavioural systems and cultural change over space and time, and to understand how these have varied in response to environmental changes. A fundamental principle is that the evidence documents a patterned relationship between the units of study (e.g., artefacts, bones and stratigraphy) and their past behavioural context, which requires the systematic collection of archaeological evidence in context and the methodological application of a range of appropriate analytical tools to elucidate the archaeological and environmental records.

In accordance with this approach, the overarching aim of this thesis is to contextually collect, describe and analyse information obtained from the recent excavations conducted at Liang Bua between 2007 and 2014, and to integrate these findings with those obtained from the 2001–2004 excavations to shed new light on the stratigraphy and chronology of the deposits and the hominin skeletal and cultural remains (and other faunal remains) preserved within them. In doing so, my specific aims are as follows:

1. To test the validity of previous stratigraphic, chronological and archaeological claims for this important site, the type locality of *H. floresiensis*;
2. To increase our knowledge of when *H. floresiensis* and modern humans used the cave and the nature of their activities; and
3. To study the preserved faunal and cultural remains to inform on the past ecological and environmental conditions experienced by these two species.

It is relatively rare for a single archaeological site in Island Southeast Asia, or elsewhere, to preserve human skeletal remains in direct association with behavioural and other faunal evidence – let alone a site that contains two species of hominin, one of

which continues to generate considerable interest and controversy. So when Professor Soejono asked me to coordinate new excavations of interdisciplinary research at Liang Bua in 2001 with Professor Michael J. Morwood and a team of other Indonesian and foreign scientists, I never expected what we would subsequently discover or the impact that these discoveries would have on interpretations of early hominin dispersals and the colonisation of Island Southeast Asia and Australasia by modern humans. In archaeology and palaeoanthropology, discoveries are meaningless without accurate, accompanying data on their temporal and spatial context. As the person responsible for overseeing the day-to-day excavations at Liang Bua since 2001, the context of these discoveries has been my principal responsibility and the focus of my research, including the work presented in this thesis. An historical account of the excavations carried out at Liang Bua between 2001 and the start of my PhD research program is presented in Appendix A, and is intended as a brief background to the new excavations described in detail in the following three chapters.

This thesis consists of four chapters in addition to the present chapter, including three (Chapters 2, 3 and 4) that (will) form the basis of journal articles; summary details on these chapters are provided below. The concluding chapter (Chapter 5) provides a synthesis of the research described in the thesis and a discussion of the implications for Island Southeast Asian archaeology and palaeoanthropology more broadly. The final chapter concludes with recommendations for future research in the region, arising from this study.

Chapter 2: presents the new stratigraphic interpretation and chronology of the sedimentary sequence of Liang Bua, which places the last appearance date of *H. floresiensis* in Liang Bua at between ~60 and 50 ka ago. This new interpretation also reduces considerably the extent of possible temporal overlap of *H. floresiensis* and

modern humans, who probably first voyaged through Island Southeast Asia at around the same time that *H. floresiensis* disappeared. The results presented in this chapter have been accepted for publication in the journal *Nature*, and this paper is referred to throughout the thesis as Sutikna *et al.* (2016): Revised stratigraphy and chronology for *Homo floresiensis* at Liang Bua in Indonesia.

Chapter 3: reports the results of ^{14}C dating of 48 new charcoal samples that have been recovered during excavations at Liang Bua, as well as the recalibration and analysis of all previously published ^{14}C ages for the site. This chapter provides details of the depositional sequence from ~46 ka cal. BP to the present across multiple Sectors. The results contained in this chapter are being prepared for submission to the *Journal of Archaeological Science*: Sutikna, T., Tocheri, M.W., Jatmiko, Saptomo, E.W., Due Awe, R., Roberts, R.G., Radiocarbon dating of charcoal from Liang Bua (Flores, Indonesia) reveals significant new insights into the depositional history of the cave over the last 50,000 years.

Chapter 4: explores the spatio-temporal distribution of the faunal and cultural remains at Liang Bua. The results are used to infer palaeoecological and palaeoenvironmental changes related to hominin behaviour at Liang Bua during the late Quaternary. This chapter provides additional detail on the composition of the archaeological finds from multiple excavated areas in the cave, and is being prepared for submission to the *Journal of Human Evolution*: Sutikna, T., Tocheri, M.W., Faith, J.T., Jatmiko, Due Awe, R., Meijer, H.J.M., Saptomo, E.W., Jungers, W.L., Roberts, R.G., The spatio-temporal distribution of archaeological finds at Liang Bua suggests modern humans arrived on Flores by ~46 thousand years ago.

These three major journal articles entail a substantial revision and reinterpretation of the stratigraphy and chronology of the Liang Bua depositional sequence, as well as a

significant improvement in our understanding of the context of the hominin skeletal and cultural remains recovered from this important site. My specific contributions to each of these multi-authored papers are described at the start of the relevant chapter.

CHAPTER 2

Revised stratigraphy and chronology for Liang Bua

2.1 Preface

The discovery in 2003 of the partial skeleton of a diminutive and primitive hominin species, *Homo floresiensis*, in Late Pleistocene sediments at Liang Bua (Flores, Indonesia) has generated wide interest and scientific debate. This discovery has ignited considerable scientific controversy in part because the *H. floresiensis*-bearing deposits, which included associated stone artefacts and remains of other extinct endemic fauna (pygmy *Stegodon*, marabou stork and vulture), were dated to between about 95 and 12 thousand calendar years (ka) ago. These ages implied that *H. floresiensis* survived on Flores long after modern humans (*H. sapiens*) had dispersed across Island Southeast Asia and reached Australia by ~50 ka ago.

This chapter focuses on testing the validity of previous interpretations of the stratigraphy and chronology of Liang Bua in relation to the skeletal and cultural remains of *H. floresiensis*. Based on the information obtained from new archaeological excavations conducted at the site between 2007 and 2014, the previous stratigraphic and chronological interpretations of the *H. floresiensis*-bearing deposits, and their stratigraphic relationships to other strata at the site, are reexamined. Several dating methods – radiocarbon, infrared stimulated luminescence (IRSL), thermoluminescence (TL), uranium-series ($^{234}U/^{230}Th$) and $^{40}Ar/^{39}Ar$ – are applied to major stratigraphic units at Liang Bua and to the skeletal remains of *H. floresiensis* and pygmy *Stegodon* recovered during previous excavations (2001–2004).

As co-director of ongoing research at Liang Bua, I have supervised all of the excavations since 2001 (2001–2004 with M.J. Morwood, R.P. Soejono and R.G.

Roberts; 2007–2009 with M.J. Morwood and Wahyu Saptomo; and 2010–present with M.W. Tocheri, Wahyu Saptomo and Jatmiko). All of these co-directors have contributed in various ways to the overall direction of this research. Since 2001, I have selected the areas for excavation and managed the collection of all field data. In terms of contributions to this chapter, I led the stratigraphic analyses, with major contributions from M.W. Tocheri, S. Wasisto, M.J. Morwood, K.E. Westaway, Rokus Due Awe, E. Wahyu Saptomo and Jatmiko, and additional input from M.W. Morley, H.J.M. Meijer, G.D. van den Bergh, B.V. Alloway, A. Brumm and R.G. Roberts. Dating analyses were conducted by B. Li and R.G. Roberts (IRSL), K.E. Westaway (TL), M. Aubert, R. Grün and A. Dosseto ($^{234}U/^{230}Th$, bones), J.-x. Zhao ($^{234}U/^{230}Th$, speleothems), and M. Storey ($^{40}Ar/^{39}Ar$). B.V. Alloway analysed the volcanic tephra, Rokus Due Awe, H.J.M. Meijer, G.D. van den Bergh, M.W. Tocheri and W.L. Jungers analysed the faunal remains, and Jatmiko analysed the stone artefacts. Radiocarbon ages for charcoal samples used in this study were analysed at DirectAMS Radiocarbon Dating Service in Bothell, Washington, USA and Oxford Radiocarbon Accelerator Unit, Oxford, UK.

I integrated the results of all of the analyses and wrote the chapter with guidance and input from R.G. Roberts and M.W. Tocheri, as well as additional input from all other co-authors.

Since submitting this thesis for examination, this chapter has been published in *Nature* as Sutikna *et al.* (2016), Revised stratigraphy and chronology for *Homo floresiensis* at Liang Bua in Indonesia. The format of the references in this chapter has been changed from the numbering system used by *Nature* to the same citation style used elsewhere in this thesis. But ‘kyr’ (as used by *Nature*) has been retained instead of the synonymous ‘ka’, which is used elsewhere in this thesis, because ‘kyr’ is embedded in several of the figures and tables in this chapter.

2.2 Revised stratigraphy and chronology for *Homo floresiensis* at Liang Bua in Indonesia

Thomas Sutikna[1,2]*, Matthew W. Tocheri[3,4]*, Michael J. Morwood[1]‡, E. Wahyu Saptomo[1,2], Jatmiko[1,2], Rokus Due Awe[1,2]‡, Sri Wasisto[2], Kira E. Westaway[5], Maxime Aubert[6,7], Bo Li[1], Jian-xin Zhao[8], Michael Storey[9], Brent V. Alloway[1,10], Mike W. Morley[1], Hanneke J. M. Meijer[4,11], Gerrit D. van den Bergh[1], Rainer Grün[12,13], Anthony Dosseto[14], Adam Brumm[7,12], William L. Jungers[15,16] & Richard G. Roberts[1]

[1] Centre for Archaeological Science, School of Earth and Environmental Sciences, University of Wollongong, Wollongong, New South Wales 2522, Australia.
[2] Pusat Penelitian Arkeologi Nasional, Jakarta 12510, Indonesia.
[3] Department of Anthropology, Lakehead University, Thunder Bay, Ontario P7B 5E1, Canada.
[4] Human Origins Program, Department of Anthropology, National Museum of Natural History, Smithsonian Institution, Washington DC 20013, USA.
[5] Traps MQ Luminescence Dating Facility, Department of Environmental Sciences, Macquarie University, Sydney, New South Wales 2109, Australia.
[6] Research Centre for Human Evolution, Place, Evolution and Rock Art Heritage Unit, Griffith University, Gold Coast, Queensland 4222, Australia.
[7] School of Earth and Environmental Sciences, University of Wollongong, Wollongong, New South Wales 2522, Australia.
[8] School of Earth Sciences, University of Queensland, Brisbane, Queensland 4072, Australia.
[9] QUADLAB, Section of Earth and Planetary System Science, Natural History Museum of Denmark, 1350 Copenhagen, Denmark.
[10] School of Geography, Environment and Earth Sciences, Victoria University of Wellington, Wellington 6012, New Zealand.
[11] Department of Natural History, University Museum of Bergen, University of Bergen, 5007 Bergen, Norway.
[12] Research Centre for Human Evolution, Environmental Futures Research Institute, Griffith University, Brisbane, Queensland 4111, Australia.
[13] Research School of Earth Sciences, Australian National University, Canberra, Australian Capital Territory 0200, Australia.
[14] GeoQuEST Research Centre, School of Earth and Environmental Sciences, University of Wollongong, Wollongong, New South Wales 2522, Australia.
[15] Department of Anatomical Sciences, Stony Brook University Medical Center, Stony Brook, New York 11794, USA.
[16] Association Vahatra, BP 3972, Antananarivo 101, Madagascar
* These authors contributed equally to this work.
‡ Deceased.

Correspondence and requests for materials should be addressed to T.S. (thomasutikna@gmail.com), M.W.T. (tocherim@gmail.com), and R.G.R. (rgrob@uow.edu.au).

Homo floresiensis, a primitive hominin species discovered in Late Pleistocene sediments at Liang Bua (Flores, Indonesia) (Brown _et al._, 2004; Morwood _et al._, 2004, 2005), has generated wide interest and scientific debate. A major reason this taxon is controversial is because the _H. floresiensis_-bearing deposits, which include associated stone artefacts (Morwood _et al._, 2004, 2005; Moore _et al._, 2009) and remains of other extinct endemic fauna (van den Bergh _et al._, 2009; Meijer _et al._, 2013), were dated to between about 95 and 12 thousand calendar years (kyr) ago (Morwood _et al._, 2004, 2005; Roberts _et al._, 2009). These ages suggested that _H. floresiensis_ survived until long after modern humans reached Australia by ~50 kyr ago (Roberts _et al._, 1990; Bowler _et al._, 2003; Clarkson _et al._, 2015). Here we report new stratigraphic and chronological evidence from Liang Bua that does not support the ages inferred previously for the _H. floresiensis_ holotype (LB1), ~18 thousand calibrated radiocarbon years before present (kyr cal. BP), or the time of last appearance of this species (about 17 or 13–11 kyr cal. BP) (Brown _et al._, 2004; Morwood _et al._, 2004, 2005, 2009; Roberts _et al._, 2009). Instead, the skeletal remains of _H. floresiensis_ and the deposits containing them are dated to between about 100 and 60 kyr ago, while stone artefacts attributable to this species range from about 190 to 50 kyr in age. Whether _H. floresiensis_ survived after 50 kyr ago – potentially encountering modern humans on Flores or other hominins dispersing through Southeast Asia, such as Denisovans (Reich _et al._, 2010, 2011) – is an open question.

The 2001–2004 excavations at Liang Bua (Fig. 2.1) revealed the skeletal remains of *H. floresiensis* (Brown *et al*., 2004; Morwood *et al*., 2004, 2005; Falk *et al*., 2005; Larson *et al*., 2007; Tocheri *et al*., 2007; Jungers *et al*., 2009; Morwood and Jungers,

2009; Kaifu *et al*., 2011; Orr *et al*., 2013) at 4–7 m depth in multiple excavated areas (referred to here as Sectors). Charcoal samples collected from similar depths near the eastern wall of the cave (Sector VII) were dated to between about 19 and 13–11 kyr cal. BP (Morwood *et al*., 2004, 2005; Roberts *et al*., 2009), whereas an age of ~74 kyr was obtained by coupled electron-spin resonance/uranium-series dating of a *Stegodon florensis insularis* molar recovered from ~4.5 m depth from near the cave centre (Sector IV) (Morwood *et al*., 2004, 2005; Roberts *et al*., 2009). This molar was found ~30 cm below a *H. floresiensis* premolar and ulna (LB2) and ~20 cm and ~130 cm above other postcranial remains (LB10 and LB3, respectively) (Morwood and Jungers, 2009).

The 2007–2014 excavations between and slightly south of these Sectors (Fig. 2.1c) have revealed new stratigraphic details that are crucial for (re)interpreting the ages inferred originally for *H. floresiensis* (Extended Data fig. 2.1 and Supplementary information video 2.1). The *H. floresiensis*-bearing deposits consist of multiple layers of fine-grained sediment interstratified by layers of weathered limestone, speleothem and loose gravel (Extended Data fig. 2.2). These deposits are conformably overlain by a ~2 m-thick sequence of five tephras (referred to here as T1–T5; Extended Data fig. 2.3 and Supplementary information section 2.1), separated by clastic sediments and flowstones (Fig. 2.2). This stratigraphic sequence forms a large pedestal that extends ~12 m laterally from the eastern wall to the cave centre, and is at least 6 m long from north to south. The pedestal is thickest (~4 m) in the middle rear of the cave, where it extends to within ~2 m of the present surface of the cave floor.

The pedestal deposits have been truncated by one or more phases of erosion, resulting in an erosional surface (i.e., an unconformity) that slopes steeply down towards the cave mouth (Fig. 2.3 and Extended Data figs 2.4 and 2.5). The specific timing and nature of the erosional events responsible for this unconformity remain

unknown, but presumably include slopewash and other hydrogeological mechanisms, given the active karst setting of the cave. This unconformity was not recognised during the 2001–2004 excavations, raising serious questions about the accuracy of previous age estimates (Morwood *et al*., 2004, 2005; Roberts *et al*., 2009) for *H. floresiensis*, which were based on inferred stratigraphic associations. To address these questions, we have applied several dating methods to the main stratigraphic units within this pedestal and to the skeletal remains of *H. floresiensis* and other fauna derived from this depositional sequence (see Supplementary information sections 2.2–2.6 for details of each dating method).

Sediment samples for infrared stimulated luminescence (IRSL) and thermoluminescence (TL) dating (Westaway and Roberts, 2006; Li *et al*., 2014) (Extended Data figs 2.6 and 2.7) were collected from the *H. floresiensis*-bearing deposits directly underlying T1 in the south baulks of Sectors XXI and XXIII, more than 2 m south of the erosional unconformity. These samples gave statistically indistinguishable weighted mean IRSL and TL ages (± 1σ) of 65 ± 5 kyr (LB12-OSL3 to -OSL6) and 71 ± 13 kyr (LB12-23-2 and -4), respectively, for the time since sand-sized grains of feldspar and quartz were last exposed to sunlight. A TL age of 89 ± 7 kyr (LB08-15-3) was obtained for the basal *H. floresiensis*-bearing deposits in Sector XV, while two further samples from the immediately underlying, gravel-rich layer (in Sectors XXI and XXIII) gave IRSL and TL ages of 128 ± 17 kyr (LB12-OSL7) and 113 ± 9 kyr (LB12-23-1), respectively. We also used $^{234}U/^{230}Th$ methods to date four samples of *in situ* speleothem from the *H. floresiensis*-bearing deposits in Sectors XII and XVII (LB07-SXII-F4 and LB09-SXVII-F1 to -F3), which gave ages (± 2σ) of between 80.8 ± 0.8 and 58.3 ± 0.5 kyr.

Three *H. floresiensis* ulnae and eight *Stegodon* bones were sampled for $^{234}U/^{230}Th$ dating, as well as a modern human femoral shaft fragment from the Holocene deposits in Sector IV (Extended Data figs 2.8 and 2.9). Owing to the open system behaviour of bone, such analyses usually yield minimum ages for bone deposition and subsequent uranium uptake (Grün *et al*., 2014). The modelled age (Sambridge *et al*., 2012) of ~7.5 kyr for the modern human bone (132A/LB/IV/27D/03) is consistent with charcoal ^{14}C ages for the underlying and overlying sediments (about 9.5 and 6.4 kyr cal. BP, respectively; Roberts *et al*., 2009). The *H. floresiensis* ulnae have modelled $^{234}U/^{230}Th$ ages (± 2σ) for individual laser-ablation tracks that range from 86.9 ± 7.9 to 71.5 ± 4.3 kyr for LB1 (Sectors VII and XI), 71.4 ± 1.1 to 66.7 ± 0.8 kyr for LB2 (Sector IV), and 66.0 ± 4.3 to 54.6 ± 2.1 kyr for LB6 (Sector XI). The *Stegodon* bone samples (all from Sector XI) span a modelled age range of 80.6 ± 11.3 to 40.5 ± 2.0 kyr, with the youngest minimum age deriving from a bone (U-s-05/LB/XI/51/04) recovered from the same sediments and depth as LB6. Delayed diffusion of uranium into the dense bone matrix of *Stegodon* may account for the youngest minimum ages appearing more recent than those obtained for the bones of *H. floresiensis*, the speleothems and the sediments.

We dated T1, which directly overlies the *H. floresiensis*-bearing deposits, using $^{40}Ar/^{39}Ar$ methods (Storey *et al*., 2012; Rivera *et al*., 2013). The inverse isochron age (± 1σ) of 79 ± 12 kyr (Extended Data fig. 2.3) is imprecise due to the low yield of radiogenic argon from the hornblende crystals, but the 2σ age range (103–55 kyr) is consistent with the luminescence and $^{234}U/^{230}Th$ ages for the underlying samples. Immediately overlying T1 is a series of interstratified sedimentary units, including T2 and several flowstones. These are in turn overlain by T3, a ~0.75 m-thick volcaniclastic mass flow deposit, formerly referred to as the 'black tuff' or similar (Morwood and Jungers, 2009; Westaway *et al*., 2009b).

Sediments between T2 and T3 in Sector XXI yielded a weighted mean IRSL age of 66 ± 9 kyr (LB12-OSL1 and -OSL2) and a TL age of 59 ± 13 kyr (LB12-23-3). Interbedded flowstones and a small stalagmite in the same Sector gave $^{234}U/^{230}Th$ ages of between 66.1 ± 0.3 and 54.4 ± 0.3 kyr (LB-S.XXI 5 #08, LB-S.XXI 8-T #09 and 8-B #10, and LB/S.XXI 10-01 and -01R), while in Sector XII – nearer the cave centre – a flowstone immediately underlying T3 (LB07-SXII-F1) was dated to 49.6 ± 0.5 kyr. Hominin skeletal remains have not been recovered from the deposits between T2 and T3. However, stone artefacts are present and these display similar raw material proportions to those found underneath T1 (~80% silicified tuff and ~20% chert), in contrast to the preference of modern humans for chert (~60%) observed at Liang Bua during the Holocene (Moore *et al*., 2009). Also present in these sediments and those underlying T1 are the remains of other extinct large-bodied taxa, including *Stegodon*, giant marabou stork and vulture (van den Bergh *et al*., 2009; Meijer *et al*., 2013). The specific processes that ultimately resulted in the extinction of these taxa and *H. floresiensis* remain poorly understood.

Overlying T3 is T4, which is covered by loose, coarse gravel in two of the southernmost Sectors excavated (XII and XXVII). Three flowstone samples (Westaway *et al*., 2007b; Roberts *et al*., 2009) with a weighted mean $^{234}U/^{230}Th$ age of 46.6 ± 0.5 kyr directly overlie the southern parts of this coarse gravel layer. From the eastern wall to the cave centre, T4 is overlain by two flowstone layers that are separated from each other by T5. At 1.89 m depth in Sector XXIII, charcoal (sample OxA-X-2648-13) from immediately above the upper surface of T5 yielded a ^{14}C age of ~46 kyr cal. BP (95% confidence interval of 47.7–44.1 kyr cal. BP).

In contrast, all of the charcoal samples used previously to infer ages of ~18 kyr cal. BP for LB1 and about 17 or 13–11 kyr cal. BP as the *terminus ante quem* for *H.*

floresiensis and *Stegodon* (Morwood *et al*., 2004, 2005; Roberts *et al*., 2009; van den Bergh *et al*., 2009) originate from deposits that unconformably overlie the remnant pedestal, based on their plotted coordinates (Fig. 2.3). These younger sediments are interstratified by three additional tephras (T6–T8; Extended Data fig. 2.10). Tephra T6 is observed at ~5.8 m depth in the northern parts of Sectors VII and XVI, followed by T7 and T8 (formerly referred to as the 'white' tuffaceous silts; Morwood *et al*., 2004, 2005; Morwood and Jungers, 2009; Westaway *et al*., 2009b) at about 3.5–5 m depth (Sectors III, IV, VII, XI, XV, XVI and XXII). The onset of accumulation of the depositional sequence above the unconformity ~20 kyr ago is consistent with a TL age of 23 ± 7 kyr for sediments collected less than 15 cm above the unconformity in Sector XVI (LB09-16-2) and two new ^{14}C ages of ~12.7 kyr cal. BP for charcoal recovered from just beneath T7 in Sector XXII (D-AMS 005953 and 005954).

Portions of the pedestal have been reworked into this younger depositional sequence. In Sector XXII, a displaced slab of intact pedestal deposit rests above the unconformity but underlies T7 (Extended Data fig. 2.10c, d). In other Sectors, eroded fragments of T1, T2 and T3 are consistently observed in the younger, overlying deposits (Morwood *et al*., 2004, 2005; Morwood and Jungers, 2009). We investigated the possibility that the luminescence ages for the sediment samples collected in 2003 from alongside LB1 and ~1 m above it (Morwood *et al*., 2004) were compromised by inadvertently sampling across the unconformity and measuring multiple grains simultaneously from this mixture. The wide spread in ages (from about 170 to 10 kyr ago) obtained for individual feldspar grains using newly developed IRSL dating procedures (Li *et al*., 2014) supports this suggestion (Extended Data fig. 2.7k, l).

The new stratigraphic and chronological evidence for Liang Bua indicates that a pedestal of remnant deposits, dating to more than ~46 kyr cal. BP, has an erosional

upper surface that slopes steeply downwards to the north and is uncomformably overlain by sediments younger than ~20 kyr cal. BP. All skeletal remains assigned to *H. floresiensis* are from the pedestal deposits dated to approximately 100–60 kyr ago, while stone artefacts reasonably attributable to this species range from about 190 kyr (Westaway *et al*., 2007a) to 50 kyr in age. Parts of Southeast Asia may have been inhabited by Denisovans (Reich *et al*., 2010, 2011) or other hominins (Mijares *et al*., 2010; van den Bergh *et al*., 2016) during this period, and modern humans had reached Australia by 50 kyr ago (Roberts *et al*., 1990; Bowler *et al*., 2003; Clarkson *et al*., 2015). But whether *H. floresiensis* survived after this time, or encountered modern humans, Denisovans or other hominin species on Flores or elsewhere, remain open questions that future discoveries may help answer.

Acknowledgements

The 2007–2014 excavations at Liang Bua were supported by an Australian Research Council (ARC) Discovery Project grant to M.J.M. (DP0770234), a Waitt Foundation/National Geographic Society grant to M.W.T and T.S. (No. 2121-2) and a Smithsonian Scholarly Studies Program award to M.W.T. Additional funding was provided by the Peter Buck Fund for Human Origins Research, the Smithsonian's Human Origins Program, the University of Wollongong (UOW) and the ARC (DP1093049 to K.E.W.). T.S. is supported by a UOW postgraduate scholarship, M.W.T. by a Canada Research Chair, M.A. and A.B. by ARC Discovery Early Career Researcher Awards (DE140100254 and DE130101560, respectively), B.L. by an ARC Future Fellowship (FT14010038), R.G.R. by an ARC Australian Laureate Fellowship (FL130100116) and B.V.A. by a Victoria University of Wellington Science Faculty Research Grant (201255). QUADLAB is funded by the Villum Foundation. Fieldwork

was authorised by Pusat Penelitian Arkeologi Nasional (Jakarta, Indonesia) and Pemerintah Daerah Kabupaten Manggarai (Flores, Nusa Tenggara Timur). We also thank I Made Geria, Valentinus N. Sene, Rick Potts, Paul Goldberg, Katerina Douka, Grace Veatch, Vince Rossi, Adam Metallo, Les Kinsley, Yasaman Jafari, Terry Lachlan, Ai Duc Nguyen, Dida Yurnaldi, Ruly Setiawan, I Dewa Kompiang and the entire Liang Bua Team from Teras, Golo Manuk and Bere.

Author contributions

M.J.M., R.P. Soejono and R.G.R. conceived and coordinated the original research program at Liang Bua (2001–2004). The new excavations were planned and directed by T.S., E.W.S and M.J.M. (2007–2009), and by T.S., M.W.T., E.W.S, J. and M.J.M. (2010–2014). T.S. led the stratigraphic analyses, with major contributions from M.W.T., S.W., M.J.M., K.E.W., R.D.A., E.W.S. and J., and additional input from M.W.M., H.J.M.M., G.D.vdB., B.V.A., A.B., W.L.J. and R.G.R. Dating analyses were conducted by B.L. and R.G.R. (IRSL), K.E.W. (TL), M.A., R.G. and A.D. ($^{234}U/^{230}Th$, bones), J.-x.Z. ($^{234}U/^{230}Th$, speleothems), and M.S. ($^{40}Ar/^{39}Ar$). B.V.A. analyzed the volcanic tephra, R.D.A., H.J.M.M., G.D.vdB., M.W.T. and W.L.J. analyzed the faunal remains, and J. analyzed the stone artefacts. T.S., M.W.T. and R.G.R. wrote the paper, with early contributions from M.J.M and additional input from all other authors.

Author information

Correspondence and requests for materials should be addressed to T.S. (thomasutikna@gmail.com), M.W.T. (tocherim@gmail.com) and R.G.R. (rgrob@uow.edu.au).

2.3 Figures

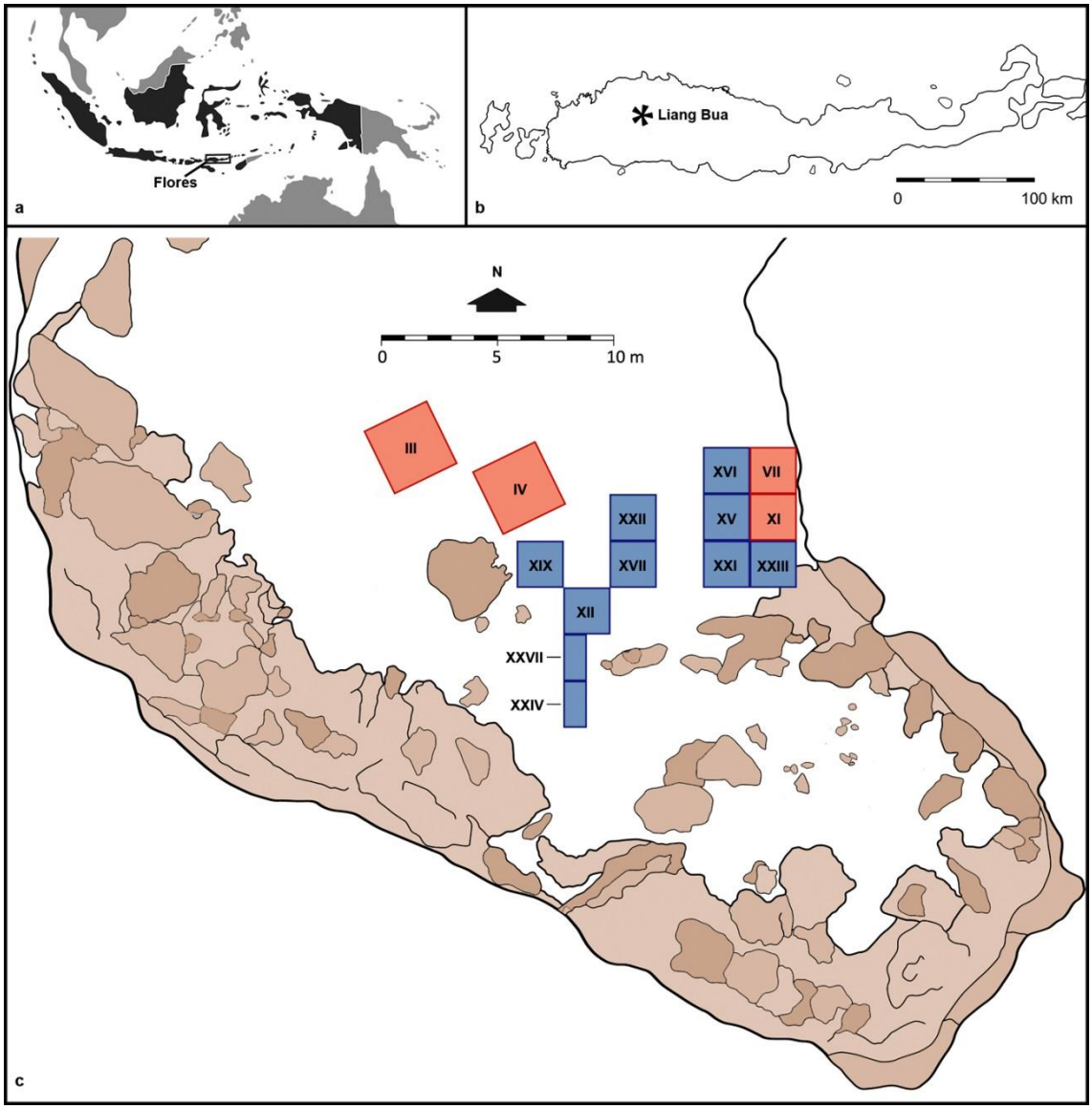

Figure 2.1 Site location. **a**, Location of Flores within Indonesia. **b**, Location of Liang Bua on Flores. **c**, Site plan of Sectors discussed in the text (the 2001–2004 and 2007–2014 excavations are shaded red and blue, respectively). The remaining cave floor sediments are shaded white, while the areas shaded brown are exposed rocks, stalagmites and other surfaces covered in speleothems.

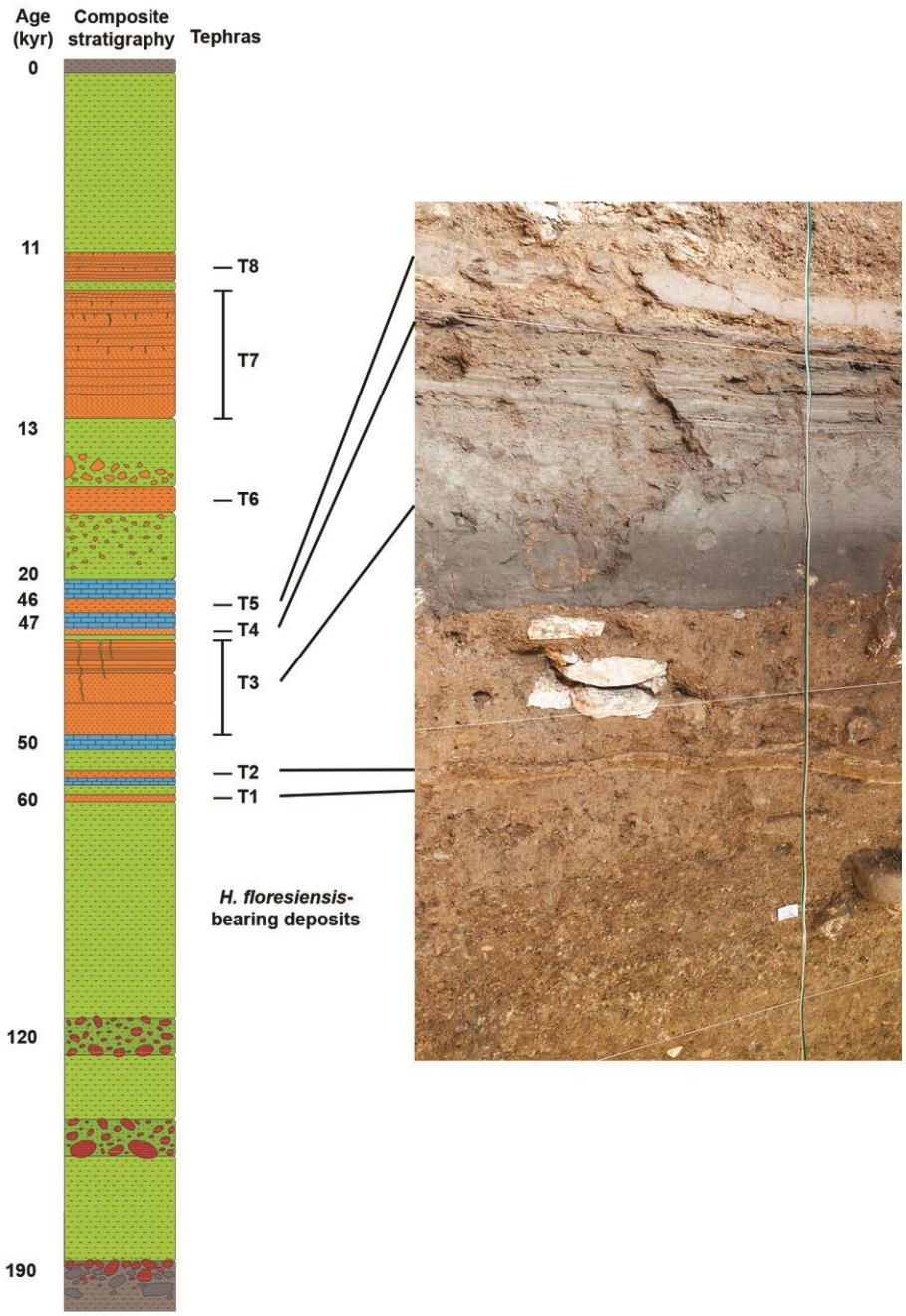

Figure 2.2 Composite stratigraphic section of deposits at Liang Bua, with approximate ages. The deposits accumulated above a fluvial conglomerate and are capped by recent sediments (both shown in grey). Skeletal remains of *Homo floresiensis* occur in deposits stratigraphically beneath a sequence of eight volcanic tephras (T1–T8), separated by calcitic speleothems (blue) and fine-grained clastic sediments (green). As the thickness, grain size and slope angle of each unit vary considerably within the cave, only the approximate relative thicknesses of the units discussed in the text are shown; the minimum depth of this composite section would exceed 15 m. See Fig. 2.3 and Extended Data fig. 2.5a for three-dimensional representations of the stratigraphy. Also indicated are units with concentrations of rounded, gravel-size clasts of igneous rock (red) or irregularly shaped, eroded fragments of T1, T2 and T3 (orange), and units with signs of bioturbation (upper parts of T3 and T7). The photograph shows T1–T5 and interstratified sediments that conformably overlie the *H. floresiensis*-bearing deposits (south baulk of Sector XXI).

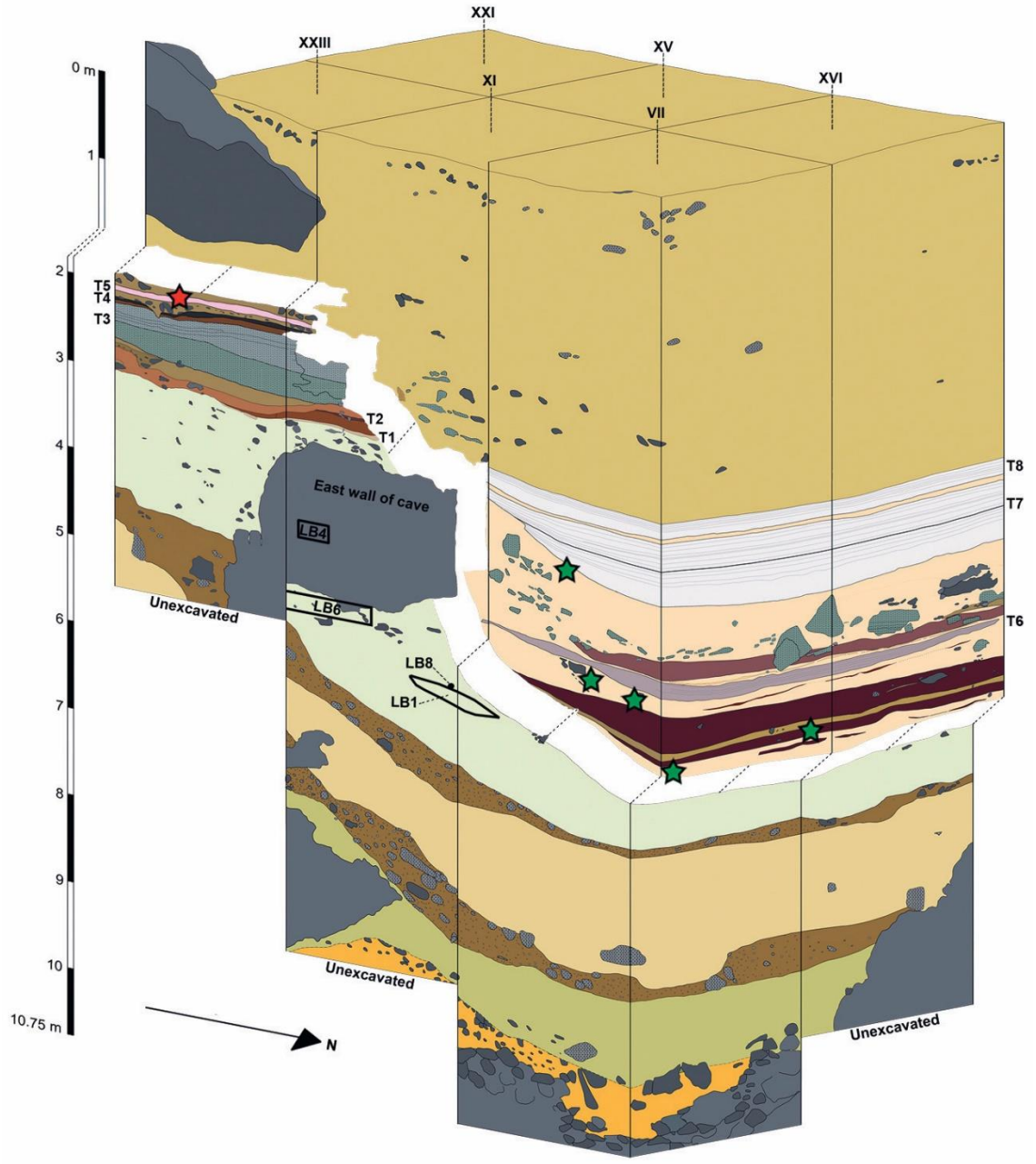

Figure 2.3 Stratigraphy of excavated Sectors near the eastern wall of the cave. Multiple specimens of *Homo floresiensis* (LB1, LB4, LB6 and LB8) were recovered previously (Brown *et al*., 2004; Morwood *et al*., 2004, 2005; Falk *et al*., 2005; Larson *et al*., 2007; Tocheri *et al*., 2007; Jungers *et al*., 2009; Morwood and Jungers, 2009; Kaifu *et al*., 2011; Orr *et al*., 2013) from sediments now recognised to directly underlie a sequence of five tephras (T1–T5) and interstratified deposits. Together, these remnant deposits form a pedestal, the top of which is dated to ~46 kyr cal. BP (charcoal sample denoted by the red star at ~2 m depth in Sector XXIII). The overlying section – separated here by a white band and dotted lines for emphasis – represents deposits (including three additional tephras, T6–T8) that rest uncomformably on the steeply sloping erosional surface of the pedestal. The green stars in Sector VII mark the respective locations (from top to bottom) of the charcoal samples dated to approximately 13.0, 18.5, 18.1, 19.0 and 19.2 kyr cal. BP, which were used erroneously (Morwood *et al*., 2004, 2005; Roberts *et al*., 2009) to infer the latest occurrences of *H. floresiensis*.

2.4 Methods

2.4.1 Archaeological excavation

The 2007–2014 excavations at Liang Bua, including eight 2 x 2 m and two 1 x 2 m areas (referred to as Sectors), proceeded in 10 cm intervals (referred to as spits) while following stratigraphic units. Timber shoring of the baulks was installed after ~2.5 m depth for safety. *In situ* findings (for example, bones, artefacts and charcoal) were plotted in three dimensions and the sediments from each spit were sieved by hand, followed by wet sieving (2 mm mesh). All recovered findings were cleaned, catalogued and transported to Pusat Penelitian Arkeologi Nasional (Jakarta, Indonesia) for curation and further study.

2.4.2 Electron microprobe analysis of volcanic glass

Bulk samples of four tephras were wet sieved at >32 μm and then dry sieved into 32–63 μm, 63–125 μm, 125–250 μm, 250–500 μm and 500 μm–1 mm fractions. Depending on the grain-size distribution of the sample, the dominant dry fraction containing the most glass material was mounted into an epoxy resin. Glass from bubble-wall shards or vesiculated pumice fragments was analysed as individual grains (>63 μm) using an electron microprobe. Major element determinations were made using a JEOL Superprobe (JXA-8230) housed at Victoria University of Wellington, New Zealand, using the ZAF correction method (Heinrich, 1991). Analyses were performed with 15 kV accelerating voltage, 8 nA beam current, and an electron beam defocused to 10–20 μm. Standardisation was achieved by means of mineral and glass standards. Rhyolitic glass standard ATHO-G (Jochum *et al*., 2006) was routinely used to monitor calibration in all analytical runs and to evaluate any day-to-day differences in calibration. All analyses were normalised to 100% (by weight) anhydrous and total iron was calculated

as FeO (Supplementary information section 2.1). The major element compositions of the four tephras and the Youngest Toba Tuff (Alloway *et al*., 2004) are displayed as bivariate plots in Extended Data fig. 2.3c-e.

2.4.3 Infrared stimulated luminescence (IRSL) dating of feldspar grains

Sediment samples were collected using opaque plastic tubes hammered horizontally into cleaned stratigraphic sections and wrapped in black plastic after removal. Field measurements of the gamma dose rate at each sample location were made using a portable gamma-ray detector (Exploranium GR-320) inserted into the emptied tube holes. Sediment samples were also collected from the tube holes for laboratory determinations of water content and beta dose rate at the University of Wollongong. The environmental dose rate of each sample was calculated as the sum of the beta dose rate (estimated from beta-counting of dried and powdered sediment samples using a Risø low-level beta multicounter system and allowing for beta-dose attenuation and other factors; Jacobs and Roberts, 2015), the *in situ* gamma dose rate, and the estimated cosmic-ray dose rate (Prescott and Hutton, 1994). The latter took account of the burial depth of each sample, the thickness of cave roof overhead, the zenith-angle dependence of cosmic rays, and the latitude, longitude and altitude of Liang Bua. Each of these external dose rate contributors were adjusted for long-term water content. The measured (field) water contents of the seven samples collected in 2012 range from 26 to 35%, but higher and lower field water contents have been reported for other sediment samples collected at Liang Bua: 15–30% (Morwood *et al*., 2004), 3–22% (Roberts *et al*., 2009) and 24–39% (Supplementary information section 2.2). We used a value of 20 ± 5% as a mid-range estimate of the long-term water content, with the standard error sufficient to cover (at 2σ) most of the field measurements. The total dose rate of each sample also

includes an estimate of the internal beta dose rate due to the radioactive decay of ^{40}K and ^{87}Rb. This estimate was based on a K concentration of 12 ± 1%, determined from energy- and wavelength-dispersive X-ray spectroscopic measurements of individual feldspar grains (Neudorf, 2012; Neudorf *et al*., 2012) (see Supplementary information section 2.2), and an assumed Rb concentration of 400 ± 100 μg g^{-1} (Huntley and Hancock, 2001). Potassium-rich feldspar (K-feldspar) grains of 90–212 or 180–212 μm diameter were extracted from the sediment samples under dim red illumination and prepared using standard procedures (Aitken, 1998), including the use of a sodium polytungstate solution of 2.58 g cm^{-3} density to separate the feldspar grains from heavier minerals. The separated grains were also washed in 10% hydrofluoric acid for 40 min to clean their surfaces and reduce the thickness of the alpha-irradiated outer layer by ~15 μm, which was taken into account in the dose rate calculation. For each sample, single aliquots composed of a few hundred grains were measured using an automated Risø TL/OSL reader equipped with infrared (875 nm) light-emitted diodes (LEDs) for stimulation (Bøtter-Jensen *et al*., 2003) and a calibrated ^{90}Sr/^{90}Y source for beta irradiations. We also made measurements of individual K-feldspar grains (180–212 μm diameter) from two samples collected in 2012 (LB12-OSL3 and -OSL4) and the two original sediment samples (LBS7-40a and LBS7-42a) collected from above and alongside the remains of LB1 (Morwood *et al*., 2004). Infrared stimulation of individual K-feldspar grains was achieved using a focussed laser beam (830 nm; Bøtter-Jensen *et al*., 2003). The IRSL emissions from the single aliquots and single grains were detected using an Electron Tubes Ltd 9235B photomultiplier tube fitted with Schott BG-39 and Corning 7-59 filters to transmit wavelengths of 320–480 nm. To estimate the equivalent dose (D_e) for each aliquot or grain (Aitken, 1998; Roberts *et al*., 2015), we initially used the multiple elevated temperature post-infrared IRSL (MET-pIRIR) regenerative-dose

procedure (Li and Li, 2011; Li *et al*., 2014; van den Bergh *et al*., 2016), in which the IRSL signals are measured by progressively increasing the stimulation temperature from 50 °C to 250 °C in 50 °C increments. The samples yielded very dim signals, however, so we used a two-step pIRIR procedure (Thiel *et al*., 2011; Li *et al*., 2014) to improve the signal-to-noise ratio. Grains were preheated at 320 °C for 60 s prior to infrared stimulation of the natural, regenerative and test doses at 50 °C for 200 s. The pIRIR signal was then measured at 290 °C for either 200 s (single aliquots) or 1 s (single grains), followed by an infrared bleach at 325 °C for 100 s at the end of each regenerative-dose cycle. Example pIRIR decay and dose-response curves are shown in Extended Data fig. 2.7a–c. Performance tests of the regenerative-dose procedure and details of residual dose measurements (Li *et al*., 2013, 2014) and anomalous fading tests (Huntley and Lamothe, 2001; Auclair *et al*., 2003) are described in Supplementary information section 2.2. We estimated the pIRIR age of each sample from the weighted mean D_e (calculated using the central age model: Galbraith *et al*., 1999; Galbraith and Roberts, 2012) divided by the environmental dose rate, and applied corrections for residual dose and anomalous fading. For the latter corrections, we used the weighted mean fading rate (0.9 ± 0.3% per decade) measured for five of the seven samples collected in 2012.

2.4.4 Thermoluminescence (TL) dating of quartz grains

Sediment samples were taken in the same manner as the IRSL samples, as were the *in situ* gamma dose rate measurements (made using an ORTEC digi-DART gamma-ray detector). Additional sediment samples were also collected for determinations of water content and beta dose rate at Macquarie University. The environmental dose rate of each sample consists of three external components, each adjusted for long-term water content

(20 ± 5%): the beta dose rate (estimated from beta-counting and allowing for beta-dose attenuation), the *in situ* gamma dose rate, and the estimated cosmic-ray dose rate. An assumed internal dose rate of 0.03 ± 0.01 Gy kyr^{-1} was also included in the total dose rate. Quartz grains were separated from the sediment samples under dim red illumination and prepared using standard procedures (Aitken, 1998), including mineral separations using 2.70 and 2.62 g cm^{-3} density solutions of sodium polytungstate to isolate the quartz and a 40% hydrofluoric acid etch for 45 min to remove the alpha-irradiated outer ~20 μm of each grain. Aliquots composed of about 10,000 quartz grains were measured using a dual-aliquot regenerative-dose TL protocol (Westaway and Roberts, 2006) to isolate the light-sensitive red emissions (Franklin *et al*., 2000). This procedure was originally developed for application at Liang Bua (Morwood *et al*., 2004) and requires two aliquots of each sample: one to estimate the D_e associated with the heat-reset TL traps and the other to measure the total TL signal, from which the D_e associated with the light-sensitive TL traps is estimated by subtraction. Measurements were made on a Risø TL/OSL reader fitted with an Electron Tubes Ltd 9658B photomultiplier tube and Schott BG-39 and Kopp 2-63 filters designed to transmit red emissions (peak transmission in the 600–620 nm range, with minimum and maximum wavelengths of 580 and 670 nm), and cooled to –22° C to reduce the background count rate. Bleaching was performed using a halogen lamp and light guide integrated into the reader, and laboratory doses were given using a ^{90}Sr/^{90}Y source mounted on the reader. The quartz grains were first heated to 260 °C at a heating rate of 5 K s^{-1} and then held at this temperature for 1000 s to induce an isothermal TL signal and reduce the unwanted glow from incandescence. Following Westaway and Roberts (2006), D_e values were estimated from the 20–30 s interval of isothermal TL (which was shown to be light-sensitive) and the final 160 s was used as background. Two of the samples contained

abundant quantities of quartz, so problems associated with inter-aliquot variability (Westaway, 2009; Demeter *et al*., 2012) were reduced by measuring 12 replicates of each pair of aliquots (Supplementary information section 2.2). As prolonged sunlight exposure is required the empty the light-sensitive TL traps, the ages obtained should be regarded as maximum estimates of the time elapsed since sediment deposition (Westaway and Roberts, 2006).

2.4.5 Uranium-series ($^{234}U/^{230}Th$) dating of bones

Samples of bone from three specimens of *Homo floresiensis*, (LB1, LB2 and LB6), one *Homo sapiens* and eight *Stegodon florensis insularis* were analysed using laser ablation uranium-series isotope measurement analysis procedures and instruments similar to those described previously (Eggins *et al*., 2005; Grün *et al*., 2014). Cuts were made perpendicular to the bone surface using a rotatory tool equipped with a thin (100 μm wide) diamond saw blade. The cut samples were mounted into aluminium cups, aligning the cross-sectioned surfaces with the outer rim of the sample holder to position the samples on the focal plane of the laser in the sampling cell. Sequential laser spot analyses were undertaken along 1–5 parallel tracks per sample, starting from the interior of each cross-sectioned bone (Extended Data figs 2.8 and 2.9 and Supplementary information section 2.3). Uranium and thorium isotopes were measured at the Australian National University using a Finnigan MAT Neptune multi-collector inductively-coupled plasma mass spectrometer (MC-ICP-MS) equipped with multiple Faraday cups and ion counters. Two ion counters were set to masses of 230.1 and 234.1, while the Faraday cups measured the masses 232, 235 and 238. Samples were ablated using a Lambda Physik LPFPro ArF excimer laser (193 nm) coupled to the MC-ICP-MS through a custom-designed Helex ablation cell. The analyses were made at regular

spacing (typically 2–3 mm) along each track, using a laser spot size of 265 μm and a 5 Hz pulse rate. The samples were initially cleaned for 5 s and ablation pits were measured for 50 s. These measurements were bracketed by analyses of reference standards to correct for instrument drift. Semi-quantitative estimates of uranium and thorium concentrations were made from repeated measurements of the SRM NIST-610 glass standard (U: 461.5 μg g^{-1}, Th: 457.2 μg g^{-1}) and uranium-isotope (activity) ratios from repeated measurements of rhinoceros tooth dentine from Hexian sample 1118 (Grün *et al*., 1998). Apparent $^{234}U/^{230}Th$ ages were estimated for each track using a diffusion–adsorption–decay (DAD) model (Sambridge *et al*., 2012), which uses the entire set of isotope measurements made along the track to calculate the rate of diffusion of ^{238}U and ^{234}U into the bone. Bones behave as geochemically 'open' systems, so the diffusion of uranium into a bone may have occurred soon after it was deposited or much later. The original isotopic signature may also be overprinted by secondary uranium uptake that is hard to recognise. As such, uranium-series ages for bones are most likely to be minimum estimates of time since deposition, with the extent of age underestimation being very difficult or impossible to evaluate (Grün *et al*., 2014). The modelled ages were calculated after rejecting data points associated with detrital contamination (U/Th elemental ratios if ≤300) and data points at the surface of the bones where secondary overprinting was suspected. Results are tabulated in Supplementary information section 2.3, with all errors given at 2σ.

2.4.6 Uranium-series ($^{234}U/^{230}Th$) dating of speleothems

Samples of calcite deposited as speleothems (flowstones and a 1 cm-tall stalagmite) were collected during excavation. Unlike bone, speleothems commonly behave as geochemically 'closed' systems, with no loss or gain of uranium after calcite

crystallisation (Hellstrom and Pickering, 2015). The cleanest portion of each sample was selected, ground to the size of a rice grain, cleaned ultrasonically and then handpicked, avoiding pieces that appeared to be porous or contaminated. Age determinations were made at the University of Queensland using a Nu Plasma MC-ICP-MS. Uranium and thorium separation procedures, MC-ICP-MS analytical protocols, details of spike calibrations, blank and 'memory' assessments, and repeat measurements of standards have been described previously (Zhou *et al*., 2011; Clark *et al*., 2014). The $^{234}U/^{230}Th$ ages were calculated using Isoplot 3.75 (Ludwig, 2012) and half-lives of 245.25 kyr (^{234}U) and 75.69 kyr (^{230}Th) (Cheng *et al*., 2000). As most samples consist of impure calcite with some degree of detrital contamination, a correction for non-radiogenic ^{230}Th was applied to the measured $^{230}Th/^{232}Th$ activity ratio of each sample using an assumed bulk-Earth $^{230}Th/^{232}Th$ activity ratio of 0.825 (with a relative error of ± 50% and assuming secular equilibrium in the $^{238}U–^{234}U–^{230}Th$ decay chain), as is typical of most other studies (Zhao *et al*., 2009). This non-radiogenic ^{230}Th correction reduces the calculated ages of the samples and increases the age uncertainties by an amount dependent on the extent of detrital contamination. All ten dated samples have measured $^{230}Th/^{232}Th$ activity ratios of >20 (Supplementary information section 2.4), so the detritally-corrected $^{234}U/^{230}Th$ ages are only slightly younger than the uncorrected (measured) ages.

2.4.7 Argon-argon ($^{40}Ar/^{39}Ar$) dating of hornblende crystals

Crystals of hornblende were obtained for the 100–150 and 150–250 μm size fractions of the T1 tephra using standard heavy liquid and magnetic separation techniques. Crystals were loaded into wells in 18 mm-diameter aluminium sample discs for neutron irradiation, along with the 1.185 million year-old Alder Creek sanidine (Rivera *et al*.,

2013) as the neutron fluence monitor. Neutron irradiation was carried out for 4 min in the cadmium-shielded CLICIT facility at the Oregon State University TRIGA reactor. Argon isotopic analyses of gas released from 6 hornblende aliquots during CO_2 laser step-heating, including a final fusion step ('fuse' in Supplementary information section 2.5), were made on a fully automated, high-resolution, Nu Instruments Noblesse multi-collector noble-gas mass spectrometer, using procedures documented previously (Storey *et al.*, 2012). One set of four experiments (Lab IDs 2598 and 2599 in Supplementary information section 2.5) consisted of strong degassing of 10 mg hornblende aliquots in square pits in the laser disc, using a beam integrator lens that gives a 'top hat' 6 x 6 mm energy profile at the focal plane. The laser was then operated at 32 W and this high-temperature, pre-fusion step measured ('D' in Supplementary information section 2.5). The fusion step was performed using a conventional focus lens. In the second set of experiments, 20 mg hornblende aliquots were loaded into 5 mm-wide channels in the laser disc and a defocussed laser beam was programmed to raster in 50 traverses, each 30 mm in length and separated by 0.1 mm. Low power (< 1 W) steps were performed initially to remove loosely trapped argon. At 1 W of laser power (step 'C'), the hornblende crystals began to glow and release significant amounts of ^{39}Ar. This and subsequent steps, including the final fusion, are reported in Supplementary information section 2.5 as Lab IDs 2584-03C to -03O (fuse) and 2584-04C to -04I (fuse). Sample gas cleanup was through an all-metal extraction line, equipped with a –130 °C cold trap (to remove H_2O) and two water-cooled SAES GP-50 getter pumps (to absorb reactive gases). Argon isotopic analyses of unknowns, blanks and monitor minerals were carried out in identical fashion during a fixed period of 400 s in 14 data acquisition cycles. ^{40}Ar and ^{39}Ar were measured on the high-mass ion counter, ^{38}Ar and ^{37}Ar on the axial ion counter and ^{36}Ar on the low-mass ion counter, with baselines measured every third

cycle. Measurement of the ^{40}Ar, ^{38}Ar and ^{36}Ar ion beams was carried out simultaneously, followed by sequential measurement of ^{39}Ar and ^{37}Ar. Beam switching was achieved by varying the field of the mass spectrometer magnet and with minor adjustment of the quad lenses. Data acquisition and reduction was performed using the program 'Mass Spec' (A. Deino, Berkeley Geochronology Center). Detector intercalibration and mass fractionation corrections were made using the weighted mean of a time series of measured atmospheric argon aliquots delivered from a calibrated air pipette (Storey *et al*., 2012). The accuracy of the primary air pipette measurements was verified by cross-referencing to data produced from a newly charged second air pipette. Decay and other constants, including correction factors for interference isotopes produced by nucleogenic reactions, are as reported in Storey *et al*. (2012). An isotope correlation (inverse isochron) plot of the data for all 28 aliquots is shown in Extended Data fig. 2.3f. The age determined from the inverse isochron is 85 ± 13 kyr for all 28 aliquots, or 79 ± 12 kyr (errors at 1σ) if the data point on the far right-hand side of the plot is excluded. In both cases, the $^{40}Ar/^{36}Ar$ intercept value is statistically indistinguishable from the atmospheric ratio of 298.6 ± 0.3 (Lee *et al*., 2006), indicating the absence of significant excess ^{40}Ar in the hornblende crystals.

2.4.8 Radiocarbon (^{14}C) dating of charcoal

Three charcoal samples recovered during excavation were sent to DirectAMS Radiocarbon Dating Service in Bothell, Washington (Supplementary information section 2.6). Samples were pretreated using acid–base–acid (ABA) procedures and the ^{14}C content was measured using accelerator mass spectrometry (Wood, 2015). Conventional ^{14}C ages in radiocarbon years before present (BP) were converted to calendar-year age ranges at the 68% and 95% confidence intervals using the SHCal13

calibration data set (Hogg *et al*., 2013) and CALIB 7.1 (http://calib.qub.ac.uk/calib/). One of these three samples yielded an 'old' radiocarbon age (>40 kyr BP), so we submitted the remaining charcoal to the Oxford Radiocarbon Accelerator Unit (ORAU) for a harsher cleaning protocol known as ABOx-SC (Bird *et al*., 1999; Brock *et al*., 2010). This pretreatment is known to improve charcoal decontamination and has been shown repeatedly to produce more reliable results for 'old' charcoal. However, the harshness of the ABOx-SC procedure often results in large material loss and sample failure, so a new preparative method (AOx-SC) has been developed and tested at the ORAU (K. Douka, personal communication). The AOx-SC procedure does not include a NaOH step and produces identical results to ABOx-SC, but with much higher yields and reduced sample failure. For the Liang Bua sample, ~100 mg and ~50 mg of hand-picked charcoal underwent ABOx-SC and AOx-SC pretreatments, respectively. Only the AOx-treated charcoal survived the wet chemistry, yielding sufficient carbon for stepped combustion, first at 630 °C and then at 1000 °C, with the latter fraction collected for graphitisation and measurement by accelerator mass spectrometry.

2.5 Extended Data figures

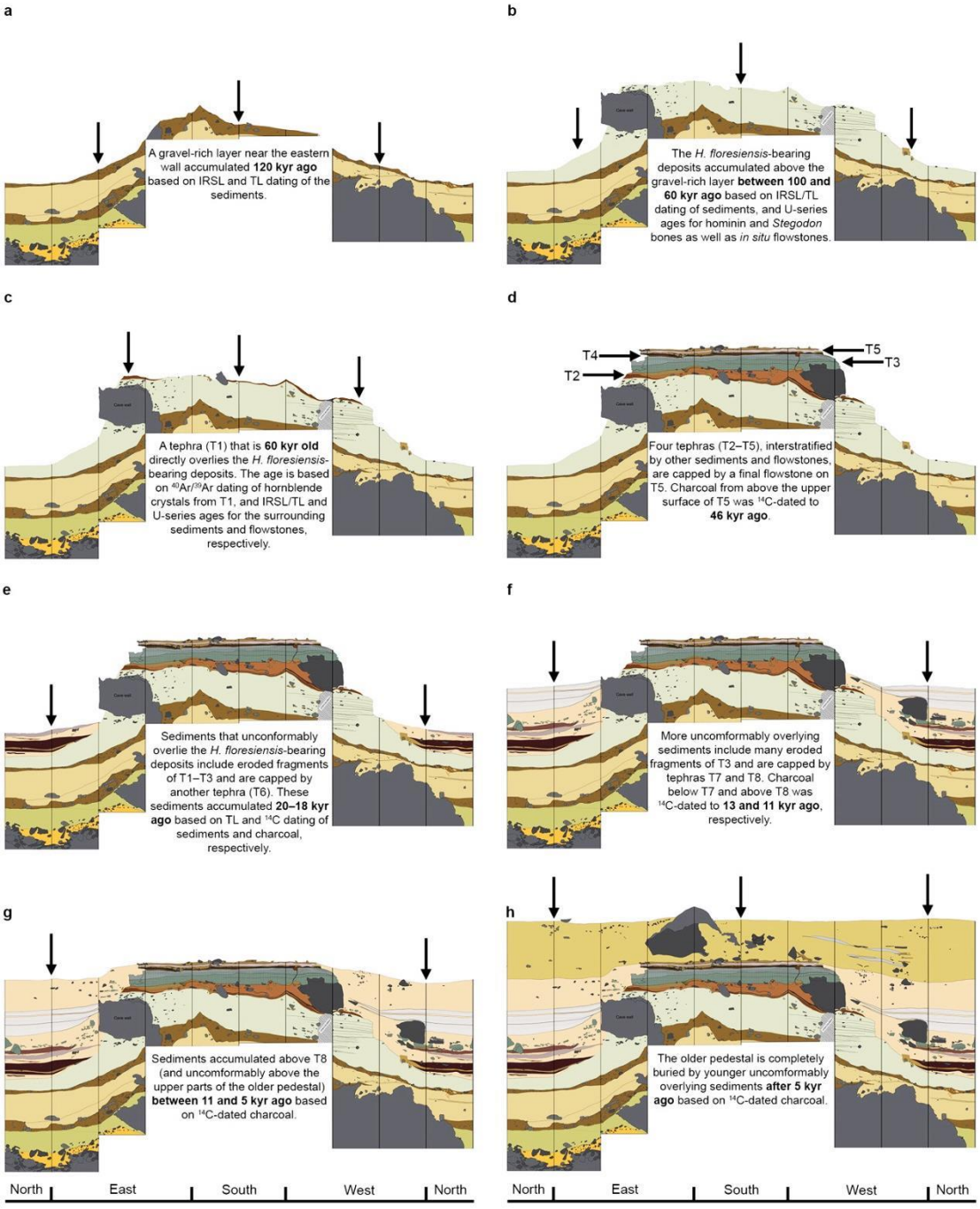

Extended Data figure 2.1 Stratigraphy of the excavated area near the eastern cave wall at eight stages of depositional history, with approximate ages indicated. Each panel (**a–h**) shows the remnant deposits exposed in the 2 m-wide baulks of the following Sectors (from left to right): north VII, east VII, XI and XXIII, south XXIII and XXI, west XXI, XV and XVI, and north XVI. The pedestal deposits shown in **b–d** were truncated by one or more phases of erosion that resulted in an erosional surface (i.e., an unconformity) that slopes steeply down towards the cave mouth (see also Supplementary information video 2.1). The black arrows relate to the accompanying text in each panel. The maximum depth excavated was 10.75 m in Sector VII (e.g., the left two panels in **h**).

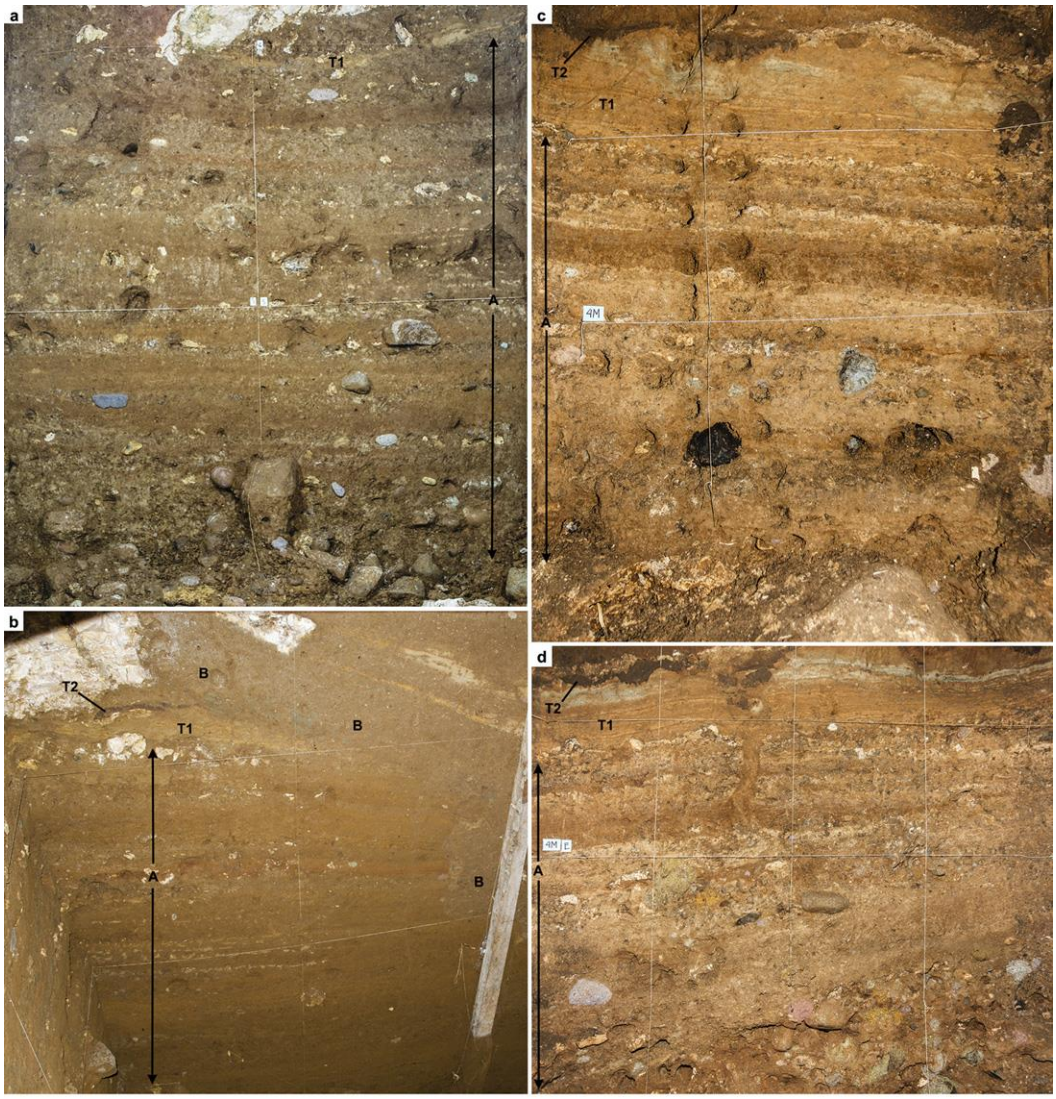

Extended Data figure 2.2 Deposits containing the remains of *Homo floresiensis*. These deposits (**A**) consist of multiple layers of fine-grained sediment interspersed with layers of weathered limestone and loose gravel, and are directly overlain by two tephras (**T1** and **T2**). **a**, South baulk of Sector XV, near the eastern cave wall. **b**, West baulk of Sector XV, also showing the uncomformably overlying deposits (**B**). **c** and **d**, North and east baulks of Sector XIX, near the cave centre.

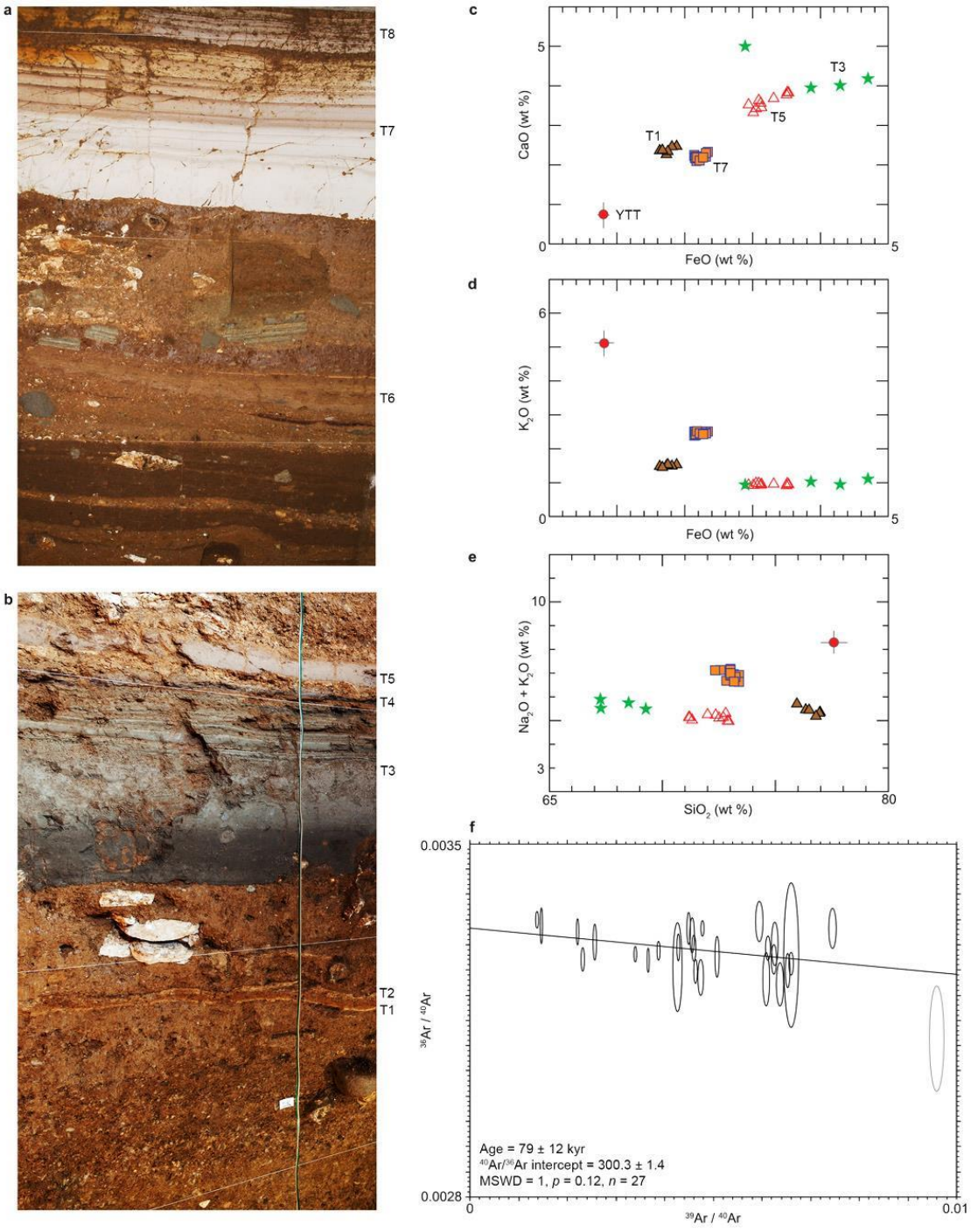

Extended Data figure 2.3 The volcaniclastic deposits at Liang Bua. **a,** Photograph of tephras T6–T8 (north baulk of Sector XVI). **b**, Photograph of tephras T1–T5 (south baulk of Sector XXI). **c**, Bivariate plot of FeO and CaO concentrations (expressed as weight %), acquired by electron microprobe analysis of glass shards from T1 (n = 6), T3 (n = 4), T5 (n = 10) and T7 (n = 15), as well as the Youngest Toba Tuff (YTT, n = 207, ± 1σ) from northern Sumatra. **d**, Bivariate plot of FeO and K_2O concentrations (symbols as in **c**). **e**, Bivariate plot of SiO_2 and Na_2O + K_2O concentrations (symbols as in **c**). **f**, Isotope correlation (inverse isochron) plot for hornblende crystals from T1. The error ellipses represent individual analyses (n = 28). The ellipse on the far right-hand side was omitted from the $^{40}Ar/^{39}Ar$ age determination of 79 ± 12 kyr (at 1σ).

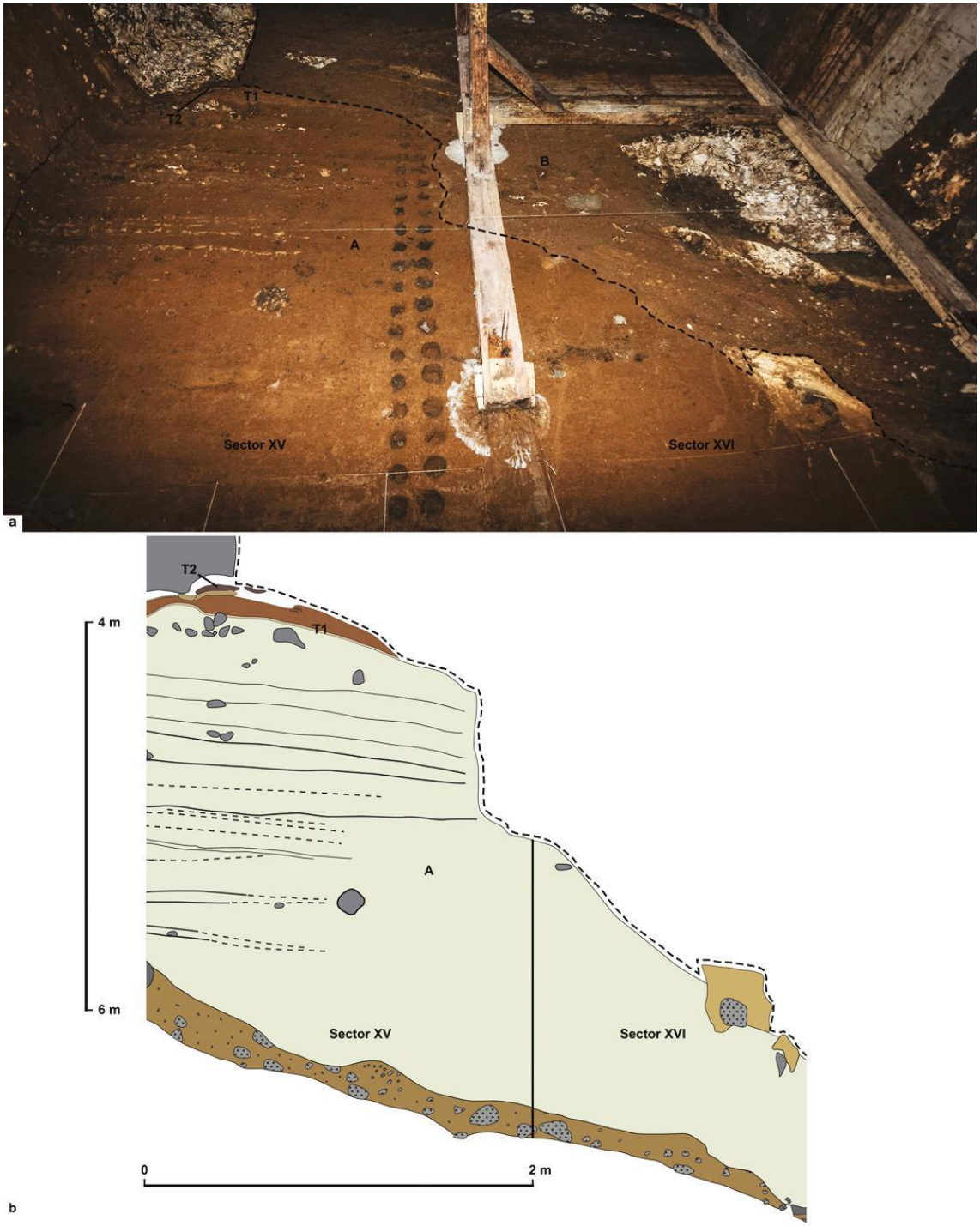

Extended Data figure 2.4 Erosional surface of the pedestal in the west baulks of Sectors XV and XVI. The dashed line marks the steeply sloping boundary between remnant deposits (**T2**, **T1** and the underlying *Homo floresiensis*-bearing sediments) that comprise part of the pedestal (**A**) and the much younger deposits (**B**) that unconformably overlie the contact. **a**, Photograph taken at an upward angle showing the sedimentary differences between the deposits above and below the erosional boundary. **b**, Illustration of the erosional surface and underlying deposits shown in **a**.

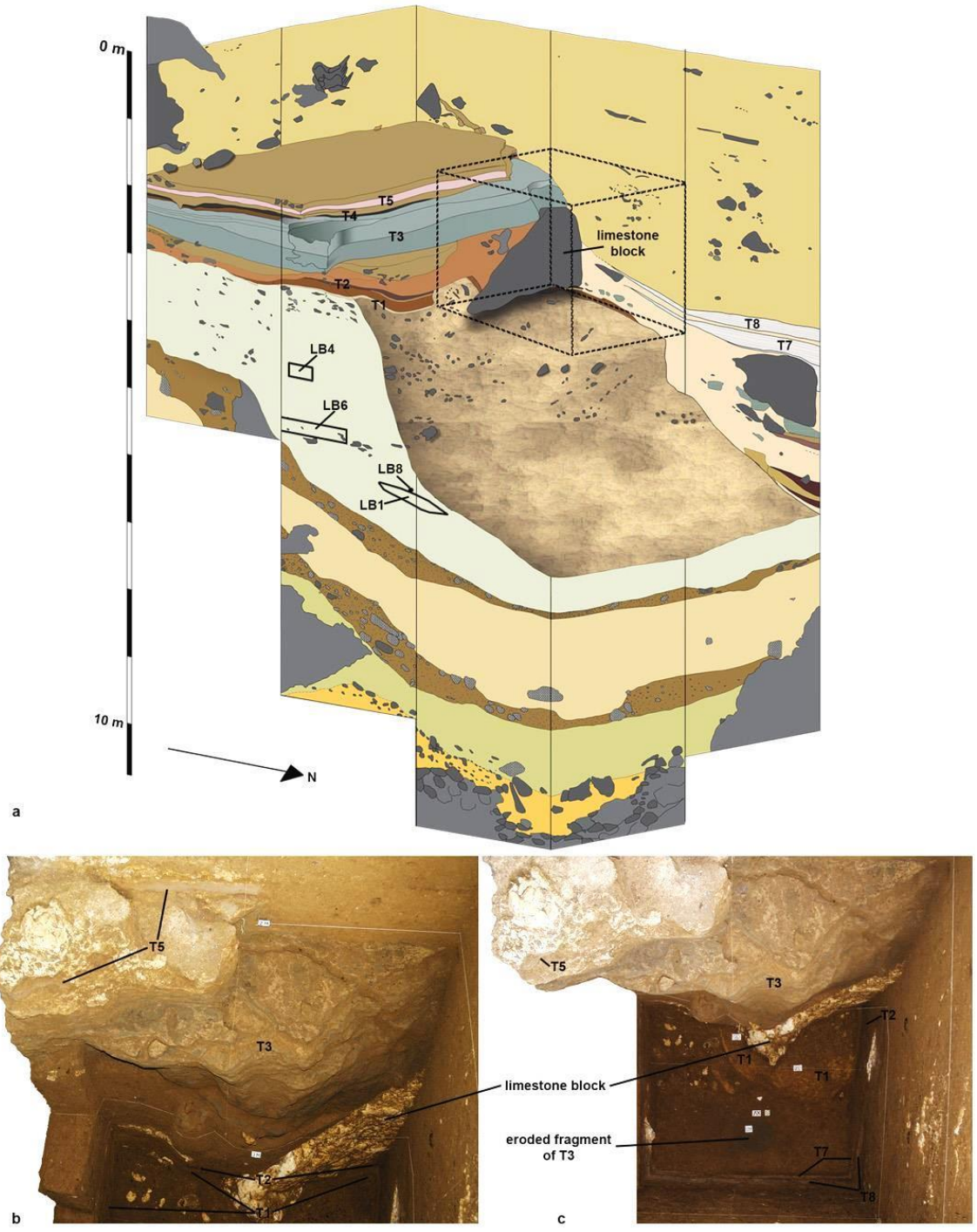

Extended Data figure 2.5 Erosional surface of the pedestal near the eastern wall of the cave. **a**, Illustration of the erosional surface and the locations of LB1, LB4, LB6 and LB8 below the boundary (see also Fig. 2.3). The deposits that unconformably overlie the pedestal are shown in the south and west baulks. The stippled cube outlines the photographed area (in Sector XV) shown in **b** and **c**. Both photographs taken from above, with north towards the bottom of the page.

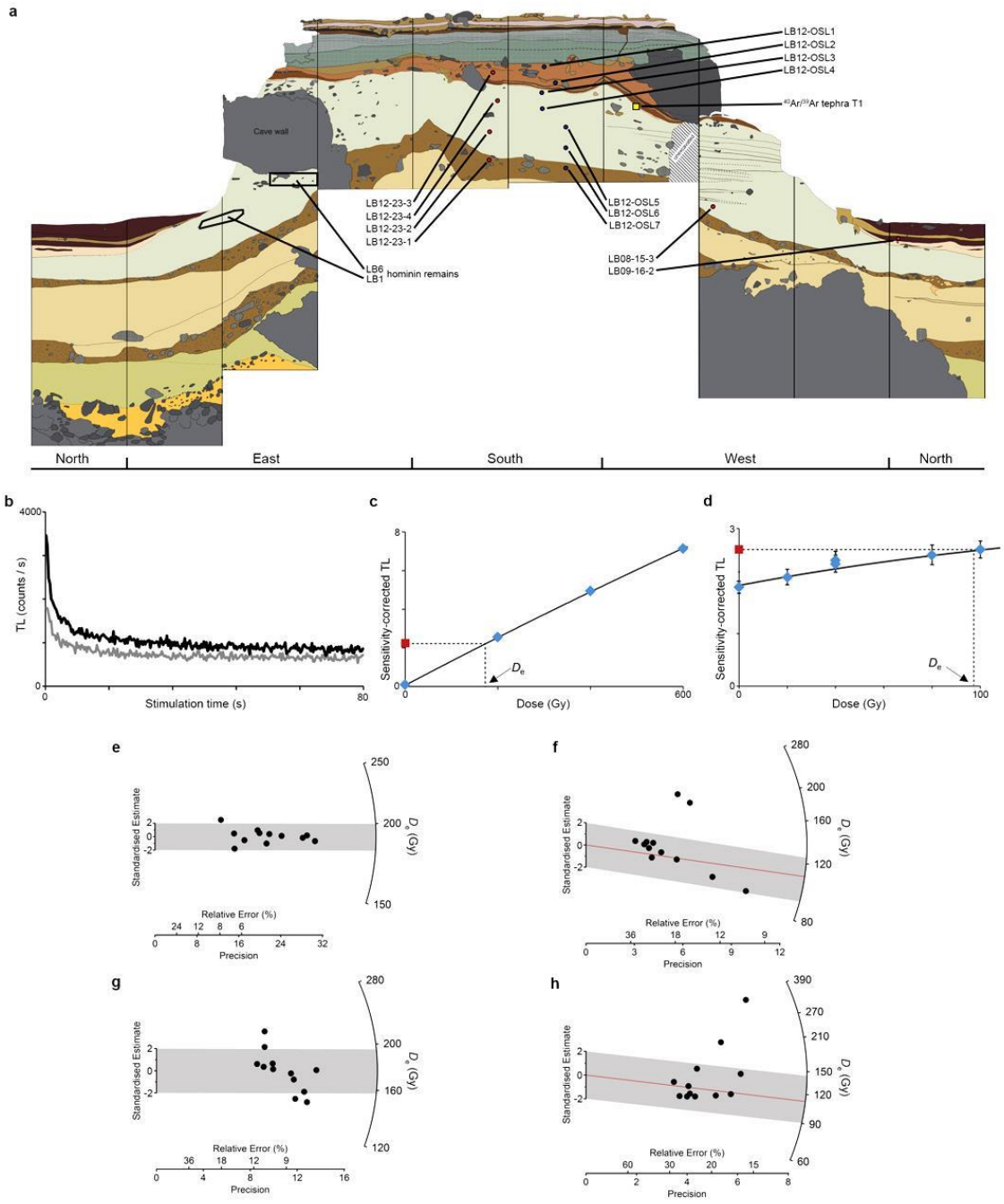

Extended Data figure 2.6 Locations of sediment samples dated in this study and TL data for quartz grains from Liang Bua. **a**, Stratigraphy of the excavated area near the eastern cave wall (Sector baulks as in Extended Data fig. 2.1) with TL samples indicated by red circles, IRSL samples by blue circles and the $^{40}Ar/^{39}Ar$ sample by a yellow square. Also shown are the TL and IRSL sample codes and the locations of hominin remains LB1 and LB6. **b**, Representative isothermal (260 °C) TL decay curves for the natural (black line) and test dose (grey line) signals from sample LB08-15-3. **c** and **d**, Regenerated TL dose-response curves for one pair of Aliquots A and B of sample LB08-15-3, respectively; the equivalent dose (D_e) is estimated by projecting the natural signal (red square) on to the dose-response curve fitted to the regenerated signals (blue diamonds). **e**, Radial plot (Galbraith *et al*., 1999; Galbraith and Roberts, 2012) of D_e values for Aliquot A (n = 12) of sample LB08-15-3; the grey band is centered on the

weighted mean D_e calculated using the central age model. **f**, Radial plot of the corresponding D_e values for Aliquot B (n = 12) of the same sample. The grey band is centered on the central age model estimate, with the two high-D_e outliers omitted. The red line intersects the right-hand axis at the D_e calculated by fitting the minimum age model (Galbraith *et al*., 1999; Galbraith and Roberts, 2012) to all 12 values. **g** and **h**, Radial plots of D_e values for Aliquots A and B of sample LB12-23-1 (symbols as in **e** and **f**).

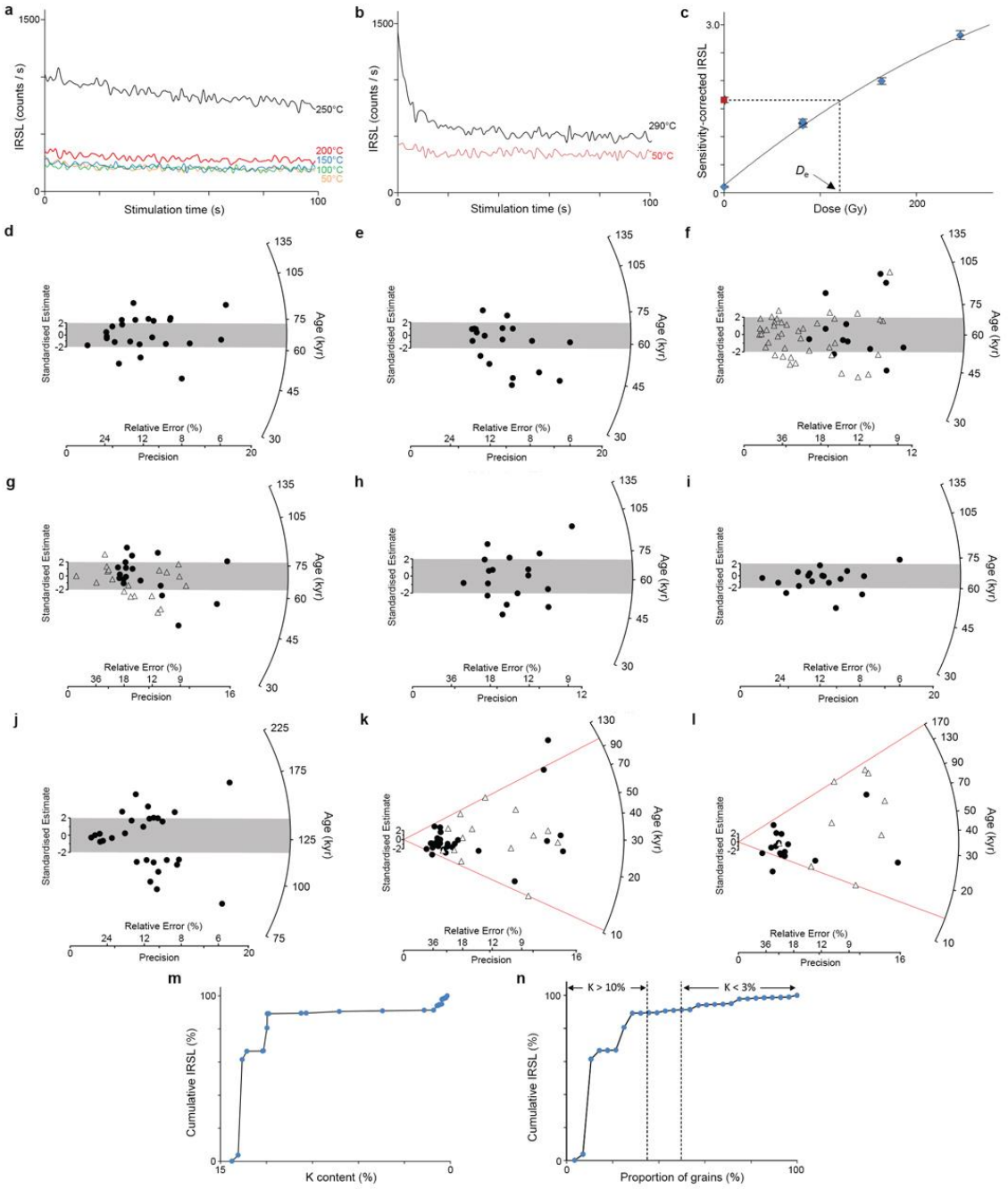

Extended Data figure 2.7 IRSL data and potassium (K) concentrations for feldspar grains from Liang Bua. **a**, Representative IRSL (50 °C) and multiple elevated temperature (100–250 °C) post-infrared IRSL (pIRIR) decay curves for a single aliquot of sample LB12-OSL1. **b**, IRSL (50 °C) and pIRIR (290 °C) decay curves for a different aliquot of LB12-OSL1. **c**, Regenerated pIRIR (290 °C) dose-response curve for the aliquot shown in **b**; the equivalent dose (D_e) is estimated by projecting the natural signal (red square) on to the dose-response curve fitted to the regenerated signals (blue diamonds). **d–j**, Radial plots of IRSL ages (corrected for residual dose and anomalous fading) for single aliquots of each sample: **d**, LB12-OSL1; **e**, LB12-OSL2; **f**, LB12-OSL3; **g**, LB12-OSL4; **h**, LB12-OSL5; **i**, LB12-OSL6; and **j**, LB12-OSL7. IRSL ages were also obtained for single grains of samples LB12-OSL3 and LB12-OSL4, and are shown as open triangles in plots **f** and **g**. The grey bands in each plot are centered on the weighted mean ages calculated using the central age model. **k** and **l**, Radial plots of

IRSL ages (corrected as for **d–j**) for samples LBS7-40a and LBS7-42a, respectively; single aliquots are shown as filled circles and single grains as open triangles. The upper and lower red lines intersect the right-hand axis at the maximum and minimum single-grain ages, respectively. **m**, Distribution of pIRIR intensities from 28 individual grains of feldspar from sample LB12-OSL3 that had been given a regenerative dose of 80 Gy. The relative contribution of each grain to the total (cumulative) pIRIR light sum is plotted as a function of K concentration (measured by wavelength-dispersive X-ray spectroscopy); note the reversed scale on the *x*-axis. **n**, Cumulative pIRIR light sum for the same 28 grains as shown in **m**, plotted as a function of grains ranked by K concentration (which decreases from left to right).

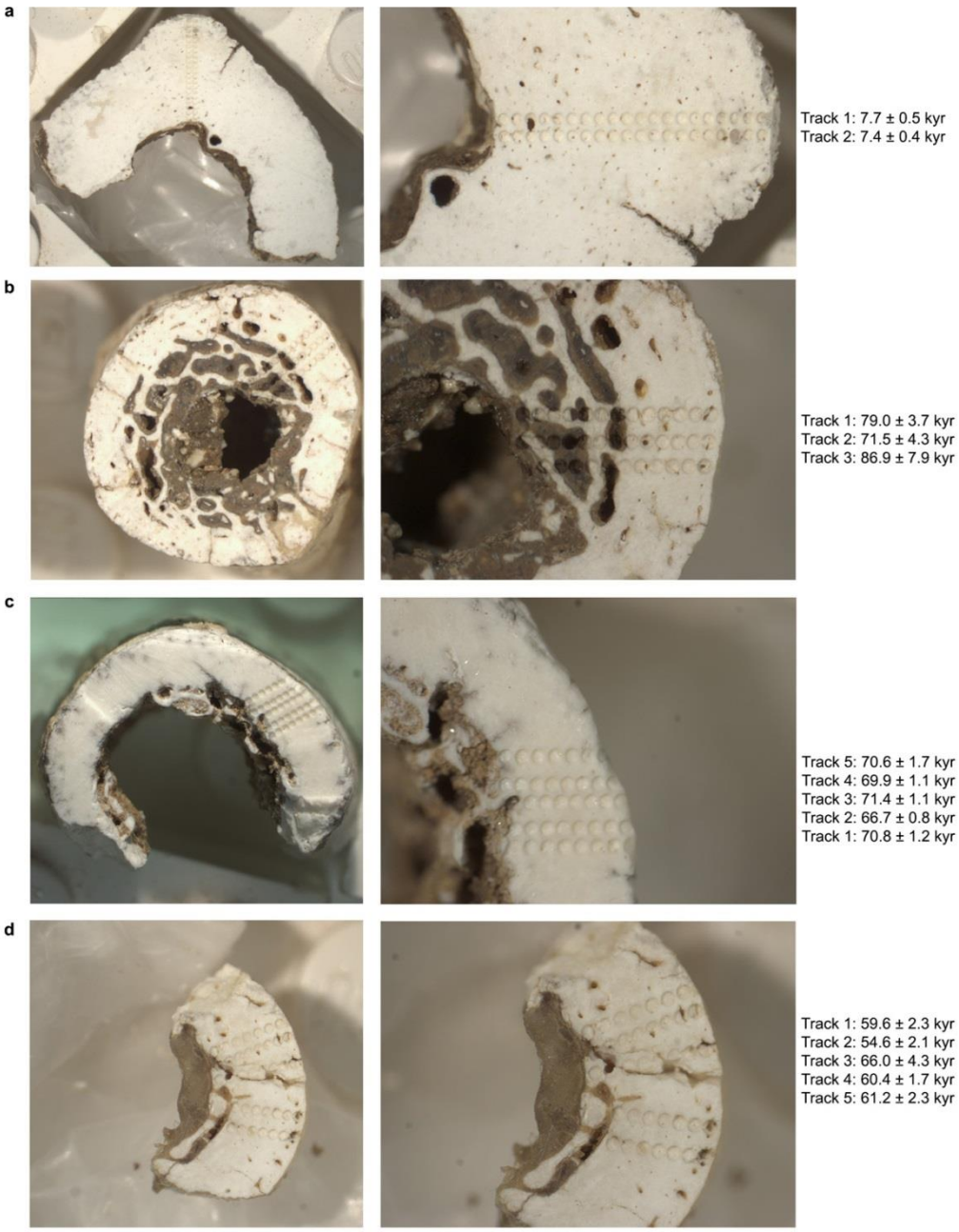

Extended Data figure 2.8 Laser-ablation uranium-series analyses of hominin bone fragments from various Sectors and spits (depth intervals), and their modelled ages. **a**, Modern human femur (132A/LB/27D/03) from Sector IV, spit 27 (265–275 cm). **b**, *Homo floresiensis* ulna (LB1/52) from Sector XI, spit 58A (575–585 cm). **c**, *H. floresiensis* ulna (LB2/1) from Sector IV, spit 42D (415–425 cm). **d**, *H. floresiensis* ulna (LB6/3) from Sector XI, spit 51 (505–515 cm). Each laser spot is 265 μm in diameter and the age errors are at 2σ.

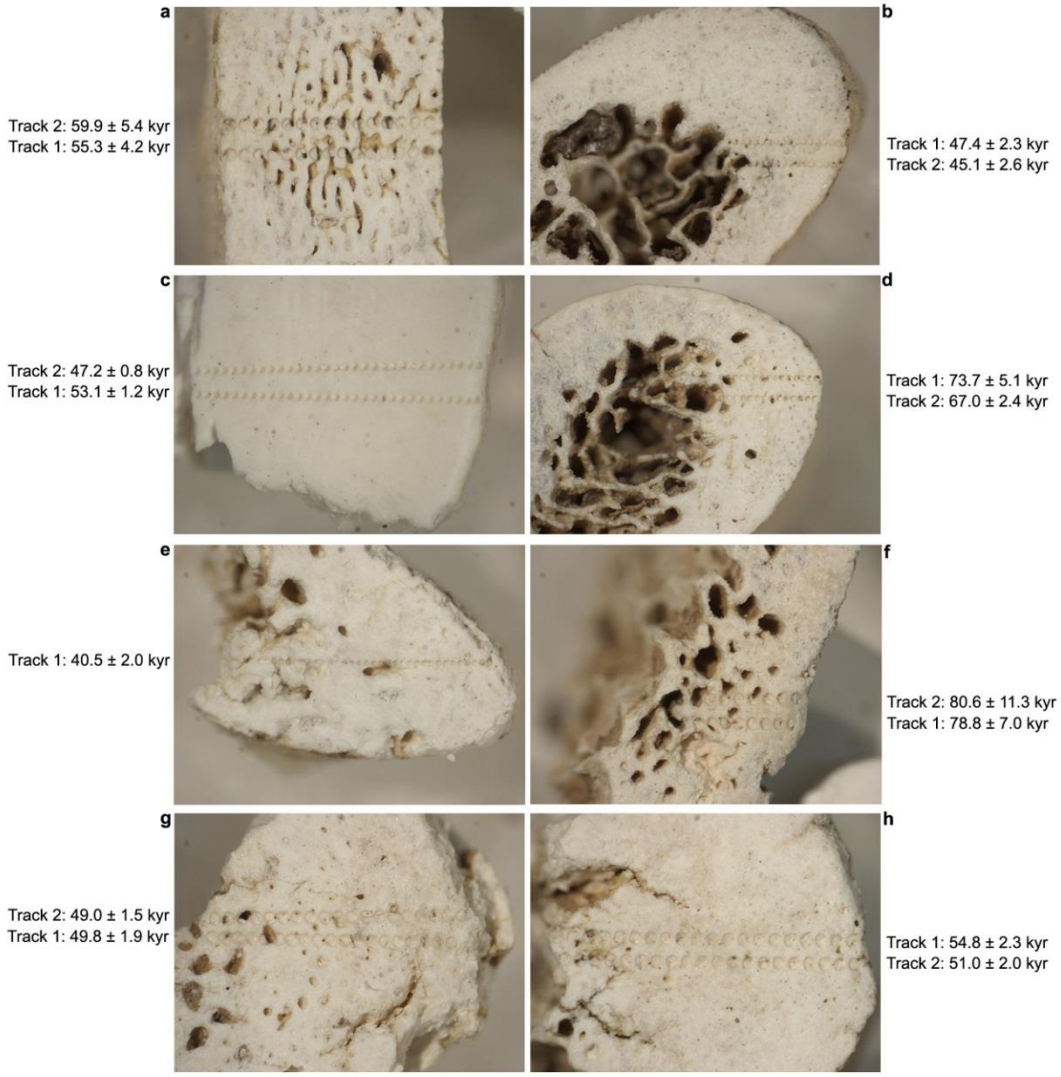

Extended Data figure 2.9 Laser-ablation uranium-series analyses of bone fragments of *Stegodon florensis insularis* from various spits (depth intervals) in Sector XI, and their modelled ages. **a**, U-s-01/LB/XI/32/04, spit 32 (315–325 cm). **b**, U-s-02/LB/XI/45/04, spit 45 (445–455 cm). **c**, U-s-03/LB/XI/47/04, spit 47 (465–475 cm). **d**, U-s-04/LB/XI/49/04, spit 49 (485–495 cm). **e**, U-s-05/LB/XI/51/04, spit 51 (505–515 cm). **f**, U-s-06/LB/XI/52/04, spit 52 (515–525 cm). **g**, U-s-07/LB/XI/65/04, spit 65 (645–655 cm). **h**, U-s-08/LB/XI/65B/04, spit 65B (645–655 cm). Each laser spot is 265 μm in diameter and the age errors are at 2σ.

Extended Data figure 2.10 Deposits stratigraphically above the unconformity in Sector XVI and displaced slab of deposit in Sector XXII. **a**, The north baulk (~2 m wide) of Sector XVI. **b**, Excavated floors (white arrow points north) of spits 61–63 (615–635 cm depth); the field of view is ~1.6 m in width. The stippled box in **a** indicates the floor of spit 63 in **b**, where fragments of T1 (+) are visible in spit 63, and fragments of T3 (*) and T1 are concentrated in the band just above the label for spit 61. Eroded fragments (between about 1 cm and 60 cm in size) of T1, T2 and T3 have been consistently

recovered from deposits unconformably overlying the erosional surface of the pedestal, indicating reworking of the pedestal deposits before ~13 kyr cal. BP. **c**, Photograph of the west baulk and parts of the south and north baulks (at left and right, respectively) of Sector XXII showing a displaced slab of deposit that contains intact portions of the uppermost part of T3 (arrow) and the overlying layers, up to and including the flowstone (fs) that caps T5. The stratigraphic position of the slab beneath T7 and T8 indicates that it broke away from its original location, slightly to the south, and slid down the steeply sloping erosional surface prior to ~13 kyr cal. BP. Also shown are the *Homo floresiensis*-bearing deposits (**A**) and the unconformably overlying deposits (**B**), which include eroded fragments of T1 (+), T2 (#) and T3 (*). **d**, Illustration of the west baulk of Sector XXII, as shown in **c**.

2.6 Supplementary information section 2.1

2.6.1 Supplementary discussion – Tephra deposits at Liang Bua

Eight centimetre- to decimetre-thick layers of volcaniclastic origin occur within stratified deposits at Liang Bua (T1–T8). All volcanic layers exhibit localised post-depositional reworking, but some exhibit bedding and sorting characteristics consistent with primary deposition within Liang Bua.

T1, T7 and T8 consist of well-sorted, vitric-rich, fine sandy- to silty-textured tephric material of regional rhyolitic origin, based on major element composition of glass shards from T1 and T7 (Extended Data fig. 2.3c–e and Supplementary table 2.1). These three tephras were deposited in Liang Bua through a combination of primary accumulation via the cave mouth and secondary aeolian and/or rain-generated run-off processes that deposited material more deeply in the recesses of the cave. All three of these rhyolitic tephras are likely related to regional eruptive events, but they cannot at this stage be matched precisely with known inter-regional tephra marker beds (such as the ~74 kyr Youngest Toba Tuff; Storey *et al*., 2012) or regionally distributed rhyolitic tephra identified within, and adjacent to, the So'a Basin in central Flores (B.V.A., unpublished data). While the wider geographic distributions and eruptive sources of T1, T7 and T8 have yet to be determined, there remains the potential for intra- and inter-regional correlations as more tephra-bearing deposits are recognised in the region and their chemical compositions are characterised.

T2, T4, T5 and T6 consist of massive to crudely normal stratified, compacted layers of moderately sorted dark grey to pink fine to very fine ash, and are all likely related to local volcanism. These four tephras are considered to represent finely comminuted (milled) ash elutriated from, and forced into, the recesses of Liang Bua by the passage of block-and-ash flows that extended down the adjacent Wae Racang river

valley. The headwaters of the Wae Racang catchment are located in a volcanic range ~14 km south of Liang Bua, near Ruteng. This volcanic range is of late Quaternary age and comprises multiple, coalesced lava domes and craters flanked by conspicuous volcaniclastic fan remnants. Some lava domes are still active today, such as Gunung Namparnos. These volcaniclastic fans have a complex architecture comprising numerous, but as yet undated, block-and-ash flow deposits. Such deposits have been identified in quarries on the flanks of Poco Likang at the tributary headwaters of the Wae Racang. Decimeter-thick sequences of coarse-grained block-and-ash flow debris have been located in side tributaries of the Wae Racang, less than 4 km upstream from Liang Bua. They exhibit extensively brecciated clasts that indicate *en masse* emplacement with percussion and associated pulverisation of constituent clasts.

T3 represents a water-supported mass flow deposit that flooded into Liang Bua from the adjacent Wae Racang river valley, most likely related to local volcanism. It is situated consistently between about 2.0 and 2.8 m depth from the eastern wall (e.g., Sector XXIII) to the cave centre (e.g., Sector XIX), and consists of three subunits. The lowermost subunit (~25–30 cm thick) is a moderately sorted, faintly bedded, upward fining, grey lithic coarse sand containing well-rounded pumiceous coarse ash and very fine lapilli with conspicuous mud rip-up clasts. The middle subunit (~15–25 cm thick) is characterised by medium to coarse sands that are severely disrupted by liquefaction/dewatering structures. The uppermost subunit (~20–30 cm thick) is characterised by millimetre- to centimetre-thick normal graded sand and silt laminations. Both subunits were deposited in quick succession, given the lack of evidence for a significant hiatus between depositional events, such as soil development or bioturbation. The sedimentological characteristics of T3 indicate its initial emplacement as a water-supported mass flow (hyperconcentrated) event (subunit 1),

which subsequently consolidated and dewatered (subunit 2). Given the absence of associated debris from the cave ceiling, it seems unlikely that the liquefaction structures in subunit 2 resulted from syn- or post-depositional volcanically and/or tectonically induced seismicity. The uppermost part of T3 (subunit 3) indicates an interval of water ponding with periodic intra-cave (rain-induced) inflow and localised redeposition. At this stage, it is unclear whether the initial emplacement of T3 represents a syn-eruptive event associated with the downstream lateral transformation of a block-and-ash flow event, or a post-eruptive event associated with flooding of the Wae Racang. The pervasive occurrence of T3 within the excavated cave deposits suggests that the level of the Wae Racang valley floor, relative to the cave entrance, was more elevated in the past than at the present day and has subsequently been down-cut. Evidence of this fluvial down-cutting is indicated by terrace remnants occupying valley margins (Roberts *et al*., 2009).

2.6.2 Supplementary table 2.1 – Major element composition of glass shards at Liang Bua

Electron microprobe analysis of volcanic glass shards from tephric (T1, T5 and T7) and water-supported mass flow deposits (T3) preserved at Liang Bua. The major element composition of the Youngest Toba Tuff is also listed (Alloway *et al*., 2004). The ATHO-G glass standard (Jochum *et al*., 2006) was used as a calibration monitor for all runs. The data were normalised to 100% (by weight) anhydrous; the totals and standard deviations shown are for the original analyses, with the difference from 100% considered as H_2O content. FeO represents total iron. Bivariate plots of individual analyses are displayed in Extended Data fig. 3c (FeO and CaO), 3d (FeO and K_2O) and 3e (SiO_2 and $Na_2O + K_2O$).

Sector	Sample	SiO_2	Al_2O_3	TiO_2	FeO	MgO	MnO	CaO	Na_2O	K_2O	Total	*n*
XVI	**T7**	73.01	14.54	0.4	2.22	0.75	0.12	2.2	4.47	2.47	97.7	15
		0.28	0.16	0.02	0.07	0.03	0.02	0.06	0.18	0.04	1.65	
XXI	**T5**	72.19	14.37	0.49	3.22	1.23	0.12	3.6	4.18	0.95	100.04	10
		0.71	0.26	0.03	0.22	0.15	0.03	0.18	0.12	0.02	1.46	
XXI	**T3**	68.08	16.22	0.34	3.94	1.49	0.16	4.29	4.66	1.01	97.48	4
		0.99	1.07	0.06	0.78	0.61	0.04	0.49	0.27	0.08	0.61	
XXI	**T1**	76.58	13.09	0.28	1.75	0.57	0.07	2.38	3.91	1.5	96.61	6
		0.4	0.11	0.02	0.09	0.04	0.01	0.08	0.17	0.03	0.65	
Youngest Toba Tuff	**YTT**	77.57	12.18	0.08	0.8	0.06	0.06	0.76	3.2	5.09	97.9	207
		0.45	0.23	0.05	0.14	0.03	0.03	0.11	0.36	0.4	1.21	
Glass standard	**ATHO-G**	75.60	12.20	0.23	3.27	0.09	0.11	1.70	3.75	2.64	99.59	49
		0.37	0.11	0.02	0.09	0.01	0.03	0.03	0.30	0.04	0.60	

2.7 Supplementary information section 2.2

2.7.1 Supplementary discussion – Luminescence dating of feldspar and quartz grains

Infrared stimulated luminescence (IRSL)

To test the suitability of the post-infrared IRSL (pIRIR) 290 °C regenerative-dose procedure for the Liang Bua samples, routine tests (Roberts *et al*., 2015) were made for 'recuperation' (the signal intensity after giving the sample a zero regenerative dose, relative to the intensity of the natural sample), 'recycling' (the signal reproducibility for a duplicate regenerative dose) and the 'residual dose' remaining after an extended bleach in a solar simulator.

The extent of recuperation and the recycling ratio are obtained for each aliquot or grain during construction of the dose-response curve for D_e estimation. We rejected aliquots (and individual grains of samples LBS7-40a and -42a) with recuperation values of more than 10% and/or recycling ratios that differed from unity by more than 10%. The elevated-temperature pIRIR traps are incompletely bleached by sunlight, even after prolonged exposure, which can result in significant residual doses at the time of sediment deposition (Li and Li, 2011; Thiel *et al*., 2011; Li *et al*., 2013, 2014: Roberts *et al*., 2015). To estimate the extent of any residual dose, we exposed 3–6 natural aliquots of samples LB12-OSL1 to -OSL7 to a solar simulator for 4 hr (duration chosen on the basis of bleaching tests on other samples: Li and Li, 2011; Li *et al*., 2013, 2014) and measured the remnant doses using the pIRIR (290 °C) procedure. The mean residual dose is less than 8 Gy in all cases (Supplementary table 2.3), with a weighted mean of 6.5 ± 0.5 Gy. The pIRIR signals were too dim to use the intensity-subtraction procedure for residual dose correction (Li *et al*., 2013), but the dose-subtraction approach (in which the residual dose of each sample is subtracted from its measured D_e)

should be satisfactory as the residual doses are small relative to the D_e values. We used the latter procedure to calculate the IRSL ages.

A 'dose recovery' test (Galbraith *et al*., 1999) was also conducted on sample LB12-OSL3, to check that a known (given) dose could be accurately recovered using the same measurement conditions as those used to estimate the D_e values (and residual doses) for the natural samples. Eight natural aliquots were bleached in a solar simulator for 4 hr and then given a laboratory beta dose of 123 Gy as a surrogate natural dose, which was measured using the pIRIR (290 °C) procedure. The resulting ratio of measured (recovered) dose to given dose is statistically consistent with unity (0.98 ± 0.04), after subtracting the residual dose for this sample, validating the suitability of these experimental conditions.

Anomalous fading tests were made on five samples using a single-aliquot measurement procedure similar to that described previously (Auclair *et al*., 2003), but with the pIRIR (290 °C) experimental conditions used in this study. The rate of fading of the sensitivity-corrected pIRIR (290 °C) signal is measured as a function of storage time at room temperature, where a 'decade' is a factor of ten in time since laboratory irradiation. The measured fading rates range from –0.7 to 1.2% per decade (but with uncertainties that overlap at 1σ) for storage times of up to 4 days (~2.4 decades). The weighted mean fading rate for these five samples is 0.9 ± 0.3% per decade, which we used to correct each of the measured ages to obtain the final, fading-corrected ages (Huntley and Lamothe, 2001) (Supplementary table 2.3). The ages are insensitive to assumptions about past water content, increasing (or decreasing) by ~0.5% for each 1% increase (or decrease) in water content.

IRSL ages can be sensitive, however, to assumptions about the internal K content, especially in contexts where the external dose rate is comparatively low. Our sample

preparation procedures are designed to separate K-rich feldspar grains, and we used X-ray diffraction to confirm the predominance of high-K feldspars (orthoclase, microcline and sanidine, in order of relative abundance). To obtain a direct measure of the K concentration, we conducted energy- and wavelength-dispersive X-ray spectroscopy (EDS and WDS, respectively) analyses of 28 grains from LB12-OSL3 that yielded detectable pIRIR signals during single-grain measurements. For each grain, 4–7 spots were sampled for EDS analysis using beam diameters ranging from a few μm to a few tens of μm, and 3–5 spots were measured for WDS analysis using an electron beam size of ~6 μm. Spots were located on relatively flat grain surfaces with an homogeneous appearance, and measurements were made using the instruments, procedures and reference standards described in Neudorf (2012) and Neudorf *et al*. (2012). The EDS and WDS analyses produced consistent results, which showed that 15 grains (~54% of the total) had K concentrations of less than 3% and that 9 grains (~32% of the total) had K contents higher than 10%. Most of the high-K grains yielded much brighter pIRIR signals than did the low-K grains. The 5 brightest grains each had K concentrations of more than 10% and, together, accounted for ~90% of the total pIRIR signal emitted by all 28 grains (Extended Data fig. 2.7m, n). A mean K concentration of 11.9% is obtained by weighting the K content of individual grains by their corresponding pIRIR sensitivities. Based on these results, we adopted a K concentration of 12 ± 1% to estimate the internal dose rates for all our samples, with the uncertainty sufficient to capture the likely range of variation in mean K content at 2σ.

The fading-corrected ages for individual aliquots and grains are displayed as radial plots (Galbraith *et al*., 1999; Galbraith and Roberts, 2012) in Extended Data fig. 2.7d–l. For all samples, the spread among these age estimates is larger than can be explained by measurement error alone, as indicated by over-dispersion (OD: Galbraith

and Roberts, 2012) values of approximately 17–43% for samples LB12-OSL1 to -OSL7, ~60% for LBS7-40a and ~80% for LBS7-42a. The OD may be due to a number of factors, such as the use of a multi-sample average fading rate for all aliquots and an average value for residual dose correction for each sample, as well as between-grain differences in the extent of bleaching before deposition and spatial variations in dose rate after burial (Roberts *et al*., 2015).

To explore the potential effect of incomplete bleaching on the single-aliquot ages, we measured 4500 and 2000 individual feldspar grains from samples LB12-OSL3 and -OSL4, respectively. Only 41 and 19 of these grains (fewer than 1% of the total measured) yielded detectable pIRIR signals (i.e., initial counts more than 3 times the background intensity), which indicates that the pIRIR signal from each aliquot (composed of a few hundred grains) is dominated by the light emitted by one or a few grains only. The distributions of fading-corrected, single-grain ages are indistinguishable from those of the single aliquots (Extended Data fig. 2.7f and 2.6g) and yield statistically consistent D_e and OD values (Supplementary table 2.3). Given the lack of evidence for incomplete bleaching, we combined the single-aliquot and single-grain data sets to estimate the burial ages of these two samples.

To allow for the observed extent of OD, whatever the sources, we used the central age model (CAM) to determine the weighted mean ages and 1σ uncertainties listed in Supplementary table 2.3. The CAM does not assume that the age estimates are statistically consistent (i.e., within measurement error of a common value), but takes into account the additional source of random variation over and above that due solely to measurement error (Galbraith *et al*., 1999; Galbraith and Roberts, 2012). Most of the single-aliquot ages (and single-grain ages for LB12-OSL3 and -OSL4) are scattered around the CAM values, but sample LB12-OSL7 shows a possible bifurcation of ages

into two discrete populations (Extended Data fig. 2.7j). One population is centered on ~80 kyr and the other on ~180 kyr, representing about 45% and 55% of aliquots, respectively. This sample was collected from the gravel-rich layer underlying the basal *Homo floresiensis*-bearing deposits and we cannot at present discount the possibility that it consists of mixed-age grains; the same note of caution applies to TL sample LB12-23-1, which was collected from the same layer and dated using multi-grain methods. Single-grain IRSL dating may help resolve this issue.

Of the 2000 and 1800 individual grains measured for samples LBS7-40a and -42a, respectively, only 14 (0.7%) and 9 (0.5%) grains gave detectable pIRIR signals. The ages of these grains are scattered widely between ~10 and ~170 kyr and the same pattern is observed in the age distribution for the single aliquots (Extended Data fig. 2.7k, l), presumably because (as with LB12-OSL3 and -OSL4) less than 1% of the few hundred grains on each aliquot are responsible for the emitted pIRIR signal. The OD values for the single grains and aliquots of these two samples are, accordingly, much larger than those of LB12-OSL1 to -OSL7. These results support our contention that LBS7-40a and -42a include a mixture of grains from different stratigraphic units on either side of the previously unrecognised unconformity. The finite mixture model (Galbraith and Roberts, 2012) can be used to estimate the ages of discrete grain populations, such as mixtures of two or three separate components, but it is applicable only to single-grain data sets and there are too few grains of LBS7-40a and -42a to fit this model reliably.

We can discern no clear evidence for discrete populations in the age distributions of samples LBS7-40a and -42a, but around two-thirds of the single-grain and single-aliquot ages for LBS7-40a appear to form a cluster at ~30 kyr. The fading-corrected CAM age for these data is 30 ± 4 kyr, and the corresponding age for the LBS7-42a data

is 36 ± 9 kyr. Neither of these 'pooled mean' ages should be considered reliable estimates of burial age for LB1, but we note that they are similar to the maximum ages of 38 ± 8 kyr (LBS7-40a) and 35 ± 4 kyr (LBS7-42a) obtained in the original Liang Bua study (Morwood *et al*., 2004; Roberts *et al*., 2009) using the light-sensitive TL emissions from aliquots consisting of ~5000 grains of quartz. For a sample composed of mixed-age grains that are measured simultaneously, the ages will represent some kind of average, with the exact value dependent on the relative proportion of grains of different ages and their luminescence intensities. The similarity of the original TL ages and pooled mean IRSL ages for LBS7-40a and -42a is consistent, therefore, with these two samples containing grains from both sides of the unconformity.

Thermoluminescence (TL)

The dual-aliquot (DA) procedure employed in this study was developed originally for TL dating of the cave sediments at Liang Bua using the heat-induced red/orange emissions from volcanically derived quartz grains (Morwood *et al*., 2004; Westaway and Roberts, 2006). A minimum of two aliquots (Aliquots A and B) are needed to estimate the D_e associated with the light-sensitive TL traps, each typically composed of several thousand quartz grains. Aliquot A is used to determine the D_e for the heat-reset TL traps and Aliquot B is used to measure the total TL signal, from which the D_e associated with the light-sensitive TL traps is obtained by subtraction. The resulting ages should conservatively be viewed as maximum estimates of the time of sediment deposition, because several hours of sunlight exposure are required to significantly deplete the light-sensitive TL traps, and not all grains on each aliquot are likely to have been fully bleached prior to burial (Westaway and Roberts, 2006).

Liang Bua samples are commonly deficient in quartz and four of the samples in this study (LB09-16-2, LB12-23-2, -3 and -4) yielded enough grains to make only two

aliquots of ~10,000 grains. Two of the samples (LB08-15-3 and LB12-23-1), however, contained sufficient quantities of quartz to make 12 replicates of both Aliquots A and B, enabling an assessment of between-aliquot differences in the extent of pre-depositional bleaching and its effect on D_e estimation. For both samples, Aliquot A showed little variation in D_e among the 12 aliquots, with OD values of 0% for LB08-15-3 and 13 ± 4% for LB12-23-1. We attribute this to the grains being uniformly heated during a volcanic event or situated in the proximity of volcanically heated materials. The CAM was used to determine the weighted mean D_e value for the heat-reset signal.

By contrast, the D_e values for the 12 aliquots of Aliquot B were over-dispersed to a much greater extent (34 ± 10% for LB08-15-3 and 40 ± 11% for LB12-23-1), owing to the presence to two outlying values in each distribution (Extended Data fig. 2.6f, h). These anomalously high-D_e values are identified as statistical outliers on the basis of having normalised median absolute deviations greater than 1.5 (Storey *et al*., 2012) and are hypothesised to arise from incomplete bleaching of some of the constituent grains when last transported. We adopted two approaches to estimate the burial ages of these two samples. First, we removed the two D_e outliers in each of the distributions, which reduced the OD values to 8 ± 10% (LB08-15-3) and 0% (LB12-23-1), and then calculated the weighted mean using the CAM. We also applied the minimum age model (MAM: Galbraith *et al*., 1999; Galbraith and Roberts, 2012) to all 12 D_e values in each distribution, as an alternative method of estimating the D_e associated with the population of most fully-bleached grains. Before running the MAM, we added a relative error of 20% to each of the D_e measurement errors, as an estimate of the inherent over-dispersion (Galbraith and Roberts, 2012). This value was chosen on the basis of the OD values obtained for three samples (12 aliquots each) of modern hillslope and river channel sediment collected in the vicinity of Liang Bua (weighted mean of 20 ± 1%),

and 12 aliquots of sample LB12-23-1 that had been bleached for 4 hr using a sunlamp (19 ± 1%). For both samples, the MAM D_e values for Aliquot B are statistically indistinguishable from the corresponding CAM D_e values: 110 ± 13 Gy for LB08-15-3 and 112 ± 14 Gy for LB12-23-1, resulting in MAM ages of 91 ± 11 and 111 ± 15 kyr, respectively. Given the consistency between the MAM and CAM D_e estimates (the latter obtained after rejecting the high-D_e outliers) and the greater precision of the latter, the burial ages listed in Supplementary table 2.3 for these two samples are those obtained using the CAM. This analysis suggests that the TL ages obtained for the other four samples, using only two aliquots of each, should provide reliable estimates of maximum age.

The *terminus post quem* caveat could be regarded as overcautious, given the overall consistency of the TL ages with the IRSL chronology and a variety of independent chronometers (Roberts *et al*., 2009 and this study). The IRSL ages are typically measured with higher precision than the TL ages, due to the indirect (subtraction) method of isolating the light-sensitive TL signal, and the pIRIR traps are also bleached more rapidly than the TL traps. Consequently, the good agreement between the two luminescence-based chronologies implies that the quartz and feldspar grains were bleached sufficiently to empty the light-sensitive TL and pIRIR traps to the same low level, and that both signals should yield ages that closely approximate the time of deposition of sediments at Liang Bua.

2.7.2 Supplementary table 2.2 – Dose rate data for IRSL and TL samples

	Sample code	Sector / depth (cm)	Grain size (μm)	Mineral / procedure [a]	Field water content (%) [b]	External dose rate (Gy/kyr) [c]			Internal dose rate (Gy/kyr) [c]	Total dose rate (Gy/kyr) [c]
						Beta	Gamma	Cosmic		
IRSL samples	LB12-OSL1	XXI / 280	90–212	feldspar / SA	26	0.41 ± 0.03	0.32 ± 0.02	0.06	0.63	1.41 ± 0.15
	LB12-OSL2	XXI / 310	90–212	feldspar / SA	35	0.44 ± 0.03	0.32 ± 0.02	0.06	0.63	1.45 ± 0.15
	LB12-OSL3	XXI / 329	180–212	feldspar / SA & SG	34	0.40 ± 0.03	0.32 ± 0.02	0.06	0.80	1.57 ± 0.11
	LB12-OSL4	XXI / 372	180–212	feldspar / SA & SG	35	0.45 ± 0.04	0.37 ± 0.02	0.06	0.80	1.68 ± 0.11
	LB12-OSL5	XXI / 410	180–212	feldspar / SA	35	0.47 ± 0.04	0.38 ± 0.02	0.06	0.80	1.71 ± 0.11
	LB12-OSL6	XXI / 450	90–212	feldspar / SA	34	0.42 ± 0.03	0.36 ± 0.02	0.06	0.63	1.47 ± 0.15
	LB12-OSL7	XXI / 495	90–212	feldspar / SA	26	0.39 ± 0.03	0.33 ± 0.02	0.05	0.63	1.40 ± 0.15
	LBS7-40a	VII / 485–490	90–212	feldspar / SA	11	0.80 ± 0.05	0.94 ± 0.05	0.05	0.63	2.42 ± 0.16
			180–212	feldspar / SG	11	0.79 ± 0.04	0.94 ± 0.05	0.05	0.80	2.58 ± 0.12
	LBS7-42a	VII / 593–598	90–212	feldspar / SA	8	0.90 ± 0.05	1.13 ± 0.06	0.05	0.63	2.71 ± 0.17
			180–212	feldspar / SG	8	0.88 ± 0.05	1.13 ± 0.06	0.05	0.80	2.86 ± 0.13
TL samples	LB08-15-3	XV / 573	90–125	quartz / DA	36	0.41 ± 0.04	0.72 ± 0.02	0.05	0.03	1.21 ± 0.05
	LB09-16-2	XVI / 640	90–125	quartz / DA	33	0.75 ± 0.03	0.94 ± 0.01	0.05	0.03	1.77 ± 0.04
	LB12-23-3	XXIII / 295	90–125	quartz / DA	36	0.42 ± 0.03	0.30 ± 0.01	0.06	0.03	0.81 ± 0.04
	LB12-23-4	XXIII / 347	90–125	quartz / DA	38	0.45 ± 0.03	0.37 ± 0.01	0.06	0.03	0.91 ± 0.04
	LB12-23-2	XXIII / 410	90–125	quartz / DA	39	0.57 ± 0.03	0.38 ± 0.01	0.06	0.03	1.04 ± 0.04
	LB12-23-1	XXIII / 490	90–125	quartz / DA	39	0.57 ± 0.03	0.36 ± 0.01	0.05	0.03	1.01 ± 0.04

[a] Procedure depends on the method of equivalent dose (D_e) determination. Potassium-rich feldspar grains were measured as single aliquots (**SA**) and/or as single grains (**SG**), while quartz grains were analysed using a dual-aliquot (**DA**) procedure.

[b] Water content at time of sample collection. The dose rates (and ages in Supplementary table 2.3) are calculated for a water content of 20 ± 5% (as explained in Methods). For the quartz samples, the calculated total dose rates increase (or decrease) by ~1% for each 1% decrease (or increase) in water content, while the effect is about half as much for the feldspar samples.

[c] All uncertainties expressed at 1σ. The cosmic-ray dose rate has a relative uncertainty of 10%, the internal dose rate of quartz has an uncertainty of ± 0.01 Gy/kyr, and the relative uncertainties on the internal dose rates of the feldspar samples are 13% and 23% for grain sizes of 180–212 and 90–212 μm, respectively. The latter uncertainties include those associated with the assumed Rb content of 400 ± 100 μg g^{-1} and the pIRIR signal-weighted K concentration of 12 ± 1% that we determined from measurements on individual grains of LB12-OSL3 (see Supplementary discussion above). It also accounts for variation in grain diameter within each of the selected size ranges, which we assumed to be Gaussian, giving mean grain sizes of 196 ± 8 and 151 ± 31 μm for the 180–212 and 90–212 μm fractions, respectively, with uncertainties that span the full size range at 2σ.

2.7.3 Supplementary table 2.3 – Equivalent doses and ages for IRSL and TL samples

	Sample code	Sector / depth (cm)	Procedure, signal [a]	Residual dose (Gy)	Equivalent dose (Gy) [b]	Over-dispersion (%) [c]	Fading rate (% per decade)	Age (kyr) [d]	
								Fading-uncorrected	Fading-corrected
IRSL samples	LB12-OSL1	XXI / 280	SA, pIRIR	4.9 ± 2.0	87 ± 8 (24)	33 ± 6	1.0 ± 0.3	62 ± 9	**67 ± 9**
	LB12-OSL2	XXI / 310	SA, pIRIR	7.6 ± 1.4	86 ± 14 (19)	29 ± 5	0.5 ± 0.6	59 ± 11	**64 ± 13**
	LB12-OSL3	XXI / 329	SA, pIRIR SG, pIRIR	5.3 ± 2.3	96 ± 11 (12) 84 ± 8 (41)	37 ± 9 43 ± 7	1.2 ± 1.4	56 ± 6	**60 ± 6**
	LB12-OSL4	XXI / 372	SA, pIRIR SG, pIRIR	7.8 ± 2.2	117 ± 9 (18) 100 ± 8 (19)	28 ± 6 26 ± 6		64 ± 6	**70 ± 7**
	LB12-OSL5	XXI / 410	SA, pIRIR	5.2 ± 1.3	98 ± 9 (17)	34 ± 7		57 ± 6	**62 ± 7**
	LB12-OSL6	XXI / 450	SA, pIRIR	5.4 ± 3.0	89 ± 5 (18)	17 ± 4	0.7 ± 0.9	60 ± 7	**66 ± 8**
	LB12-OSL7	XXI / 495	SA, pIRIR	7.0 ± 0.8	164 ± 12 (28)	33 ± 5	–0.7 ± 1.2	117 ± 15	**128 ± 17**
	LBS7-40a	VII / 485–490	SA, pIRIR SG, pIRIR		64 ± 8 (28) 78 ± 14 (14)	60 ± 9 64 ± 13		28 ± 3	**30 ± 4**
	LBS7-42a	VII / 593–598	SA, pIRIR SG, pIRIR		68 ± 13 (16) 144 ± 42 (9)	75 ± 14 88 ± 21		33 ± 8	**36 ± 9**
TL samples	LB08-15-3	XV / 573	DA, heat DA, light		191 ± 5 (12) 108 ± 7 (10)	0 8 ± 10		158 ± 8 **89 ± 7**	
	LB09-16-2	XVI / 640	DA, heat DA, light		134 ± 11 (1) 40 ± 13 (1)			76 ± 6 **23 ± 7**	
	LB12-23-3	XXIII / 295	DA, heat DA, light		246 ± 19 (1) 48 ± 10 (1)			304 ± 28 **59 ± 13**	
	LB12-23-4	XXIII / 347	DA, heat DA, light		273 ± 15 (1) 66 ± 18 (1)			300 ± 21 **73 ± 20**	
	LB12-23-2	XXIII / 410	DA, heat DA, light		292 ± 16 (1) 72 ± 17 (1)			281 ± 19 **69 ± 17**	
	LB12-23-1	XXIII / 490	DA, heat DA, light		176 ± 9 (12) 114 ± 8 (10)	13 ± 4 0		174 ± 11 **113 ± 9**	

[a] Measurement procedure used to estimate the equivalent dose (D_e): single-aliquot (**SA**), single-grain (**SG**) and dual-aliquot (**DA**) regenerative-dose procedures. Luminescence signal used for dating: **pIRIR**, post-infrared IRSL (290 °C); **heat**, heat-reset TL; **light**, light-sensitive TL.

[b] Weighted mean ± 1σ uncertainty, calculated using the central age model for all samples. Two high-D_e outliers were rejected from both the LB08-15-3 and LB12-23-1 data sets prior to running the model (see Supplementary discussion above). The numbers of aliquots or grains used for D_e determination are enclosed in parentheses, and a systematic error of 2% was added (in quadrature) to the propagated random errors to allow for any bias associated with calibration of the laboratory beta sources. The D_e values for samples LB12-OSL1 to -OSL7 are corrected for the measured residual doses in the adjacent (left-hand) column.

[c] Over-dispersion (OD) value ± 1σ uncertainty, calculated using the central age model. The OD represents the spread in D_e values remaining after taking measurement uncertainties into account (Galbraith and Roberts, 2012). The OD would be zero if 95% of the individual D_e values in each sample were consistent with a common D_e value at 2σ.

[d] Calculated as the central age model D_e divided by the total dose rate (see Supplementary table 2.2), with the uncertainty expressed at 1σ. The weighted mean of the 5 measured fading rates (0.9 ± 0.3%) was used to correct the IRSL ages for anomalous fading. The most reliable estimates of depositional age are highlighted in **bold**: the fading-corrected IRSL ages and the TL ages obtained from the light-sensitive signal. The IRSL ages for LB12-OSL3 and -OSL4 are based on the results from both the SA and SG measurements. The ages listed for samples

LBS7-40a and -42a are included for comparison with those reported in Morwood *et al*. (2004), but they are not considered reliable estimates of burial time for LB1 (see Supplementary discussion above). To determine the weighted mean age for different samples, each age was weighted by the inverse square of its standard error, which included only random sources of error; the total systematic error was added in quadrature afterwards.

2.8 Supplementary information section 2.3

2.8.1 Supplementary table 2.4 – Laser-ablation uranium-series dating of hominin bones

Laser-ablation uranium-series isotope analyses and dating results for bones of 1 modern human (132A/LB/IV/27D/03) and 3 specimens of *Homo floresiensis* (LB1/52, LB2/1 and LB6/3). All errors are at 2σ. Data are listed for every spot measured along each of 2–5 tracks across each cut section of bone (see Extended Data fig. 2.8 for photos of each sample). All tracks are from the interior to the exterior of the bones. Ages cannot be calculated for spot measurements with $^{230}Th/^{234}U$ ratios much greater than 1 and are accordingly left blank. Analyses with U/Th ratios of ≤ 300 (marked in red) and data points suspected of being affected by uranium leaching or secondary overprinting (marked in blue) were also not used to calculate the DAD model ages (shown in **bold**).

132A/LB/IV/27D/03		U (ppm)	Th (ppb)	U/Th	$^{230}Th/^{238}U$	$^{230}Th/^{238}U$ error	$^{234}U/^{238}U$	$^{234}U/^{238}U$ error	Age (kyr)	Age error
Track 1	1	18.0	14	1296	0.0606	0.0023	1.2729	0.0048	5.3	0.2
	2	11.7	13	928	0.0668	0.0024	1.2654	0.0061	5.9	0.2
	3	13.7	80	172	0.0927	0.0029	1.2728	0.0103	8.2	0.3
	4	18.2	16	1174	0.0614	0.0020	1.2660	0.0032	5.4	0.2
	5	19.3	15	1274	0.0666	0.0018	1.2652	0.0045	5.9	0.2
	6	23.0	3	7335	0.0655	0.0013	1.2657	0.0045	5.8	0.1
	7	25.1	9	2915	0.0658	0.0019	1.2677	0.0034	5.8	0.2
	8	26.1	3	9386	0.0664	0.0016	1.2538	0.0086	5.9	0.1
	9	24.4	4	5952	0.0683	0.0016	1.2673	0.0036	6.0	0.2
	10	26.6	6	4426	0.0698	0.0015	1.2651	0.0030	6.2	0.1
	11	33.4	3	12267	0.0642	0.0014	1.2730	0.0064	5.6	0.1
	12	27.2	1	18156	0.0707	0.0015	1.2579	0.0080	6.3	0.1
	13	27.4	3	8353	0.0700	0.0014	1.2688	0.0034	6.2	0.1
	14	26.8	2	13479	0.0719	0.0015	1.2660	0.0035	6.4	0.1
	15	25.5	14	1786	0.0758	0.0011	1.2668	0.0048	6.7	0.1
	16	22.4	2	12938	0.0795	0.0019	1.2613	0.0057	7.1	0.2
	17	22.8	2	9959	0.0765	0.0017	1.2631	0.0034	6.8	0.2
	18	25.1	3	7967	0.0887	0.0017	1.2692	0.0047	7.9	0.2
	19	24.5	5	5288	0.0851	0.0015	1.2727	0.0031	7.5	0.1
	20	23.7	11	2255	0.0837	0.0014	1.2693	0.0060	7.4	0.1
								DAD fit	**7.7**	**0.5**
Track 2	1	12.3	3	3844	0.0643	0.0037	1.2720	0.0141	5.7	0.3
	2	12.7	3	4349	0.0619	0.0028	1.2777	0.0067	5.4	0.3
	3	12.5	8	1598	0.0679	0.0026	1.2753	0.0084	6.0	0.2
	4	14.2	1	13855	0.0695	0.0033	1.2768	0.0072	6.1	0.3
	5	19.8	11	1825	0.0595	0.0020	1.2764	0.0060	5.2	0.2
	6	18.0	16	1116	0.0648	0.0030	1.2732	0.0109	5.7	0.3
	7	20.0	17	1195	0.0713	0.0026	1.2740	0.0050	6.3	0.2
	8	27.2	1	20592	0.0686	0.0019	1.2787	0.0042	6.0	0.2
	9	26.7	14	1857	0.0688	0.0021	1.2719	0.0141	6.1	0.2
	10	32.3	3	12082	0.0667	0.0024	1.2981	0.0151	5.7	0.2
	11	33.9	2	20865	0.0696	0.0025	1.2729	0.0028	6.1	0.2
	12	37.7	10	3922	0.0619	0.0017	1.2787	0.0090	5.4	0.2
	13	30.7	1	29412	0.0670	0.0025	1.2732	0.0076	5.9	0.2
	14	25.2	7	3499	0.0680	0.0032	1.2802	0.0130	5.9	0.3
	15	28.9	13	2301	0.0783	0.0025	1.2720	0.0074	6.9	0.2
	16	29.0	7	3918	0.0805	0.0020	1.2769	0.0063	7.1	0.2
	17	27.5	9	2950	0.0773	0.0032	1.2807	0.0057	6.8	0.3
	18	30.1	1	20878	0.0671	0.0031	1.2763	0.0037	5.9	0.3
	19	19.6	2	11341	0.0913	0.0044	1.2734	0.0061	8.1	0.4
	20	14.8	4	3458	0.0870	0.0051	1.2759	0.0106	7.7	0.5
								DAD fit	**7.4**	**0.5**

LB1/52		U (ppm)	Th (ppb)	U/Th	$^{230}Th/^{238}U$	$^{230}Th/^{238}U$ error	$^{234}U/^{238}U$	$^{234}U/^{238}U$ error	Age (kyr)	Age error
Track 1	1	25.1	1395	18	0.5408	0.0453	1.3901	0.0044	52.4	5.6
	2	38.4	213	181	0.8523	0.0060	1.3660	0.0036	100.8	1.2
	3	29.5	283	104	0.7263	0.0116	1.3569	0.0066	80.3	1.9
	4	26.2	343	76	0.6912	0.0111	1.3615	0.0029	74.5	1.7
	5	18.0	801	22	0.8054	0.0257	1.3480	0.0066	94.4	4.7
	6	32.0	14	2371	0.7205	0.0072	1.3652	0.0043	78.6	1.2
	7	16.0	1036	15	0.8435	0.0183	1.3540	0.0044	100.7	3.5
	8	41.1	27	1550	0.7460	0.0088	1.3624	0.0035	82.9	1.4
	9	35.8	5	7555	0.6830	0.0066	1.3552	0.0027	73.8	1.0
	10	27.6	17	1672	0.6471	0.0068	1.3621	0.0044	68.1	1.0
	11	31.0	10	3080	0.6452	0.0063	1.3548	0.0042	68.3	1.0
	12	27.9	2	12565	0.7268	0.0055	1.3656	0.0033	79.6	0.9
	13	9.9	29	338	1.1211	0.0128	1.3961	0.0062	156.3	4.0
								DAD fit	**79.0**	**3.7**
Track 2	1	15.2	1319	12	0.9831	0.0479	1.3572	0.0109	129.4	12.0
	2	16.9	1237	14	0.9232	0.0142	1.3535	0.0170	116.6	4.2
	3	1.8	1491	1	2.6753	0.3790	1.2959	0.0152		
	4	0.9	204	4	0.8756	0.0749	1.3361	0.0340	109.4	17.2
	5	11.1	532	21	0.8879	0.0366	1.3533	0.0109	109.3	7.7
	6	27.3	168	163	0.7469	0.0096	1.3645	0.0059	82.8	1.6
	7	1.7	930	2	1.9846	0.1580	1.2998	0.0244		
	8	25.3	135	187	0.7032	0.0156	1.3606	0.0113	76.4	2.6
	9	30.2	85	354	0.6905	0.0205	1.3598	0.0200	74.5	3.5
	10	32.6	6	5094	0.6414	0.0107	1.3650	0.0128	67.0	1.8
	11	37.6	6	6571	0.5918	0.0067	1.3561	0.0037	60.8	0.9
	12	31.0	4	8093	0.6720	0.0085	1.3762	0.0094	70.6	1.4
	13	10.8	11	1025	1.0250	0.0186	1.3841	0.0078	134.1	4.8
								DAD fit	**71.5**	**4.3**
Track 3	1	19.4	427	45	0.8694	0.0090	1.3513	0.0045	106.0	1.9
	2	6.9	2353	3	1.6032	0.0474	1.3383	0.0072		
	3	1.1	744	1	1.9951	0.2124	1.3068	0.0601		
	4	28.5	675	42	0.7907	0.0071	1.3548	0.0059	91.1	1.4
	5	12.8	1363	9	1.0655	0.0342	1.3498	0.0084	152.4	10.5
	6	34.9	51	688	0.6697	0.0107	1.3497	0.0038	72.3	1.6
	7	35.1	13	2643	0.8024	0.0060	1.3604	0.0062	92.5	1.3
	8	33.6	3	11851	0.6504	0.0071	1.3558	0.0026	69.0	1.0
	9	30.6	33	940	0.6343	0.0086	1.3537	0.0029	66.8	1.2
	10	29.5	2	16120	0.7828	0.0062	1.3618	0.0056	89.0	1.2
	11	6.8	41	165	1.1940	0.0161	1.3946	0.0063	179.4	6.0
								DAD fit	**86.9**	**7.9**

LB2/1		U (ppm)	Th (ppb)	U/Th	$^{230}Th/^{238}U$	$^{230}Th/^{238}U$ error	$^{234}U/^{238}U$	$^{234}U/^{238}U$ error	Age (kyr)	Age error
Track 1	1	56.8	28	2034	0.4436	0.0128	1.3253	0.0040	43.7	1.5
	2	58.6	4	13659	0.5979	0.0061	1.3142	0.0022	64.4	0.9
	3	43.8	2	19335	0.6080	0.0042	1.3104	0.0037	66.1	0.7
	4	57.7	2	32616	0.6198	0.0038	1.3129	0.0019	67.7	0.6
	5	58.8	1	61464	0.6147	0.0032	1.3136	0.0023	66.9	0.5
	6	57.3	2	37009	0.6224	0.0032	1.3063	0.0027	68.6	0.5
	7	51.6	5	11222	0.6060	0.0046	1.3086	0.0037	66.0	0.7
	8	52.8	15	3584	0.6424	0.0059	1.3125	0.0028	71.1	0.9
								DAD fit	**70.8**	**1.2**
Track 2	1	44.0	29	1501	0.5963	0.0082	1.3208	0.0041	63.7	1.2
	2	46.8	4	12391	0.6121	0.0126	1.3177	0.0069	66.2	1.9
	3	48.9	2	30015	0.6058	0.0056	1.3276	0.0056	64.6	0.9
	4	55.4	1	42103	0.6126	0.0035	1.3141	0.0048	66.6	0.6
	5	52.4	1	76115	0.5955	0.0040	1.3213	0.0037	63.6	0.6
	6	50.2	1	46785	0.5770	0.0112	1.3215	0.0077	61.0	1.6
	7	42.4	2	20440	0.5976	0.0208	1.3249	0.0078	63.7	3.0
	8	50.1	12	4166	0.5880	0.0127	1.3142	0.0037	63.0	1.8
								DAD fit	**66.7**	**0.8**
Track 3	1	28.0	584	48	0.5664	0.0101	1.3099	0.0029	60.3	1.4
	2	55.5	3	18645	0.6343	0.0025	1.3180	0.0064	69.5	0.6
	3	52.1	1	47357	0.6125	0.0046	1.3177	0.0034	66.3	0.7
	4	54.7	1	42271	0.6338	0.0042	1.3154	0.0021	69.6	0.7
	5	57.7	2	33613	0.6366	0.0042	1.3168	0.0024	69.9	0.6
	6	55.7	1	43911	0.6248	0.0034	1.3145	0.0058	68.3	0.7
	7	54.4	3	16019	0.6167	0.0035	1.3098	0.0026	67.5	0.5
	8	57.7	19	3108	0.6265	0.0086	1.3098	0.0020	68.9	1.3
								DAD fit	**71.4**	**1.1**
Track 4	1	56.1	16	3585	0.6021	0.0078	1.3152	0.0017	65.0	1.1
	2	54.5	6	8981	0.6355	0.0033	1.3195	0.0021	69.5	0.5
	3	52.4	1	52352	0.6214	0.0039	1.3241	0.0021	67.1	0.6
	4	54.8	1	58980	0.6349	0.0042	1.3199	0.0039	69.4	0.7
	5	54.7	1	53718	0.6211	0.0042	1.3219	0.0060	67.2	0.8
	6	52.4	1	36824	0.6073	0.0094	1.3135	0.0046	65.8	1.4
	7	54.2	3	18437	0.6182	0.0037	1.3144	0.0043	67.3	0.6
	8	54.9	15	3671	0.6422	0.0079	1.3117	0.0028	71.1	1.2
								DAD fit	**69.9**	**1.1**
Track 5	1	50.3	25	2044	0.5895	0.0052	1.3150	0.0019	63.2	0.8
	2	49.9	3	19862	0.6229	0.0040	1.3172	0.0039	67.8	0.7
	3	54.2	1	68895	0.6288	0.0050	1.3176	0.0021	68.7	0.8
	4	52.0	2	33547	0.6457	0.0035	1.3177	0.0022	71.2	0.6
	5	55.0	1	36695	0.6170	0.0052	1.3079	0.0084	67.7	1.0
	6	44.9	6	7561	0.6189	0.0043	1.3122	0.0028	67.6	0.7
	7	43.0	12	3513	0.5607	0.0029	1.3103	0.0023	59.5	0.4
								DAD fit	**70.6**	**1.7**

LB6/3		U (ppm)	Th (ppb)	U/Th	$^{230}Th/^{238}U$	$^{230}Th/^{238}U$ error	$^{234}U/^{238}U$	$^{234}U/^{238}U$ error	Age (kyr)	Age error
Track 1	1	48.9	33	1492	0.3805	0.0203	1.3490	0.0082	35.6	2.2
	2	38.2	8	4709	0.5198	0.0074	1.3636	0.0138	51.2	1.1
	3	51.4	10	5257	0.5453	0.0092	1.3448	0.0051	55.4	1.2
	4	58.4	2	31145	0.5735	0.0062	1.3458	0.0047	59.0	0.9
	5	40.7	1	35007	0.5442	0.0094	1.3538	0.0034	54.7	1.2
	6	26.1	1	47813	0.5500	0.0087	1.3698	0.0034	54.6	1.1
	7	18.2	1	14971	0.7205	0.0098	1.3691	0.0068	78.3	1.6
								DAD fit	**56.9**	**2.3**
Track 2	1	38.4	5	7842	0.5090	0.0116	1.3520	0.0038	50.4	1.4
	2	36.5	22	1651	0.5141	0.0065	1.3481	0.0034	51.3	0.8
	3	42.6	9	4574	0.5244	0.0105	1.3533	0.0038	52.3	1.3
	4	48.3	4	11112	0.5566	0.0070	1.3481	0.0062	56.7	1.0
	5	38.6	6	6684	0.5481	0.0077	1.3513	0.0046	55.4	1.0
	6	27.2	2	12491	0.4829	0.0112	1.3674	0.0066	46.6	1.4
	7	20.0	19	1055	0.6064	0.0169	1.3688	0.0083	62.0	2.3
	8	12.3	1	9065	0.7300	0.0240	1.3641	0.0065	80.2	3.9
								DAD fit	**54.6**	**2.1**
Track 3	1	42.0	4	10729	0.5619	0.0069	1.3475	0.0039	57.4	0.9
	2	32.2	22	1489	0.6076	0.0101	1.3511	0.0048	63.3	1.4
	3	42.5	1	35306	0.5655	0.0058	1.3431	0.0036	58.1	0.8
	4	53.3	5	10629	0.5641	0.0039	1.3475	0.0032	57.7	0.6
	5	33.8	1	60478	0.5510	0.0038	1.3463	0.0023	56.0	0.5
	6	36.7	1	55890	0.5234	0.0050	1.3491	0.0047	52.4	0.7
	7	18.9	3	6308	0.5910	0.0149	1.3656	0.0085	60.1	2.1
	8	21.4	40	532	0.6213	0.0084	1.3631	0.0033	64.4	1.2
								DAD fit	**66.0**	**4.3**
Track 4	1	44.0	21	2113	0.5765	0.0084	1.3520	0.0029	59.0	1.1
	2	52.4	2	34090	0.5595	0.0056	1.3415	0.0049	57.4	0.8
	3	45.8	1	56401	0.5709	0.0057	1.3458	0.0060	58.7	0.8
	4	38.1	1	46671	0.5715	0.0061	1.3540	0.0022	58.3	0.8
	5	27.6	33	838	0.6023	0.0080	1.3576	0.0095	62.2	1.2
	6	18.2	1	20163	0.5858	0.0132	1.3688	0.0032	59.3	1.7
	7	12.3	13	937	0.8004	0.0140	1.3755	0.0052	90.5	2.4
								DAD fit	**60.4**	**1.7**
Track 5	1	36.3	6	5827	0.5533	0.0072	1.3468	0.007	56.3	1
	2	42.4	5	8068	0.5497	0.0059	1.3431	0.0047	56	0.8
	3	40.1	1	65641	0.5685	0.0051	1.3561	0.0035	57.8	0.7
	4	33.9	1	37865	0.5935	0.0062	1.3555	0.0024	61.1	0.8
	5	30.2	1	38764	0.5800	0.0076	1.3607	0.0036	59	1
	6	21.8	2	8837	0.6220	0.0054	1.3701	0.0049	64	0.8
	7	15.8	80	196	0.8118	0.0083	1.3805	0.0027	91.9	1.4
								DAD fit	**61.2**	**2.3**

2.8.2 Supplementary table 2.5 – Laser-ablation uranium-series dating of Stegodon bones

Laser-ablation uranium-series isotope analyses and dating results for bones of 8 specimens of *Stegodon florensis insularis* from Sector XI. All errors are at 2σ. Data are listed for every spot measured along each pair of tracks (or a single track in the case of U-s-05/LB/XI/51/04) across each cut section of bone (see Extended Data fig. 2.9 for photos of each sample). All tracks are from the interior to the exterior of the bones. Analyses with U/Th ratios of ≤ 300 (marked in red) and data points suspected of being affected by uranium leaching or secondary overprinting (marked in blue) were not used to calculate the DAD model ages (shown in **bold**).

U-s-01/ LB/XI/ 32/04		U (ppm)	Th (ppb)	U/Th	$^{230}Th/^{238}U$	$^{230}Th/^{238}U$ error	$^{234}U/^{238}U$	$^{234}U/^{238}U$ error	Age (kyr)	Age error
Track 1	1	15.8	53	300	0.4651	0.0106	1.3113	0.0032	46.9	1.3
	2	32.4	30	1096	0.3940	0.0105	1.3101	0.0029	38.5	1.2
	3	20.2	33	606	0.4049	0.0060	1.3056	0.0050	39.9	0.7
	4	19.1	101	189	0.3534	0.0096	1.3132	0.0044	33.8	1.1
	5	26.2	37	708	0.3975	0.0093	1.3145	0.0023	38.7	1.1
	6	24.0	44	539	0.3828	0.0084	1.3107	0.0030	37.2	1.0
	7	23.0	25	920	0.3778	0.0096	1.3188	0.0042	36.3	1.1
	8	22.6	105	215	0.4147	0.0080	1.3071	0.0050	41.0	1.0
	9	11.1	287	39	0.5390	0.0109	1.3100	0.0049	56.5	1.5
	10	18.7	145	129	0.4338	0.0055	1.3058	0.0053	43.3	0.7
	11	24.1	88	273	0.5041	0.0079	1.3140	0.0042	51.7	1.0
	12	14.1	147	96	0.5111	0.0093	1.3168	0.0064	52.5	1.3
	13	24.9	15	1708	0.4459	0.0086	1.3155	0.0048	44.4	1.1
	14	22.3	8	2904	0.4673	0.0056	1.3165	0.0051	47.0	0.7
	15	17.6	5	3237	0.5320	0.0087	1.3193	0.0076	55.1	1.2
								DAD fit	**55.3**	**4.2**
Track 2	1	20.0	22	893	0.4869	0.0142	1.3122	0.0042	49.6	1.8
	2	26.3	11	2341	0.4978	0.0078	1.3098	0.0024	51.1	1.0
	3	18.5	29	632	0.4792	0.0065	1.3045	0.0089	49.0	0.9
	4	21.1	58	362	0.5030	0.0066	1.3126	0.0031	51.7	0.9
	5	20.4	30	683	0.4063	0.0079	1.3116	0.0043	39.8	0.9
	6	19.8	72	275	0.5081	0.0090	1.3123	0.0039	52.3	1.2
	7	15.7	43	367	0.4203	0.0060	1.3144	0.0041	41.4	0.7
	8	20.1	95	212	0.4701	0.0051	1.3130	0.0031	47.5	0.7
	9	20.6	44	467	0.4614	0.0119	1.3142	0.0022	46.3	1.5
	10	22.4	32	690	0.4326	0.0056	1.3088	0.0042	43.1	0.7
	11	21.2	35	599	0.5303	0.0089	1.3169	0.0030	55.0	1.2
	12	29.0	5	6182	0.5366	0.0086	1.3065	0.0042	56.4	1.2
	13	22.8	26	874	0.5194	0.0085	1.3163	0.0030	53.6	1.1
	14	28.4	14	1975	0.5030	0.0074	1.3149	0.0028	51.5	1.0
	15	16.0	69	232	0.5603	0.0089	1.3188	0.0091	58.9	1.3
								DAD fit	**59.9**	**5.4**

U-s-02/ LB/XI/ 45/04		U (ppm)	Th (ppb)	U/Th	$^{230}Th/^{238}U$	$^{230}Th/^{238}U$ error	$^{234}U/^{238}U$	$^{234}U/^{238}U$ error	Age (kyr)	Age error
Track 1	1	15.6	17	907	0.366	0.015	1.344	0.0128	34.2	1.7
	2	12.6	10	1204	0.483	0.015	1.339	0.0045	47.9	1.8
	3	13.9	8	1806	0.438	0.013	1.348	0.0090	42.1	1.5
	4	12.5	6	1937	0.431	0.011	1.338	0.0047	41.7	1.3
	5	13.4	6	2248	0.409	0.010	1.333	0.0054	39.3	1.1
	6	11.0	3	3205	0.472	0.012	1.344	0.0096	46.3	1.5
	7	11.6	4	2871	0.547	0.011	1.335	0.0060	56.2	1.5
	8	12.9	4	3418	0.522	0.010	1.336	0.0063	52.9	1.4
	9	10.4	3	2999	0.458	0.011	1.337	0.0055	44.9	1.3
	10	9.0	22	406	0.535	0.011	1.335	0.0052	54.6	1.5
	11	13.7	5	2492	0.448	0.013	1.329	0.0043	44.0	1.6
	12	13.6	5	2668	0.508	0.010	1.335	0.0063	51.2	1.2
	13	11.6	2	5469	0.489	0.011	1.327	0.0041	49.2	1.4
	14	12.8	5	2370	0.477	0.009	1.321	0.0049	47.9	1.1
	15	11.8	9	1382	0.431	0.012	1.328	0.0054	42.1	1.5
	16	13.8	4	3202	0.392	0.011	1.331	0.0050	37.6	1.3
	17	10.4	4	2581	0.413	0.010	1.330	0.0046	39.9	1.1
								DAD fit	**47.4**	**2.3**
Track 2	1	9.2	213	43	0.622	0.018	1.338	0.0062	66.2	2.6
	2	1.3	47	29	0.561	0.037	1.361	0.0266	56.6	5.1
	3	0.9	239	4	1.093	0.088	1.306	0.0436	173.9	40.1
	4	9.0	157	57	0.653	0.011	1.347	0.0053	70.1	1.6
	5	14.0	13	1064	0.478	0.020	1.342	0.0043	47.1	2.4
	6	15.3	80	191	0.394	0.011	1.323	0.0059	38.0	1.3
	7	14.5	103	140	0.467	0.008	1.337	0.0053	46.0	1.0
	8	11.3	6	2005	0.466	0.008	1.335	0.0047	46.0	0.9
	9	13.0	10	1292	0.447	0.012	1.339	0.0036	43.6	1.5
	10	10.6	5	2104	0.512	0.008	1.338	0.0050	51.5	1.1
	11	9.6	16	616	0.503	0.015	1.349	0.0075	49.9	1.9
	12	9.9	6	1570	0.446	0.014	1.325	0.0080	44.0	1.7
	13	8.9	3	3180	0.456	0.012	1.329	0.0082	45.1	1.5
	14	10.2	1	6814	0.375	0.009	1.322	0.0067	35.9	1.1
	15	10.5	1	8590	0.407	0.008	1.330	0.0041	39.2	1.0
	16	10.6	3	3459	0.459	0.010	1.325	0.0046	45.5	1.2
								DAD fit	**45.1**	**2.6**

U-s-03/ LB/XI/ 47/04		U (ppm)	Th (ppb)	U/Th	$^{230}Th/^{238}U$	$^{230}Th/^{238}U$ error	$^{234}U/^{238}U$	$^{234}U/^{238}U$ error	Age (kyr)	Age error
Track 1	1	51.3	2	28803	0.5151	0.0052	1.3146	0.0045	53.1	0.7
	2	29.6	0	78573	0.4758	0.0083	1.3033	0.0056	48.6	1.1
	3	39.4	1	40100	0.4671	0.0084	1.3119	0.0048	47.2	1.1
	4	47.2	2	25712	0.4962	0.0065	1.3035	0.0055	51.3	0.9
	5	49.2	2	26874	0.4673	0.0053	1.3122	0.0059	47.2	0.7
	6	52.6	2	33220	0.4674	0.0070	1.3102	0.0069	47.3	0.9
	7	51.0	2	31615	0.4655	0.0065	1.3050	0.0050	47.3	0.8
	8	46.1	2	26241	0.4619	0.0071	1.3074	0.0054	46.7	0.9
	9	52.6	2	25865	0.4641	0.0075	1.3005	0.0057	47.3	1.0
	10	49.9	1	81937	0.4770	0.0080	1.3050	0.0062	48.7	1.1
	11	45.3	2	25137	0.4612	0.0067	1.3087	0.0049	46.6	0.9
	12	52.4	1	39472	0.4796	0.0055	1.2985	0.0051	49.4	0.7
	13	52.5	3	18738	0.4784	0.0068	1.3093	0.0060	48.7	0.9
	14	49.0	3	14640	0.4749	0.0069	1.3084	0.0041	48.3	0.9
	15	43.6	2	20111	0.4471	0.0066	1.3038	0.0044	45.1	0.8
	16	52.1	3	20331	0.4570	0.0067	1.3070	0.0046	46.1	0.9
	17	48.7	2	22504	0.4395	0.0070	1.3031	0.0060	44.2	0.9
	18	47.9	3	18745	0.4398	0.0095	1.3028	0.0045	44.2	1.2
	19	49.4	3	14532	0.4459	0.0076	1.3060	0.0044	44.8	0.9
	20	49.1	6	8806	0.4304	0.0061	1.3002	0.0053	43.2	0.8
	21	51.9	2	27387	0.4519	0.0084	1.3036	0.0038	45.7	1.1
	22	51.6	3	16077	0.4370	0.0061	1.3059	0.0036	43.7	0.8
	23	49.4	4	13888	0.4371	0.0079	1.3077	0.0048	43.7	1.0
	24	44.6	16	2832	0.4252	0.0071	1.3011	0.0042	42.5	0.9
	25	47.0	3	15608	0.4246	0.0085	1.3083	0.0035	42.1	1.0
	26	46.6	2	22928	0.4176	0.0084	1.3012	0.0050	41.6	1.0
	27	45.0	3	16195	0.4183	0.0077	1.3022	0.0050	41.6	0.9
	28	41.4	2	21478	0.4057	0.0079	1.3092	0.0061	39.9	1.0
	29	30.7	4	8211	0.3942	0.0093	1.3056	0.0055	38.7	1.1
	30	34.7	14	2535	0.4458	0.0069	1.3064	0.0053	44.8	0.9
								DAD fit	**53.1**	**1.2**
Track 2	1	48.3	3	14397	0.4711	0.0073	1.3055	0.0070	48.0	1.0
	2	36.8	0	167199	0.4830	0.0107	1.3057	0.0049	49.4	1.4
	3	36.4	2	16574	0.4657	0.0060	1.3088	0.0065	47.1	0.8
	4	47.3	2	29534	0.4833	0.0074	1.3141	0.0045	49.1	1.0
	5	48.3	3	17594	0.4721	0.0082	1.3036	0.0080	48.2	1.1
	6	49.4	2	26285	0.4722	0.0080	1.3132	0.0058	47.7	1.0
	7	50.6	1	43024	0.4668	0.0066	1.3060	0.0053	47.4	0.9
	8	52.0	2	29515	0.4675	0.0076	1.3105	0.0051	47.3	1.0
	9	52.1	1	46480	0.4634	0.0088	1.3097	0.0044	46.8	1.1
	10	49.3	0	126916	0.4627	0.0081	1.3071	0.0041	46.8	1.0
	11	50.4	1	98336	0.4483	0.0069	1.3066	0.0043	45.1	0.9
	12	42.3	0	151291	0.4691	0.0064	1.3084	0.0064	47.6	0.9
	13	51.3	1	48537	0.4751	0.0063	1.3100	0.0047	48.2	0.8
	14	48.1	0	114019	0.4431	0.0075	1.2985	0.0044	44.8	0.9
	15	46.9	1	72792	0.4492	0.0079	1.3050	0.0052	45.3	1.0
	16	38.4	1	64732	0.4678	0.0097	1.3083	0.0052	47.4	1.2
	17	40.7	2	24935	0.4618	0.0097	1.3048	0.0047	46.8	1.2
	18	41.1	0	85723	0.4484	0.0058	1.3036	0.0036	45.2	0.7
	19	46.9	1	50405	0.4448	0.0063	1.3061	0.0049	44.7	0.8
	20	43.0	2	21432	0.4380	0.0081	1.3086	0.0043	43.7	1.0
	21	37.9	1	45244	0.4105	0.0093	1.3032	0.0052	40.7	1.1
	22	39.9	1	33496	0.4136	0.0078	1.3027	0.0039	41.1	0.9
	23	39.4	1	35193	0.4499	0.0097	1.3046	0.0038	45.4	1.2
	24	37.7	1	29133	0.3899	0.0085	1.3028	0.0046	38.3	1.0
	25	40.1	1	28917	0.4187	0.0111	1.3080	0.0055	41.4	1.3
	26	40.5	1	43624	0.4225	0.0081	1.2992	0.0044	42.3	1.0
	27	42.3	1	62104	0.4236	0.0080	1.3039	0.0043	42.2	1.0
	28	41.0	0	118676	0.4146	0.0084	1.3014	0.0039	41.2	1.0
	29	34.9	1	46063	0.4164	0.0072	1.3061	0.0047	41.3	0.9
	30	28.5	2	15935	0.4208	0.0092	1.3071	0.0053	41.7	1.1
								DAD fit	**47.2**	**0.8**

	U-s-04/ LB/XI/ 49/04	U (ppm)	Th (ppb)	U/Th	$^{230}Th/^{238}U$	$^{230}Th/^{238}U$ error	$^{234}U/^{238}U$	$^{234}U/^{238}U$ error	Age (kyr)	Age error
Track 1	1	70.6	60	1185	0.4200	0.0169	1.3253	0.0121	40.9	2.0
	2	30.3	109	279	0.6373	0.0118	1.3375	0.0116	68.4	1.9
	3	71.1	53	1351	0.4510	0.0182	1.3392	0.0074	44.0	2.2
	4	94.9	26	3581	0.5090	0.0136	1.3442	0.0080	50.8	1.7
	5	85.5	12	7120	0.5376	0.0115	1.3332	0.0028	55.0	1.5
	6	80.8	8	9962	0.5696	0.0109	1.3272	0.0062	59.6	1.5
	7	60.7	18	3365	0.5605	0.0126	1.3249	0.0060	58.5	1.8
	8	62.5	11	5483	0.6328	0.0071	1.3348	0.0036	68.0	1.1
	9	71.7	8	9206	0.5282	0.0131	1.3318	0.0030	53.9	1.7
	10	46.7	5	8781	0.6228	0.0091	1.3417	0.0035	66.1	1.3
	11	52.1	19	2778	0.5657	0.0095	1.3384	0.0033	58.4	1.3
	12	52.9	11	4804	0.5553	0.0105	1.3378	0.0034	57.1	1.4
	13	44.6	12	3779	0.6297	0.0073	1.3369	0.0050	67.4	1.1
	14	34.0	22	1558	0.5788	0.0094	1.3453	0.0076	59.8	1.4
	15	37.5	110	339	0.6528	0.0073	1.3473	0.0071	70.0	1.2
								DAD fit	**73.7**	**5.1**
Track 2	1	71.8	144	497	0.4589	0.0242	1.3395	0.0043	44.9	2.9
	2	67.3	20	3393	0.6110	0.0086	1.3393	0.0040	64.6	1.2
	3	74.2	5	14285	0.5794	0.0120	1.3324	0.0032	60.6	1.7
	4	63.5	9	7404	0.5720	0.0128	1.3327	0.0039	59.6	1.8
	5	54.8	34	1592	0.6070	0.0103	1.3361	0.0037	64.2	1.5
	6	72.8	5	14061	0.5935	0.0084	1.3334	0.0033	62.5	1.2
	7	67.4	3	20936	0.5308	0.0122	1.3392	0.0037	53.8	1.6
	8	39.4	12	3231	0.6786	0.0070	1.3273	0.0039	75.4	1.1
	9	39.7	4	9707	0.6735	0.0089	1.3371	0.0039	73.8	1.4
	10	36.5	9	3844	0.6095	0.0100	1.3336	0.0054	64.7	1.5
	11	52.4	12	4437	0.5974	0.0125	1.3427	0.0048	62.4	1.8
	12	39.6	25	1607	0.5852	0.0130	1.3426	0.0044	60.8	1.8
	13	34.6	13	2643	0.5922	0.0082	1.3479	0.0046	61.4	1.2
	14	41.9	3	14297	0.5919	0.0106	1.3404	0.0046	61.8	1.5
								DAD fit	**67.0**	**2.4**

U-s-05/ LB/XI/ 51/04		U (ppm)	Th (ppb)	U/Th	$^{230}Th/^{238}U$	$^{230}Th/^{238}U$ error	$^{234}U/^{238}U$	$^{234}U/^{238}U$ error	Age (kyr)	Age error
Track 1	1	10.6	29	362	0.2563	0.0153	1.3090	0.0071	23.6	1.6
	2	16.6	15	1116	0.2362	0.0107	1.3053	0.0040	21.6	1.1
	3	12.7	2	5700	0.3257	0.0057	1.2993	0.0063	31.2	0.7
	4	16.1	3	4946	0.2481	0.0111	1.3045	0.0036	22.8	1.1
	5	15.5	26	601	0.2529	0.0106	1.3069	0.0040	23.3	1.1
	6	15.7	4	3985	0.3181	0.0050	1.2988	0.0048	30.3	0.6
	7	14.7	7	1996	0.3107	0.0089	1.3084	0.0051	29.3	1.0
	8	17.5	2	9304	0.2776	0.0084	1.3041	0.0044	25.9	0.9
	9	13.0	9	1473	0.2866	0.0085	1.2941	0.0046	27.1	0.9
	10	15.6	12	1289	0.3372	0.0061	1.3068	0.0059	32.2	0.7
	11	17.4	10	1725	0.2838	0.0119	1.3092	0.0039	26.4	1.3
	12	19.2	10	1852	0.2501	0.0067	1.3026	0.0050	23.1	0.7
	13	22.2	21	1075	0.2992	0.0061	1.3087	0.0036	28.1	0.7
	14	24.8	5	5132	0.3174	0.0077	1.3121	0.0052	29.9	0.8
	15	27.1	5	5557	0.2993	0.0063	1.2981	0.0034	28.3	0.7
	16	22.9	4	5267	0.2891	0.0080	1.3051	0.0043	27.1	0.9
	17	25.5	5	4678	0.2934	0.0106	1.3014	0.0032	27.6	1.1
	18	20.6	3	7717	0.3044	0.0073	1.3007	0.0032	28.8	0.8
	19	26.1	4	6320	0.2955	0.0053	1.3027	0.0038	27.8	0.6
	20	27.0	38	718	0.2542	0.0095	1.3060	0.0034	23.4	1.0
	21	23.5	16	1464	0.3302	0.0047	1.3040	0.0045	31.5	0.5
	22	18.7	2	9223	0.3161	0.0064	1.3030	0.0039	30.0	0.7
	23	27.8	4	6383	0.3313	0.0089	1.2972	0.0075	31.8	1.0
	24	27.4	1	24869	0.3398	0.0074	1.3060	0.0058	32.5	0.8
	25	23.4	2	10011	0.3201	0.0075	1.3125	0.0029	30.2	0.8
	26	22.9	4	5924	0.3102	0.0071	1.3073	0.0044	29.3	0.8
	27	25.0	4	5810	0.3656	0.0072	1.3060	0.0033	35.4	0.8
	28	25.1	2	13842	0.3522	0.0069	1.3144	0.0063	33.6	0.8
	29	28.1	6	5061	0.3796	0.0057	1.3043	0.0026	37.0	0.7
	30	31.6	2	18569	0.3558	0.0061	1.2964	0.0029	34.6	0.7
	31	33.4	2	13657	0.3804	0.0063	1.2982	0.0030	37.3	0.7
	32	24.6	4	5487	0.4057	0.0057	1.3003	0.0031	40.2	0.7
	33	21.7	1	15988	0.4248	0.0067	1.3123	0.0032	42.0	0.8
	34	19.3	5	3785	0.4739	0.0078	1.3087	0.0050	48.2	1.0
	35	16.4	22	747	0.4838	0.0066	1.3144	0.0030	49.1	0.8
								DAD fit	**40.5**	**2.0**

	U-s-06/ LB/XI/ 52/04	U (ppm)	Th (ppb)	U/Th	$^{230}Th/^{238}U$	$^{230}Th/^{238}U$ error	$^{234}U/^{238}U$	$^{234}U/^{238}U$ error	Age (kyr)	Age error
Track 1	1	17.8	428	42	0.3424	0.0261	1.3750	0.0375	30.8	2.9
	2	37.2	203	183	0.3864	0.0132	1.3157	0.0127	37.4	1.6
	3	19.0	97	197	0.5532	0.0174	1.3359	0.0077	56.9	2.4
	4	15.4	120	129	0.5137	0.0103	1.3312	0.0085	52.1	1.4
	5	37.2	39	947	0.4522	0.0132	1.3299	0.0023	44.5	1.6
	6	32.9	47	700	0.5287	0.0112	1.3351	0.0089	53.8	1.5
	7	24.2	18	1375	0.5731	0.0106	1.3366	0.0048	59.5	1.5
	8	24.9	19	1276	0.5431	0.0109	1.3316	0.0034	55.8	1.5
	9	32.6	13	2444	0.5359	0.0081	1.3193	0.0026	55.6	1.1
	10	31.4	7	4729	0.6162	0.0078	1.3211	0.0033	66.6	1.2
	11	37.9	9	4063	0.6353	0.0067	1.3203	0.0023	69.4	1.0
	12	38.4	7	5296	0.6814	0.0075	1.3166	0.0026	76.8	1.2
								DAD fit	**78.8**	**7.0**
Track 2	1	5.8	297	20	0.7719	0.0330	1.3271	0.0096	90.9	6.0
	2	13.4	378	35	0.7177	0.0173	1.3381	0.0064	80.7	2.9
	3	13.5	337	40	0.5213	0.0372	1.3283	0.0072	53.2	4.9
	4	17.5	18	955	0.4624	0.0066	1.3333	0.0066	45.6	0.8
	5	18.5	19	990	0.5751	0.0112	1.3303	0.0056	60.2	1.6
	6	24.0	7	3589	0.5599	0.0070	1.3308	0.0051	58.1	1.0
	7	24.6	56	439	0.6296	0.0115	1.3262	0.0056	68.1	1.7
	8	28.1	7	4125	0.5823	0.0081	1.3226	0.0080	61.7	1.2
	9	30.2	10	3003	0.6209	0.0145	1.3202	0.0083	67.3	2.2
	10	37.6	10	3719	0.6635	0.0089	1.3205	0.0029	73.7	1.4
								DAD fit	**80.6**	**11.3**

	U-s-07/ LB/XI/ 65/04	U (ppm)	Th (ppb)	U/Th	$^{230}Th/^{238}U$	$^{230}Th/^{238}U$ error	$^{234}U/^{238}U$	$^{234}U/^{238}U$ error	Age (kyr)	Age error
Track 1	1	157.8	48	3274	0.4244	0.0064	1.3516	0.0060	40.4	0.8
	2	92.4	122	756	0.4821	0.0108	1.3484	0.0035	47.3	1.3
	3	59.9	333	180	0.5461	0.0089	1.3578	0.0056	54.8	1.2
	4	106.6	122	870	0.4666	0.0076	1.3584	0.0035	45.0	0.9
	5	99.2	27	3654	0.5426	0.0059	1.3619	0.0034	54.1	0.8
	6	74.2	41	1812	0.4529	0.0114	1.3664	0.0037	43.1	1.3
	7	115.5	31	3755	0.4962	0.0061	1.3644	0.0021	48.3	0.7
	8	101.4	62	1633	0.5444	0.0055	1.3693	0.0029	53.9	0.7
	9	95.7	56	1719	0.5494	0.0073	1.3649	0.0021	54.8	0.9
	10	91.3	103	882	0.5382	0.0037	1.3630	0.0032	53.5	0.5
	11	107.4	10	11135	0.5288	0.0065	1.3611	0.0020	52.4	0.8
	12	97.1	47	2073	0.5462	0.0044	1.3554	0.0027	54.9	0.6
	13	97.4	68	1438	0.5220	0.0043	1.3580	0.0027	51.7	0.5
	14	108.3	91	1188	0.5299	0.0079	1.3509	0.0023	53.1	1.0
	15	132.8	32	4142	0.5018	0.0032	1.3415	0.0040	50.0	0.4
	16	127.5	50	2538	0.4779	0.0040	1.3420	0.0039	47.1	0.5
	17	85.8	24	3513	0.4355	0.0041	1.3351	0.0032	42.4	0.5
	18	117.5	106	1113	0.4642	0.0069	1.3276	0.0080	46.1	0.9
	19	108.9	24	4576	0.4299	0.0041	1.3379	0.0064	41.6	0.5
								DAD fit	**49.8**	**1.9**
Track 2	1	98.8	18	5512	0.5078	0.0107	1.3596	0.0037	49.9	1.3
	2	74.2	164	452	0.5099	0.0129	1.3639	0.0035	50.0	1.6
	3	72.0	67	1080	0.4780	0.0057	1.3579	0.0166	46.4	1.0
	4	78.6	53	1485	0.4865	0.0129	1.3662	0.0075	47.1	1.6
	5	67.0	281	239	0.6278	0.0083	1.3572	0.0091	65.7	1.3
	6	78.2	299	261	0.4995	0.0051	1.3668	0.0033	48.6	0.6
	7	88.1	12	7204	0.4986	0.0104	1.3626	0.0117	48.7	1.4
	8	77.1	5	17031	0.5148	0.0083	1.3645	0.0036	50.5	1.0
	9	95.0	7	14263	0.5382	0.0106	1.3693	0.0136	53.2	1.5
	10	89.1	63	1410	0.5251	0.0058	1.3621	0.0035	51.9	0.7
	11	78.2	27	2880	0.4642	0.0078	1.3659	0.0056	44.4	0.9
	12	86.3	48	1804	0.5022	0.0080	1.3588	0.0045	49.3	1.0
	13	75.0	16	4752	0.4725	0.0126	1.3631	0.0044	45.5	1.5
	14	86.6	16	5519	0.5361	0.0065	1.3676	0.0155	53.0	1.1
	15	94.6	11	8784	0.5325	0.0095	1.3747	0.0077	52.2	1.2
	16	96.1	107	895	0.4569	0.0071	1.3557	0.0049	44.0	0.9
	17	64.2	96	669	0.4086	0.0097	1.3629	0.0286	38.3	1.5
	18	104.3	80	1300	0.4361	0.0105	1.3466	0.0071	42.0	1.2
	19	111.9	65	1711	0.4609	0.0070	1.3421	0.0097	45.1	0.9
								DAD fit	**49.0**	**1.5**

	U-s-08/ LB/XI/ 65B/04	U (ppm)	Th (ppb)	U/Th	$^{230}Th/^{238}U$	$^{230}Th/^{238}U$ error	$^{234}U/^{238}U$	$^{234}U/^{238}U$ error	Age (kyr)	Age error
Track 1	1	44.0	55	802	0.3554	0.0103	1.3627	0.0036	32.5	1.1
	2	48.7	19	2602	0.3879	0.0065	1.3579	0.0035	36.2	0.7
	3	43.1	71	603	0.3531	0.0058	1.3624	0.0082	32.3	0.7
	4	40.6	107	381	0.2907	0.0063	1.3566	0.0029	26.0	0.6
	5	50.0	61	822	0.3843	0.0083	1.3561	0.0022	35.8	0.9
	6	58.5	16	3728	0.4014	0.0040	1.3505	0.0055	37.9	0.5
	7	54.2	18	3066	0.4198	0.0039	1.3521	0.0037	39.9	0.5
	8	52.1	19	2729	0.4387	0.0049	1.3562	0.0016	41.9	0.6
	9	44.7	31	1447	0.4331	0.0061	1.3515	0.0042	41.4	0.7
	10	61.6	9	6483	0.4104	0.0066	1.3562	0.0020	38.7	0.7
	11	60.5	19	3257	0.4259	0.0054	1.3505	0.0022	40.6	0.6
	12	59.7	12	5126	0.3901	0.0041	1.3551	0.0019	36.5	0.4
	13	66.5	9	7433	0.4184	0.0041	1.3543	0.0016	39.7	0.5
	14	61.0	8	7303	0.4409	0.0038	1.3541	0.0044	42.2	0.5
	15	68.4	5	13381	0.4512	0.0027	1.3555	0.0024	43.4	0.3
	16	83.1	12	7219	0.4997	0.0032	1.3570	0.0038	49.1	0.4
	17	73.2	10	7518	0.5112	0.0039	1.3632	0.0050	50.1	0.5
	18	61.5	8	7553	0.5096	0.0040	1.3688	0.0067	49.7	0.6
	19	56.4	13	4370	0.4802	0.0041	1.3602	0.0019	46.6	0.5
	20	57.2	21	2686	0.5229	0.0034	1.3651	0.0021	51.5	0.4
								DAD fit	**54.8**	**2.3**
Track 2	1	40.5	12	3374	0.4512	0.0068	1.3746	0.0100	42.6	0.9
	2	35.1	29	1221	0.4044	0.0033	1.3668	0.0031	37.7	0.4
	3	38.1	35	1104	0.3912	0.0082	1.3604	0.0030	36.4	0.9
	4	39.2	54	728	0.4111	0.0090	1.3823	0.0183	37.9	1.2
	5	55.7	24	2324	0.4005	0.0068	1.3663	0.0061	37.3	0.8
	6	49.5	31	1582	0.4027	0.0058	1.3685	0.0110	37.4	0.7
	7	47.2	15	3206	0.3870	0.0040	1.3656	0.0046	35.8	0.5
	8	45.3	32	1409	0.4372	0.0084	1.3620	0.0024	41.5	1.0
	9	50.9	3	14646	0.4262	0.0031	1.3667	0.0037	40.1	0.4
	10	56.6	10	5705	0.4402	0.0052	1.3631	0.0058	41.8	0.6
	11	62.6	11	5934	0.4199	0.0077	1.3489	0.0139	40.0	1.0
	12	60.7	9	6996	0.4358	0.0060	1.3547	0.0028	41.6	0.7
	13	54.7	17	3309	0.4594	0.0069	1.3693	0.0039	43.8	0.8
	14	59.3	23	2596	0.4874	0.0062	1.3638	0.0027	47.3	0.8
	15	64.2	5	12101	0.4770	0.0055	1.3650	0.0031	46.0	0.7
	16	61.8	7	8973	0.4872	0.0043	1.3690	0.0044	47.0	0.5
	17	67.5	34	1989	0.4866	0.0079	1.3684	0.0032	47.0	0.9
	18	76.9	9	8702	0.4949	0.0049	1.3651	0.0035	48.1	0.6
	19	64.5	10	6575	0.4893	0.0087	1.3580	0.0095	47.7	1.1
	20	66.0	28	2355	0.4681	0.0045	1.3639	0.0070	45.0	0.6
								DAD fit	**51.0**	**2.0**

2.9 Supplementary information section 2.4

2.9.1 Supplementary table 2.6 – Uranium-series dating of speleothems

Uranium (^{238}U, ^{234}U) and thorium (^{232}Th, ^{230}Th) isotopic analyses and $^{230}Th/^{234}U$ ages for *in situ* calcitic flowstones and a small stalagmite (LB/S.XXI 10-01 and -01R). The corrected ages listed in the far right-hand column are considered the most accurate. All uncertainties are expressed at 2σ.

Sample code [a]	Sector / depth (cm)	U (ppm)	^{232}Th (ppb)	$^{230}Th/^{232}Th$	$^{230}Th/^{238}U$	$^{234}U/^{238}U$	Uncorrected age (kyr)	Corrected initial $^{234}U/^{238}U$	Corrected age (kyr)
LB07-SXII-F1	XII / 245–255	0.05210 ± 0.00010	1.102 ± 0.007	54.77 ± 0.44	0.382 ± 0.002	1.033 ± 0.002	50.2 ± 0.4	1.038 ± 0.003	49.6 ± 0.5
LB-S.XXI 5 #08	XXI / 255–260	0.09635 ± 0.00004	0.053 ± 0.001	2250 ± 14	0.404 ± 0.001	1.026 ± 0.001	54.6 ± 0.2	1.030 ± 0.001	54.6 ± 0.2
LB-S.XXI 8-T #09	XXI / 255–260	0.08685 ± 0.00003	0.830 ± 0.001	128.16 ± 0.55	0.404 ± 0.002	1.023 ± 0.001	54.7 ± 0.3	1.027 ± 0.001	54.4 ± 0.3
LB-S.XXI 8-B #10	XXI / 255–260	0.08339 ± 0.00003	0.407 ± 0.001	252.41 ± 0.94	0.406 ± 0.001	1.028 ± 0.001	54.7 ± 0.3	1.033 ± 0.001	54.6 ± 0.3
LB/S.XXI 10-01R	XXI / tip of stalagmite	0.28140 ± 0.00013	7.335 ± 0.014	53.57 ± 0.23	0.460 ± 0.002	1.027 ± 0.002	64.7 ± 0.4	1.033 ± 0.003	64.0 ± 0.5
LB/S.XXI 10-01	XXI / top of stalagmite	0.33919 ± 0.00016	1.049 ± 0.005	459.1 ± 2.6	0.468 ± 0.002	1.027 ± 0.001	66.2 ± 0.3	1.033 ± 0.001	66.1 ± 0.3
LB07-SXII-F4	XII / 482	0.27760 ± 0.00020	6.288 ± 0.032	57.78 ± 0.38	0.431 ± 0.002	1.031 ± 0.002	58.9 ± 0.4	1.037 ± 0.002	58.3 ± 0.5
LB09-SXVII-F1	XVII / 583	0.10263 ± 0.00013	2.609 ± 0.008	64.23 ± 0.48	0.538 ± 0.003	1.017 ± 0.002	81.5 ± 0.7	1.022 ± 0.003	80.8 ± 0.8
LB09-SXVII-F2	XVII / 565	0.12253 ± 0.00016	1.043 ± 0.005	175.6 ± 1.6	0.492 ± 0.003	1.023 ± 0.002	71.1 ± 0.6	1.028 ± 0.003	70.8 ± 0.6
LB09-SXVII-F3	XVII / 568	0.10027 ± 0.00010	4.189 ± 0.001	36.89 ± 0.14	0.507 ± 0.002	1.022 ± 0.002	74.4 ± 0.5	1.027 ± 0.002	73.2 ± 0.8

[a] Sample LB/S.XXI 10-01R is the very tip (~0.03 g) of a 1 cm-tall stalagmite, and sample LB/S.XXI 10-01 is a larger portion (~0.12 g) of the top section of the same stalagmite.

2.10 Supplementary information section 2.5

2.10.1 Supplementary table 2.7 – $^{40}Ar/^{39}Ar$ dating of tephra T1

Laser step-heating experiments on hornblende crystals of 100–150 μm (Lab ID 2598) and 150–250 μm (Lab IDs 2584 and 2599) size fractions. All uncertainties are expressed at 1σ.

Lab ID [a]	Relative argon isotopic abundances (V)					Ca/K	$\%^{40}Ar^{*}$ [b]	Age (kyr)
	^{40}Ar	^{39}Ar	^{38}Ar	^{37}Ar	^{36}Ar			
QL-OSU-28B; J = 0.0000170 ± 0.000000097								
2584-03C	3.256E-03 ± 1.6E-06	4.837E-06 ± 7.8E-08	2.157E-06 ± 4.9E-08	7.360E-05 ± 1.2E-06	1.090E-05 ± 1.2E-07	29.82 ± 0.69	0.36 ± 1.07	77 ± 226
2584-03D	4.573E-03 ± 1.7E-06	1.080E-05 ± 1.0E-07	3.197E-06 ± 5.7E-08	2.494E-04 ± 2.3E-06	1.500E-05 ± 1.1E-07	45.13 ± 0.60	2.36 ± 0.71	314 ± 95
2584-03E	5.543E-03 ± 2.5E-06	2.070E-05 ± 1.3E-07	4.066E-06 ± 6.1E-08	5.540E-04 ± 3.6E-06	1.830E-05 ± 1.4E-07	52.47 ± 0.48	2.42 ± 0.74	205 ± 62
2584-03F	7.297E-03 ± 2.6E-06	2.890E-05 ± 1.7E-07	5.583E-06 ± 6.8E-08	8.154E-04 ± 4.9E-06	2.420E-05 ± 1.5E-07	55.28 ± 0.47	1.88 ± 0.60	151 ± 48
2584-03G	4.800E-03 ± 2.0E-06	2.280E-05 ± 1.4E-07	3.760E-06 ± 5.6E-08	6.673E-04 ± 3.8E-06	1.580E-05 ± 1.2E-07	57.47 ± 0.49	3.09 ± 0.73	207 ± 49
2584-03H	2.187E-03 ± 1.3E-06	1.330E-05 ± 1.3E-07	1.901E-06 ± 4.1E-08	4.025E-04 ± 2.7E-06	7.423E-06 ± 8.9E-08	59.23 ± 0.71	0.13 ± 1.21	7 ± 63
2584-03I	3.933E-03 ± 1.9E-06	2.040E-05 ± 1.4E-07	2.982E-06 ± 5.5E-08	6.073E-04 ± 3.9E-06	1.300E-05 ± 1.6E-07	58.26 ± 0.56	2.22 ± 1.24	136 ± 76
2584-03J	1.389E-03 ± 1.2E-06	8.639E-06 ± 9.7E-08	1.193E-06 ± 4.1E-08	2.607E-04 ± 2.3E-06	4.556E-06 ± 7.6E-08	59.15 ± 0.84	3.57 ± 1.63	182 ± 83
2584-03K	8.464E-04 ± 1.2E-06	3.697E-06 ± 7.6E-08	7.691E-07 ± 3.8E-08	1.186E-04 ± 1.7E-06	2.786E-06 ± 7.5E-08	62.86 ± 1.59	2.84 ± 2.66	207 ± 194
2584-03L	2.774E-03 ± 1.5E-06	1.300E-05 ± 1.2E-07	2.184E-06 ± 4.9E-08	4.164E-04 ± 3.1E-06	9.315E-06 ± 9.9E-08	62.94 ± 0.76	0.95 ± 1.07	64 ± 73
2584-03M	6.797E-04 ± 1.0E-06	6.673E-06 ± 9.0E-08	6.179E-07 ± 3.5E-08	2.026E-04 ± 2.2E-06	2.170E-06 ± 7.1E-08	59.52 ± 1.03	7.04 ± 3.13	228 ± 101
2584-03N	5.103E-04 ± 9.5E-07	3.462E-06 ± 7.3E-08	4.225E-07 ± 3.5E-08	1.253E-04 ± 1.6E-06	1.706E-06 ± 7.4E-08	70.91 ± 1.75	2.12 ± 4.31	100 ± 203
2584-03O fuse	2.763E-03 ± 1.6E-06	7.273E-06 ± 8.9E-08	2.101E-06 ± 5.2E-08	2.499E-04 ± 2.5E-06	9.193E-06 ± 1.0E-07	67.34 ± 1.07	1.36 ± 1.10	164 ± 133
2584-04C	7.293E-03 ± 2.5E-06	1.030E-05 ± 1.1E-07	5.065E-06 ± 7.1E-08	1.397E-04 ± 1.6E-06	2.450E-05 ± 1.3E-07	26.63 ± 0.43	0.05 ± 0.54	11 ± 119
2584-04D	9.496E-03 ± 2.9E-06	3.300E-05 ± 1.7E-07	7.086E-06 ± 8.0E-08	8.757E-04 ± 5.4E-06	3.140E-05 ± 1.5E-07	52.05 ± 0.42	2.06 ± 0.48	188 ± 44
2584-04E	5.025E-03 ± 2.2E-06	2.370E-05 ± 1.5E-07	4.107E-06 ± 6.4E-08	6.836E-04 ± 4.3E-06	1.670E-05 ± 1.3E-07	56.62 ± 0.51	1.69 ± 0.78	114 ± 52
2584-04F	4.745E-03 ± 1.8E-06	2.080E-05 ± 1.4E-07	3.757E-06 ± 6.0E-08	6.106E-04 ± 4.0E-06	1.580E-05 ± 1.3E-07	57.67 ± 0.55	1.66 ± 0.82	120 ± 59
2584-04G	1.161E-02 ± 3.2E-06	5.680E-05 ± 2.3E-07	9.371E-06 ± 9.2E-08	1.656E-03 ± 8.0E-06	3.910E-05 ± 1.8E-07	57.16 ± 0.36	0.53 ± 0.47	34 ± 31
2584-04H	3.670E-03 ± 1.8E-06	2.450E-05 ± 1.5E-07	3.186E-06 ± 5.5E-08	7.461E-04 ± 4.8E-06	1.210E-05 ± 1.3E-07	59.66 ± 0.53	3.05 ± 1.05	145 ± 50
2584-04I fuse	4.365E-03 ± 1.8E-06	9.898E-06 ± 9.3E-08	3.342E-06 ± 5.8E-08	3.200E-04 ± 2.7E-06	1.460E-05 ± 1.2E-07	63.36 ± 0.80	0.75 ± 0.81	105 ± 114
QL-OSU-28C; J = 0.0000170 ± 0.000000045								
2598-01D	2.785E-03 ± 1.6E-06	1.350E-05 ± 1.2E-07	2.311E-06 ± 4.5E-08	4.324E-04 ± 2.2E-06	9.122E-06 ± 1.0E-07	62.61 ± 0.66	3.46 ± 1.10	226 ± 72
2598-01 fuse	2.263E-03 ± 1.4E-06	1.450E-05 ± 1.4E-07	2.006E-06 ± 4.5E-08	4.795E-04 ± 2.8E-06	7.599E-06 ± 9.7E-08	64.79 ± 0.74	1.43 ± 1.29	71 ± 64
2598-02D	2.421E-03 ± 1.5E-06	1.580E-05 ± 1.4E-07	2.096E-06 ± 4.5E-08	4.793E-04 ± 2.4E-06	7.926E-06 ± 1.1E-07	59.54 ± 0.62	3.86 ± 1.31	188 ± 64
2598-02 fuse	6.454E-03 ± 2.1E-06	4.370E-05 ± 1.9E-07	5.740E-06 ± 6.6E-08	1.487E-03 ± 5.9E-06	2.150E-05 ± 1.5E-07	66.67 ± 0.40	2.61 ± 0.68	123 ± 32
2598-03D	1.947E-03 ± 1.3E-06	1.480E-05 ± 1.3E-07	1.658E-06 ± 4.5E-08	4.712E-04 ± 2.3E-06	6.613E-06 ± 8.0E-08	62.22 ± 0.61	0.56 ± 1.23	23 ± 51
2598-03 fuse	5.091E-03 ± 2.0E-06	3.200E-05 ± 1.8E-07	4.339E-06 ± 7.7E-08	1.069E-03 ± 4.5E-06	1.700E-05 ± 1.3E-07	65.55 ± 0.47	1.72 ± 0.75	87 ± 38
QL-OSU-28C; J = 0.0000170 ± 0.000000035								
2599-01D	4.058E-03 ± 1.9E-06	1.870E-05 ± 1.4E-07	3.330E-06 ± 5.2E-08	5.869E-04 ± 2.8E-06	1.370E-05 ± 1.3E-07	61.51 ± 0.55	0.56 ± 0.99	39 ± 69
2599-01 fuse	4.109E-03 ± 1.8E-06	2.640E-05 ± 1.6E-07	3.505E-06 ± 5.5E-08	8.389E-04 ± 3.9E-06	1.370E-05 ± 1.3E-07	62.33 ± 0.48	2.39 ± 0.92	119 ± 46

[a] Lab ID 2584-03M is the data point on the far right-hand side of Extended Data fig. 2.3f, which was excluded from the inverse isochron used to calculate the $^{40}Ar/^{39}Ar$ age of 79 ± 12 kyr.

[b] Radiogenic ^{40}Ar yield.

2.11 Supplementary information section 2.6

2.11.1 Supplementary table 2.8 – Radiocarbon (^{14}C) dating of charcoal

Charcoal pieces were recovered *in situ* (exact locations indicated by coordinates) and pretreated using acid–base–acid (ABA) procedures. Previous ^{14}C dating studies at Liang Bua have suggested that ABA pretreatment is more effective at reducing sample contamination by 'old' carbon (e.g., from dissolved limestone) than are less rigorous chemical pretreatments (Roberts *et al.*, 2009). However, ABA procedures may not remove all sources of contamination by modern carbon, and the effect of such contamination increases with sample age (Wood, 2015). For example, a 50,000 year-old sample contaminated with just 0.5% of modern carbon would give a measured age of ~40,000 years BP. Sample D-AMS 007548 falls in a challenging time period for ^{14}C dating, so the remaining charcoal from this sample was subjected to a more stringent cleaning procedure (AOx-SC), described in Methods. We consider the resulting age (OxA-X-2648-13) to be more accurate.

Sample code	Sector / depth (cm)	Coordinates (x, y, z)	δ^{13}C (‰) [a]	Conventional ^{14}C age (years BP) [b]	Calibrated age range (kyr cal. BP) [c]	
					68% CI	95% CI
D-AMS 007548	XXIII / 189	16, 76, 189	–22.2	40,417 ± 332	44.30–43.59	44.61–43.27
OxA-X-2648-13	XXIII / 189	16, 76, 189	–24.4	42,500 ± 900	46.56–44.91	47.66–44.13
D-AMS 005954	XXII / 431	76, 185, 431	–28.2	10,949 ± 42	12.79–12.72	12.87–12.70
D-AMS 005953	XXII / 432	65, 186, 432	–28.1	10,910 ± 36	12.76–12.71	12.80–12.70

[a] Values for prepared graphite measured by AMS and used to correct the conventional ages for isotopic fractionation.

[b] Radiocarbon years before present (BP) ± 1σ, where 'present' is defined (by convention) as A.D. 1950.

[c] Calendar-year age ranges reported at the 68% and 95% confidence interval (CI), with calibrations performed using the SHCal13 data set (Hogg *et al.*, 2013) and CALIB 7.1 (http://calib.qub.ac.uk/calib/).

CHAPTER 3

Radiocarbon dating of charcoal samples from Liang Bua

3.1 Preface

The discovery and initial dating of *Homo floresiensis* at Liang Bua raised major questions about when modern humans first arrived on Flores and whether these two hominin species ever occupied the island at the same time (Brown *et al*., 2004; Morwood *et al*., 2004). If *H. floresiensis* survived until ~17 or 13–11 thousand calibrated radiocarbon years before present (ka cal. BP), as originally suggested (Morwood *et al*., 2004, 2005, 2009; Roberts *et al*., 2009), then it provided 30–40 millennia of potential overlap with modern humans on the island. However, the first evidence of modern humans on Flores was also from Liang Bua and restricted to the last 11 ka (Morwood *et al*., 2004, 2005, 2009).

The revised stratigraphic interpretation and chronology of the sedimentary sequence of Liang Bua presented in Chapter 2 of this thesis (Sutikna *et al*., 2016) places the last appearance date of *H. floresiensis* at Liang Bua between ~60 and 50 ka ago, removing most but not all of the possible temporal span of overlap with modern humans, given the evidence that the latter species had probably reached Australia by ~60–50 ka (Roberts *et al*., 1990, 1994). But this new interpretation also suggests that sediments between ~46 and 20 ka in age are currently missing from the excavated areas at Liang Bua. This gap in the stratigraphic record at Liang Bua leaves many key questions unanswered, including whether there were indeed any late-surviving populations of *H. floresiensis* and/or whether modern humans arrived on the island earlier than ~11 ka ago.

This chapter presents the results of radiocarbon dating of 48 new charcoal samples recovered during excavations at Liang Bua as well as recalibration and analysis of all previously reported ^{14}C dates from the site. Linear regression analyses (least-squares) are used to evaluate whether the relationships between sample depth and age in each Sector are statistically significant from a slope of 0 while analysis of covariance (ANCOVA) is used to test whether the regression slopes of each Sector are significantly different than one another. Together, these results provide important details about the site's depositional sequence from ~46 ka ago to the present and clarify issues relating to the stratigraphic gap between ~46 and 20 ka ago and also regarding the chronology of the Holocene sequence across multiple Sectors.

As co-director of ongoing research at Liang Bua, I have supervised all of the excavations since 2001 (2001–2004 with M.J. Morwood, R.P. Soejono and R.G. Roberts; 2007–2009 with M.J. Morwood and Wahyu Saptomo; and 2010–present with M.W. Tocheri, Wahyu Saptomo and Jatmiko). Although all of these co-directors have contributed in various ways to the overall direction of this research, I have selected the areas for excavation and managed the collection of all field data since 2001, including the selection of the charcoal samples used in this chapter. In terms of contributions to this chapter, I led the stratigraphic analyses and divisions of the sequence into the units/subunits used, with input from M.W. Tocheri, Jatmiko, E. Wahyu Saptomo, Rokus Due Awe and R.G. Roberts. I conducted all of the analyses and wrote the chapter, with guidance on the statistics from M.W. Tocheri and additional input from all other co-authors. This chapter has been prepared for submission to the *Journal of Archaeological Science*.

Radiocarbon dating of charcoal from Liang Bua (Flores, Indonesia) reveals significant new insights into the depositional history of the cave over the last 50,000 years

Thomas Sutikna[1,2], Matthew W. Tocheri[3,4], Jatmiko[2,1], E. Wahyu Saptomo[2,1], Rokus Due Awe[2,1,‡], Richard G. Roberts[1]

[1]Centre for Archaeological Science, School of Earth and Environmental Sciences, University of Wollongong, Wollongong, New South Wales 2522, Australia.
[2]Pusat Penelitian Arkeologi Nasional, Jakarta 12510, Indonesia.
[3]Department of Anthropology, Lakehead University, Thunder Bay, Ontario P7B 5Z5, Canada.
[4]Human Origins Program, National Museum of Natural History, Smithsonian Institution, Washington DC 20013, USA.
‡Deceased.

Correspondence and requests for materials should be addressed to T.S. (thomasutikna@gmail.com).

Abstract

New stratigraphic and chronological details from the excavated areas of Liang Bua (Flores, Indonesia) show that the skeletal remains of *Homo floresiensis* are between 60 and 100 thousand years (ka) old. Although stone artefacts reasonably attributable to this species have also been recovered from sediments that are up to ~50 ka in age, whether this primitive hominin species survived past 50 ka ago is an open question. The results of this study significantly refine and extend our understanding of the past 50 ka depositional sequence at Liang Bua. We report the discovery of deposits at Liang Bua dated here to between ~41 and 25 thousand calibrated radiocarbon (^{14}C) years before present (ka cal. BP). This discovery provides future studies the opportunity to address questions regarding potentially late-surviving populations of *H. floresiensis* and/or the early presence of modern humans on the island. Furthermore, the depositional ages of tephras T7 and T8 – which represent key stratigraphic markers between the terminal Pleistocene and early Holocene sediments at Liang Bua – are constrained more precisely to between 13.1 and 11.7 ka cal. BP. From the eastern wall to the cave centre, the Holocene sequence at Liang Bua appears essentially similar, providing a useful stratigraphic and chronological framework for reconstructing the depositional history of the site and further analyses of its archaeological and faunal assemblages.

3.2 Introduction

The revised stratigraphy and chronology of Liang Bua (Chapter 2 of this thesis; Sutikna *et al*., 2016) has resolved some major questions about the depositional sequence of this important archaeological site. For instance, this new evidence suggests that all skeletal and cultural remains of *H. floresiensis* are between about 100–60 thousand years (ka) old and 190–50 ka old, respectively (Sutikna *et al*., 2016), and – in contrast to

previous suggestions (Morwood *et al*., 2004, 2005, 2009; Roberts *et al*., 2009) – do not extend until ~17 or 13–11 thousand calibrated radiocarbon (^{14}C) years before present (ka cal. BP, where the 'present' is defined by convention as A.D. 1950)[1]. However, this new interpretation also raises two important new questions about the stratigraphy and chronology of deposits that are younger than ~46 ka. To address these research questions, we use the stratigraphic information obtained during the 2007–2014 excavations and all ^{14}C ages obtained for charcoal samples from Liang Bua, including 48 new ages presented here for the first time. We document the stratigraphic provenance of these newly dated samples and discuss the implications of this evidence for interpreting the depositional sequence at Liang Bua over the last 50 millennia.

The first question concerns the major gap in the stratigraphic record between about 46 and 20 ka (Fig. 3.1). Is this gap the result of a depositional hiatus or one or more erosional periods, or are deposits of this age range preserved elsewhere at Liang Bua in areas not yet excavated? This gap in the stratigraphic record covers a crucial time period for hominin prehistory on Flores. At present, the earliest evidence for modern humans on Flores derives from the Holocene sequence at Liang Bua and suggests a relatively continuous presence at the site after ~11 ka (Morwood *et al*., 2004, 2005, 2009; Moore *et al*., 2009). In contrast, archaeological evidence suggests modern humans were on Timor, an island east of Flores, by ~42 ka ago (O'Connor *et al*., 2011; O'Connor, 2015) and had reached Australia no later than 50–47 ka ago (Roberts *et al*., 1990, 1994, 1998; Roberts and Jones, 2001; Turney *et al*., 2001; Bowler *et al*., 2003; Allen and O'Connell, 2014; Clarkson *et al*., 2015; O'Connell and Allen, 2015; Hiscock, 2015; Saltré *et al*., 2016). The discovery of deposits between 46 and 20 ka old at Liang

[1] Henceforth in this study, we have abbreviated 'ka cal. BP' to 'ka' as all of the ^{14}C ages have been calibrated and are equivalent to calendar years before A.D. 1950 (see 'Methods' below).

Bua or elsewhere on Flores would provide critical details for addressing questions regarding potentially late-surviving populations of *H. floresiensis* and/or an earlier presence of modern humans on the island.

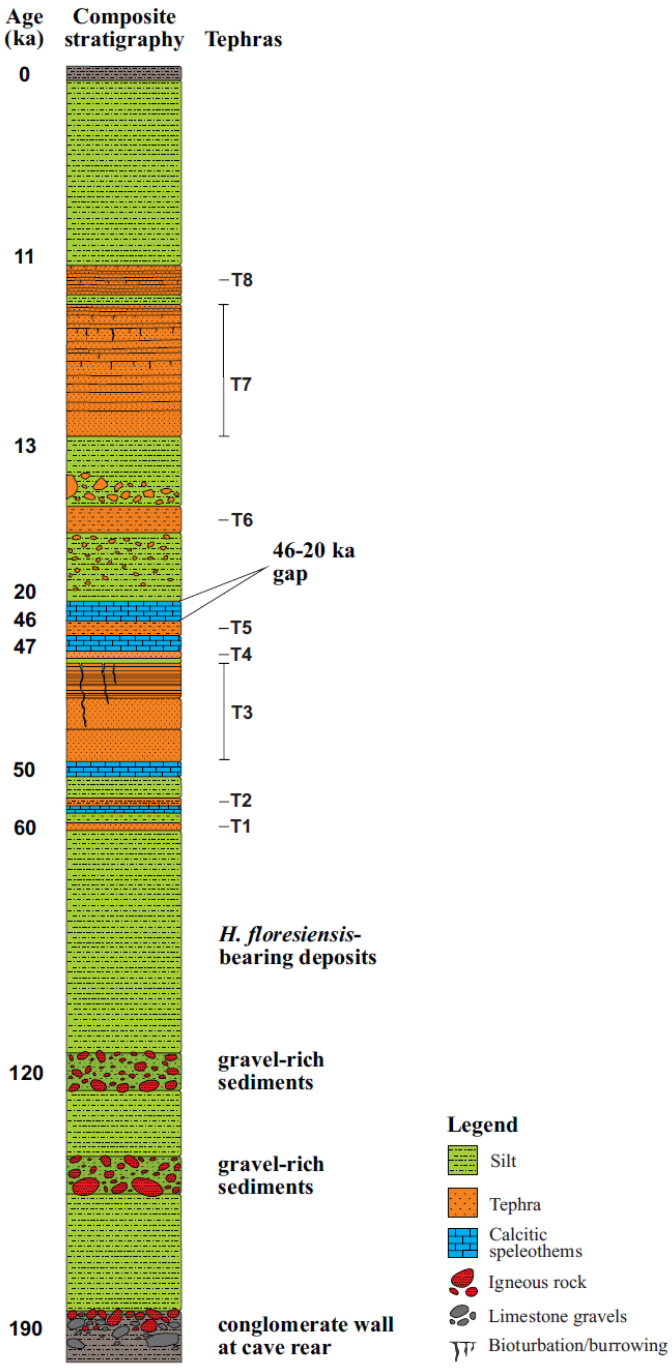

Figure 3.1 Composite section of the Liang Bua depositional sequence, showing the tephras and other key stratigraphic markers with approximate ages. The modern soil and basal sediments are shaded grey at the top and bottom of the section, respectively. Note the gap in the section between 46 and 20 ka, constrained by flowstone directly overlying T5 and the charcoal sample dated by ^{14}C to ~46 ka cal BP.

The second question arising from our improved appreciation of the site's stratigraphic complexities in the older deposits (>46 ka; Sutikna *et al*., 2016) is how valid is it to apply the published ^{14}C chronology for Sectors III, IV, VII and XI (Roberts *et al*., 2009) to estimate the ages of the deposits excavated since 2008 (Fig. 3.2)? Twenty-eight ^{14}C ages were reported by Roberts *et al*. (2009). Fourteen of the 20 Holocene ages are from Sector IV (an area excavated on nine separate occasions between 1978 and 2003) and nine of these ages were obtained using methods of charcoal pretreatment that may not have been sufficiently stringent to remove all modern carbon contaminants (e.g., acid wash only). Hence, the applicability of these ages to deposits in other Sectors requires more empirical support. Two new ^{14}C ages of ~12.7 ka from just beneath tephra T7 in Sector XXII (D-AMS-005953 and -005954; Sutikna *et al*., 2016) support the previous age estimate of ~13 ka obtained from a similar stratigraphic position in Sector VII (ANUA-27115). However, the oldest ^{14}C ages of ~11 ka from above tephra T8 in Sector IV (ANUA-19209, -19211 and GrN-14306) (Roberts *et al*., 2009; Figs 3.1 and 3.2) have yet to be confirmed by evidence in other Sectors. Additional charcoal samples from other Sectors may also enable the ages of tephras T7 and T8 to be constrained more precisely.

To address these research questions, we use the stratigraphic information obtained during the 2007–2014 excavations and all ^{14}C ages obtained for charcoal samples from Liang Bua, including 48 new ages presented here for the first time. We document the stratigraphic provenance of these newly dated samples and discuss the implications of this evidence for interpreting the depositional sequence at Liang Bua over the last 50 millennia.

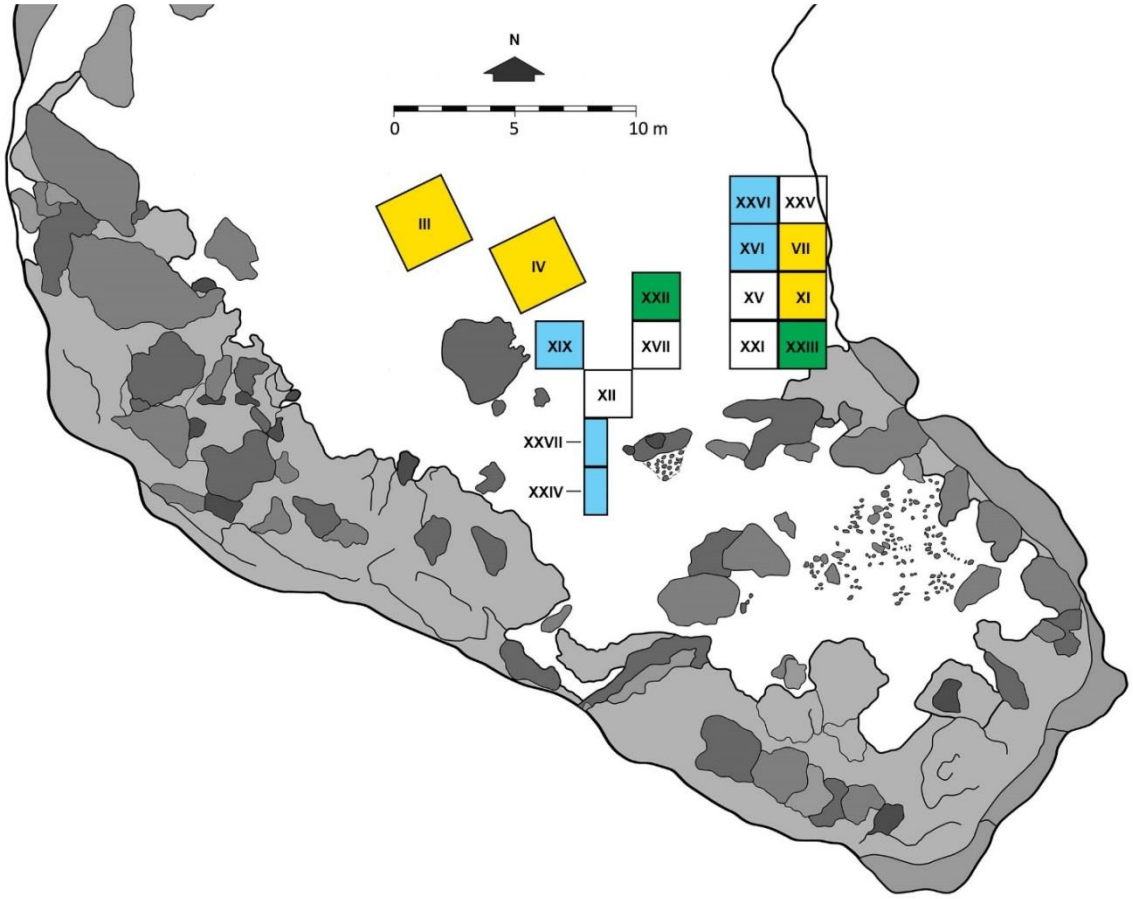

Figure 3.2 Site plan of Liang Bua and excavated Sectors. Sectors from which charcoal has been dated by ^{14}C are shaded: yellow, ages reported by Roberts *et al*. (2009); green, ages reported in Chapter 2 of this thesis (Sutikna *et al*., 2016); blue, ages reported in this study. The remaining cave floor sediments are shaded white, while the areas shaded gray are exposed rocks, stalagmites and other surfaces covered in speleothems.

3.3 Methods

Radiocarbon dating of charcoal samples from the Liang Bua depositional sequence has been a major component of the overall chronology program for the site. Previously, 28 ages were obtained from four excavated units (Sectors III, IV, VII and XI) (Roberts *et al*., 2009). The conventional (i.e., uncalibrated) ^{14}C ages for these charcoal samples ranged from 16.1 to 0.19 ka BP, with corresponding median calibrated ages of 19.2 to 0.14 ka cal. BP using the IntCal04 dataset, Calib 5.0 (Reimer *et al*., 2004) and a Southern Hemisphere offset of 40 ± 13 years (Hogg *et al*., 2002; Roberts *et al*., 2009).

An updated calibration dataset for the Southern Hemisphere (SHCal13) is now available (Hogg *et al*., 2013), so we have recalibrated all 28 published ^{14}C ages from Liang Bua, along with the ages for the new samples described below, using SHCal13 and the CALIB 7.1 program (http://calib.qub.ac.uk/calib/), which also includes a revised Southern Hemisphere offset. Calibration involved converting conventional ^{14}C ages in radiocarbon years BP to calendar-year age ranges at the 68% and 95% confidence intervals (CIs) (Tables 3.1–3.5). Henceforth in this study, we refer only to the calibrated ^{14}C ages and their 95% CI ranges.

The ages of the two ^{14}C samples from Sector XXII (D-AMS-005953 and -005954, ~12.7 ka) and one from Sector XXIII (OxA-X-2648-13, ~46 ka) were reported previously (Sutikna *et al*., 2016). Forty-eight additional charcoal samples, recovered during excavation of five other Sectors (XVI, XIX, XXIV, XXVI and XXVII), were selected for ^{14}C dating. These samples were sent to DirectAMS Radiocarbon Dating Service in Bothell, Washington, where they were pretreated using acid–base–acid (ABA) procedures and the ^{14}C content was measured using accelerator mass spectrometry (AMS) (Wood, 2015). All ages were corrected for isotopic fractionation using their respective δ^{13}C values, which were measured on the prepared graphite using the AMS spectrometer.

Excavations between 2008 and 2014 included five Sectors. Sectors XVI, XIX and XXVI were each 2 x 2 m squares, whereas only the western halves (1 x 2 m areas) of Sectors XXIV and XXVII were excavated (Fig. 3.2). The excavation of each Sector proceeded in intervals of 10 cm (referred to as spits), while following stratigraphic units. For safety, the excavation walls (baulks) were shored with timber after ~2.5 m depth. During excavation of each spit, charcoal and other findings recovered *in situ* were plotted in three dimensions. Sediments from each spit were labelled, hand-sieved

and then wet-sieved using 2 mm mesh. Initial cataloguing of all findings took place in the field. All charcoal pieces dated in this study were collected directly from combustion features (hearths) or as fragments that vary from coarse-sand to gravel in size. The exact excavated positions of these pieces were recorded as three-dimensional coordinates, and no dated pieces were collected from the sieved sediments. All findings were then packed and shipped to Pusat Penelitian Arkeologi Nasional (National Research Centre for Archaeology) in Jakarta, Indonesia for further cleaning, cataloguing, curation and study.

For each Sector, the statistical relationship between the median calibrated ^{14}C ages and their depths beneath the present surface of the cave floor was examined using least-squares linear regression analysis (Neter *et al*., 1996). Depth was used as the independent variable (i.e., the predictor) and age as the dependent variable. The slopes of the fitted lines were tested for significant deviation from zero (i.e., no relationship between the independent and dependent variables), while analyses of their respective residuals were used to evaluate if the assumptions of the regression model were reasonably met—for example, whether the linear function was appropriate, the error variance was constant, and the errors were normally distributed. Analysis of covariance (ANCOVA) was used to evaluate the null hypothesis that, for different Sectors, the fitted regression lines with slopes significantly different from zero have equal slopes (i.e., lie parallel to each other) (Neter *et al*., 1996). If the null hypothesis was rejected, then pairwise comparisons of the least-squares means for all Sectors were examined using the Tukey-Kramer adjustment for post hoc multiple comparisons (Neter *et al*., 1996), to determine which regression lines differed significantly. This adjustment ensured that an ‘alpha value’ of 0.05 applied to the entire family of pairwise

comparisons. All statistical analyses were conducted in SAS/STAT software, version 9.0 for Microsoft Windows (SAS Institute Inc., Cary, USA).

Table 3.1 Recalibration of published ^{14}C ages for charcoal samples from Liang Bua[1].

					Age			
		Depth		$\delta^{13}C$	^{14}C	Median Calibrated	Calibrated Range (ka)	
	Sample Code	(cm)	Methods[2]	(‰)	(yr BP)	(yr cal. BP)	68% CI[3]	95% CI[3]
III	ANUA-23607	363	ABOX (850) / AMS	–25.0	1,490 ± 210	1,361	1.58–1.17	1.76–0.93
	ANUA-23610	446	ABOX (850) / AMS	–25.0	13,800 ± 230	16,641	16.97–16.29	17.35–16.00
IV	GrN-15870	20	ABA / GPC	–25.8	190 ± 35	174	0.23–0.17	0.29–0.13
	GrN-15871	30	ABA / GPC	–26.0	550 ± 40	530	0.54–0.51	0.56–0.50
	GrN-14301	40	ABA / GPC	–26.2	450 ± 25	484	0.50–0.47	0.51–0.45
	GrN-14302	40	Acid / GPC	–24.8	580 ± 70	552	0.56–0.51	0.66–0.49
	GrN-15872	50	ABA / GPC	–26.3	460 ± 70	461	0.53–0.44	0.55–0.32
	GrN-14303	50	Acid / GPC	–25.5	465 ± 35	491	0.51–0.47	0.53–0.45
	GrN-14304	150	Acid / GPC	–25.0	3,390 ± 270	3,609	3.93–3.32	4.30–2.92
	GrN-14305	170	Acid / GPC	–26.2	3,820 ± 120	4,160	4.30–3.98	4.45–3.84
	ANUA-19207	230	ABOX (910) / AMS	–25.0	5,620 ± 130	6,377	6.51–6.27	6.67–6.17
	GrN-14306	310	Acid / GPC	–25.0	9,830 ± 490	11,268	11.99–10.55	12.67–10.12
	ANUA-19214	340	ABOX (910) / AMS	–25.0	8,250 ± 160	9,163	9.41–9.01	9.52–8.72
	ANUA-19206	340	ABOX (650) / AMS	–25.0	8,810 ± 150	9,833	9.93–9.56	10.20–9.53
	ANUA-19211	398.5	ABOX (910) / AMS	–25.0	9,410 ± 190	10,625	10.79–10.28	11.18–10.21
	ANUA-19209	398.5	ABOX (650) / AMS	–25.0	9,640 ± 170	10,921	11.18–10.72	11.35–10.41
	ANUA-19203	490	ABOX (650) / AMS	–25.0	13,880 ± 210	16,750	17.06–16.42	17.39–16.16
	ANUA-19210	490	ABOX (910) / AMS	–25.0	13,950 ± 240	16,848	17.20–16.48	17.53–16.17
VII	ANUA-27115	463	ABOX (650, 850) / AMS	–25.0	11,160 ± 220	12,985	13.14–12.75	13.41–12.67
	ANUA-27117	575	ABOX (850) / AMS	–25.0	14,845 ± 240	18,012	18.31–17.73	18.58–17.45
	ANUA-27116	588	ABOX (650, 850) / AMS	–25.0	15,300 ± 240	18,497	18.77–18.25	18.97–17.94
	ANUA-31229	652	ABOX (850) / AMS	–25.0	15,750 ± 310	19,004	19.36–18.66	19.74–18.31
	ANUA-32717	670	ABOX (850) / AMS	–25.0	16,130 ± 280	19,413	19.72–19.04	20.07–18.79
XI	Wk-16351	30	ABA / AMS	–24.8	94 ± 33	83	0.24–0.02	0.26–0.00
	Wk-16352	60	ABA / AMS	–25.1	502 ± 32	511	0.52–0.50	0.54–0.49
	Wk-16353	90	ABA / LSC	–26.7	2662 ± 35	2,752	2.77–2.73	2.85–2.70
	Wk-16354	150	ABA / AMS	–29.6	4526 ± 39	5,154	5.28–5.16	5.30–5.03
	Wk-16355	230	ABA / AMS	–26.9	7499 ± 47	8,276	8.27–8.20	8.37–8.18
XXII	D-AMS-005953	431	ABA / AMS	–28.2	10,949 ± 42	12,766	12.79–12.72	12.87–12.70
	D-AMS-005954	432	ABA / AMS	–28.1	10,910 ± 36	12,739	12.76–12.71	12.80–12.70
XXIII	D-AMS-007548	189	ABA / AMS	–22.2	40,417 ± 332	43,946	44.30–43.59	44.61–43.27
	OxA-X-2648-13	189	AOx (630, 1000) / AMS	–24.4	42,500 ± 900	45,771	46.56–44.91	47.66–44.13

[1] Sector III, IV, VII and XI ages from Roberts *et al*. (2009); Sector XXII and XXIII ages from Sutikna *et al*. (2016).

[2] Sample pretreatments include acid only (Acid), acid–base–acid (ABA), acid–base wet oxidation (ABOX) and acid wet oxidation (AOx). The wet oxidation samples were step-combusted at different temperatures (shown in parentheses). Techniques for measuring ^{14}C content include gas proportional counting (GPC), liquid scintillation counting (LSC) and accelerator mass spectrometry (AMS).

[3] CI, confidence intervals.

3.4 Results

3.4.1 Recalibration of published ^{14}C ages for Liang Bua

The published and recalibrated ^{14}C ages from Liang Bua are listed in Table 3.1. As these recalibrated ages use SHCal13—the standard calibration dataset for the

Southern Hemisphere (Hogg *et al*., 2013)—they supersede previously published estimates. Most of the median recalibrated ages are identical to, or differ only slightly from those reported by Roberts *et al*. (2009), but typically the 68% and 95% CIs are narrower. Sample Wk-16351 yielded a conventional ^{14}C age of 94 ± 33 years BP, which falls outside the calibration range of SHCal13 using CALIB 7.1, so we instead used the OxCal 4.2 program to calibrate this age (https://c14.arch.ox.ac.uk/oxcal/OxCal).

3.4.2 Discovery of deposits dating to between about 41 and 25 ka

Sector XXIV

This Sector is in the middle rear of the cave, 2 m to the south of Sector XII (Fig. 3.2). The present cave floor slopes ~30° upwards from just south of Sector XII to the conglomerate wall at the rear of the cave. In 2011, the western half of Sector XXIV (1 x 2 m in area) was excavated to a depth of ~4 m. The primary goal of this excavation was to document the possible southernmost extent of tephra T3 (~50–47 ka), a key stratigraphic layer that overlies all known *H. floresiensis* remains (Sutikna *et al*., 2016). This tephra was observed across the entire area of Sector XII (excavated in 2007) at around 2.2–2.8 m depth, with its base angled slightly upwards toward the south. Thus, the aim was to observe whether T3 was present in Sector XXIV and, if so, whether it abutted the stratigraphically underlying deposits. If T3 was not present in Sector XXIV, then it must have terminated at some point in the area between Sectors XII and XXIV (Fig. 3.2).

Table 3.2 New ^{14}C ages for charcoal samples from Sectors XXIV and XXVII.

		Depth		$\delta^{13}C$	Age			
					^{14}C	Median Calibrated	Calibrated Range (ka)	
	Sample Code	(cm)	Methods[1]	(‰)	(yr BP)	(yr cal. BP)	68% CI[2]	95% CI[2]
XXIV	D-AMS-007550	143	ABA / AMS	–26.3	27,954 ± 125	31,605	31.75–31.42	32.03–31.29
	D-AMS-005947	152	ABA / AMS	–28.1	30,168 ± 158	34,161	34.32–33.98	34.52–33.85
	D-AMS-007546	153	ABA / AMS	–28.0	27,466 ± 120	31,263	31.36–31.16	31.46–31.07
	D-AMS-007547	154	ABA / AMS	–23.7	27,587 ± 107	31,328	31.43–31.27	31.53–31.13
	D-AMS-007549	201	ABA / AMS	–33.2	29,074 ± 153	33,258	33.49–33.04	33.66–32.82
XXVII	D-AMS-007555	137	ABA / AMS	–22.1	20,516 ± 58	24,616	24.77–24.45	24.95–24.36
	D-AMS-007551	237	ABA / AMS	–21.7	36,323 ± 259	40,930	41.25–40.64	41.48–40.31
	D-AMS-007552	239	ABA / AMS	–27.1	33,817 ± 173	38,284	38.54–38.07	38.70–37.67
	D-AMS-007553	250	ABA / AMS	–20.4	22,288 ± 94	26,463	26.61–26.28	26.85–26.14

[1] ABA, acid–base–acid pretreatment; AMS, accelerator mass spectrometry measurement technique.

[2] CI, confidence intervals.

During the excavation of Sector XXIV, T3 was encountered in the northern part as a thin lens that sloped upward toward the south and terminated ~60 cm from the north baulk (Fig. 3.3). Although the main goal of the excavation had been achieved with the identification of T3, further questions arose because more than 3,000 faunal specimens per cubic metre were recovered – almost double that from any other Sector. This large accumulation of faunal remains suggested either a major difference in the taphonomy of the deposits or perhaps their age.

A charcoal sample from 152 cm depth in Sector XXIV (D-AMS-005947) was selected for ^{14}C dating and returned an unexpectedly early age of ~34 ka (Table 3.2). This result was 15 millennia older than any of the ^{14}C ages obtained previously at Liang Bua (Roberts *et al.*, 2009) (Table 3.1), which raised the possibility that much of the unexplored rear of the cave may preserve deposits within the critical time interval (46–20 ka ago) missing from the other excavated areas. Accordingly, four additional charcoal samples were selected for dating: three from the same stratigraphic layer and similar depths (143, 152 and 153 cm) as sample D-AMS-005947, and one from the underlying stratigraphic layer at 201 cm depth (Fig. 3.3). These four samples yielded ages of ~34–31 ka (Table 3.2 and Fig. 3.3), thereby corroborating the original age determination.

Furthermore, evidence of fire use – a hearth – was found in the west baulk of Sector XXIV in sediments dated to between ~41 and 24 ka cal. BP (Fig. 3.3). Micromorphology analyses have recently confirmed anthropogenic burning activity in these sediments, which contain ash and charcoal (Morley *et al*., 2016).

Table 3.3 New ^{14}C ages for charcoal samples from Sector XXVI.

					Age		
		Depth		δ^{13}C	^{14}C	Median Calibrated	Calibrated Range (ka)
	Sample Code	(cm)	Methods[1]	(‰)	(yr BP)	(yr cal. BP)	68% CI[2]	95% CI[2]
XXVI	D-AMS-005940	45	ABA / AMS	–26.6	460 ± 24	493	0.51–0.49	0.52–0.45
	D-AMS-005941	66	ABA / AMS	–27.5	774 ± 27	673	0.68–0.66	0.72–0.65
	D-AMS-005942	89	ABA / AMS	–26.3	1,233 ± 31	1,107	1.11–1.06	1.18–1.05
	D-AMS-005943	104	ABA / AMS	–23.0	2,018 ± 25	1,937	1.93–1.90	2.00–1.88
	D-AMS-005945	127	ABA / AMS	–20.5	2,143 ± 25	2,075	2.10–2.04	2.15–2.01
	D-AMS-005944	116	ABA / AMS	–21.7	2,196 ± 29	2,153	2.16–2.09	2.21–2.06
	D-AMS-005946	140	ABA / AMS	–22.8	2,337 ± 29	2,326	2.35–2.31	2.36–2.30
	D-AMS-005948	143	ABA / AMS	–27.4	2,639 ± 29	2,741	2.76–2.72	2.78–2.70
	D-AMS-005949	171	ABA / AMS	–9.6	4,062 ± 52	4,498	4.54–4.41	4.65–4.38
	D-AMS-005950	178	ABA / AMS	–22.7	4,067 ± 28	4,487	4.49–4.44	4.58–4.42
	D-AMS-005951	247	ABA / AMS	–29.9	5,557 ± 26	6,310	6.32–6.28	6.40–6.28
	D-AMS-005952	279	ABA / AMS	–24.3	7,391 ± 32	8,157	8.20–8.15	8.22–8.03
	D-AMS-013410	411	ABA / AMS	–26.1	10,237 ± 37	11,881	11.97–11.81	12.03–11.75
	D-AMS-013409	395	ABA / AMS	–23.9	10,350 ± 41	12,089	12.11–11.97	12.30–11.94

[1] ABA, acid–base–acid pretreatment; AMS, accelerator mass spectrometry measurement technique.
[2] CI, confidence intervals.

Table 3.4 New ^{14}C ages for charcoal samples from Sector XVI.

					Age		
		Depth		δ^{13}C	^{14}C	Median Calibrated	Calibrated Range (ka)
	Sample Code	(cm)	Methods[1]	(‰)	(yr BP)	(yr cal. BP)	68% CI[2]	95% CI[2]
XVI	D-AMS-013388	88	ABA / AMS	–19.0	1,643 ± 28	1,489	1.53–1.47	1.55–1.42
	D-AMS-013389	89	ABA / AMS	–30.8	1,275 ± 27	1,141	1.18–1.09	1.19–1.07
	D-AMS-013390	98	ABA / AMS	–21.3	2,180 ± 27	2,127	2.16–2.08	2.18–2.04
	D-AMS-013391	100	ABA / AMS	–16.6	2,054 ± 29	1,964	1.98–1.93	2.02–1.89
	D-AMS-013392	105	ABA / AMS	–18.6	2,587 ± 29	2,627	2.75–2.70	2.75–2.68
	D-AMS-013393	109	ABA / AMS	–14.6	2,365 ± 28	2,343	2.36–2.32	2.44–2.31
	D-AMS-013394	117	ABA / AMS	–21.6	3,142 ± 29	3,302	3.30–3.25	3.39–3.21
	D-AMS-013395	120	ABA / AMS	–10.9	2,746 ± 29	2,806	2.80–2.76	2.86–2.75
	D-AMS-013397	133	ABA / AMS	–15.2	3,258 ± 28	3,431	3.46–3.39	3.50–3.37
	D-AMS-013396	133	ABA / AMS	–30.5	3,614 ± 29	3,872	3.92–3.83	3.98–3.82
	D-AMS-013399	139	ABA / AMS	–22.4	3,301 ± 28	3,487	3.51–3.45	3.57–3.44
	D-AMS-013398	143	ABA / AMS	–21.3	4,029 ± 32	4,470	4.52–4.47	4.54–4.39
	D-AMS-013401	150	ABA / AMS	–18.3	3,575 ± 26	3,804	3.87–3.82	3.90–3.70
	D-AMS-013400	153	ABA / AMS	–28.4	4,141 ± 28	4,614	4.63–4.53	4.71–4.52
	D-AMS-013403	155	ABA / AMS	–26.1	3,796 ± 30	4,115	4.16–4.08	4.24–4.06
	D-AMS-013404	157	ABA / AMS	–24.0	4,085 ± 29	4,513	4.49–4.44	4.62–4.42
	D-AMS-013402	159	ABA / AMS	–21.2	3,897 ± 29	4,279	4.30–4.23	4.41–4.22
	D-AMS-013406	196	ABA / AMS	–19.3	5,398 ± 30	6,139	6.15–6.11	6.22–6.09
	D-AMS-013405	202	ABA / AMS	–26.1	5,214 ± 31	5,931	5.95–5.91	6.00–5.89
	D-AMS-013407	303	ABA / AMS	–26.3	8,635 ± 33	9,547	9.56–9.52	9.63–9.49
	D-AMS-013408	497	ABA / AMS	–23.3	11,107 ± 42	12,928	13.00–12.85	13.06–12.79

[1] ABA, acid–base–acid pretreatment; AMS, accelerator mass spectrometry measurement technique.
[2] CI, confidence intervals.

Linear regression analysis of these five ages as a function of depth results in a slope that is not significantly different from zero ($p = 0.50$; $R^2 = 0.166$). The poor linear fit is because the oldest age (~34 ka) derives from a similar depth to the three youngest ages (~31 ka). However, as all five ages are from within ~60 cm of each other vertically, it is likely that these two stratigraphic layers include deposits that are 34.5–31.1 ka in age (upper and lower 95% CIs for the oldest and youngest ages, respectively). Moreover, these ^{14}C results are consistent with speleothem U-series ages of ~47 ka obtained in 2004 from a test excavation, 0.5 x 0.5 m in area and ~2 m in depth, mostly in the eastern half of Sector XXIV, but extending into the southern part of Sector XXVII (Fig. 3.2) (Westaway *et al*., 2007a; Roberts *et al*., 2009). Previous studies had interpreted these U-series results as dating the same eroded 'conglomerate' or gravel-rich sediments as occur stratigraphically beneath the *H. floresiensis* deposits in Sectors VII and XI (Westaway *et al*., 2007a, 2009b; Roberts *et al*., 2009) (see Fig. 3.1). By contrast, the 2011 excavations of Sector XXIV suggested that this gravel-rich layer and its dated speleothems stratigraphically overlay tephra T3 (Sutikna *et al*., 2016). To resolve this issue, we subsequently excavated Sector XXVII.

Sector XXVII

This Sector, excavated in 2014, occurs directly between Sectors XXIV (to the south) and XII (to the north) (Fig. 3.2). Given the initial ^{14}C age of ~34 ka in 152 cm depth of Sector XXIV, the goal of this new excavation was to observe the stratigraphic connections between Sectors XXIV and XII and obtain additional samples for ^{14}C dating. The stratigraphy followed that of Sector XXIV, showing that these deposits continued to slope downward to the north (Fig. 3.3). Other important stratigraphic details included the presence of tephra T4 above T3, as seen in other Sectors (e.g., XI, XXI, XXIII and XV) but not in Sector XXIV. Instead, T4 terminated against the

inclining lens of T3 near the southern extent of Sector XXVII and was overlain by gravel-rich sediments – the same layer where the aforementioned small test excavation had terminated (Fig. 3.3).

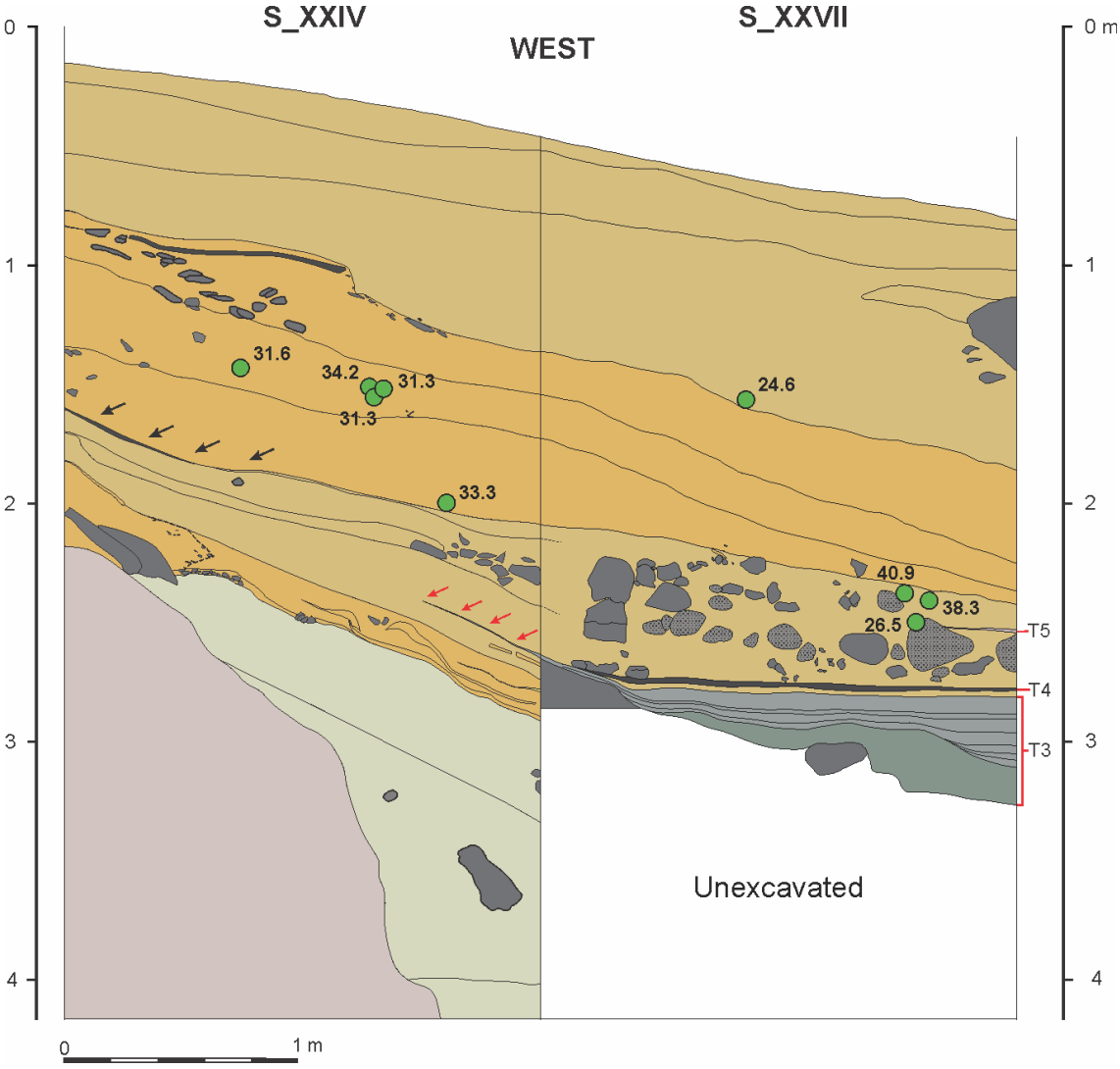

Figure 3.3 Stratigraphic profile of the western baulks of Sectors XXIV (at left) and XXVII (at right). The locations of the dated charcoal samples are shown projected on to the west wall as green circles with their median calibrated ^{14}C ages (in ka). Colours are used to illustrate the spatial extent of each stratigraphic layer, with clasts of limestone and gravel shown in dark grey. Black arrows indicate a combustion feature (a hearth). Red arrows indicate the termination of T3 in Sector XXIV and tephras T3, T4 and T5 are indicated in the right margin.

Four charcoal samples from between 137 and 250 cm depth in Sector XXVII yielded ages of between 41.5 and 24.4 ka (upper and lower 95% CIs for the oldest and

youngest ages, respectively; Table 3.2; Fig. 3.3). Linear regression analysis of these four ages as a function of depth results in a slope that is not significantly different from zero (p = 0.44; R^2 = 0.312). In this instance, the poor linear fit is because the second youngest age (~26.5 ka; D-AMS-007553) is from the deepest sample (250 cm); we interpret this charcoal sample as having been reworked from a younger layer by post-depositional processes. Otherwise, the ^{14}C ages for sector XXVII show reasonable stratigraphic consistency with those from Sector XXIV and indicate that immediately above the gravel-rich sediments and the ~47 ka speleothems that cover them – and which both overlie T3 and T4 – is up to 1 m of deposit that accumulated between 41.5 and 24.4 ka ago. This new ^{14}C chronology shows unequivocally that these gravel-rich sediments are not the same age as those underlying the *H. floresiensis*-bearing sediments along the east wall of the cave (see Figs 3.1 and 3.3). Instead, it provides further support for an age of more than ~41 ka for the *H. floresiensis*-bearing deposits at Liang Bua.

3.4.3 Dating of the Holocene sediments and tephras T7 and T8

Sector XXVI

Sectors XXVI and XXV are immediately adjacent to the north baulks of Sectors XVI and VII, respectively, and were excavated together in 2012 and 2014 (Fig. 3.2). The main goals of these excavations (which are ongoing) include obtaining new details about the Holocene stratigraphy and chronology. Fourteen charcoal samples from Sector XXVI yielded ^{14}C ages of ~12–0.5 ka (Table 3.3). The depths of these samples from the present cave surface ranged from 45 to 411 cm (Fig. 3.4), with the ages increasing with depth, as expected from stratigraphic principles. Three pairs of samples (D-AMS-005944 and -005945, -005949 and -005950, and -013409 and -013410) have

ages that are statistically indistinguishable at the 95% CI in each case (Table 3.3). For each pair of samples, the difference in depth is relatively small (7–16 cm), so we interpret the fact that their respective ages are indistinguishable as evidence for short-term episodes of more rapid sediment accumulation, superimposed on a fairly steady rate of deposition over the last 12 millennia.

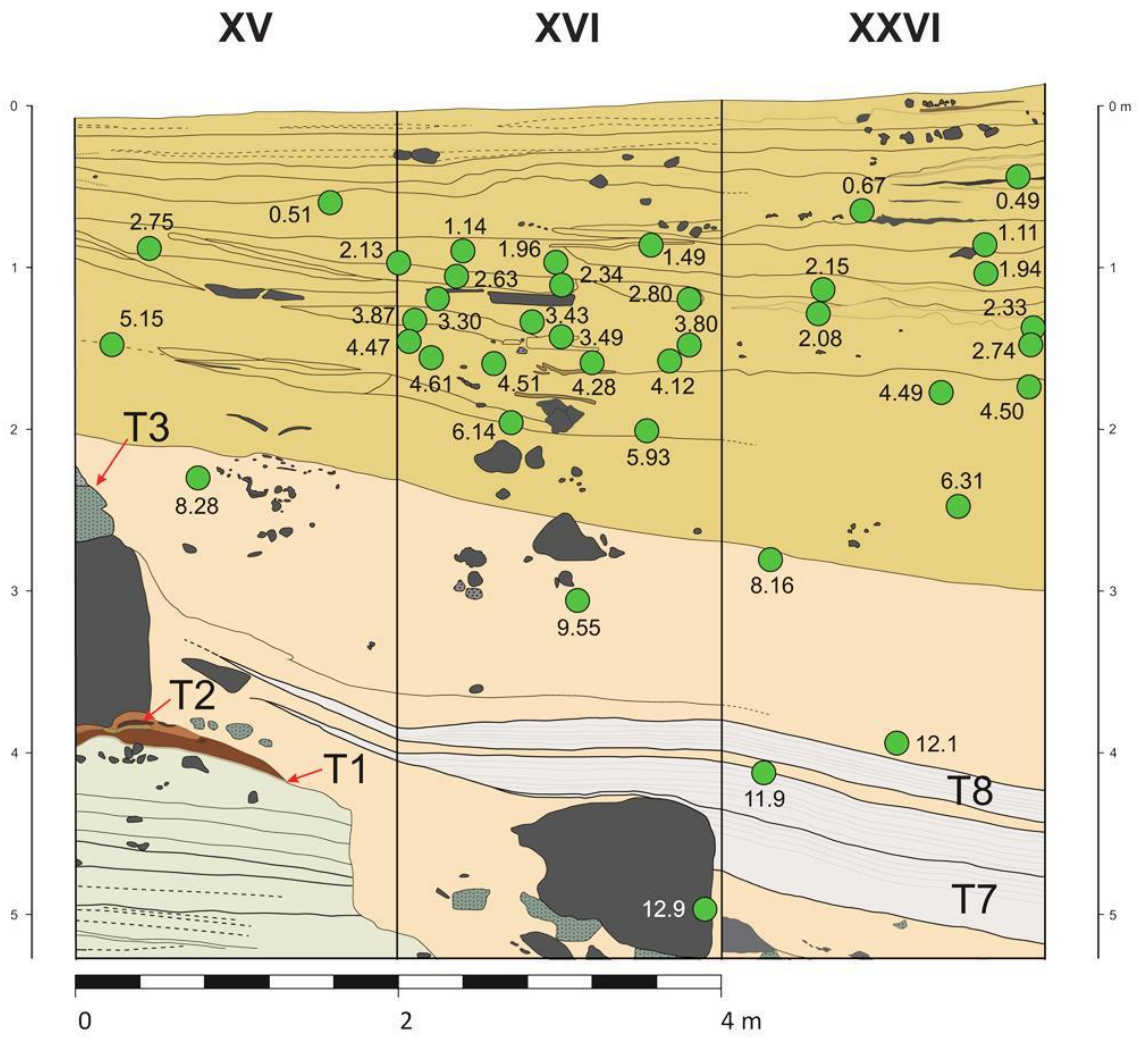

Figure 3.4 Stratigraphic profile of the western baulks of Sectors XV, XVI and XXVI (left, middle and right panels, respectively). The locations of the dated charcoal samples are shown projected on to the west wall as green circles with their median calibrated ^{14}C ages (in ka). Tephras T1, T2, T3, T7 and T8 are also indicated.

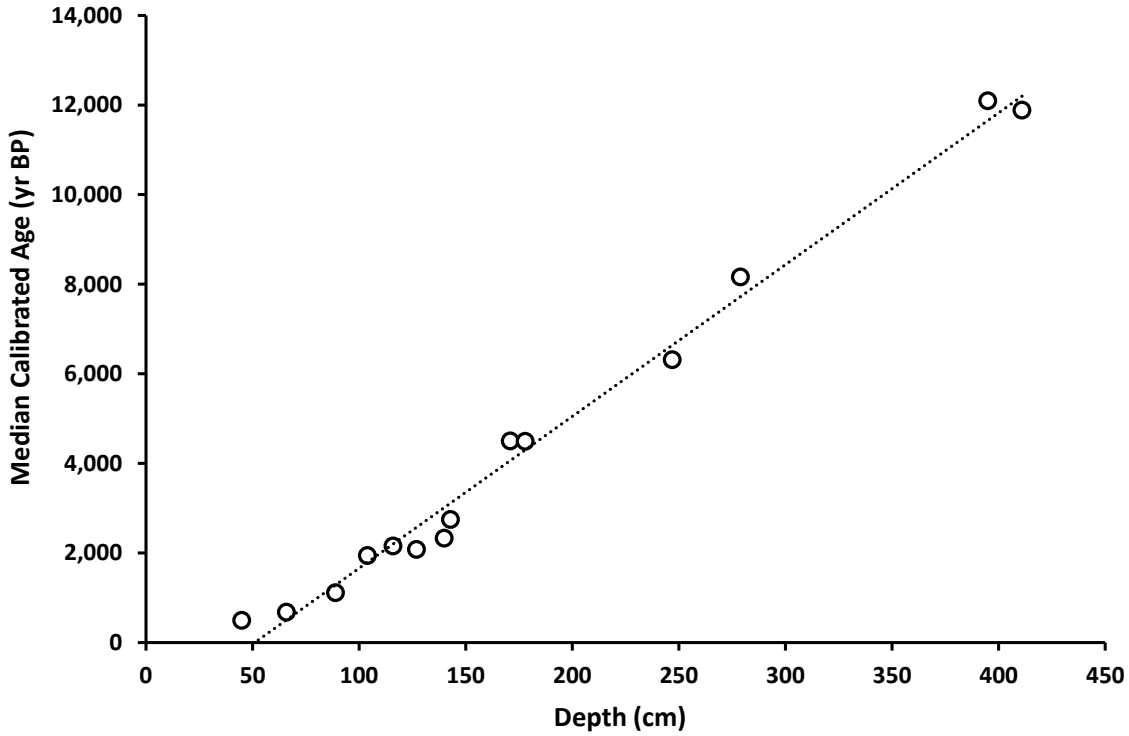

Figure 3.5 Linear regression fit to the ^{14}C ages (circles) from the Holocene sequence in Sector XXVI. The fitted line is defined as $y = 33.89x - 2200$, with $R^2 = 0.989$.

Regression analysis of the Sector XXVI ages as a function of depth produces a fitted line with a slope significantly different from zero and an R^2 value of 0.989 (Fig. 3.5). In other words, 99% of the observed variation in age is explained by a linear relationship with depth. These results suggest an average sedimentation rate of ~30 cm/ka in this Sector since the deposition of tephra T8, or ~32 cm/ka since that of tephra T7.

Sector XVI

Sectors XVI and XV are located immediately adjacent to the eastern baulks of Sectors VII and XI, respectively, and were excavated together in 2008 and 2009 (Fig. 3.2). The primary goal of these excavations was to expand the areas where most of the remains of *H. floresiensis* had been discovered, including the holotype (LB1) (Brown *et al*., 2004). It was during the excavation of these Sectors that the presence of an

unconformity was first recognised, but its implications were still not fully appreciated at that time. Twenty-one charcoal samples from Sector XVI were collected from depths of 88–497 cm below the present surface of the cave floor (Fig. 3.4) and yielded ^{14}C ages of between ~1 and 13 ka (Table 3.4).

Overall, there is reasonable correspondence between age, stratigraphic unit and depth (Fig. 3.4). However, samples from the southern half of the Sector are almost always older than those from similar depths in the northern half, essentially following the deposits as they slope downward towards the north at depths of ~1 m and deeper. In the southern half of this Sector, the ^{14}C ages range from 9.6 to 1.1 ka (upper and lower 95% CIs for the oldest and youngest ages, respectively) and all of these are ordered by increasing depth, with two statistically indistinguishable ages (95% CIs) of 4.7–4.5 and 4.6–4.4 ka for samples from depths of 153 and 157 cm depth, respectively. Sequentially ordered ^{14}C ages were obtained for the northern half of Sector XVI, ranging from 6.0 to 1.4 ka (upper and lower 95% CIs for the oldest and youngest ages, respectively).

Linear regression analysis of all 20 Holocene ages as a function of depth results in a model with a slope significantly different from zero (p = < 0.001), with 97.0% of the observed variation in age explained by sample depth (Fig. 3.6). If only the ages from the northern half of the square are considered, the proportion of total variation in age due to a linear relationship with depth increases to 99.9% and the slope of the line changes only slightly (Fig. 3.6). In contrast, analysis of the ages from the southern half of the Sector results in a model with a steeper slope and less of the total variation in age – but still a substantial fraction (95.6%) – explained as a linear function of depth (Fig. 3.6). These results give average sedimentation rates of around 21 and 27 cm/ka in the southern and northern halves of Sector XVI, respectively.

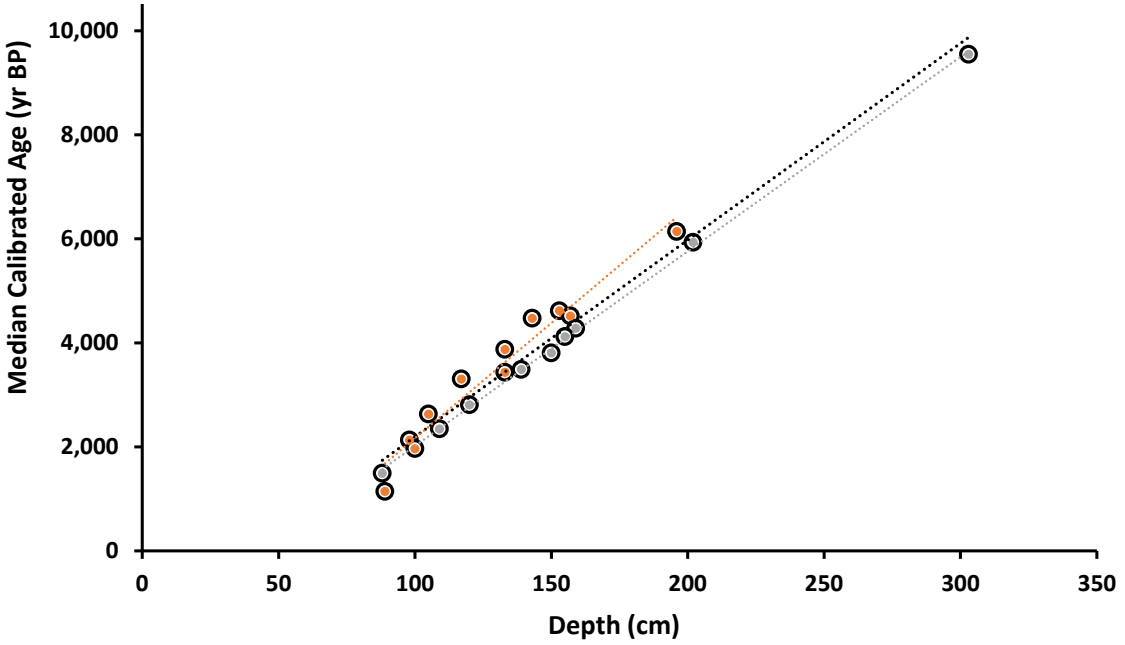

Figure 3.6 Linear regression analyses of the ^{14}C ages (circles) from the Holocene sequence in Sector XVI. The fitted lines are as follows: all samples (black), $y = 37.83x - 1589.2$, $R^2 = 0.970$; southern half (orange), $y = 44.29x - 2261.1$, $R^2 = 0.956$; northern half (grey), $y = 37.41x - 1722.7$, $R^2 = 0.999$.

Sector XIX

This Sector, excavated in 2009 and 2010, occurs slightly to the south of Sector IV (Fig. 3.2). Three charcoal samples collected from depths of 100–131 cm below the present surface of the cave floor yielded a ^{14}C age range of 5.1–3.3 ka (upper and lower 95% CIs for the oldest and youngest ages, respectively; Table 3.5). The youngest age is for the deepest sample, which was collected near the northern baulk ~1 m further north than the other two samples. This trend, in which the ^{14}C ages follow the stratigraphic evidence of a downward slope of the deposits towards the north (Fig. 3.7), is similar to that seen in Sector XVI and explains the lack of simple relation of age to depth.

Table 3.5 New ^{14}C ages for charcoal samples from Sector XIX.

					Age (yr BP)	Cal. Age Range (ka)	
	Sample Code	Depth[a]	Methods	$\delta^{13}C$	^{14}C	Median Cal.	1σ	2σ
XIX	D-AMS-013413	131	ABA / AMS	–23.4	3,174	3,355	3.39–3.34	3.41–3.32
	D-AMS-013411	100	ABA / AMS	–26.3	3,498	3,722	3.73–3.68	3.83–3.63
	D-AMS-013412	124	ABA / AMS	–16.7	4,431	4,950	4.98–4.87	5.05–4.85

Sectors IV and XI

The recalibrated ^{14}C ages for the Holocene deposits (i.e., above T8) in Sectors IV and XI were also regressed against depth to facilitate comparison with the ages for Sectors XVI and XXVI. Among the Sector IV samples, two have ages obtained using two different step-combustion temperatures (650 and 910°C). Each pair of ages are not independent observations, as they are derived from the same piece of charcoal, so we have included only the ages for the 910°C step-combustion, as these are considered the most accurate (Roberts *et al*., 2009). Linear regression analysis of the Sector IV ages clearly identifies sample GrN-14306 as a statistical outlier, with a 'studentised deleted residual value' of 10.7—far greater than the standard cutoff value of around |3.0| used to identify outliers (Neter *et al*., 1996). This result is not surprising; Roberts *et al*. (2009) noted the stratigraphically inconsistent age for this sample and attributed this inconsistency to the less stringent pretreatment methods used for this piece of charcoal (i.e., acid wash only), which may have increased the extent of sample contamination by non-elemental carbon compounds. For these reasons, we excluded this sample from further statistical analyses.

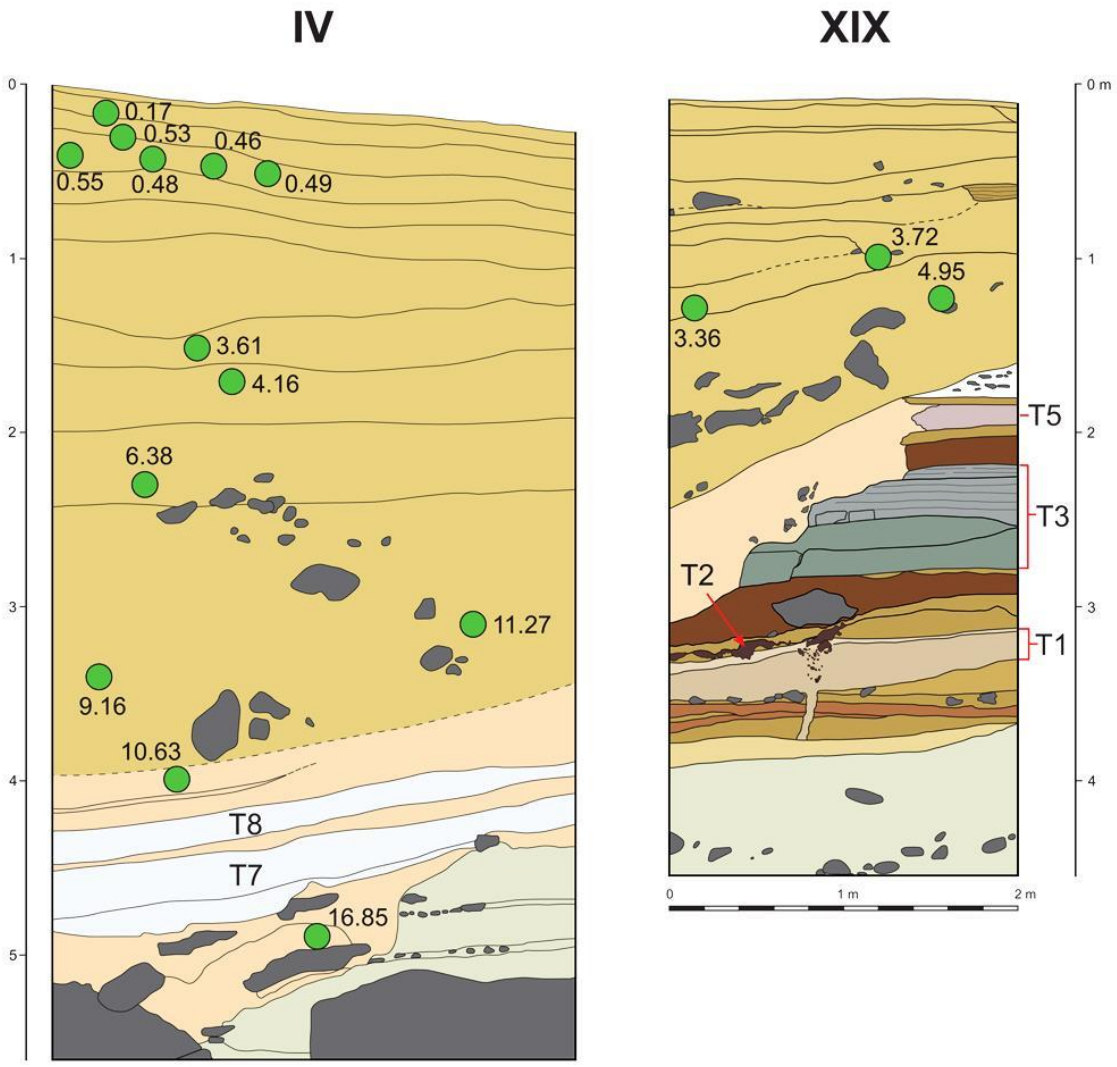

Figure 3.7 Stratigraphic profile of the eastern baulks of Sectors IV and XIX (left and right panels, respectively). Note that there is 50 cm of unexcavated deposit between the two baulks and that the orientation of Sector IV is at an angle relative to Sector XIX (see Fig. 3.2). The locations of dated charcoal samples are shown projected on to the east wall as green circles with their median calibrated ^{14}C ages (in ka). Tephras T1, T2, T3, T5, T7 and T8 are also indicated.

With GrN-14306 removed from the dataset, the slope of the fitted linear function for Sector IV is significantly different from zero ($p < 0.001$) (Fig. 3.8) and analyses of the residuals suggests the assumptions of the model are not violated. The linear model explains almost all (99.6%) of the observed variation in age with depth, and corresponds to an average sedimentation rate of ~36 cm/ka since deposition of T8.

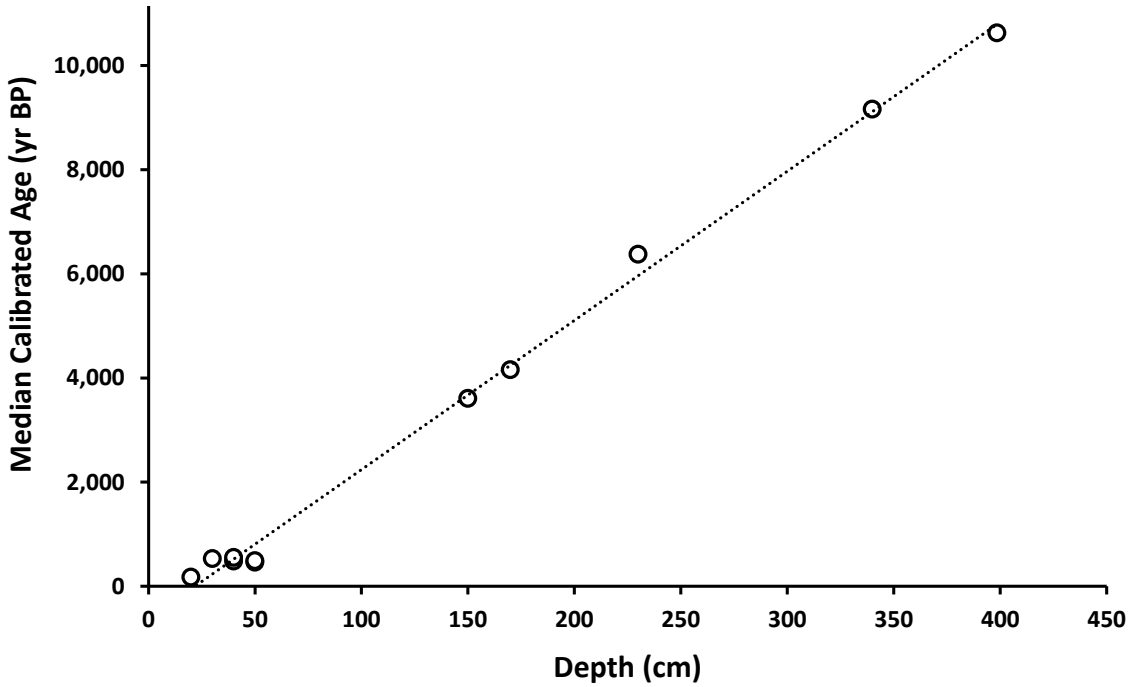

Figure 3.8 Linear regression fit to the ^{14}C ages (circles) from the Holocene sequence in Sector IV. The fitted line is defined as $y = 28.65x - 625.97$, with $R^2 = 0.996$.

Linear regression analysis of the Sector XI ages clearly identifies the youngest sample (Wk-16352) from 60 cm depth as a statistical outlier (studentised deleted residual value of –25.2). The top 75 cm of sediments in the Sectors near the eastern wall maintain a relatively horizontal profile (Fig. 3.4), whereas deposits deeper than 75 cm in Sectors XI/XV and VII/XVI slope downwards to the north. There is no stratigraphic basis, therefore, to exclude this outlier from the regression analysis, but we note that the model assumptions are violated and the results should, therefore, be treated with caution. The linear model provides a reasonable fit to these data (Fig. 3.9): the slope is significantly different from zero (p = 0.008) and 98.5% of the variation in age is explained as a function of depth. These results suggest an average sedimentation rate in Sector XI of ~22 cm/ka between about 8.3 and 0.5 ka ago, or ~25 cm/ka between about 8.3 and 2.8 ka ago.

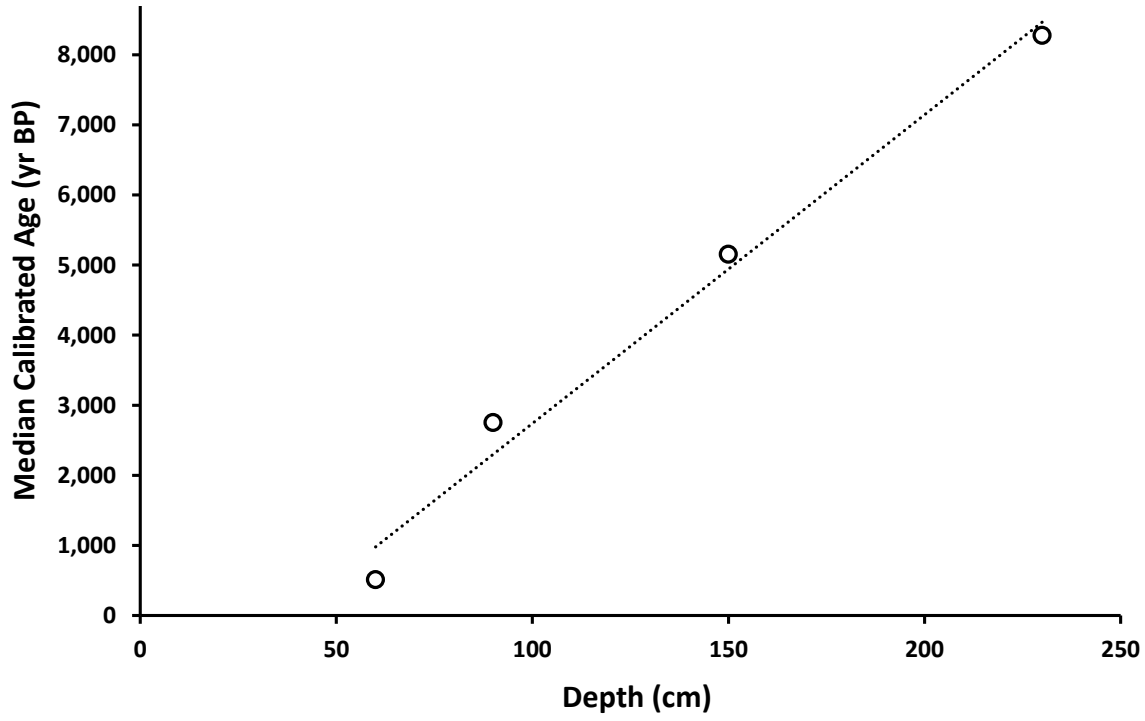

Figure 3.9 Linear regression analysis of the ^{14}C ages (circles) from the Holocene sequence in Sector XI. The fitted line is defined as $y = 44.04x - 1661.44$, with $R^2 = 0.985$.

3.5 Discussion

Since Roberts *et al*. (2009), an additional 51 charcoal samples from five new excavated Sectors at Liang Bua have yielded a ^{14}C age range of 47.7–0.45 ka (upper and lower 95% CIs for the oldest and youngest ages, respectively). These ages, and the stratigraphic information obtained during excavation, extend our knowledge about the depositional sequence preserved at Liang Bua in two major ways. First, the gap between ~46 and 20 ka in the stratigraphic record has been significantly reduced by the discovery of deposits dated by ^{14}C to ~41–25 ka in the middle rear of the cave (Sectors XXIV and XXVII; Table 3.2) and to ~46 ka in Sector XXIII (Sutikna *et al*., 2016; Table 3.1). Second, the chronological resolution of the Holocene sequence has been significantly refined and the ages of tephras T7 and T8 have been constrained more precisely.

3.5.1 Implications for the Late Pleistocene history of sedimentation at Liang Bua after 50 ka

The ways in which modern humans dispersed around the world during the past 100 millennia are topics of major significance and interest (Rasmussen *et al*., 2011; Reich *et al*., 2011; Pickrell and Reich, 2014; Liu *et al*., 2015). Current genetic data suggest that many of these dispersals out of Africa were probably unsuccessful, with no direct descendants surviving among today's human population worldwide (Fu *et al*., 2014; Pickrell and Reich, 2014). The earliest documented dispersal to Asia appears to have occurred by ~80 ka ago (Bae *et al*., 2014; Liu *et al*., 2015; Curnoe *et al*., 2016), but ancient DNA analyses are required to test whether these population have any living descendants. Ancestors of the present-day Aboriginal inhabitants of Australia and New Guinea left Africa ~70 ka ago (Rasmussen *et al*., 2011) and first reached Sahul (Pleistocene Australia and New Guinea) by at least 47–48 ka ago (Allen and O'Connell, 2014; O'Connell and Allen, 2015) or probably as early as 50–60 ka ago (Roberts *et al*., 1990, 1994, 1998; Roberts and Jones, 2001; Turney *et al*., 2001; Bowler *et al*., 2003; Clarkson *et al*., 2015; Hiscock, 2015; Bergström *et al*., 2016; Saltré *et al*., 2016).

However, there is a paucity of archaeological evidence of modern humans in Island Southeast Asia and the Indonesian archipelago earlier than 20 ka ago. The oldest archaeological evidence of modern humans on Timor is ~42 ka (O'Connor *et al*., 2011; O'Connor, 2015), with additional evidence afterwards (O'Connor *et al*., 2002a, 2002b; O'Connor, 2007; O'Connor and Aplin, 2007). In contrast, the oldest evidence of modern humans on Flores is from deposits at Liang Bua dated to ~11 ka ago (Morwood *et al*., 2004, 2005, 2009; Moore *et al*., 2009). If the latter were true, then the time of arrival of modern humans on Flores was surprisingly late and is challenging to explain,

underscoring how little is currently known about past human dispersals across the Indonesian archipelago (O'Connor, 2007).

The results of our recent excavations at Liang Bua have shown that the majority of deposits dated to between 46 and 20 ka have remained largely unexcavated by previous work. The combined Sectors XXIV and XXVII trench (1 m wide x 4 m long) suggests that these deposits likely span much of the rear of the cave (~100 m^2 in area) and occur 0.5–2 m beneath the present-day surface of the cave floor. A series of nine ^{14}C ages from Sectors XXIV and XVII in this rear area yielded ages of ~41 to 25 ka for deposits that overlie speleothems dated to ~47 ka (Fig. 3.3) (Westaway *et al*., 2007a; Roberts *et al*., 2009). Not all of these ^{14}C ages are in correct stratigraphic order, which can be explained as the result of some mixing of materials that may have occurred due to scuffing and treadage prior to consolidation of the sediments. We attribute such mixing to biological activities, including possible hominin activity, particularly as all nine of these ^{14}C ages derive from layers ~1.15 m-thick in total. Some charcoal may have been transported via past burrowing activities of insects or small mammals, but any evidence of this (e.g., infilled burrows) was not directly observed during excavation. Regardless of the exact explanation for these localised stratigraphic anomalies, these ^{14}C ages – in conjunction with the 47.7–44.1 ka age (95% CI) for the sample directly above tephra T5 in Sector XXIII (Sutikna *et al*., 2016) – suggest that no major temporal gap occurs in the Liang Bua sequence from ~190 ka to the present.

The combustion features discovered in the sediments dated to between ~41 and 24 ka cal. BP in Sector XXIV (Morley *et al*., 2016) are suggestive of a modern human presence at Liang Bua long before the deposition of tephra T8, ~12 ka ago. Further research into the archaeological findings from Sectors XXIV and XXVII – and from other Sectors – could usefully test the current interpretation that modern humans arrived

on Flores only after deposition of tephra T8 (see below). This topic is investigated in Chapter 4 of this thesis.

3.5.2 Refinement of the chronology of the terminal Pleistocene and Holocene deposits

Tephras T7 and T8 were dated previously to ~13–11 ka based on ^{14}C ages for charcoal obtained from beneath T7 in Sector VII and above T8 in Sector IV (Morwood *et al*., 2004, 2005; Roberts *et al*., 2009). Recalibration of these ^{14}C ages using the latest available datasets (Hogg *et al*., 2013) yields age ranges (95% CI) of 13.4–12.7 and 11.3–10.4 ka for these immediately pre-T7 and post-T8 samples, respectively. Two recently reported ^{14}C age ranges (95% CI) of 12.8–12.7 and 12.9–12.7 ka for charcoal samples from just beneath T7 in Sector XXII (Sutikna *et al*., 2016) are statistically indistinguishable and consistent with this chronology.

To further refine the terminal Pleistocene and Holocene tephra sequence at Liang Bua, we selected charcoal samples recovered from sediments directly underlying T7 in Sector XVI, from the thin layer of sediments that separate T7 and T8 in Sector XXVI, and from immediately above T8 in Sector XXVI (Fig. 3.4). These samples yielded ^{14}C age ranges (95% CI) of 13.1–12.8 ka beneath T7, 12.0–11.7 ka between T7 and T8, and 12.3–11.9 ka above T8. The latter two ages (both from Sector XXVI) are statistically indistinguishable. Taken together with the two ages from Sector XXII mentioned above, these results constrain the time of deposition of T7 to 13.1–11.7 ka and of T8 to 12.3–11.7 ka (upper and lower 95% CIs for the oldest and youngest ages, respectively). These are modest, but important, refinements of the previously published constraints of 13.4–10.2 ka for both tephras (Roberts *et al*., 2009), halving the time interval during which both tephras were deposited, from ~3 millennia to 1.4 ka or less.

Previous ^{14}C dating of the Holocene sequence at Liang Bua was carried out primarily in the cave centre (Sectors IV and III), with additional evidence from along the eastern wall (Sector XI) (Roberts *et al*., 2009). In this study, we explored in more detail the ages of the Holocene deposits near the eastern wall as well as from the cave centre. For the five charcoal samples from Sector XI, four of the ages appear systematically older than those collected from similar depths in Sectors XVI and XXVI (Fig. 3.4). A similar pattern is observed between the southern and northern parts of Sector XVI, and between both parts of Sectors XVI and XXVI. An ANCOVA for these four age/depth datasets results in significant pairwise differences between all but the data for Sector XI and the southern part of Sector XVI (Fig. 3.10). The least-squares mean slopes for the fitted regression lines to the ages for Sectors XI, XVI south, XVI north and XXVI are 5.16, 4.60, 4.08 and 3.53, respectively–that is, the regression slope decreases and the sedimentation rate increases towards the mouth (north) of the cave. These results support the stratigraphic interpretation of these deposits that suggests the sediments above T8, to a depth of ~75 cm, have been deposited on a downward sloping surface (Fig. 3.4), which has provided more space for sediments to accumulate in the more northerly Sectors.

Including Sector IV in an ANCOVA with the data for Sectors near the eastern wall yields similar results to the previous analysis, with significant pairwise differences between Sectors IV and XI and the southern part of XVI ($p < 0.001$). The fact that the linear relationship between age and depth in Sector IV is not significantly different from that in Sectors XXVI and the northern part of XVI is important (Fig. 3.10). Although only three charcoal samples have been dated from Sector XIX, immediately south of Sector IV, these ages are systematically older than those collected from similar depths in Sectors IV and XVI and they more closely follow the pattern observed in Sector XI.

Overall, these results suggest that the Holocene sequence is essentially similar from the eastern wall to the cave centre, providing an important framework for reconstructing the depositional history of Liang Bua not only during the Holocene, but also during the Late Pleistocene (Fig. 3.11).

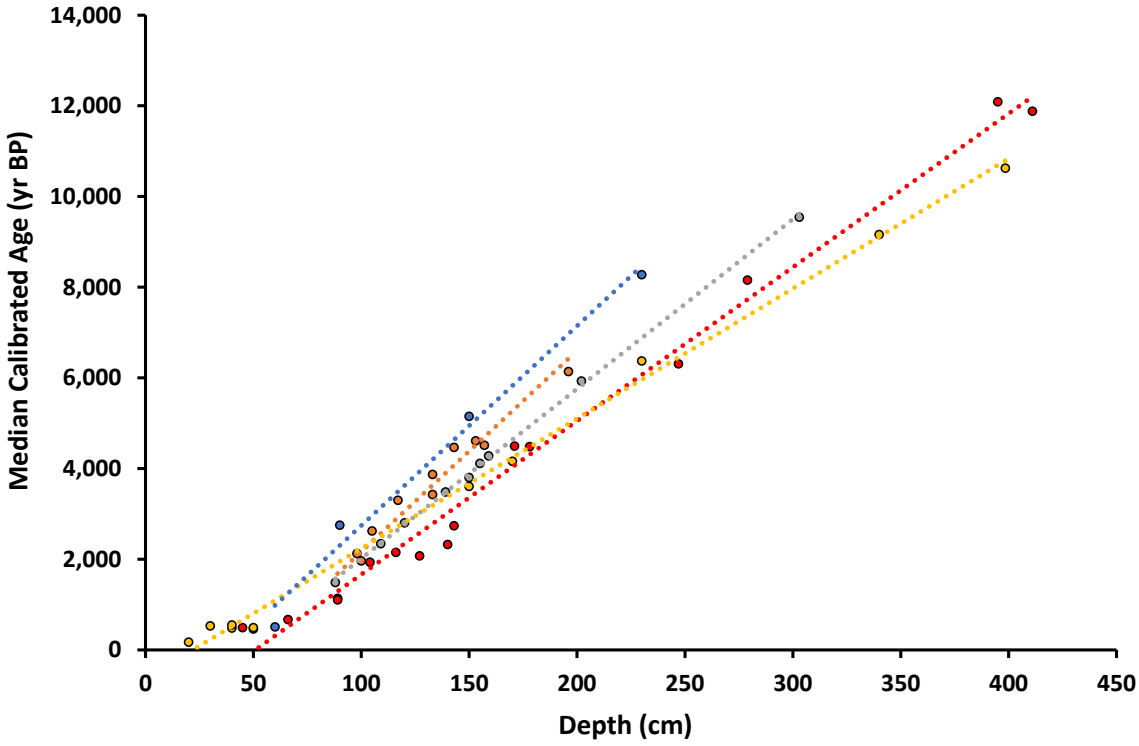

Figure 3.10 Linear regression analysis of the ^{14}C ages by depth for the Holocene and terminal Pleistocene deposits in Sectors aligned south to north as follows: XI (blue), XVI south (orange), XVI south (grey) and XXVI (red). Sector IV (yellow) lies further to the west (Fig. 3.2). ANCOVA results indicate that the regression slopes of Sectors XI and XVI south are significantly different from the others ($p < 0.05$), essentially tracking the stratigraphic observations that the deposits slope downward towards the north. The regression slopes of Sectors XVI north, XXVI and IV are not significantly different from each other.

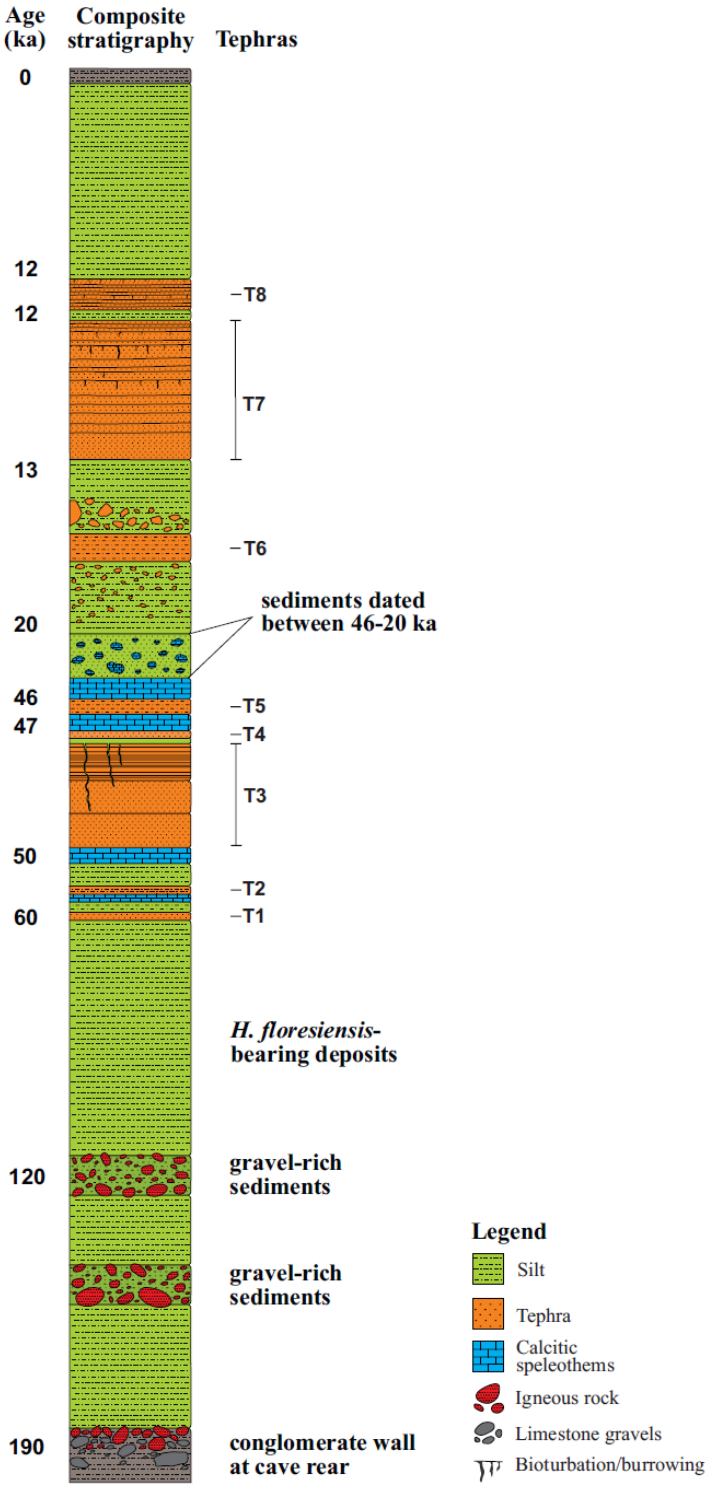

Figure 3.11 Composite section of the Liang Bua depositional sequence, showing the tephras and other key stratigraphic markers with approximate ages. The modern soil and basal sediments are shaded grey at the top and bottom of the section, respectively. Note that the previous gap between 46 and 20 ka (Fig. 3.1) now contains sediments dated to this interval in Sectors XXIV and XXVII as a result of this study. The depositional age of T8 is now more tightly constrained to ~12 ka, based on new ^{14}C ages for charcoal samples collected from immediately below and above this tephra.

The general depositional pattern emerging from Liang Bua is sediment deposition followed by erosional processes that have planed off the upper portions of the pre-existing deposits in the more northerly Sectors. As a result, the erosional surfaces consistently slope downwards to the north. The late Holocene – represented by the uppermost 75 cm of deposit – is the only period during which this pattern does not appear to dominate the stratigraphic sequence at Liang Bua. This suggests that, from ~1 ka ago, the previously recurring erosional periods became reduced in frequency and/or magnitude relative to the rate of sediment deposition, such that the most recent deposits at the site more closely preserve their original horizontal placement. Exactly how this pattern relates to the geomorphological evolution of the cave is still poorly understood, but a likely possibility is that the base of the cave also slopes downward to the north.

3.6. Conclusions

The results of this study significantly refine and extend our understanding of the past 50 ka depositional sequence at Liang Bua (Fig. 3.11). The discovery of deposits at Liang Bua that are here dated to between ~41 and 25 ka presents the opportunity to address questions regarding potentially late-surviving populations of *H. floresiensis* and/or the early presence of modern humans on the island. The latter topic is investigated further in Chapter 4.

Future work will also target the rear area of the cave for new excavations aimed at recovering additional evidence within this critical time interval. The depositional ages of tephras T7 and T8 – which represent key stratigraphic markers between the terminal Pleistocene and early Holocene sediments at Liang Bua – have been constrained more precisely to between 13.1 and 11.7 ka. Moreover, from the eastern wall to the centre of the cave, the Holocene sequence appears essentially similar and provides a useful

stratigraphic and chronological framework for reconstructing the depositional history at Liang Bua and to guide analyses of its archaeological and faunal assemblages – as will now be discussed in Chapter 4.

CHAPTER 4

The spatio-temporal distribution of archaeological finds at Liang Bua

4.1 Preface

The discovery and initial dating of *Homo floresiensis* at Liang Bua raised major questions about when modern humans first arrived on Flores and whether these two hominin species ever occupied the island at the same time (Brown *et al*., 2004; Morwood *et al*., 2004). If *H. floresiensis* survived until ~17 or 13–11 thousand calibrated radiocarbon years before present (ka cal. BP), as originally suggested (Morwood *et al*., 2004, 2005, 2009; Roberts *et al*., 2009), then it provided 30–40 millennia of potential overlap with modern humans on the island. However, the first evidence of modern humans on Flores was also from Liang Bua and restricted to the last 11 ka (Morwood *et al*., 2004, 2005, 2009).

The revised stratigraphic interpretation and chronology of the sedimentary sequence of Liang Bua (Chapters 2 and 3 of this thesis; Sutikna *et al*., 2016) has resolved some questions about *H. floresiensis*, while raising new ones about a possible earlier arrival of modern humans on Flores. Chapter 2 of this thesis (Sutikna *et al*., 2016) places the last appearance date of *H. floresiensis* at Liang Bua around 50 ka ago, removing most but not all of the possible spatio-temporal span of overlap, given the evidence of modern humans on Australia by ~50 ka (Roberts *et al*., 1990, 1994). Chapter 3 of this thesis revised the age of the first evidence of modern humans at Liang Bua to ~12 ka cal. BP, immediately following the deposition of tephra T8. However, if all of the skeletal and cultural remains of *H. floresiensis* are between ~100–60 ka and ~190–50 ka old, respectively, then is there any evidence of hominin behaviour between ~50 ka and 12 ka cal. BP at Liang Bua?

Previous analyses of archaeological materials from Liang Bua included samples thought to be derived from deposits between ~50 ka and 13–11 ka cal. BP (e.g., Moore *et al*., 2009; van den Bergh *et al*., 2009). At the time of the analyses, however, these were unknowingly combined with samples older than ~50 ka because of the misinterpretation of the stratigraphy. Thus, a reassessment of the archaeological finds at Liang Bua is required because the temporal range between ~50 ka and 12 ka cal. BP is critical for evaluating the timing, tempo and mode of modern human dispersal to Flores and throughout Island Southeast Asia.

This chapter is focused on reexamining the spatio-temporal distribution of the faunal and cultural remains at Liang Bua in the context of the revised stratigraphic and chronological interpretations. The results are used to infer details about palaeoecological and palaeoenvironmental changes and their relationship to signals of hominin behaviour at Liang Bua during the late Quaternary. Building upon the results presented in Chapters 2 and 3 of this thesis, this chapter provides more detail on the composition of archaeological finds discovered from multiple excavated areas of the site.

Changes in the abundances of faunal taxa and raw materials used to manufacture stone artefacts between stratigraphic units/subunits are examined using several univariate and multivariate statistical techniques. Chord distance analysis (Ludwig and Reynolds, 1988; Gavin *et al*., 2003) is used to measure changes in abundance across successive pairs of stratigraphic units/subunits. Pairwise comparisons of all chord distances between units/subunits are subject to cluster analysis using the unweighted pair group method with arithmetic mean to evaluate similarities of units/subunits based on their respective taxonomic and raw material compositions. The Shannon evenness index (Magurran, 1988) is used to quantify how evenly taxa and raw materials are

distributed within stratigraphic units/subunits. Correspondence analysis is used to examine the relationship of stratigraphic units/subunits with the faunal and raw material assemblages. This multivariate statistical technique provides an overall measure of faunal and raw material change across all units simultaneously (Cannon, 2001; Lyman, 2008). To further aid the interpretation of the correspondence analysis results, differences in abundance across two or more successive units were evaluated using the Cochran chi-square test for linear trends (Cannon, 2001; Lyman, 2008). Together, these various statistical techniques provide important insights into the rich archaeological sequence at Liang Bua.

As co-director of ongoing research at Liang Bua, I have supervised all of the excavations since 2001 (2001–2004 with M.J. Morwood, R.P. Soejono and R.G. Roberts; 2007–2009 with M.J. Morwood and Wahyu Saptomo; and 2010–present with M.W. Tocheri, Wahyu Saptomo and Jatmiko). All of these co-directors have contributed in various ways to the overall direction of this research. Since 2001, I have selected the areas for excavation and managed the collection of all field data. In terms of contributions to this chapter, I led the stratigraphic analyses and divisions of the sequence into the units/subunits used, with input from M.W. Tocheri, E. Wahyu Saptomo and R.G. Roberts. Rokus Due Awe, H.J.M. Meijer, M.W. Tocheri and W.L. Jungers identified the faunal remains. Jatmiko and I identified the stone artefact raw materials. I conducted all of the analyses and wrote the chapter, with guidance on the statistics from M.W. Tocheri and J.T. Faith and additional input from all other co-authors. This chapter has been prepared for submission to the *Journal of Human Evolution*.

The spatio-temporal distribution of archaeological finds at Liang Bua suggests modern humans arrived on Flores by ~46 thousand years ago

Thomas Sutikna[1,2], Matthew W. Tocheri[3,4], J. Tyler Faith[5], Jatmiko[2,1], Rokus Due Awe[2,1,‡], Hanneke J. M. Meijer[6,7,4], E. Wahyu Saptomo[2,1], William L. Jungers[8], Richard G. Roberts[1]

[1]Centre for Archaeological Science, School of Earth and Environmental Sciences, University of Wollongong, Wollongong, New South Wales 2522, Australia.
[2]Pusat Penelitian Arkeologi Nasional, Jakarta 12510, Indonesia.
[3]Department of Anthropology, Lakehead University, Thunder Bay, Ontario P7B 5Z5, Canada.
[4]Human Origins Program, National Museum of Natural History, Smithsonian Institution, Washington DC 20013, USA.
[5]Archaeology Program, School of Social Science, University of Queensland, Brisbane QLD 4072, Australia.
[6]Department of Ornithology, Senckenberg Forschungsinstitut und Naturmuseum, 60325 Frankfurt, Germany.
[7]University Museum, Department of Natural History, University of Bergen, 5007 Bergen, Norway.
[8]Department of Anatomical Sciences, Stony Brook University Medical Center, Stony Brook, New York 11794, USA.
‡Deceased.

Correspondence and requests for materials should be addressed to T.S. (thomasutikna@gmail.com).

Abstract

Liang Bua, the type site of *Homo floresiensis*, is a limestone cave on the Indonesian island of Flores with sedimentary deposits that range in age from about 190 thousand years (ka) ago to the present. Recent revision of the stratigraphy and chronology of this depositional sequence suggests that evidence of *H. floresiensis* occurs until ~50 ka ago, rather than nearer to the Late Pleistocene–Holocene boundary. Here we examine the compositions of the faunal communities (by broad taxonomic groups) and stone artefacts (by raw materials) throughout the ~190 ka time interval preserved in the sequence. Major shifts are observed in both the faunal and stone artefact assemblages that reflect marked changes in palaeoecology and hominin behaviour. The results of these analyses suggest that *H. floresiensis* and *Stegodon florensis insularis*, along with giant marabou stork and vulture, were likely extinct by about 50 ka ago. Moreover, a significant shift in raw material preference, coupled with the presence of two likely modern human teeth, provide credible evidence that *Homo sapiens* arrived on Flores by ~46 thousand calibrated radiocarbon years before present (ka cal. BP), the earliest cultural and biological evidence of modern humans in Indonesia.

4.2 Introduction

Liang Bua is a large limestone cave on the Indonesian island of Flores, which is part of the chain of Lesser Sunda Islands. The cave is located approximately 14 km northwest of Ruteng, the capital of Manggarai Regency of West Flores, and is about 500 m above sea level (Fig. 4.1a, b). Multiple archaeological excavations at Liang Bua have been conducted since 1965 and large numbers of stone artefacts and faunal remains have been recovered (Morwood *et al*., 2004, 2005, 2009; Brumm *et al*., 2006;

van den Hoek Ostende, 2006; Moore and Brumm, 2007; Moore *et al*., 2009; van den Bergh *et al*., 2008, 2009; Meijer and Due Awe, 2010; Meijer *et al*., 2013, 2015) (Fig. 4.2). Liang Bua is most widely known as the type locality of *Homo floresiensis* (Brown *et al*., 2004; Morwood *et al*., 2004), a hominin species anatomically more primitive than modern humans and Neandertals, but whose precise phylogenetic relationships to other species of early *Homo* remain unresolved (Brown *et al*., 2004; Morwood *et al*., 2005; Argue *et al*., 2006; Larson *et al*., 2007, 2009; Tocheri *et al*., 2007; Jungers *et al*., 2009a, b; Kaifu *et al*., 2011, 2015a, b; Orr *et al*., 2013).

New stratigraphic and dating evidence suggests that all skeletal and cultural remains of *H. floresiensis* are between about 100–60 and 190–50 ka old, respectively (Sutikna *et al*., 2016), and do not extend to ~17 or 13–11 ka cal. BP as suggested previously (Morwood *et al*., 2004, 2005, 2009; Roberts *et al*., 2009). Based on this new stratigraphic and chronological framework, we examine here the faunal assemblage from 12 excavated areas (referred to as Sectors) in combination with the stone artefact assemblage from eight Sectors (Fig. 4.1c), to present a current and comprehensive broad-scale spatio-temporal analysis of the palaeoecological record at Liang Bua and the raw materials used for stone artefact manufacture.

4.2.1 Previous studies

Previous studies of the Liang Bua faunal and stone artefact assemblages have been based only on materials from between one and five Sectors (I, III, IV, VII and XI) and before the complexities of the stratigraphy were fully understood (van den Bergh *et al*., 2008, 2009; Hocknull *et al*., 2009; Moore *et al*., 2009; Meijer and Due Awe, 2010; Meijer *et al*., 2013; Locatelli *et al*., 2012, 2015). In addition to the remains of *H. floresiensis*, the Liang Bua faunal assemblage includes at least three other ‘large’ taxa

(i.e., greater than 5 kg)—*Stegodon florensis insularis* (stegodont), *Leptoptilos robustus* (giant stork) and *Trigonoceps* sp. (vulture)—that are not present on Flores today.

Figure 4.1 Site location and plan: **a**, Location of Flores island within the Indonesian archipelago; **b**, Location of Liang Bua on Flores island; **c**, Liang Bua plan and Sectors discussed in the text.

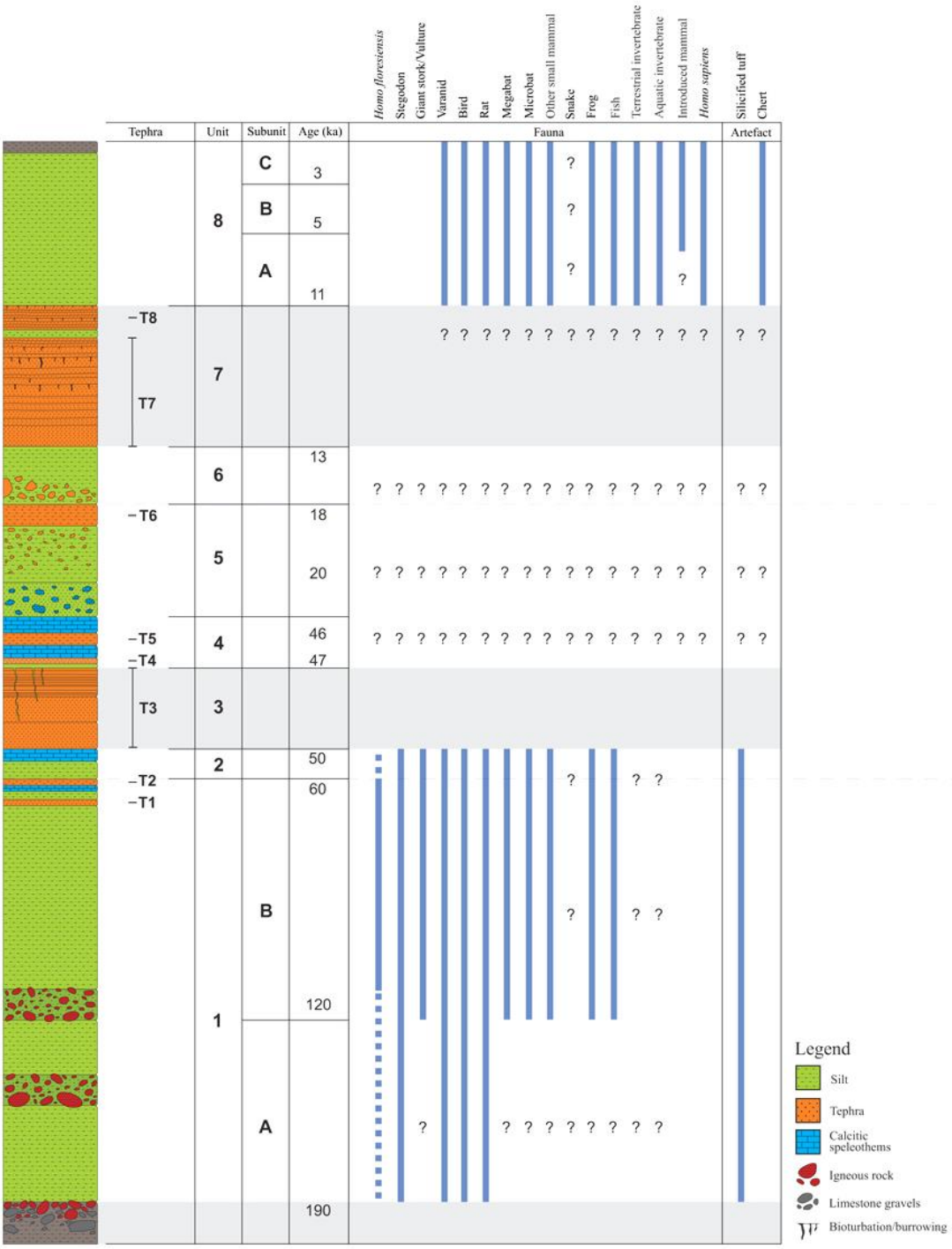

Figure 4.2 Composite stratigraphy at Liang Bua with approximate ages and units/subunits based on Sutikna *et al*. (2016). The modern soil and basal sediments are shaded grey at the top and bottom of the section, respectively. Eight identified tephras (T1–T8) define the eight main units/subunits used in this chapter (Units 1A–8C). The data shown for the fauna and stone artefacts are based on samples obtained during the 2001–2004 excavations. Based on this revised stratigraphy and chronology, the vertical blue lines show the known faunal presence (Morwood and Jungers, 2009; van den Bergh *et al*., 2009; Meijer *et al*., 2013) and the raw material preferred by hominins for stone artefacts (Moore *et al*., 2009). The dotted vertical lines indicate presumed presence of *H. floresiensis* based on stone artefacts (Sutikna *et al*., 2016). Question marks highlight new uncertainties raised by the results of previous publications, in combination with the revised stratigraphic and chronological framework for the site.

S. florensis insularis is an endemic form of proboscidean that is most likely the direct descendant of *S. florensis florensis* (van den Bergh *et al*., 2008), which is known from several sites in the Soa Basin of central Flores that have been dated to between ~850 and 700 ka (Morwood *et al*., 1998). The linear dimensions of *S. florensis insularis* molars are ~30% smaller than those of *S. florensis florensis*, suggesting that the Liang Bua stegodonts were also smaller in overall body size compared to their Soa Basin ancestors (van den Bergh *et al*., 2008). However, adult male *S. florensis insularis* may have reached similar body sizes to those of adult female *S. florensis florensis*, given the slight overlap between the largest and smallest elements (dental and postcranial) observed at Liang Bua and the Soa Basin, respectively (van den Bergh *et al*., 2008). A specific body mass estimate for *S. florensis insularis* is not provided by van den Bergh *et al*. (2008); however, an average adult body mass of ~500 kg is probably reasonable, given the estimate of ~850 kg, on average, for *S. florensis florensis* (van den Bergh *et al*., 2008). Although the Liang Bua stegodonts are small for proboscideans in general, they were likely the largest animals alive on Flores during the Late Pleistocene and would have played important ecological roles both as an herbivore (Owen-Smith, 1988) and as prey (hunted and/or scavenged) in the island's ecosystem. Thus, the exact timing of *Stegodon* extinction on Flores has significant implications for reconstructions of the island's palaeoecology.

Based on inferred stratigraphic associations between stegodont remains and radiocarbon-dated charcoal samples from Sector VII at Liang Bua, *S. florensis insularis* was thought to have gone extinct about 13–11 ka cal. BP (Morwood *et al.*, 2004, 2005; van den Bergh *et al*., 2008, 2009; Meijer and Due Awe, 2010). However, because these inferred stratigraphic associations have since been shown to be erroneous, the true extinction date of this taxon is now less certain, but probably lies between ~50 ka and

~13 ka cal. BP (Sutikna *et al*., 2016). The Sector VII stegodont remains are typically very poorly preserved and contrast strongly with those recovered from Sector XI (van den Bergh *et al*., 2008). In fact, the latter authors thought that the fragmentary *Stegodon* remains from Sector VII had probably "washed down from the elevated area" above, in Sector XI (van den Bergh *et al*., 2008: 18), but were of comparable age based on the stratigraphic interpretation at that time (Morwood *et al*., 2005). In light of the new interpretations, these "youngest" *Stegodon* elements were probably reworked into the ~19–13 ka cal. BP sediments, which are now recognised to unconformably overlie a remnant pedestal of much older deposits (≥46 ka cal. BP) (Sutikna *et al*., 2016).

Giant marabou stork (*Leptoptilos robustus*) and vulture (*Trigonoceps* sp.), both large carnivorous birds, have been documented in the Late Pleistocene deposits at Liang Bua that also contain the remains of both *Stegodon* and *H. floresiensis* (Meijer and Due Awe, 2010; Meijer *et al*., 2013, 2015). Although the diet of these birds likely included smaller mammals (e.g., rats) and other birds, scavenging on the carcasses of *Stegodon* probably comprised a significant component of their feeding behaviour (Meijer *et al*., 2013). Whether their extinction is tied directly to that of *Stegodon* and/or *H. floresiensis* is, therefore, a key palaeoecological question that remains unanswered (Meijer *et al*., 2015).

Living populations of Komodo dragon (*Varanus komodoensis*) survive on the islands of Komodo, Rinca and Padar (all immediately west of Flores) and on the northern coast of Flores (Auffenberg, 1981). The distribution of this reptilian predator on Flores was clearly wider in the past, as remains of this taxon have been recovered from deposits at both Liang Bua and multiple sites within the Soa Basin (van den Bergh *et al*., 2009; Hocknull *et al*., 2009). Hocknull *et al*. (2009) concluded that Komodo dragons survived around Liang Bua until ~2 ka ago; however, all of the Liang Bua

bones they examined were derived from Late Pleistocene deposits (see their Table S1), and only a single mandibular fragment was identified from Holocene sediments by van den Bergh *et al*. (2009). A lone mandibular fragment could easily have been reworked from older deposits, or possibly even transported from the coast by modern humans ~2 ka ago, raising doubts about whether Komodo dragons survived in the vicinity of Liang Bua until and into the Holocene. Further complicating matters is that the remains of another large varanid (*Varanus hooijeri* Brongersma, 1958), thought to be extinct today, are present throughout the Liang Bua sequence and are especially prevalent in the Holocene sediments (van den Bergh *et al*., 2009). Although *V. hooijeri* has distinctive, blunt-shaped teeth and is thought to be smaller overall than *V. komodoensis* (van den Bergh *et al*., 2009), distinguishing between fragmentary postcranial remains of these two taxa presents challenges, especially given how little is known about body size variation in this taxon.

Other fauna recorded and/or studied at Liang Bua include one or multiple species of bat, bird, shrew, murine rodent (i.e., rats), civet cat, porcupine, macaque, dog, deer, pig, bovid and horse, as well as terrestrial, freshwater and marine molluscs (Morwood *et al*., 2004, 2005; van den Hoek Ostende, 2006; van den Bergh *et al*., 2009; Locatelli *et al*., 2012, 2015; Meijer *et al*., 2013, 2015). Many of these taxa were likely introduced to Flores by modern humans during the Holocene, based on an earlier study of the Liang Bua fauna from Sectors I, III, IV, VII and XI (van den Bergh *et al*., 2009). This initial research documented the following first appearance dates for these introduced mammals at Liang Bua: ~7 ka for the Sulawesi warty pig (*Sus celebensis*); ~4 ka for Eurasian pigs (*Sus scrofa*), Javanese porcupines (*Hystrix javanica*), long-tailed macaques (*Macaca fascicularis*) and Masked palm civets (*Paradoxurus hermaphrodites*); and within the last ~500 years for deer (*Rusa* sp.), dog (*Canis familiaris*), bovid (*Bos sp.*) and horse

(*Equus* sp.). Marine molluscs recovered at Liang Bua are dominated by Veneridae and Nautilidae, but these are found only in sediments that postdate ~4 ka and were most likely brought in or traded from coastal areas by modern humans. However, beyond these major faunal shifts, which occurred mostly from the mid-Holocene onward, relatively little is known about the Liang Bua fauna in terms of their taxonomy, phylogeny and palaeoecology.

Stone artefacts are present throughout the Liang Bua stratigraphic sequence. In the most detailed study of the Liang Bua stone artefacts to date (Moore *et al*., 2009), only a small number of characteristics distinguish the tool assemblages made by *H. floresiensis* from those made by modern humans. Both assemblages are technologically similar in terms of the reduction sequence and knapping techniques used (e.g., freehand, burination, truncation and bipolar), but they vary in terms of raw material selection and the number of stone artefacts that show evidence of edge-gloss and/or exposure to fire (Moore *et al*., 2009). For instance, the stone artefact assemblages attributed to modern humans are all Holocene in age and include the only evidence of edge-glossed flakes; ~18% of the stone artefacts shows evidence of exposure to fire (compared to less than 1% of the Late Pleistocene assemblages attributed to *H. floresiensis*) and ~60% are made from chert (compared to only ~16% of the *H. floresiensis* assemblages) (Moore *et al*., 2009).

The discovery of the skeletal and associated cultural remains of *H. floresiensis*, and the initial interpretation that it and *S. florensis insularis* survived on Flores until ~17 or ~13–11 ka cal. BP (Morwood *et al*., 2004, 2005, 2009), suggested that these taxa overlapped with modern humans – if not on Flores itself, then at least in the surrounding region – for around 30 to 40 millennia. The earliest evidence for modern humans on Flores was also from Liang Bua and suggested initial arrival at ~11 ka cal. BP

(Morwood *et al*., 2004, 2005, 2009; Moore *et al*., 2009). Such a late arrival of modern humans on Flores was unexpected and challenging to explain, given the evidence for modern humans on Timor by ~42 ka ago (O'Connor, 2007) and in Australia by ~50 ka ago (Roberts *et al*., 1990, 1994; Bowler *et al*., 2003; Allen and O'Connell, 2014; Clarkson *et al*., 2015; O'Connell and Allen, 2015).

4.2.2 Research objectives

The revised stratigraphic interpretation of the Liang Bua sedimentary sequence, along with the geochronological evidence that supports it (Chapters 2 and 3 of this thesis; Sutikna *et al*., 2016), requires a reappraisal of the excavated faunal remains and stone artefacts. Previous analyses of this material unknowingly did not include samples dated to between ~50 ka and 11 ka cal. BP or pooled them with samples older than ~50 ka (e.g., van den Bergh *et al*., 2008, 2009; Moore *et al*., 2009). As this time interval is critical for addressing questions surrounding the timing and nature of modern human dispersal through Island Southeast Asia and across Flores (including the palaeoecology before and after the arrival of *H. sapiens*), the aim of this study is to reexamine the faunal and stone artefact evidence from Liang Bua to shed new and/or additional light on these major issues. We focus in particular on the implications for understanding ecological change through time, as it relates to signals of hominin behaviour in the cave.

4.3 Materials and methods

4.3.1 Stratigraphic units

In this study, we used the eight tephras that occur within the Liang Bua depositional sequence (Sutikna *et al.*, 2016) to define eight main stratigraphic units (Units 1–8). The oldest and youngest units are further divided into two (1A–B) and

three (8A–C) subunits, respectively (Table 4.1 and Fig. 4.2). Unit 1 is defined as the deposits underlying and including tephras T1 and T2 (which were emplaced ~60 ka). All of the sediments underlying the gravel-rich layer in the Sectors near the eastern cave wall and in the oldest parts of other Sectors comprise Unit 1A (~190–120 ka), whereas the *H. floresiensis*-bearing deposits and the capping pair of tephras are defined as Unit 1B (~120–60 ka).

Sediments occurring between T2 and the bottom of T3 comprise Unit 2 (~60–50 ka), while tephra T3 constitutes Unit 3 (~50–47 ka). Unit 4 (~47–46 ka) is defined as all sediments between the top of T3 and the top of the flowstone that immediately overlies T5, and Unit 5 comprises all sediments that occur stratigraphically above this flowstone up to and including T6 (~46–18 ka). Sediments overlying T6 and underlying T7 comprise Unit 6 (~18–13 ka), while those of T7 up to and including T8 constitute Unit 7 (~12 ka). Unit 8 includes all sediments above T8. Sediments between about 12 and 5 ka cal. BP comprise Unit 8A; those between about 5 and 3 ka cal. BP make up Unit 8B and include the first evidence of pottery at Liang Bua (Morwood *et al*., 2009); and those younger than ~3 ka cal. BP constitute Unit 8C.

Table 4.1 Summary of the Liang Bua assemblages examined in this study.

Unit	Approximate Age Range (ka)	Unit Description	NISP[1] Vertebrates[2]	Invertebrates[3]	Stone Artefacts[4]
8C	3–0	Neolithic to Present	16,128	3,076	3,269
8B	5–3	Mesolithic to Neolithic transition	16,157	5,234	945
8A	12–5	above T8 to terminal Mesolithic	26,154	456	372
7	13–12	T7 to T8	438	0	0
6	18–13	above T6 to beneath T7	13,627	1	602
5	46–18	above T5-capping flowstone to T6	11,124	15	770
4	47–46	above T3 to flowstone above T5	543	16	57
3	50–47	T3	0	0	0
2	60–50	between T2 and T3	4,116	1	31
1B	120–60	*H. floresiensis*- bearing sediments	156,949	39	4,308
1A	190–120	underlying gravel-rich layer	30,607	8	80
		Total NISP	275,843	8,846	10,434

[1]NISP, number of identified specimens

[2]Excluding hominin taxa

[3]Includes aquatic and terrestrial taxa

[4]Sample examined for raw material

4.3.2 Faunal assemblage

More than 340,000 faunal elements were recovered from 12 sectors (I, IV, VII, XI, XV, XVI, XVII, XIX, XXI, XXII, XXIII and XXIV) (Fig. 4.1). Of these, 284,689 specimens were identified (number of identified specimens, NISP) to one of 14 broad taxonomic levels that together account for more than 99% of NISP in each stratigraphic unit (Table 4.2). These taxonomic abundances were analysed assuming that all skeletal elements represent animals that died during the depositional accumulation of the stratigraphic unit from which they were recovered. However, elements attributed to *Stegodon*, giant marabou stork and vulture recovered from Units 4 and above show taphonomic signs of reworking (van den Bergh *et al*., 2009) as do tephras T1–T3 (Sutikna *et al*., 2016). Thus, an additional analysis was conducted assuming that these taxa were already extinct and that their skeletal elements most likely derived from Unit 1B. Together, these quantitative analyses measure faunal structure throughout the

assemblage and enable exploration of temporal patterns of palaeoecological change at Liang Bua over the past ~190 ka.

The degree of faunal change between units was quantified using chord distance (CD), a measure of taxonomic dissimilarity using relative abundance data (Ludwig and Reynolds, 1988; Gavin *et al*., 2003). Assemblages with identical or very similar faunal compositions will have CD values equal or close to 0, whereas those with no or few taxa in common will be equal or close to the square root of 2 (i.e., ~1.4). Pairwise comparisons of all CD values between units were also subject to cluster analysis using the unweighted pair group method with arithmetic mean (UPGMA), which evaluates unit similarities based on descriptor variables (in this case, taxonomic group composition) (Legendre and Legendre, 1998).

The Shannon evenness index (Magurran, 1988) was used to measure taxonomic evenness throughout the sequence. This statistic equals the Shannon diversity index divided by the logarithm of the number of taxa present, providing a measure of how evenly individuals are distributed among all of the taxa present within an assemblage (Magurran, 1988). The numerator (i.e., the Shannon diversity index) takes into account how many taxa and individuals are present. Assemblages with an uneven distribution of taxa, in which some taxa are very abundant and others are very rare, will result in evenness values approaching 0, whereas those with an even distribution (i.e., all taxa are similarly abundant) will approach 1 (Magurran, 1988).

Finally, correspondence analysis was used to examine the relationship between stratigraphic units based on the taxonomic abundances within each unit. This multivariate statistical technique provides an overall measure of faunal change across all units simultaneously. To aid in the interpretation of the correspondence analysis results, differences in the abundance of a taxonomic group between two or more successive

units were evaluated using the Cochran test for linear trends; this is a type of chi-square analysis that is ideally suited for statistical analysis of abundance data among rank-ordered samples (Cannon, 2001; Lyman, 2008).

Table 4.2 Number of identified specimens (NISP) by stratigraphic unit and taxon.

	Stratigraphic Unit										
Taxon	1A	1B	2	4	5	6	7	8A	8B	8C	Total
Bird	167	1,562	80	7	151	170	13	282	131	180	2,743
Stork/Vulture	0	115	2	0	0	2	0	0	0	0	119
Fish	3	326	2	1	6	17	0	152	196	110	813
Frog	470	2,404	78	14	373	428	14	3,318	3,611	1,719	12,429
Stegodon	478	10,633	23	7	169	355	0	9	0	1	11,675
Large Mammal (introduced)	0	0	0	0	0	0	0	82	496	833	1,411
MegaBat	264	1,379	44	30	701	713	21	2,077	1,023	521	6,773
MicroBat	447	2,813	124	42	1,374	2,303	96	3,074	1,302	1,050	12,625
Other Small Mammal	41	160	4	0	63	46	1	34	12	52	413
Rat	28,641	135,776	3,742	429	8,202	9,339	290	15,922	8,943	11,506	222,790
Snake	6	231	5	11	39	193	2	924	224	81	1,716
Varanid	90	1,550	12	2	46	61	1	280	219	75	2,336
Aquatic Invertebrate	6	25	0	3	9	0	0	169	4,251	2,495	6,958
Terrestrial Invertebrate	2	14	1	13	6	1	0	287	983	581	1,888
Total	30,615	156,988	4,117	559	11,139	13,628	438	26,610	21,391	19,204	284,689

4.3.3 Stone artefact assemblage

A total of 10,434 stone artefacts (excluding debitage) was sampled from eight sectors (XV, XVII, XIX, XXI, XXIII, XXIV, XXV and XXVI) and examined for raw material lithology. Seven raw materials were identified in the sample (silicified tuff, chert, silicified limestone, jasper, chalcedony, andesite and quartz) that together account for 100% of specimens in each unit (Table 4.3). The same quantitative methods as used for the palaeoecological analyses were used to examine the raw material abundances relative to each stratigraphic unit, to explore the degree of change in raw material preference at Liang Bua over the past ~190 ka.

Table 4.3 Number of identified specimens (NISP) by stratigraphic unit and raw material (excluding debitage).

	Stratigraphic Unit									
Raw Material	1A	1B	2	4	5	6	8A	8B	8C	Total
Silicified Tuff	56	3,014	20	21	317	153	154	375	1,048	5,158
Chert	9	751	4	32	299	324	128	345	1,598	3,490
Silicified Limestone	1	219	1	0	18	14	36	77	337	703
Jasper	0	68	1	2	16	4	15	58	106	270
Chalcedony	7	78	1	0	39	53	3	18	41	240
Andesite	7	175	4	2	76	50	35	70	131	550
Quartz	0	3	0	0	5	4	1	2	8	23
Total	80	4,308	31	57	770	602	372	945	3,269	10,434

4.4 Results

4.4.1 Faunal assemblage

Specimen counts (NISP) across stratigraphic units for taxa identified at Liang Bua are summarised in Table 4.2. The total NISP for vertebrates and invertebrates was 275,843 and 8,846, respectively (Table 4.1). No faunal remains were recovered from T3, so Unit 3 is not included in the analyses reported below.

Figure 3.3 shows the CD values for the faunal assemblages across successive pairs of assigned depositional units. Of all successive pairs, Units 1A to 1B followed by Units 1B to 2 shows the least amount of change (CD $\leq$ 0.07). The change observed from Units 2 to 4 (CD = 0.10), which represents before and after T3 (Unit 3, ~50–47 ka), is similar to but slightly larger than all subsequent changes (CD = 0.08–0.09), until deposition of T8. Therefore, a gradual but noticeable shift in faunal community composition occurs through the Late Pleistocene sequence, following the deposition of T3.

From the terminal Late Pleistocene to the early Holocene, represented here by Units 7 (~13–11 ka cal. BP) to 8A (~11–5 ka cal. BP), the amount of faunal change (CD = 0.22) is more than double that observed in any of the previous unit pairs. Furthermore, the amount of change (CD = 0.44) doubles again from Units 8A to 8B (~5–3 ka cal. BP), which represents the Neolithic transition. From Units 8B to 8C, the amount of

change (CD = 0.31) is less than that of the previous unit pair (8A to 8B), but greater than any of the other comparisons. Overall, greater amounts of faunal change are observed within the Holocene units compared to the Late Pleistocene units.

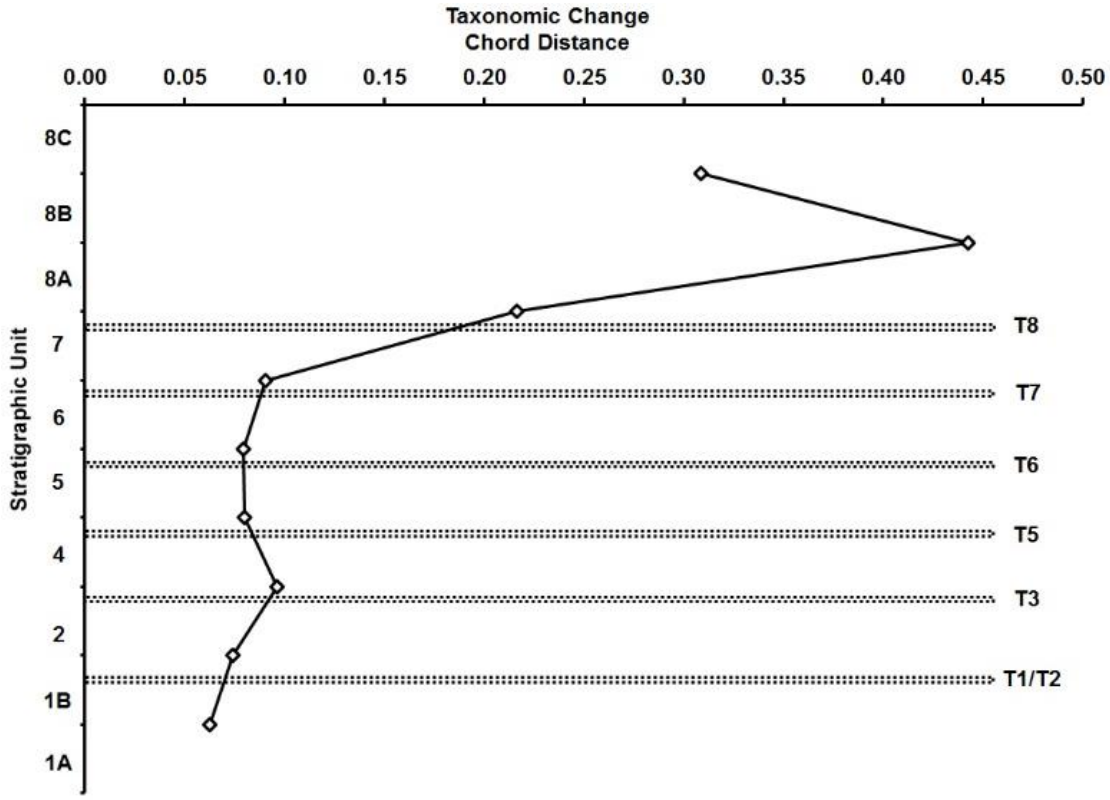

Figure 4.3 Chord distance (CD) values (dimensionless) for the faunal assemblages across successive pairs of assigned depositional units at Liang Bua. The tephras are denoted as T1–T8. CD values close to zero indicate no change between units, while higher values indicate more change.

UPGMA analysis of all pairwise chord distances between units results in two main clusters, with Unit 8B forming one cluster and all other units forming the other (Fig. 4.4). Within this second cluster, 8C is most unlike all of the remaining units, which form two additional clusters. The first of these includes Units 1A, 1B, 2 and 4, while the second includes Units 5, 6, 7 and 8A. In the former cluster, Units 1A, 1B and 2 are more similar to one another than any are to Unit 4; and in the latter cluster, Units 5 and 6 are most similar to each other, followed by Unit 7 and, lastly, Unit 8A.

Analysis of taxonomic evenness throughout the stratigraphic sequence, using the Shannon evenness index, also indicates major differences between the assemblages of Units 1 and 2 compared to Units 4 and above (Fig. 4.5). An overall trend of increasing evenness (i.e., all taxa are similarly abundant) is observed from the base to the top of the sequence, but with the most marked shifts in evenness occurring between Units 2 and 4, and between the subunits of Unit 8. Although the Shannon evenness index can be sensitive to sample size, we find no significant relationship between NISP and the evenness index among the different units (r = –0.32, p = 0.37 and Spearman's rho (r_s) = –0.08, p = 0.83).

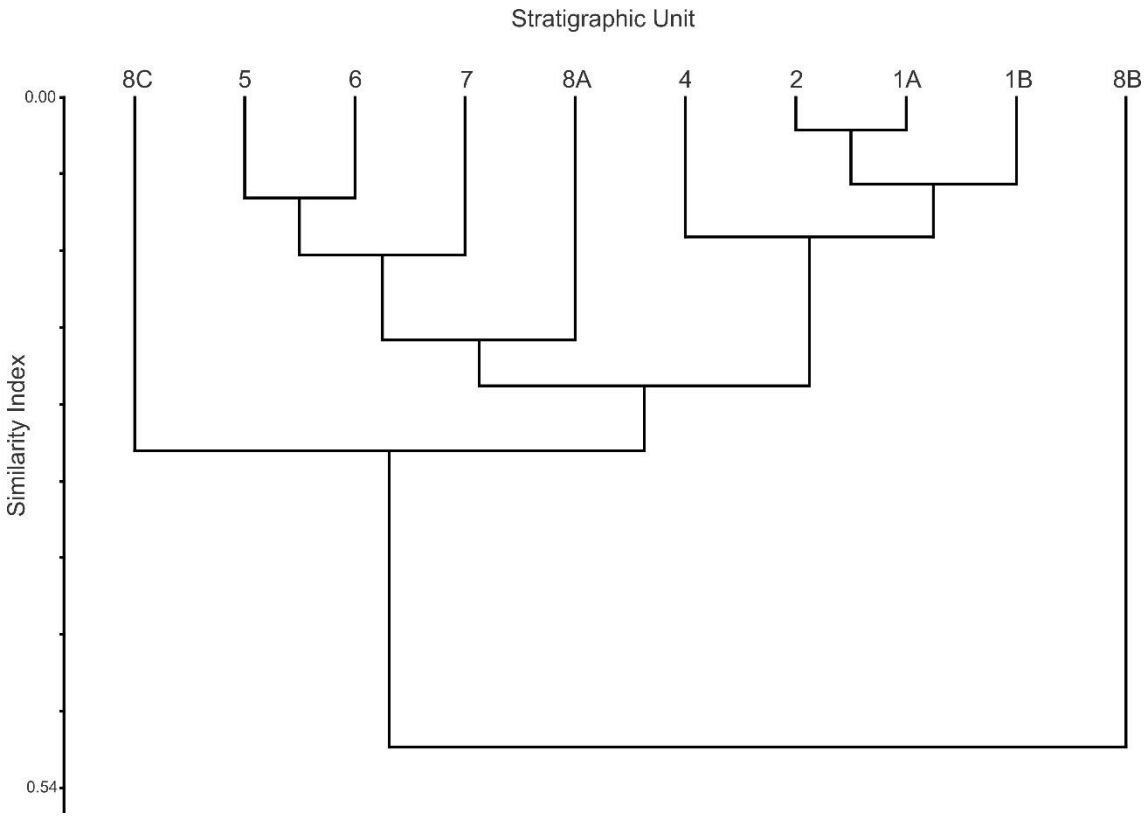

Figure 4.4 Unweighted pair group method with arithmetic mean (UPGMA) cluster analysis of stratigraphic units at Liang Bua. The dendrogram is based on a similarity index (dimensionless) calculated using the matrix of all pairwise chord distances between units. Deeper branches between units indicate less similarity in faunal structure (e.g., Unit 1B compared with all other units).

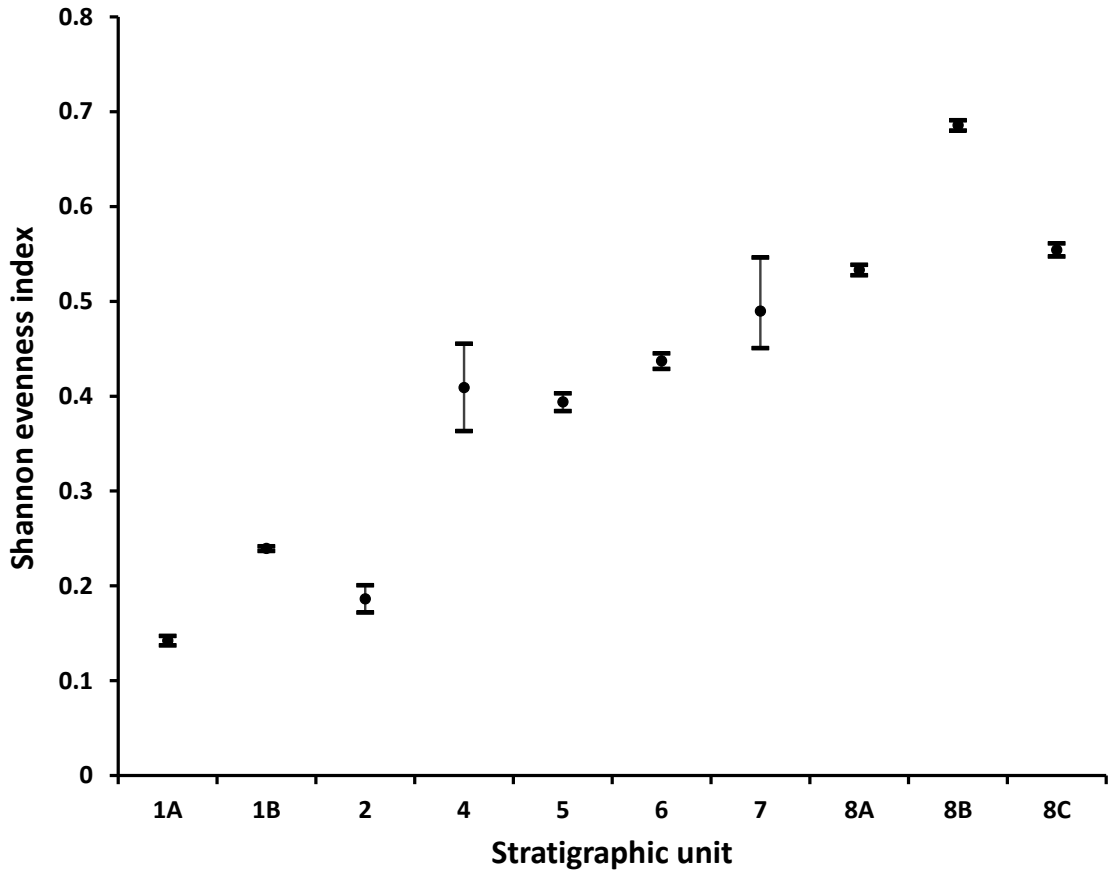

Figure 4.5 Taxonomic evenness throughout the stratigraphic sequence, determined using the Shannon evenness index. Approximate 95% confidence intervals for the index of each unit were estimated using the bootstrap procedure (9999 resamples with replacement) provided in PAST, version 3 (Hammer, 2015). Greater evenness is indicated by higher index values. Note the significant differences between the indices of assemblages of Units 1A–2 compared to Units 4–8C.

Axes 1 and 2 of the correspondence analysis explain 70.7% and 21.3% of the variance in faunal taxonomic abundance, respectively (Fig. 4.6). Units 1 and 2 show the most negative scores along axis 1; these deposits are dominated by rats (≥86.5% of NISP; Fig. 4.7) and also contain stegodont remains (0.6 to 6.8% of NISP; Fig. 4.8) and low numbers of the other taxonomic groups (≤3% of NISP). Units 4 to 7 follow a noticeable trend, shifting to more negative values along axis 2 with each successive unit and having more positive axis 1 values than Units 1 and 2. These changes are driven by a decrease in rat abundance ($\chi^2_{\text{trend}} = -22.34$, $p < 0.0001$), in conjunction with increasing

abundances of frog (χ^2_{trend} = 17.93, p < 0.0001), snake (χ^2_{trend} = 27.69, p < 0.0001), 'megabat' (Megachiroptera) (χ^2_{trend} = 54.64, p < 0.0001) and, especially, 'microbat' (Microchiroptera) (χ^2_{trend} = 100.47, p < 0.0001) (Figs 4.9–4.12). However, Unit 4 shows an increase in both aquatic (χ^2_{trend} = 1.84, p = 0.03) and terrestrial invertebrates (χ^2_{trend} = 12.63, p < 0.0001) relative to Units 1A, 1B and 2, whereas these taxa decrease in abundance in the subsequent Units 5, 6 and 7 (χ^2_{trend} = –4.80, p < 0.0001 and χ^2_{trend} = –8.93, p < 0.0001, respectively) (Figs 4.13 and 4.14). The relative abundance of these invertebrates in Unit 4 explains why it falls slightly to the right of the otherwise clear trend line from Units 1A to 7 (Fig. 4.6).

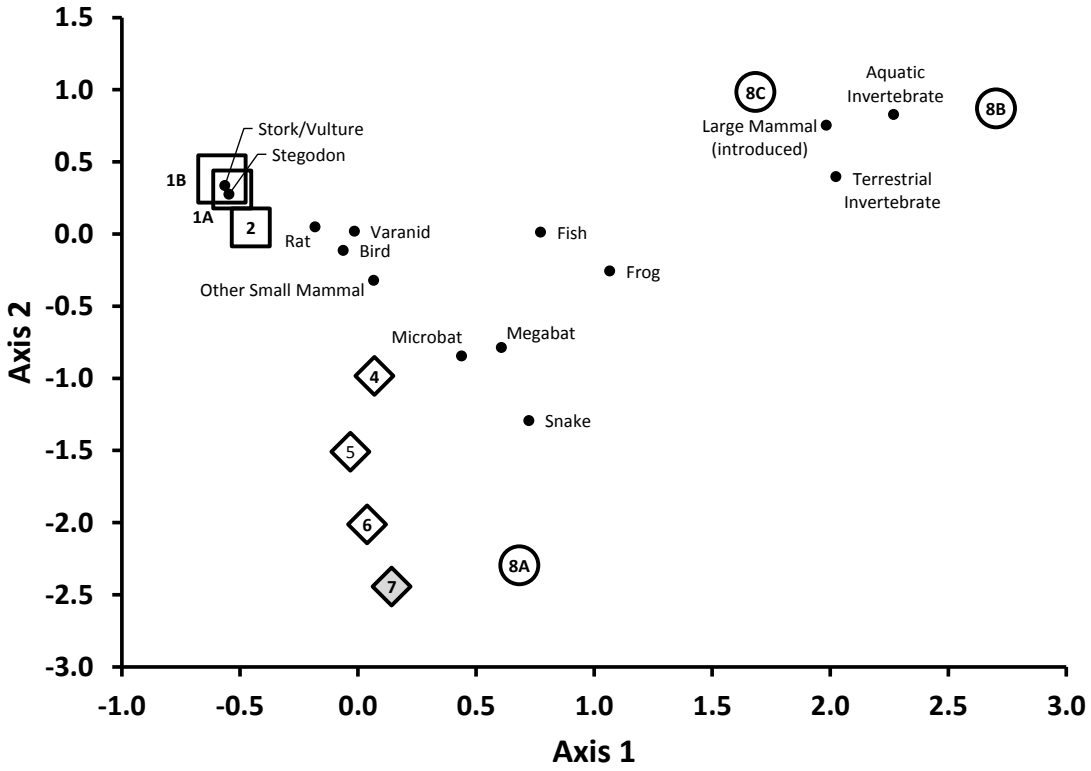

Figure 4.6 Correspondence analysis of faunal taxa abundances within stratigraphic units. Axes 1 and 2 explain 70.7% and 21.3% of the variance, respectively. Unit symbols: >50 ka, squares; 50 to 12 ka, diamonds (with unit containing T7 and T8 denoted in grey); 12 ka to present, circles.

Unit 8A departs more markedly than Unit 4 from the trend of Units 1A–7. This unit, which accumulated during the early Holocene, shifts positively along axis 1 from

Unit 7 by an amount almost equal to that observed for the entire depositional sequence up to Unit 7 (Fig. 4.6). This marked shift is partly explained by a 3.2–12.7% increase in the number of frog specimens (χ^2_{trend} = 5.47, p < 0.0001) and a 0.5–3.5% increase in the number of snake remains (χ^2_{trend} = 3.41, p = 0.0003) from Unit 7 to Unit 8A (Figs 4.9 and 4.10). Compared to all previous units, Unit 8A also marks the first time that a new large mammal, in this case pig (0.3% of vertebrate NISP), is observed at Liang Bua (χ^2_{trend} = 21.61, p < 0.0001), while the abundances of aquatic and terrestrial invertebrates (0.64% and 1.08% of total NISP, respectively) return to values similar to those for Unit 4 (0.54% and 2.33% of total NISP, respectively) (Figs 4.13–4.15).

Unit 8B displays dramatic positive shifts along axes 1 and 2 indicating major faunal changes relative to Unit 8A and all previous units. These shifts are consistent with our analysis of chord distances, and are due to a 12.7–22.4% increase in frog (χ^2_{trend} = 21.92, p < 0.0001) and a 0.3–3.1% increase in introduced large mammal remains (including pigs, civet cats, deer, macaques and porcupines) (χ^2_{trend} = 23.34, p < 0.0001) (Figs 4.9 and 4.15). Moreover, aquatic (NISP = 4,251; χ^2_{trend} = 65.69, p < 0.0001) and terrestrial invertebrate taxa (NISP = 983; χ^2_{trend} = 23.20, p < 0.0001) dominate the Unit 8B assemblage (Figs 4.13 and 4.14).

From Unit 8B to Unit 8C, aquatic and terrestrial invertebrates decline in abundance (χ^2_{trend} = –15.76, p < 0.0001 and χ^2_{trend} = –7.90, p < 0.0001, respectively) and frog remains drop to 10.7% (χ^2_{trend} = –23.98, p < 0.0001), whereas introduced large mammal remains increase to 5.2% (χ^2_{trend} = 9.09, p < 0.0001) and rat abundance increases to 74.3% (χ^2_{trend} = 14.14, p < 0.0001) (Figs 4.7, 4.9 and 4.13–4.15). Together, these changes result in the axis 1 score of Unit 8C shifting to a more negative value than that of Unit 8B, while the axis 2 score shifts slightly to a more positive value (Fig. 4.6).

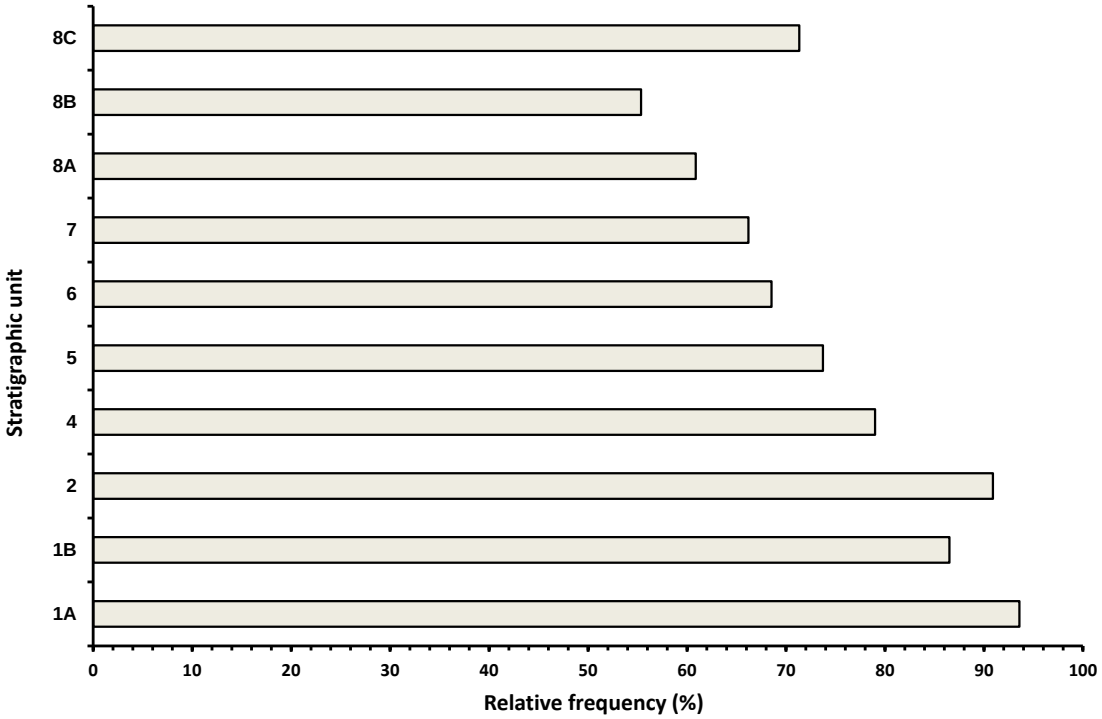

Figure 4.7 Relative frequencies (calculated as % vertebrate NISP) of rat by stratigraphic unit at Liang Bua. There is a consistent decrease in rat abundance from Units 2 to 8B. The *x*-axis ranges between 0 and 100%.

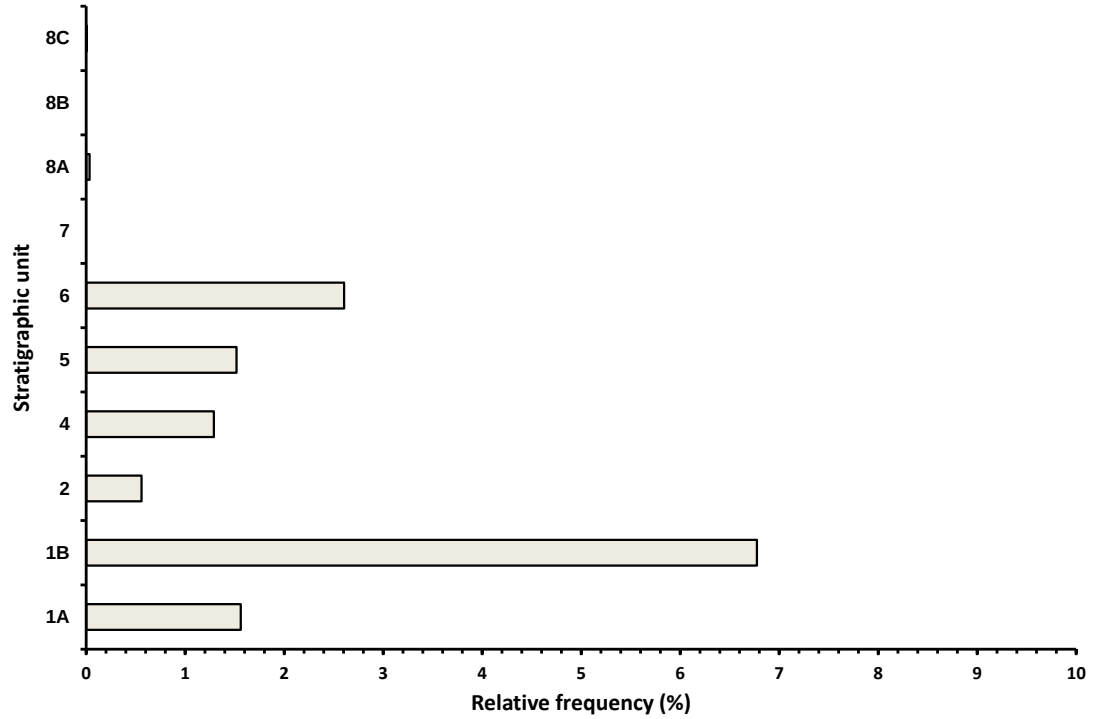

Figure 4.8 Relative frequencies (calculated as % vertebrate NISP) of stegodont by stratigraphic unit at Liang Bua. *Stegodon* remains from Units 4–6 and 8A may be reworked from Units 1A–2 (see text for discussion). Note the *x*-axis ranges between 0 and 10%.

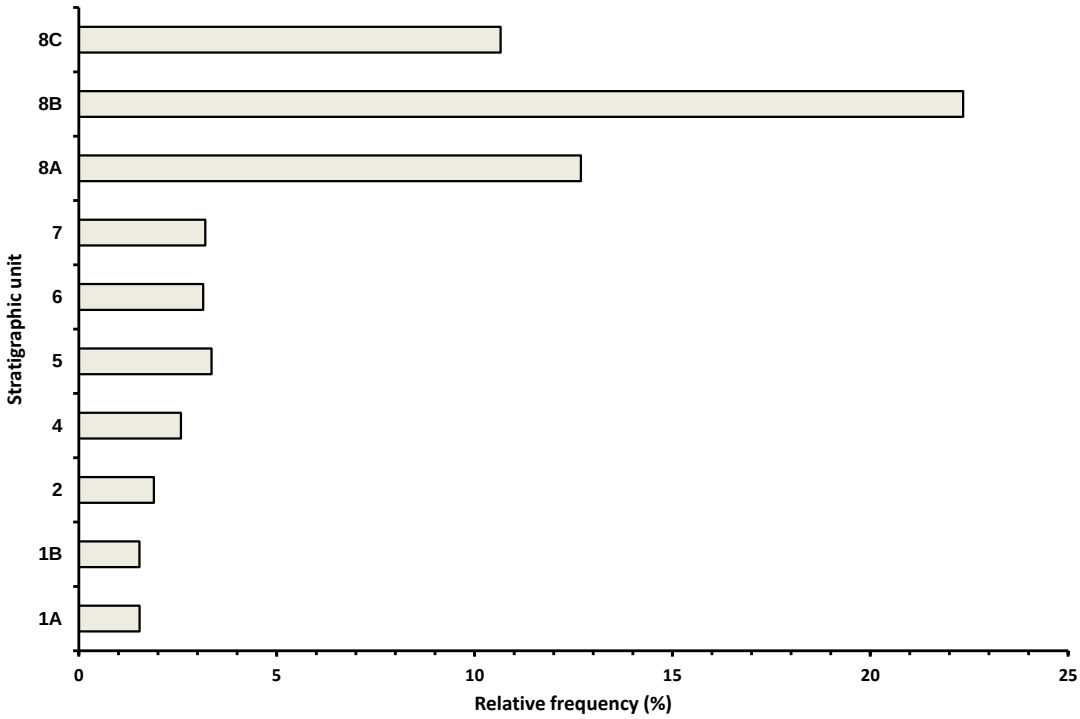

Figure 4.9 Relative frequencies (calculated as % vertebrate NISP) of frog by stratigraphic unit at Liang Bua. Frog remains are most abundant in the Holocene units (8A–8C). Note the *x*-axis ranges between 0 and 25%.

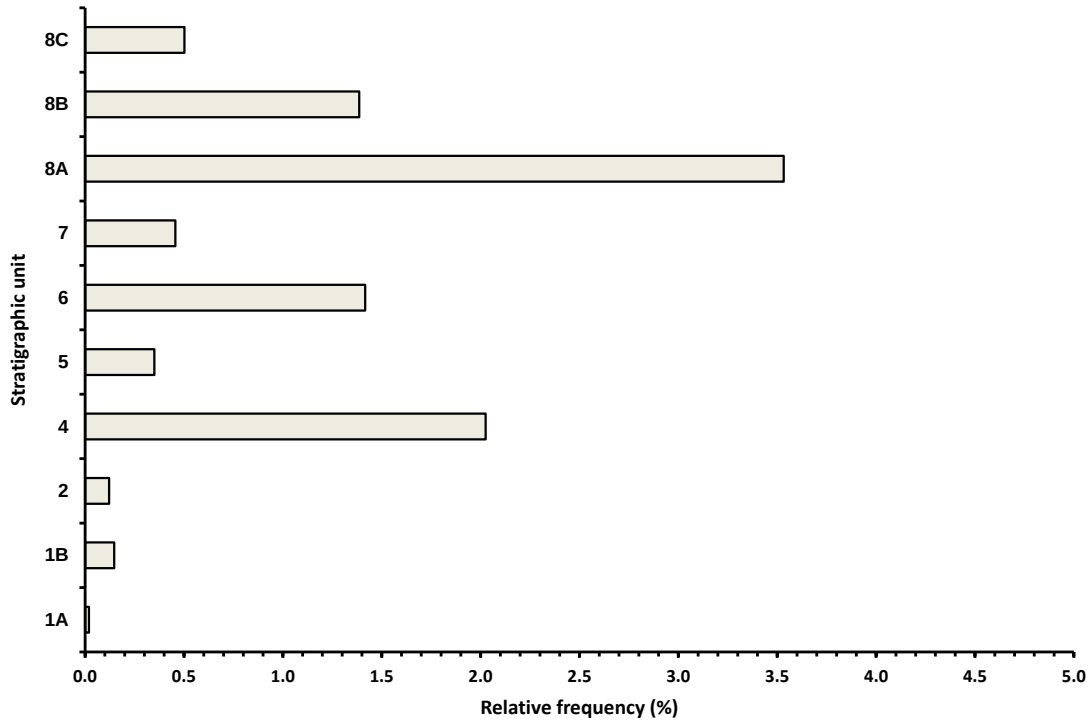

Figure 4.10 Relative frequencies (calculated as % vertebrate NISP) of snake by stratigraphic unit at Liang Bua. Note the *x*-axis ranges between 0 and 5%.

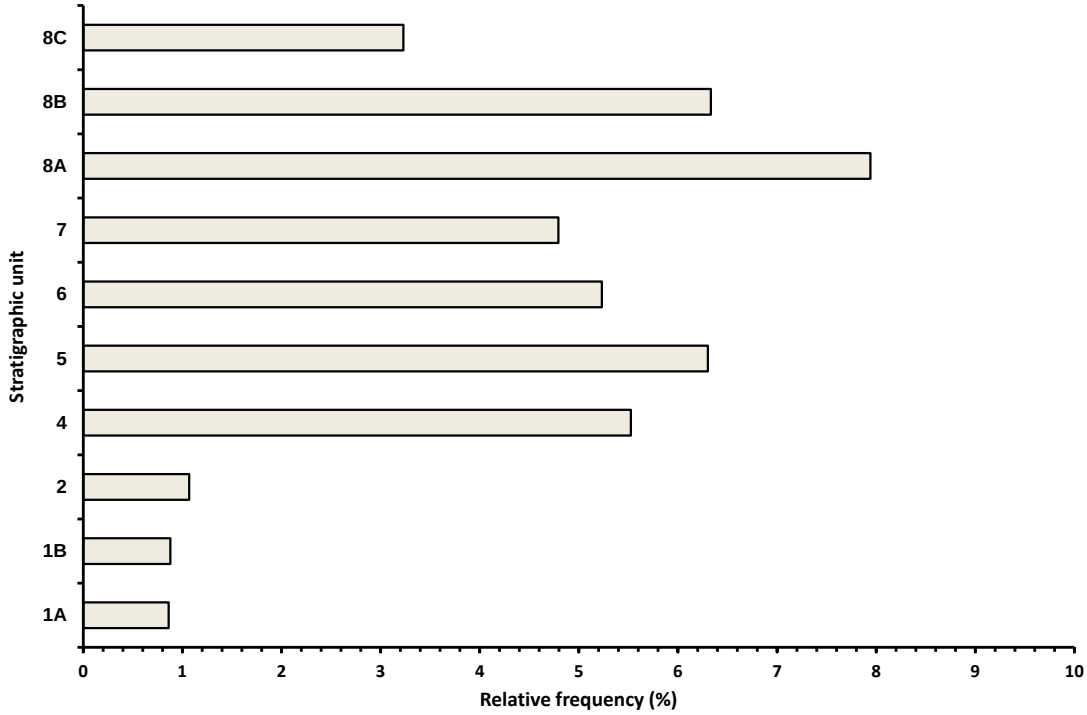

Figure 4.11 Relative frequencies (calculated as % vertebrate NISP) of megabat by stratigraphic unit at Liang Bua. The largest abundances are observed above tephra T3, in Units 4–8C. Note the *x*-axis ranges between 0 and 10%.

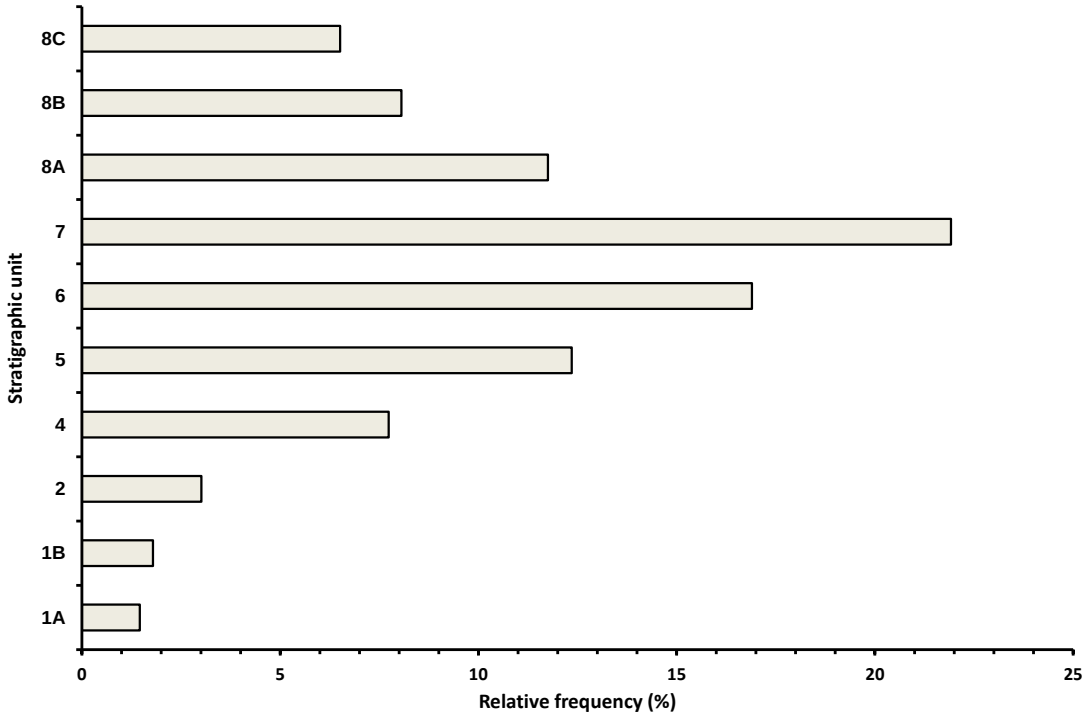

Figure 4.12 Relative frequencies (calculated as % vertebrate NISP) of microbat by stratigraphic unit at Liang Bua. As with the megabat, the highest abundances occur in Units 4–8C. Note the *x*-axis ranges between 0 and 25%.

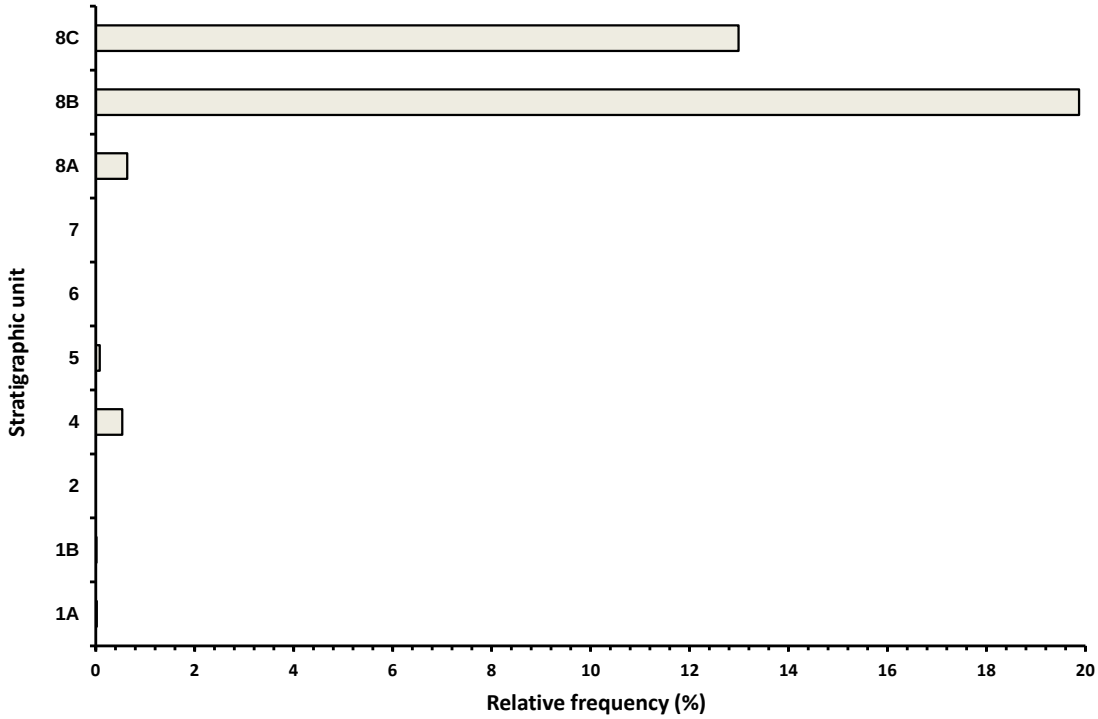

Figure 4.13 Relative frequencies (calculated as % total faunal NISP) of aquatic invertebrate by stratigraphic unit at Liang Bua. By far the largest abundances are in Units 8B and 8C. Note the *x*-axis ranges between 0 and 20%.

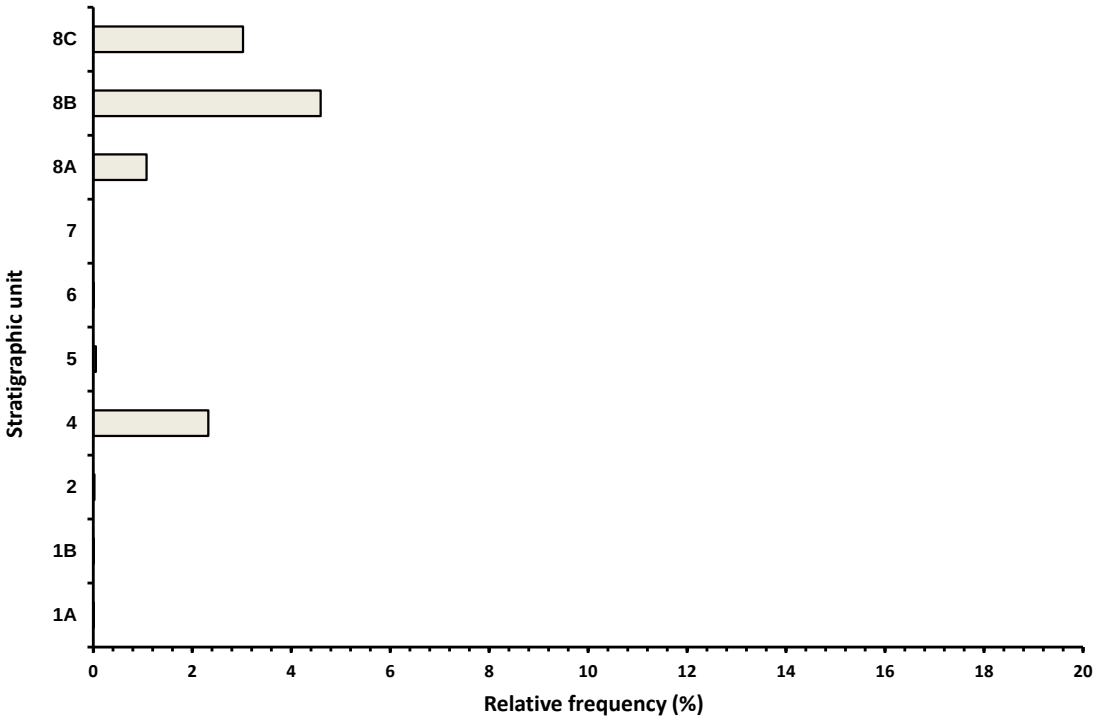

Figure 4.14 Relative frequencies (calculated as % total faunal NISP) of terrestrial invertebrate by stratigraphic unit at Liang Bua. Note the *x*-axis ranges between 0 and 20%.

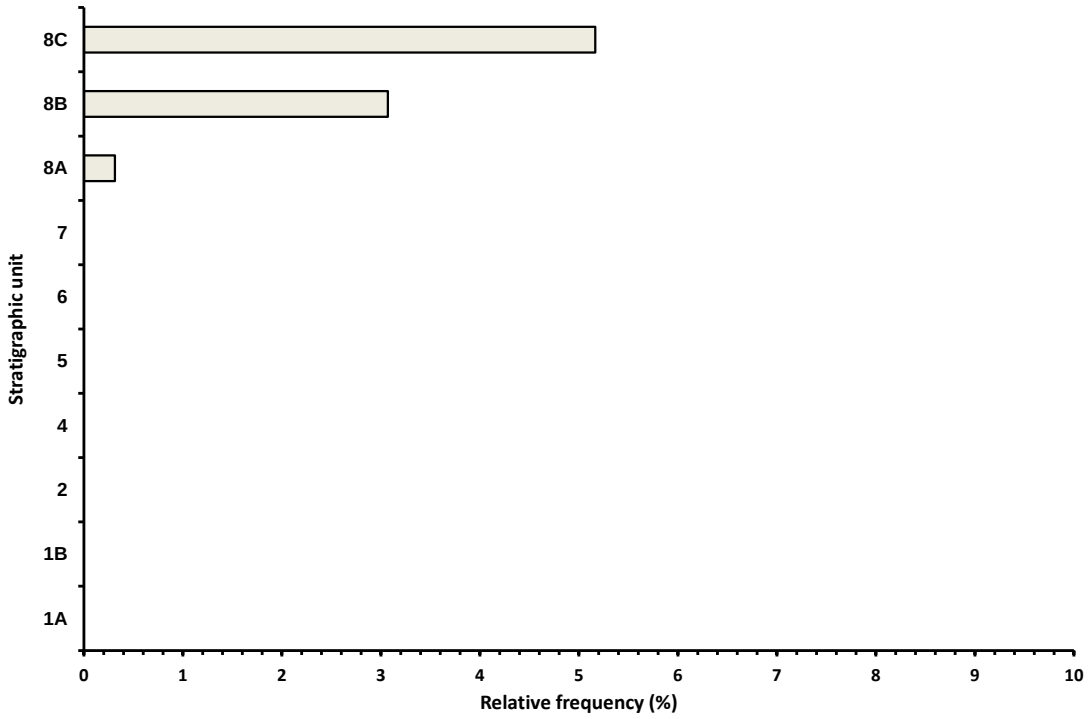

Figure 4.15 Relative frequencies (calculated as % vertebrate NISP) of introduced large mammal by stratigraphic unit at Liang Bua. These only occur in Units 8A–8C. Note the *x*-axis ranges between 0 and 10%.

Essentially identical results are obtained in analyses that assume *Stegodon* and stork/vulture are extinct in Units 4 and above, and that any remains attributed to these units were reworked from the pedestal deposits. The CD values between successive units change minimally between the two analyses and act only to slightly reduce the amounts of observed change from Units 5 to 7 (Fig. 4.16). In the correspondence analysis, the only noteworthy differences between the two analyses (aside from the inverted *y*-axis, which is a statistical artefact) are slight increases along axis 1 in the separation distances of Units 2 and 4, and of Units 5 and 6 (Fig. 4.17). However, the UPGMA results differ more substantially in the second analysis, in that Unit 4 now forms part of the cluster that includes Units 5–8A, rather than clustering with Units 1A–2 (Fig. 4.18).

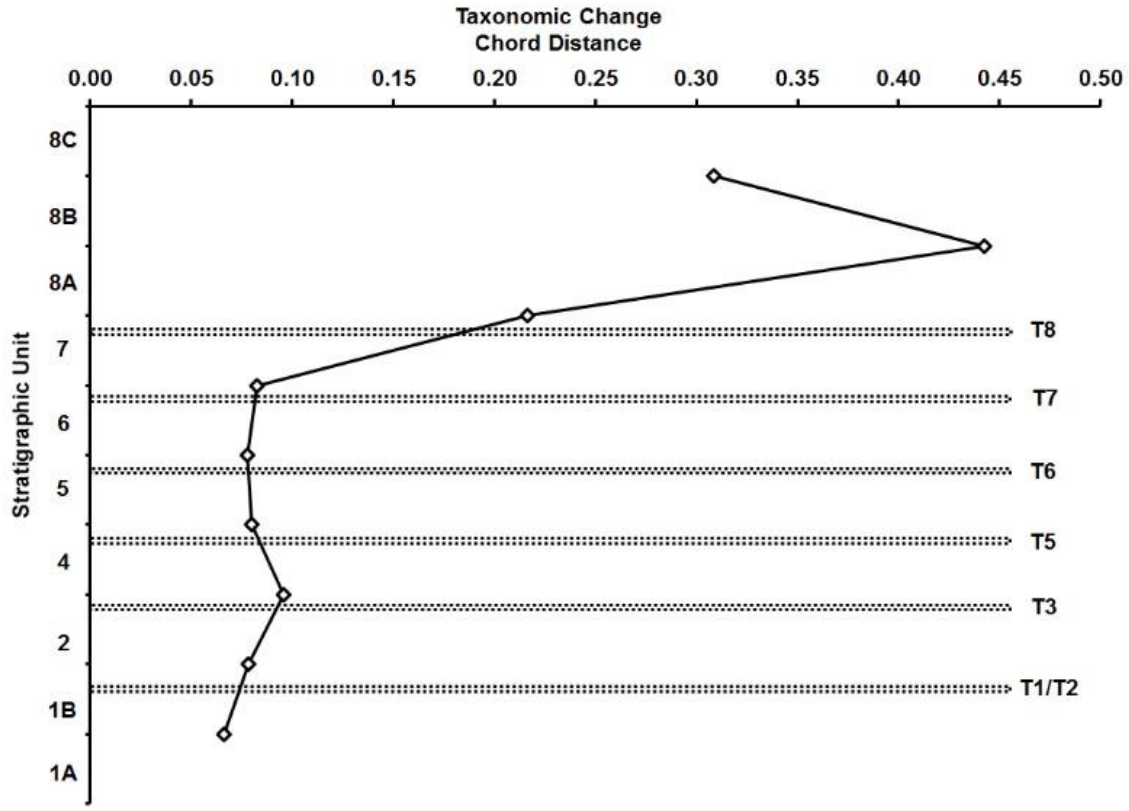

Figure 4.16 Chord distance (CD) values for the faunal assemblages across successive pairs of assigned depositional units at Liang Bua, assuming *Stegodon* and stork/vulture are extinct in Units 4 and above. The tephras are denoted as T1–T8. CD values close to zero indicate no change between units, while higher values indicate more change.

If *Stegodon* and stork/vulture remains are, in fact, eroding out of the older pedestal deposits and being incorporated into the younger, uncomformably overlying sediments – as suggested by previous analyses (van den Bergh *et al*., 2008) – then the deposits in front (downslope) of the remnant pedestal should contain larger numbers of these taxa than do the sediments preserved stratigraphically and elevationally above the pedestal. We tested this prediction by using *Stegodon* NISPs for Unit 5, which includes the thickest deposits both upslope and downslope of the remnant pedestal; stork/vulture remains are extremely rare throughout the entire sequence and, after Units 1B and 2, are observed only in Unit 6, where they comprise 0.01% of vertebrate NISP. Unit 5 has a vertebrate NISP of 11,124 from four Sectors (VII, XVI, XXII and XXIV). In three of these Sectors, Unit 5 lies immediately above (and in front of) the downward-sloping

unconformity and contains *Stegodon* elements at 9.44% of 1,250 (Sector VII, 535–635 cm depth), 5.49% of 765 (Sector XVI, 465–645 cm depth) and 43.75% of 16 (Sector XXII, 485–495 cm depth) vertebrate NISP. In contrast, Unit 5 in Sector XXIV (175–195 cm depth) is located more than 4 m south of and 2 m above this erosional boundary and contains only 0.02% of 9,093 vertebrate NISP. These results support our proposition that *Stegodon* and stork/vulture elements recovered from Units 4 and above do not represent animals that died during the depositional accumulation of these units, but instead represent elements reworked from older deposits.

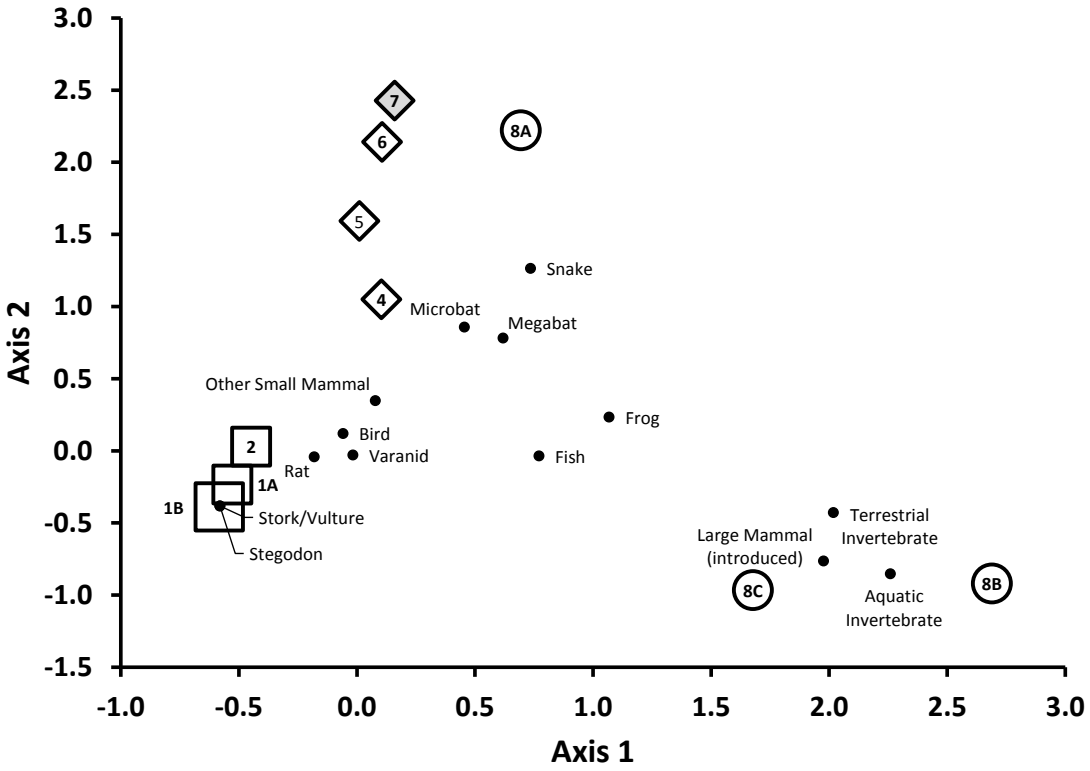

Figure 4.17 Correspondence analysis of faunal taxa abundances within stratigraphic units, assuming *Stegodon* and stork/vulture are extinct in Units 4 and above. Axes 1 and 2 explain 70.0% and 21.9% of the variance, respectively. Unit symbols as in Fig. 4.6. Note that in comparison with Fig. 4.6, axis 2 is inverted; this is solely a statistical artefact and otherwise both plots are essentially identical.

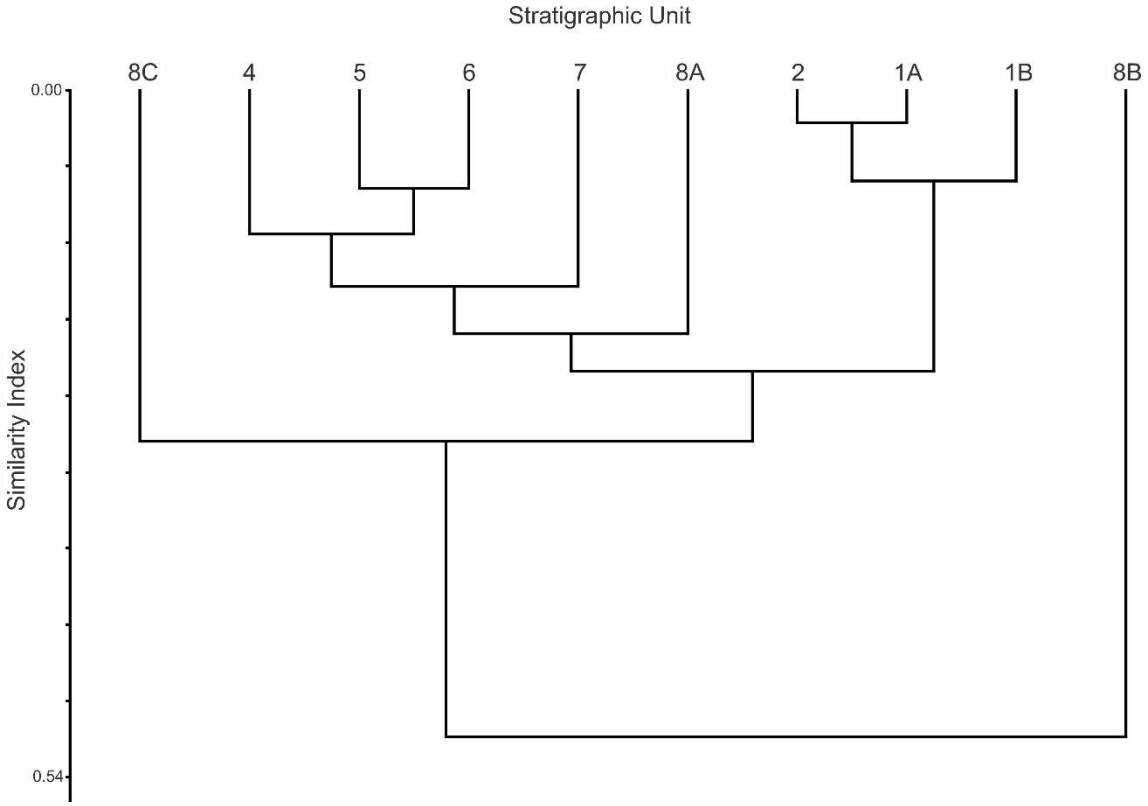

Figure 4.18 Unweighted pair group method with arithmetic mean (UPGMA) cluster analysis of stratigraphic units at Liang Bua, assuming *Stegodon* and stork/vulture are extinct in Units 4 and above. The dendrogram is based on a similarity index (dimensionless) calculated using the matrix of all pairwise chord distances between units. Deeper branches between units indicate less similarity in faunal structure (e.g., Units 1A–2 are more similar to each other than any of them are to Units 4–8A).

4.4.2 Stone artefact assemblage

Stone artefact raw material abundances (raw material NISP) within each stratigraphic unit at Liang Bua are summarised in Table 4.1. Of the 10,434 stone artefacts, 5,158 were made of silicified tuff, 3,490 of chert, 703 of silicified limestone, 550 of andesite, 270 of jasper, 240 of chalcedony and 23 of quartz (Table 4.3). No artefacts were recovered from Units 3 or 7 (Table 4.1), so these units are not included in the analyses below.

The CD values for raw material abundances in successive unit pairs are plotted in Figure 4.19. Of all successive pairs, the least amount of change (CD = 0.08) is observed

from Units 8A to 8B, followed by Units 1B to 2 (CD = 0.15) and Units 1A to 1B (CD = 0.16). All other unit pairs show more substantial amounts of change (CDs of between 0.26 and 0.78). The largest shift occurs from Units 2 to 4, which marks the transition across T3 (Unit 3, ~50–47 ka).

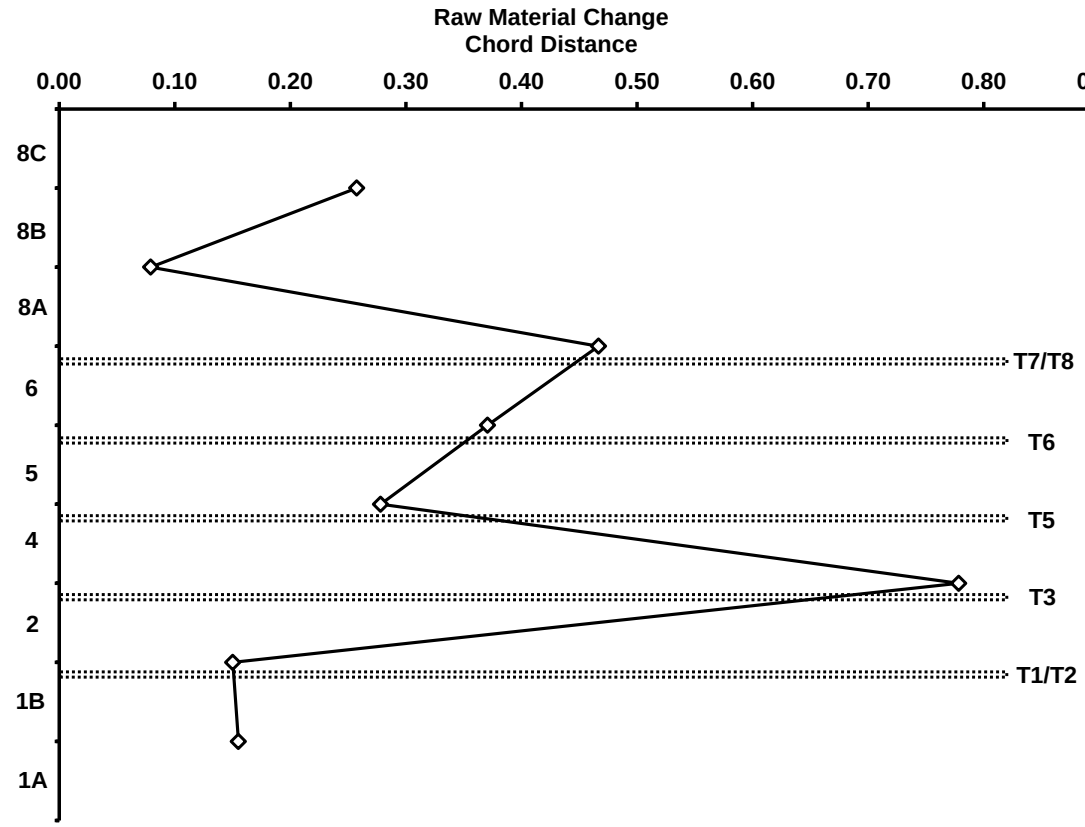

Figure 4.19 Chord distance (CD) values for raw material abundances across successive pairs of assigned depositional units at Liang Bua. The tephras are denoted as T1–T8. CD values close to zero indicate no change between units, while higher values indicate more change.

The observed changes in raw material proportions are not strongly associated with those of faunal composition, based on a quantitative comparison of their respective CD values: r = –0.34, p = 0.42 and Spearman's rho (r_s) = 0.02, p = 0.98. For example, the largest raw material shift occurs from Units 2 to 4 and, thus, precedes the pronounced taxonomic changes across the Pleistocene–Holocene transition and throughout the Holocene sequence (Units 7–8C).

UPGMA cluster analysis of all pairwise CD values between units results in two main clusters, with Units 1A–2 forming one cluster and all other units forming the other (Fig. 4.20). Within the latter, there are two clusters. The first includes Units 4, 6 and 8C, while the second includes Units 5, 8A and 8B. In the former cluster, Units 4 and 8C are more similar to each other than either is to Unit 6, whereas in the latter cluster, Units 8A and 8B share more similarities than either do with Unit 5.

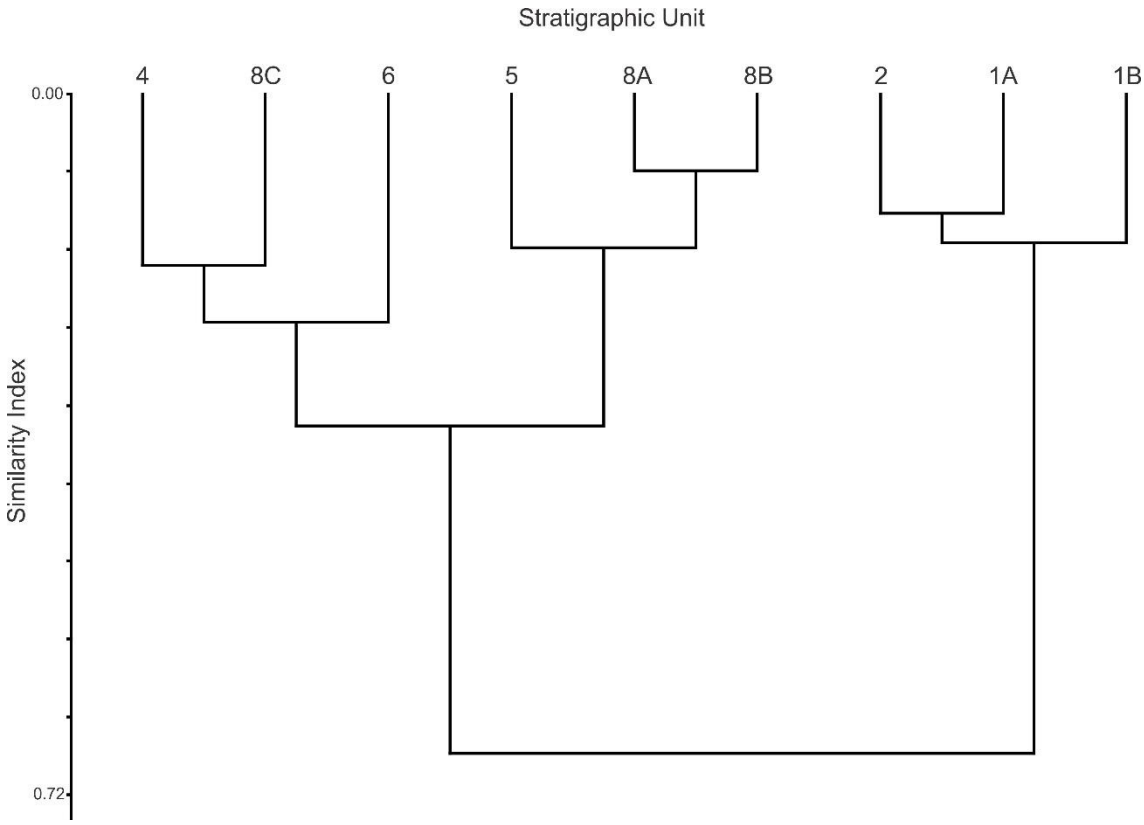

Figure 4.20 Unweighted pair group method with arithmetic mean (UPGMA) cluster analysis of raw material abundance by stratigraphic unit at Liang Bua. The dendrogram is based on a similarity index (dimensionless) calculated using the matrix of all pairwise chord distances between units. Deeper branches between units indicate less similarity in raw material used (e.g., Units 1A–2 are more similar to each other than any of them are to Units 4–8C).

Analysis of raw material evenness throughout the stratigraphic sequence, using the Shannon evenness index, indicates that the major difference between artefact assemblages occurs between Unit 1B and Units 4–8C (Fig. 4.21). No significant correlation is observed between artefact NISP and the evenness index (r = –0.63, p =

0.07 and Spearman's rho (r_s) = 0.11, p = 0.78). The 95% confidence intervals of Units 1A and 2 overlap with the evenness scores of all other units (i.e., 1B and 4–8C).

In the correspondence analysis, axes 1 and 2 together explain 94% of the total variance in raw material abundance (Fig. 4.22). The two main clusters observed show the same pattern as seen in the UPGMA analysis, with one cluster including Units 1A–2 and the second including Units 4 and above. Units 1 and 2 have the most negative scores on axis 1; these deposits are dominated by silicified tuff (≥65% of NISP) and have low frequencies of the other raw materials (≤17% each of NISP) (Fig. 4.23). Units 4–8C have more positive scores on axis 1, primarily due to increased frequencies of chert (34–68% of NISP) and lower frequencies of silicified tuff (25–41% of NISP) (Figs 4.23 and 4.24).

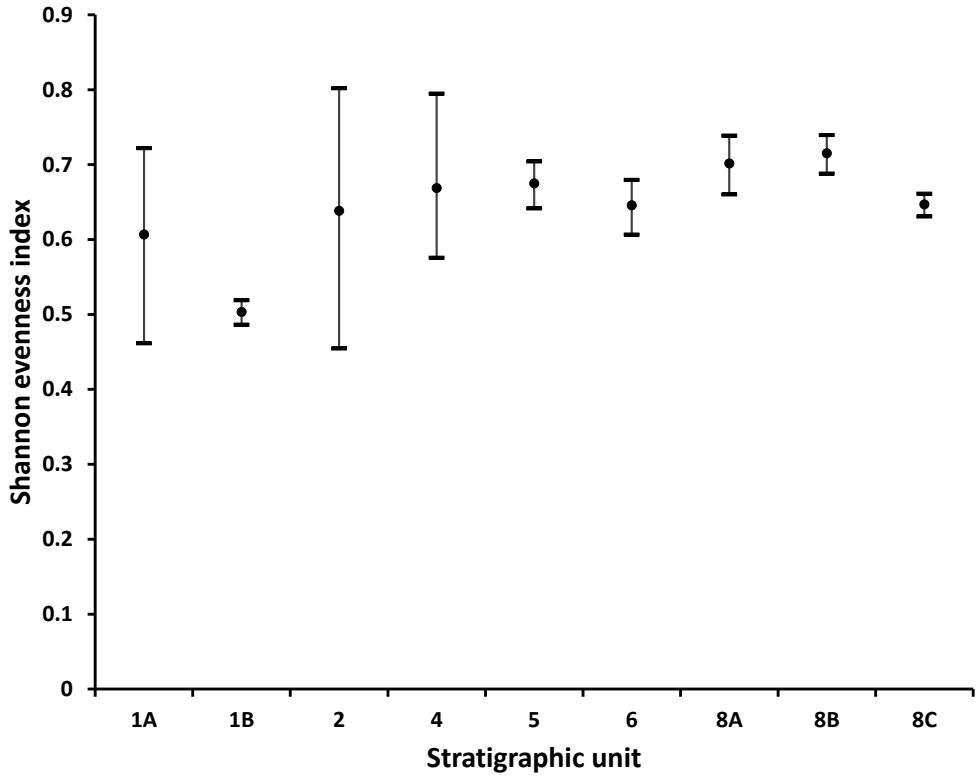

Figure 4.21 Raw material evenness throughout the stratigraphic sequence, determined using the Shannon evenness index. Approximate 95% confidence intervals for the index of each unit were estimated using the bootstrap procedure (9999 resamples with replacement) provided in PAST, version 3 (Hammer, 2015). Greater evenness is indicated by higher index values. Note the significant differences between the indices of assemblages of Unit 1B compared to Units 4–8C.

From Units 1A to 8C, silicified tuff shows a decrease in abundance (χ^2_{trend} = –19.96, $p < 0.0001$), whereas chert increases in abundance (χ^2_{trend} = 20.74, $p < 0.0001$). However, no linear trends are observed for silicified tuff in Units 1A to 2 (χ^2_{trend} = –0.15, $p = 0.88$) or in Units 4 to 8C (χ^2_{trend} = –1.95, $p = 0.05$). Instead, the significant decline in silicified tuff is due specifically to the shift that occurs from Units 1B to 4 (χ^2_{trend} = –2.46, $p < 0.01$). Similarly, chert shows no trends in Units 1A to 2 (χ^2_{trend} = 0.75, $p = 0.45$) or in Units 4 to 8C (χ^2_{trend} = 1.89, $p = 0.06$), with the significant increase in chert due specifically to the shift that occurs from Units 2 to 4 (χ^2_{trend} = 2.71, $p < 0.01$). If this trend of increasing abundance is measured from Units 1B to 4, then the associated probability decreases considerably (χ^2_{trend} = 5.08, $p < 0.0001$).

Axis 2, which explains 17.3% of the variance, reflects higher frequencies of chalcedony in Units 1A, 5 and 6 (8.8%, 5.1% and 8.8%, respectively), quartz in Units 5 (0.6%) and 6 (0.7%), jasper in Unit 8B (6.1%) and silicified limestone in Units 8A–8C (9.7%, 8.1% and 10.3%, respectively) (Figs 3.25–3.28). Neither chalcedony nor quartz displays a significant trend from Units 1A to 8C (χ^2_{trend} = –1.57, $p = 0.12$ and χ^2_{trend} = 1.76, $p = 0.08$, respectively), but jasper and silicified limestone increase significantly in abundance (χ^2_{trend} = 6.22, $p < 0.0001$ and χ^2_{trend} = 8.62, $p < 0.0001$, respectively). Further inspection of these data shows that the significant increase in abundance of these raw materials is due to their larger relative abundances in Units 8A–8C than in the older units.

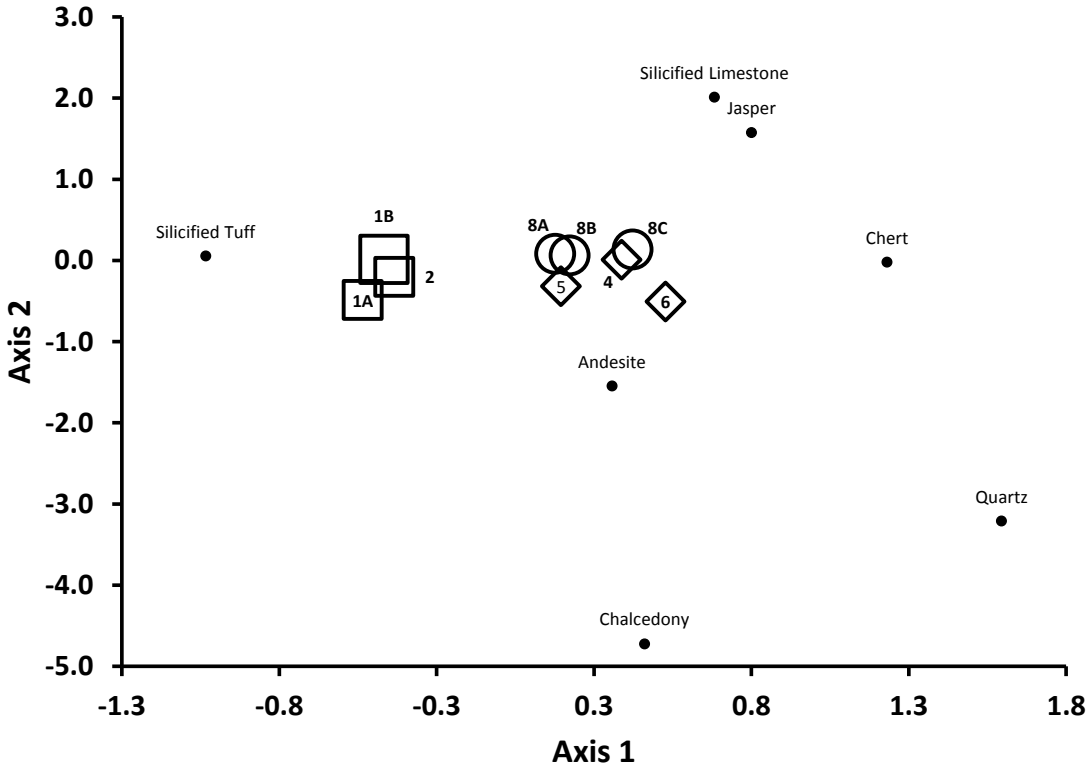

Figure 4.22 Correspondence analysis of raw material abundances within stratigraphic units. Axes 1 and 2 explain 76.7% and 17.3% of the variance, respectively. Unit symbols as in Fig. 4.6. Variance along Axis 1 is mainly explained by the abundances of chert and silicified tuff.

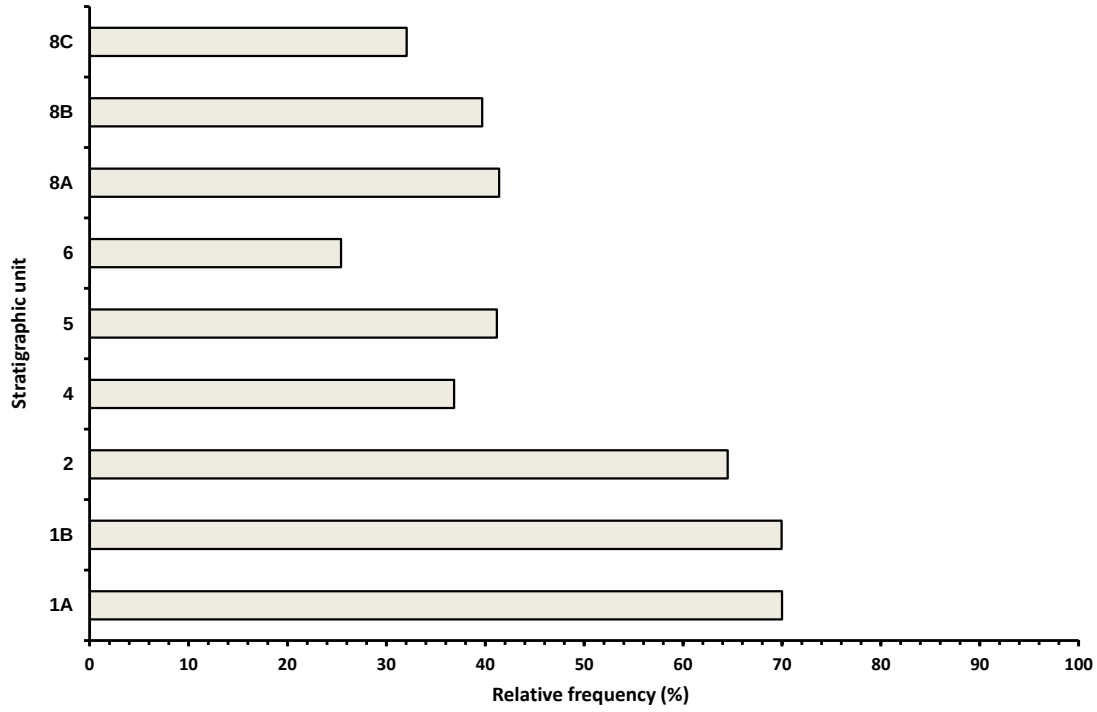

Figure 4.23 Relative frequencies (calculated as % raw material NISP) of silicified tuff by stratigraphic unit at Liang Bua. The largest abundances are in Units 1A–2. The *x*-axis ranges between 0 and 100%.

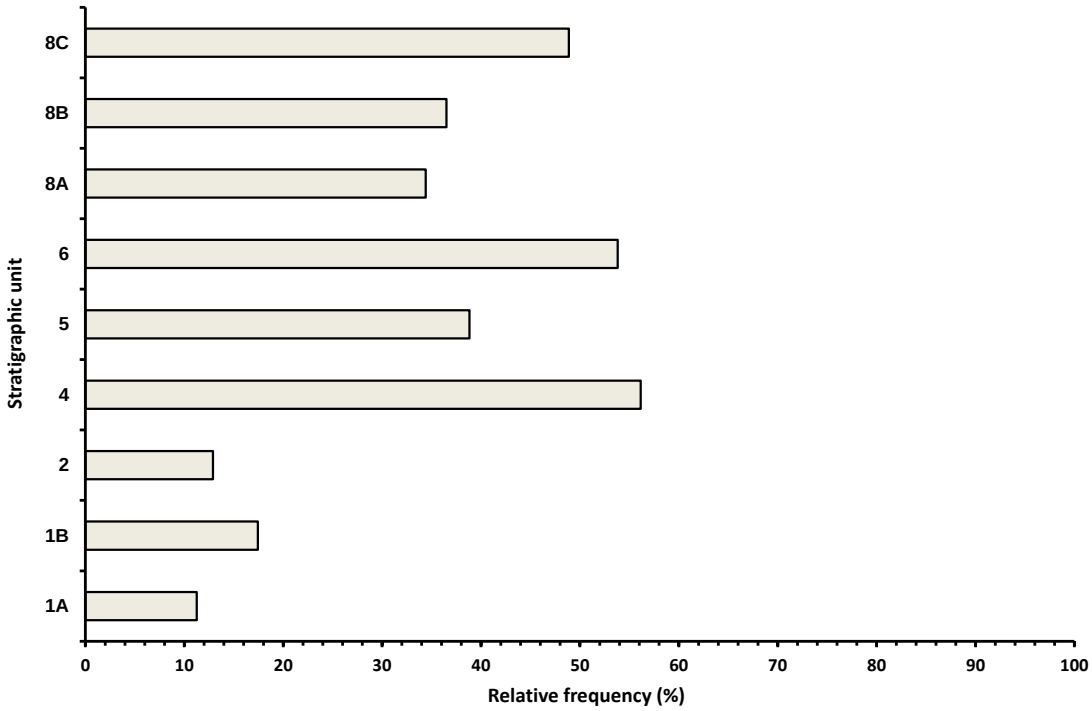

Figure 4.24 Relative frequencies (calculated as % raw material NISP) of chert by stratigraphic unit at Liang Bua. Chert is most abundant in Units 4–8C. As with Fig. 4.23, the *x*-axis ranges between 0 and 100%.

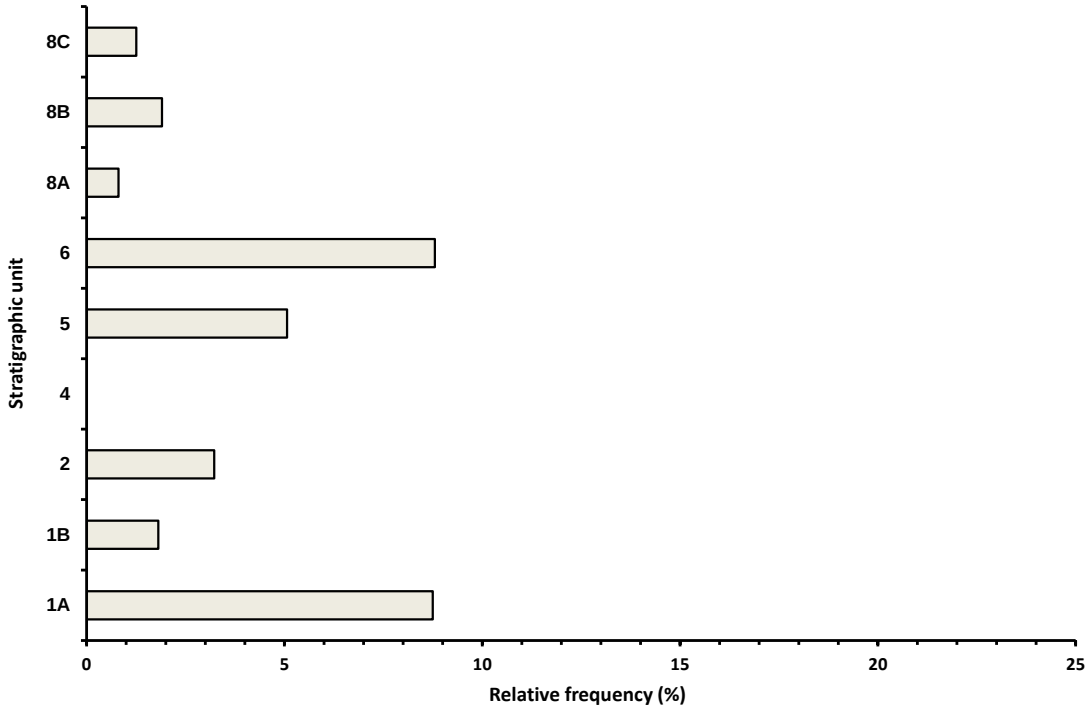

Figure 4.25 Relative frequencies (calculated as % raw material NISP) of chalcedony by stratigraphic unit at Liang Bua. Note the *x*-axis ranges between 0 and 25%.

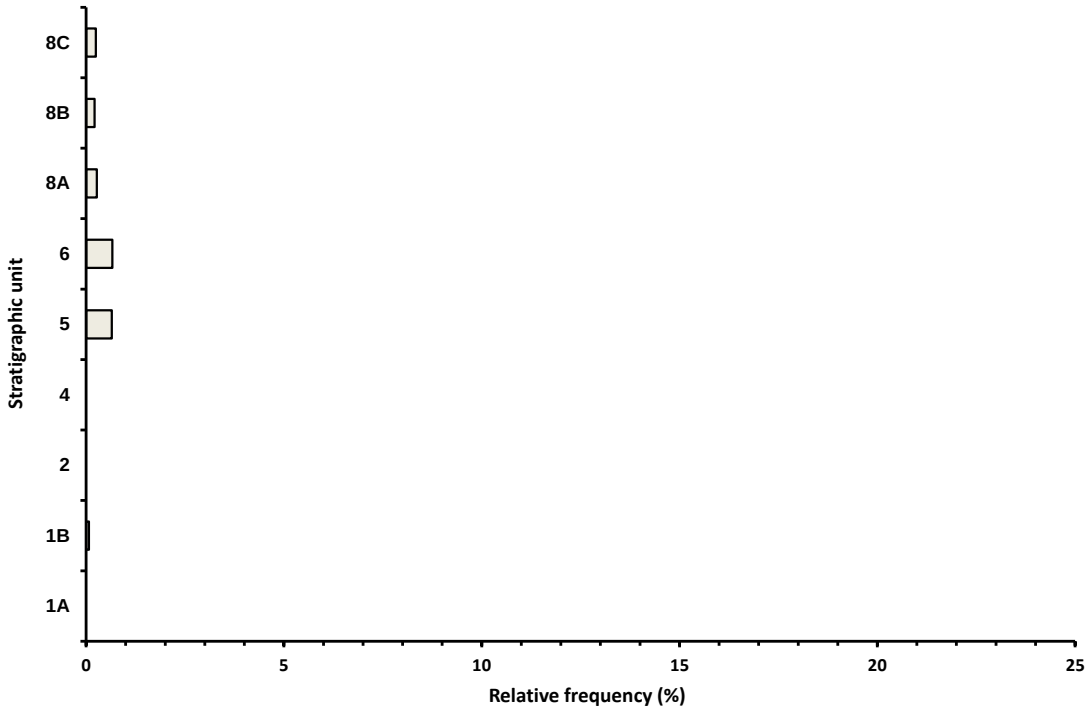

Figure 4.26 Relative frequencies (calculated as % raw material NISP) of quartz by stratigraphic unit at Liang Bua. Note the *x*-axis ranges between 0 and 25%.

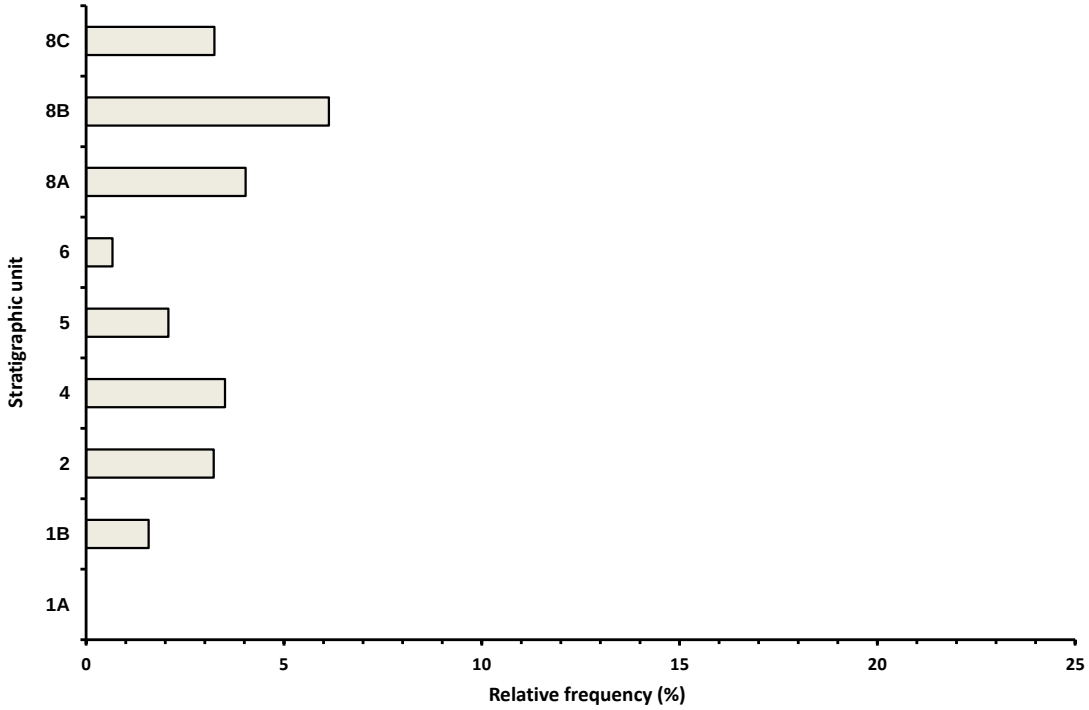

Figure 4.27 Relative frequencies (calculated as % raw material NISP) of jasper by stratigraphic unit at Liang Bua. Note the *x*-axis ranges between 0 and 25%.

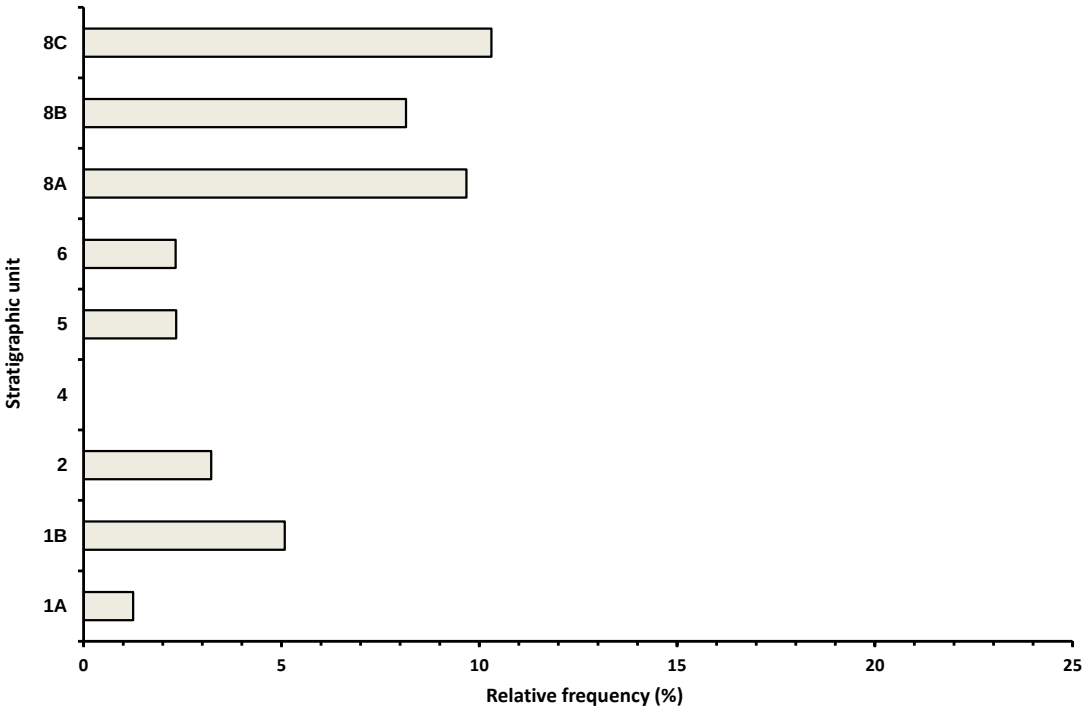

Figure 4.28 Relative frequencies (calculated as % raw material NISP) of silicified limestone by stratigraphic unit at Liang Bua. Note the *x*-axis ranges between 0 and 25%.

4.5 Implications for palaeoecology and human behaviour

Liang Bua provides evidence for substantial changes through time in both faunal community and stone artefact raw material composition (Figs 4.3 and 4.19). However, these observed changes occurred largely independent of one another (r = –0.34, p = 0.42; r_s = 0.02, p = 0.98). From ~190 to 50 ka ago, the faunal and stone artefact assemblages of Units 1A–2 are reasonably uniform in their taxonomic and raw material abundances, respectively. Rats dominate this faunal assemblage, accounting for more than 86% of vertebrate NISP, with all other taxa comprising less than 7% each (Table 4.2 and Figs 4.7–4.15). The dominant raw material for stone artefacts is silicified tuff (≥65% of NISP), with the other raw materials comprising less than 20% each (Table 4.3 and Figs 4.23–4.28).

The main faunal distinction among these units is that *Stegodon* elements comprise 6.8% of vertebrate NISP in Unit 1B and only 1.6% and 0.6% in Units 1A and 2,

respectively (Table 4.2 and Fig. 4.8). This probably signifies that hominin behaviour contributed at least partly to the assemblage because Unit 1B contains 55.1% of the total faunal NISP and 41.3% of the total stone artefacts for all units combined, despite the fact that the duration of Unit 1B (~60 ka) constitutes only ~30% of the total time span sampled. Similarly, varanids (most likely Komodo dragon) are more than twice as common in Unit 1B than in any other Late Pleistocene unit (Table 4.2 and Fig. 4.29). Stork/vulture also comprise 6.9% of all bird remains within this unit – almost three times that of Unit 2 and six times that of Unit 6, which are the only other units containing these taxa (Table 4.2 and Fig. 4.30). Moreover, all skeletal remains assigned to *H. floresiensis* currently derive from Unit 1B (Sutikna *et al*., 2016). The clear association in Unit 1B – and to a lesser extent in Units 1A and 2 – of skeletal elements of *Stegodon*, giant marabou stork, vulture and large varanids, as well as the skeletal and cultural remains of *H. floresiensis*, suggests that a very different ecosystem (or at least the fauna >5 kg) existed on Flores prior to the volcanic eruption that resulted in the deposition of T3 at Liang Bua around 50–47 ka ago.

Tephra T3 is a volcaniclastic mass flow deposit that is up to ~0.75 m thick and includes ~0.27 m depth of pumiceous coarse ash and conspicuous mud rip-up clasts; the volcanic event that produced T3 is likely to have originated nearby to Liang Bua (Sutikna *et al*., 2016). This eruption undoubtedly had an initial devastating effect on the ecosystem of the surrounding region. But ecosystems typically can recover relatively quickly (i.e., within decades) from such major volcanic disturbances (e.g., the 1883 Krakatau eruption in Indonesia), although the exact nature and timescale of recovery varies considerably (Whittaker *et al*., 1992; del Moral and Grishin, 1999). Immediately following T3 at Liang Bua, the compositions of both the stone artefact and faunal assemblages change significantly (Figs 4.6, 4.17 and 4.22). The preferred raw material

used for making stone artefacts shifts from silicified tuff to chert, representing a major change in hominin behaviour (Figs 4.23 and 4.24).

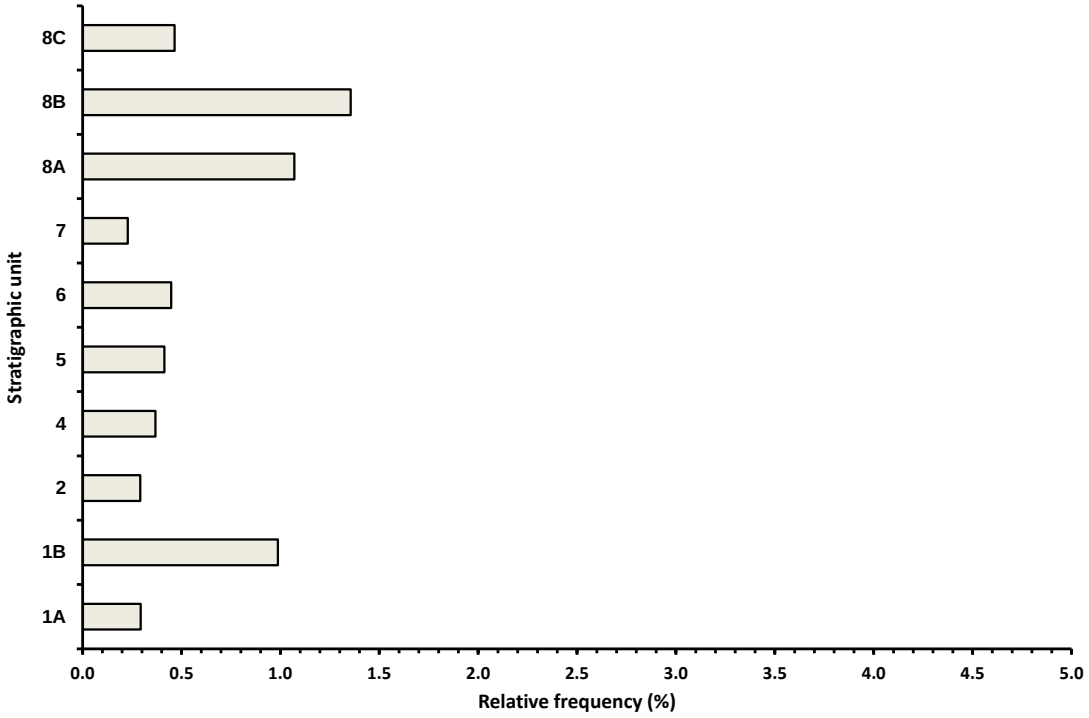

Figure 4.29 Relative frequencies (calculated as % vertebrate NISP) of varanid by stratigraphic unit at Liang Bua. Note the *x*-axis ranges between 0 and 5%.

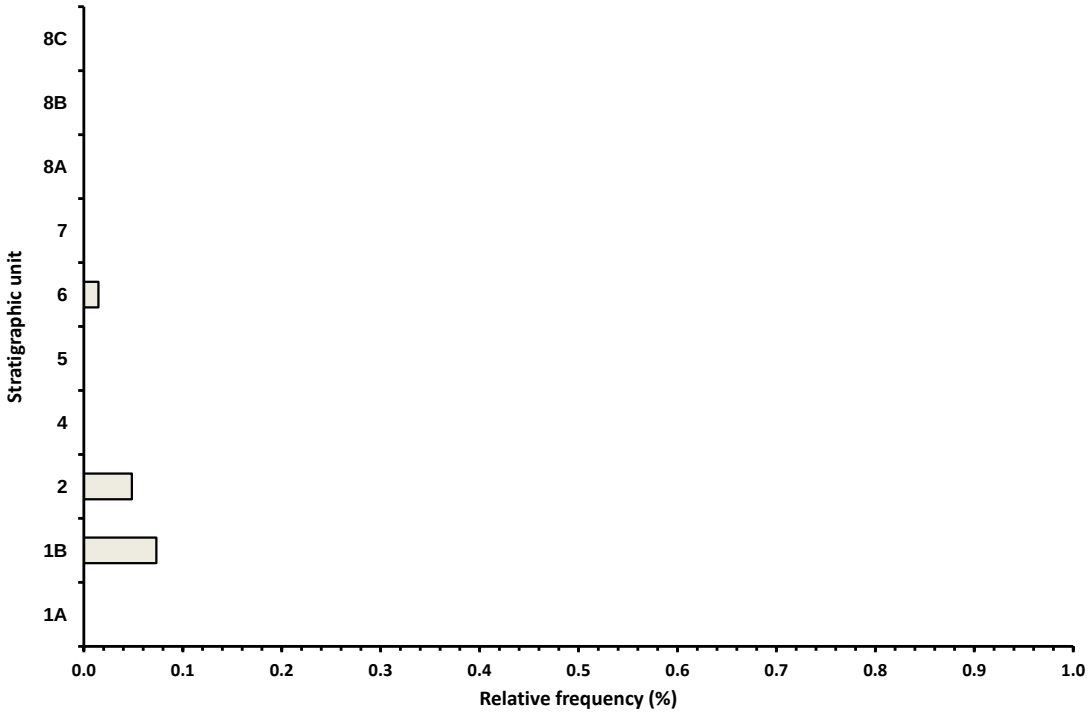

Figure 4.30 Relative frequencies (calculated as % vertebrate NISP) of stork/vulture by stratigraphic unit at Liang Bua. Note the *x*-axis ranges between 0 and 1%.

There are two possible explanations for this dramatic shift in raw material selection. First, one or more surviving populations of *H. floresiensis* returned to Liang Bua following T3 and they had a much stronger preference for using chert than did earlier populations, either because chert was more available in the immediate vicinity of the cave than it had been previously or because hominins chose to transport the chert from more distant localities. An alternative possibility is that *H. floresiensis* did not return to Liang Bua following T3, either because it had gone extinct or was surviving elsewhere on Flores, and the observed preference for chert provides the earliest evidence of modern humans on Flores (or, less likely, another species of hominin, as yet unrecognised). Based on the results of previous studies of the Liang Bua stone artefacts (Moore, 2005, 2007; Brumm *et al*., 2006; Moore and Brumm, 2007, 2009; Moore *et al*., 2009), we consider the arrival of modern humans as the more plausible option. One of the major distinctions between the Late Pleistocene stone artefact assemblages attributed to *H. floresiensis* and those attributed to Holocene modern humans is the clear preference for chert by the latter (Moore *et al*., 2009). It should be noted that the samples studied for raw material proportions by Moore *et al*. (2009) did not include any artefacts from deposits that are now dated to between about 47 and ~13 ka cal. BP. Instead, the artefacts studied by Moore *et al*. (2009), and assumed by them to fall within this time interval, are now recognised as ~190 to 50 ka in age.

The large shift in raw material preference after T3 is not the only change observed in Unit 4 plausibly related to hominin behaviour. Both aquatic and terrestrial invertebrates (i.e., molluscs) exhibit a significant increase in abundance compared to the underlying, older units ($\chi^2_{\text{trend}} = 1.84$, $p = 0.03$ and $\chi^2_{\text{trend}} = 12.63$, $p < 0.0001$, respectively) (Figs 4.13 and 4.14). Although such shifts in mollusc remains could be reasonably attributed to a variety of taphonomic factors, their significant increase in

Unit 4 deserves further explanation, given the importance of this resource to modern humans at many other prehistoric sites across Southeast Asia (Gosden and Robertson, 1991; O'Connor *et al*., 2002; Veth *et al*., 2005; O'Connor and Aplin, 2007; Szabó *et al*., 2007). Previous work on Liang Bua molluscs has suggested that subsistence collecting by modern humans did not occur until the Holocene (van den Bergh *et al*., 2009). However, the samples studied suffer from the same issues as noted above for the stone artefacts—that is, researchers thought they were sampling deposits 50–11 ka old when, in fact, they were > 50 ka in age. The absolute numbers of mollusc remains in Unit 4 are small, comprising only three aquatic (freshwater) and 13 terrestrial specimens, and they all derive from less than 30 cm depth of deposit that underlies a 5–10 cm-thick layer of flowstone near the eastern wall of the cave. The time span represented by Unit 4 is relatively short (~47 ka to ~46 ka cal. BP), giving a sediment deposition rate of ~30 cm/ka. As the number of faunal specimens recovered from this unit is extremely low relative to the other stratigraphic units (Table 4.2), this interval of ~1 ka may record only a small number of occurrences, so the proportion of molluscs within the assemblage is likely to be significant in this context.

Further evidence that modern humans were likely present at Liang Bua during the accumulation of Unit 4 derives from two isolated hominin teeth—a left maxillary 3rd premolar and a right mandibular 2nd molar (Fig. 4.31a, b). The roots of these teeth are not preserved, but the crowns are in reasonable condition, are only moderately worn, and are considerably larger than those of *H. floresiensis* and phenetically more similar to those of modern humans. The maxillary premolar is 7.9 mm long mesiodistally and 11.2 mm wide buccolingually, which is large relative to published data for modern humans (Voisin *et al*., 2012) and LB1 (Brown *et al*., 2009; Kaifu *et al*., 2015) (Fig. 4.32). Its buccolingual width is also greater than the mean values for Australian

Aboriginal (10.3 mm), North Asian (9.5 mm) and European (8.8 mm) population samples measured by Brown (online dataset).

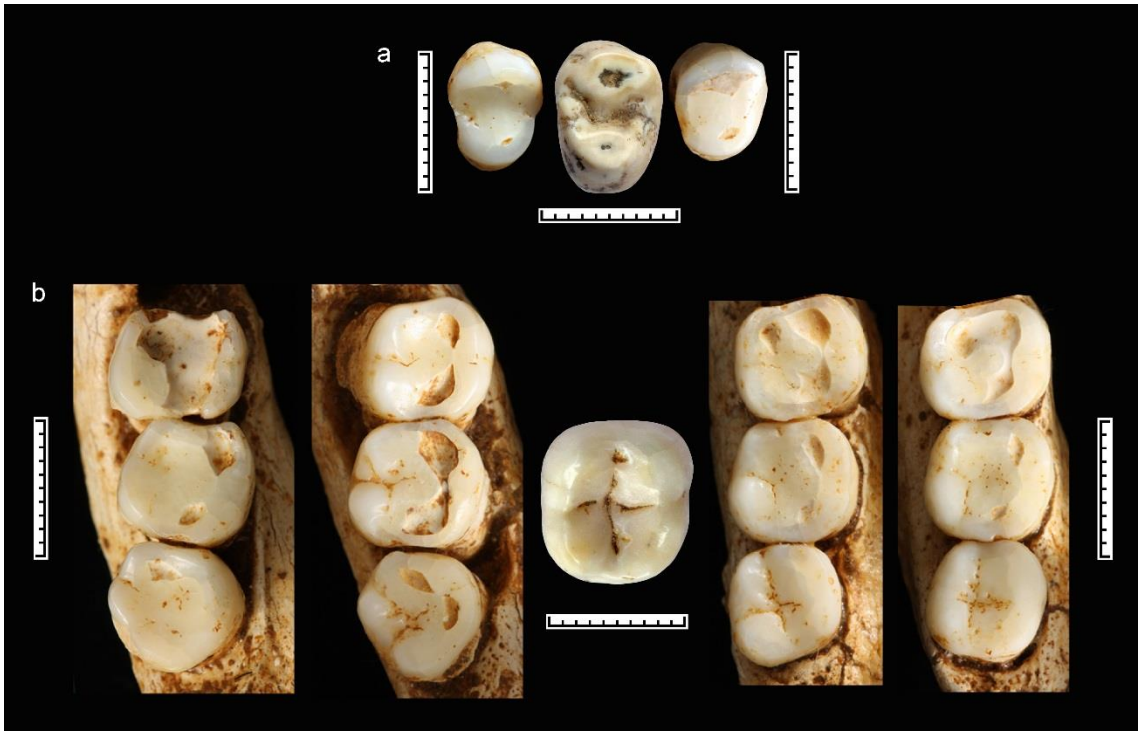

Figure 4.31 The left maxillary 3rd premolar (**a**, centre) and right mandibular 2nd molar (**b**, centre) from Unit 4 at Liang Bua. In **a**, the right (mirrored) and left maxillary 3rd premolars of LB1 are shown at left and right, respectively (modified from Kaifu *et al*., 2015). In **b**, the left (mirrored) and right mandibular 1st–3rd molars of LB1 are shown at the far left and second from left, respectively, and the left (mirrored) and right mandibular 1st–3rd molars of LB6 are shown at the far right and second from right, respectively (modified from Kaifu *et al*., 2015). Note the difference in shape and absolute and relative cusp size between the teeth of *H. floresiensis* and the two teeth from Unit 4 (1 cm scale shown).

Compared to published data on the mandibular 2nd molars of LB1, LB6 (Brown and Maeda, 2009; Kaifu *et al*., 2015) and modern humans (Voisin *et al*., 2012), the molar from Unit 4 is mesiodistally long and buccolingually wide. It is more than 1 mm longer than it is wide, distinguishing it clearly from the crown shapes of LB1 and LB6, but falling within the range of variation observed among modern human molars (Fig. 4.33). Its buccolingual width of 11.0 mm falls within the range of mean values for Australian Aboriginal (11.9 mm), North Asian (10.3 mm) and European (10.0 mm)

population samples (Brown, 2016). Together, the size and shape of these two isolated teeth fall within the range of variation of modern humans in general, and of Australian Aboriginals in particular, and they are unlike the teeth of LB1 and LB6. If the latter two specimens are typical of *H. floresiensis*, then it is reasonable to conclude that the two teeth from Unit 4 belong to *Homo sapiens*.

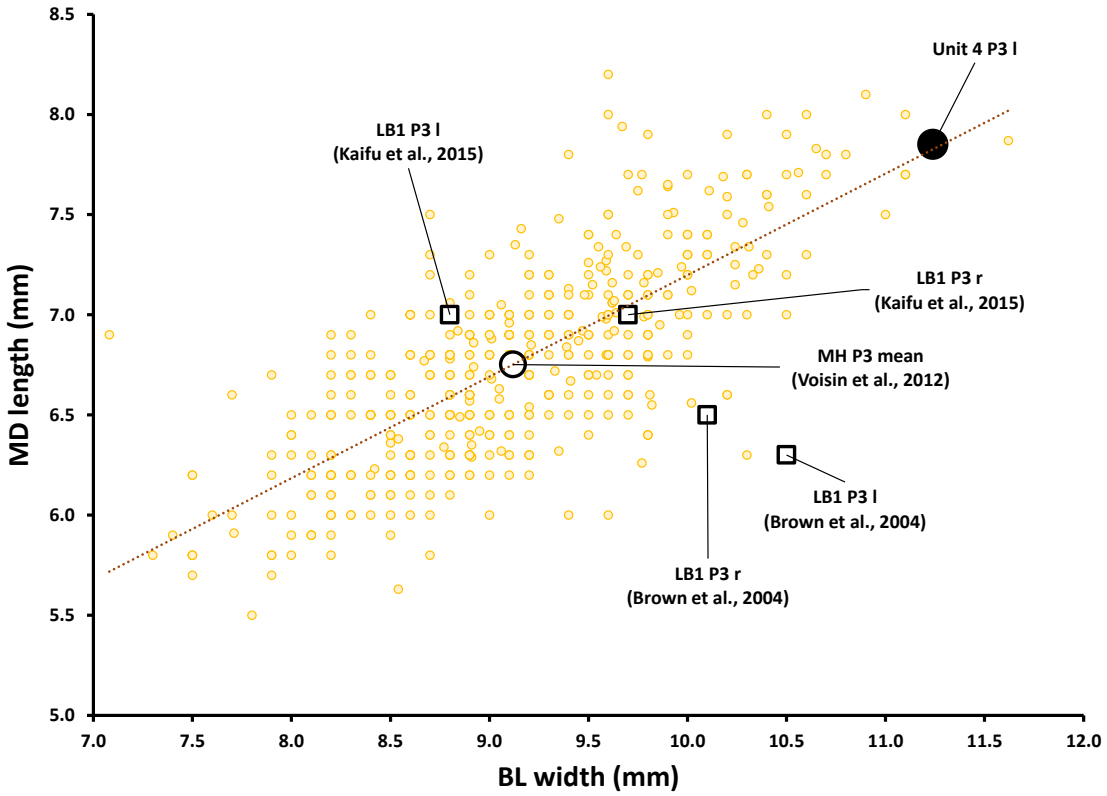

Figure 4.32 Mesiodistal (MD) lengths and buccolingual (BL) widths of maxillary 3rd premolars from *H. floresiensis* (LB1) (Brown *et al.*, 2004; Kaifu *et al.*, 2015), modern humans (*N* = 502) (Voisin *et al.*, 2012) and Unit 4 at Liang Bua (~46 ka cal. BP, shown by the filled circle). The dotted line is the linear regression for the dataset of modern human premolars.

Apart from these two intriguing teeth in Unit 4, the dramatic shift in choice of raw material for stone artefact manufacture and the possibly human-mediated increase in abundance of shellfish remains in this unit, the subsequent Late Pleistocene units suggest a mostly consistent trend in environmental conditions, based on the faunal record. From Unit 4 to Unit 7 (~47 ka to 11 ka cal. BP), rats continue to decline significantly in relative abundance, while the remains of frogs, snakes, megabats and,

especially, microbats increase (Figs 4.7 and 4.9–4.12). Although we lack taphonomic observations needed to rule out changes in the accumulators of the fauna, these taxonomic trends collectively imply substantial ecological changes occurred in the area around Liang Bua as it recovered from the effects of at least two volcanic eruptions ~50–47 ka ago. The rise in abundance of megabat remains suggests that fruiting trees increased, while the increase in microbat and frog remains implies that abundant numbers of insects were likely present during this period also. Chert and silicified tuff show no statistically significant trends in Units 4–7 (Figs 4.23 and 4.24), so we attribute the observed variations in raw material proportions to fluctuations arising from low sample numbers (Table 4.3), rather than to any significant shifts in hominin behaviour.

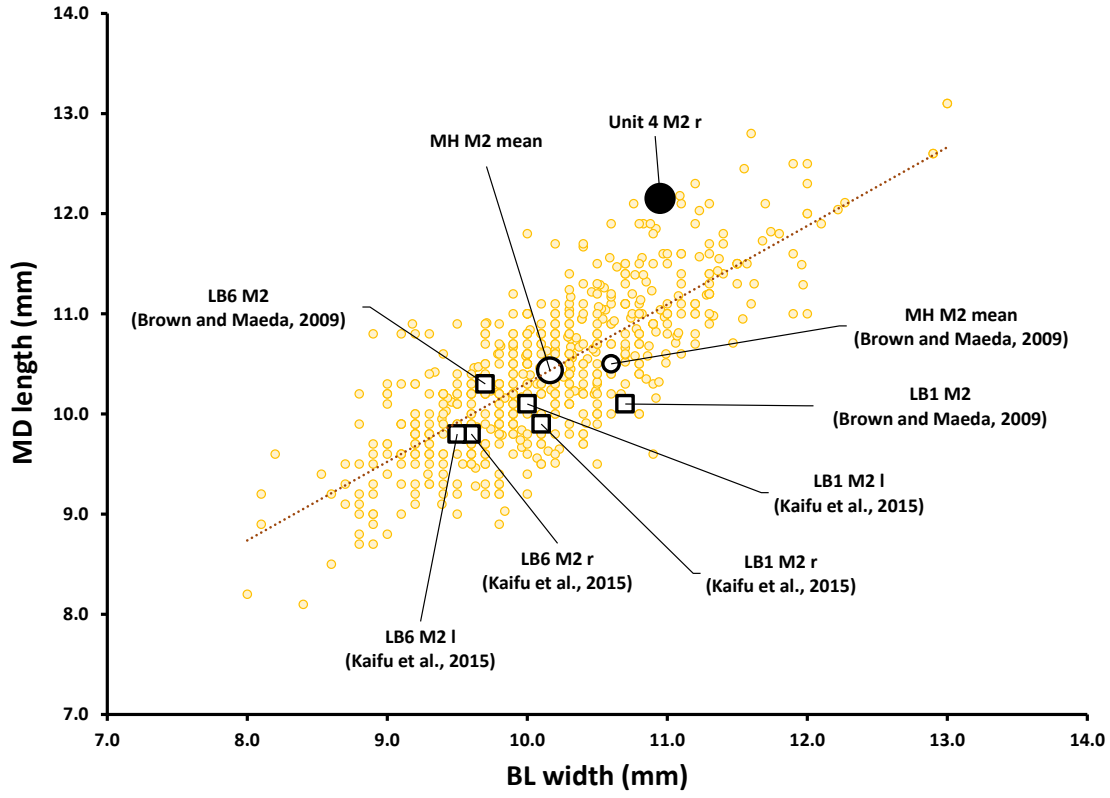

Figure 4.33 Mesiodistal (MD) lengths and buccolingual (BL) widths of mandibular 2nd molars from *H. floresiensis* (LB1 and LB6) (Brown *et al*., 2004; Kaifu *et al*., 2015), modern humans (*N* = 502) (Voisin *et al*., 2012), modern humans (*N* = 1181) (Brown and Maeda, 2009) and Unit 4 at Liang Bua (~46 ka cal. BP, shown by the filled circle). The dotted line is the linear regression for the dataset of modern human molars.

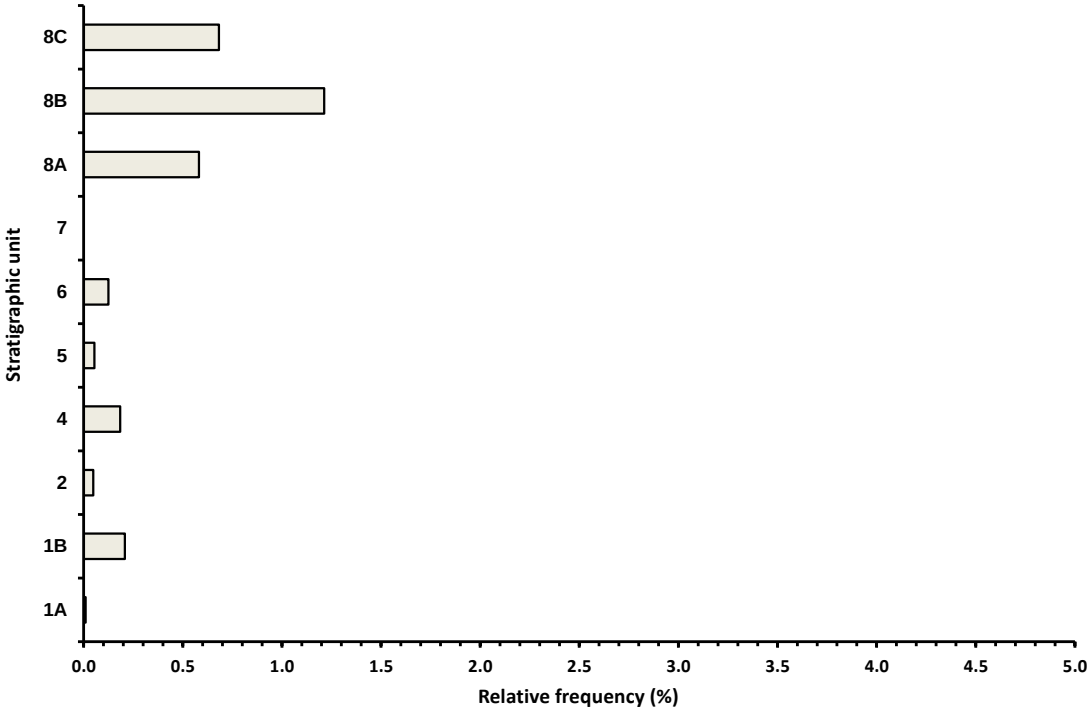

Figure 4.34 Relative frequencies (calculated as % vertebrate NISP) of fish by stratigraphic unit at Liang Bua. Note the *x*-axis ranges between 0 and 5%.

This same overall ecological trend of faunal abundances continues into the early to middle part of the Holocene (Unit 8A, ~12–5 ka cal. BP), but the 9.5% increase in frogs (Fig. 4.9) suggests a much wetter environment, and expansion of moist rainforest may also explain the 3.2% increase in megabats (Fig. 4.11). These trends are consistent with palaeoenvironmental data that suggest wet and relatively stable conditions during this period (Westaway *et al*., 2009a, b). Fish remains comprise 0.6% of vertebrate NISP in Unit 8A, which is a small but likely significant amount, as it represents the first time in the entire sequence that fish surpass 0.2% of vertebrate NISP (Fig. 4.34). Aquatic and terrestrial invertebrates also return at low frequencies (0.6% and 1.1% of total NISP, respectively), after being absent in Units 5–7 (Figs 4.13 and 4.14), and varanids (most likely *V. hooijeri*) reach 1.1% of vertebrate NISP, more than double that in any unit since Unit 1B (Fig. 4.29). The increases in fish, aquatic invertebrate and varanid remains most likely represent the refuse of modern human subsistence practices.

Compared to the preceding four Late Pleistocene units (Units 4–7), it appears that early to mid-Holocene modern human populations exploited freshwater resources to a greater extent than did their ancestors during the preceding 35–40 millennia. Whether this behavioural shift was due to the increased availability of these resources and/or to some other factor (e.g., location of resource processing, population growth, changes in cultural practices) is not yet certain. But whatever the exact reason, it is clear that these human subsistence behaviours had intensified at Liang Bua by the mid-Holocene.

In Unit 8B (~5–3 ka cal. BP), significant increases in the proportions of vertebrate NISP are observed for fish (1.2%), frogs (22.4%) and varanids (1.4%) in comparison with those of Unit 8A (Figs 4.9, 4.29 and 4.34). Aquatic invertebrates rise to 19.9% of total faunal NISP and the proportion of land snails jumps to 4.6% (Figs 4.13 and 4.14). Introduced large mammals (e.g., pig, porcupine, macaque and civet cat) comprise 3.1% of vertebrate NISP in Unit 8B, compared to just 0.3% in Unit 8A and nil in all of the earlier units (Fig. 4.15). Pottery sherds also make their first appearance at Liang Bua in Unit 8B (Morwood *et al*., 2009), but the raw material proportions of the stone artefacts maintain the same pattern as first seen in Unit 4, more than ~40 ka earlier (Fig. 4.22). Together, this evidence speaks to intensified human exploitation of the natural environment, coupled with deliberate modification of the ecosystem through the introduction of non-endemic animal species to provide additional food resources. While the faunal assemblages in the preceding units show glimpses of an ephemeral hunter–gatherer subsistence economy, Unit 8B marks the transition to a Neolithic lifestyle in the area surrounding Liang Bua. The presence of pottery by itself does not necessarily suggest that farming was underway around Liang Bua by the mid-Holocene, but it certainly indicates that people were attempting to store resources. Coupled with the faunal evidence in Unit 8B, the appearance of pottery suggests that the population of

modern humans in the area was on the rise and that people were quickly becoming, or were already, more sedentary.

The notable shifts in faunal community composition in Unit 8B mostly recede to previous patterns of abundance in Unit 8C (~3 ka to the present) (Fig. 4.6). Fish, frogs and varanids decline in relative abundance to 0.7%, 10.7% and 0.5%, respectively (Figs 4.9, 4.29 and 4.34), and aquatic and terrestrial invertebrates also decrease in relative abundance to 13% and 3% of total faunal NISP, respectively (Figs 4.13 and 4.14). In contrast, introduced large mammals increase to 5.2% of vertebrate NISP (Fig. 4.15) and rats increase to 71.3%—the first time in more than ~45 millennia that these murine rodents have not declined further in abundance (i.e., since before the volcanic eruption 50–47 ka ago) (Fig. 4.7). The evidence from Unit 8C suggests that human use of the cave over the last 3 ka differed from that during the first 9 ka of the Holocene, which we interpret as indicating more significant human-induced changes to the surrounding landscape (e.g., clearing for cultivation and animal domestication).

4.6 Conclusions

This study has resolved many questions about the spatio-temporal distribution of faunal and cultural remains at Liang Bua (Fig. 4.35) and revealed significant shifts in the taxonomic and raw material composition of these assemblages throughout the stratigraphic sequence. These shifts reflect palaeoecological changes likely related to changing environmental conditions and hominin and other animal behaviours over the last ~190 ka.

Previous studies of the palaeoenvironment and palaeoclimate of Flores (Westaway *et al*., 2007a, b; 2009a, b) have suggested that changing conditions on Flores during the late Quaternary likely impacted on the regional ecology and human

activities. However, the wide age ranges for many of the stratigraphic units analysed in this study preclude precise correlation with the higher resolution palaeoenvironmental and palaeoclimatic datasets for the region. Successive volcanic eruptions have also likely had a major influence on the responses of hominins, other biota and the climate of Flores, and may have played a role in the extinction of *H. floresiensis* and other taxa larger than 5 kg. There are, therefore, compelling reasons to conduct further research into the roles of changing climate and volcanic activity on the documented changes in faunal composition at Liang Bua.

Our analyses indicate that the most marked shift in faunal structure occurred immediately after deposition of tephra T3 ~50 ka ago. Further major change is recorded after another volcanic eruption that resulted in the deposition of T7 and T8 between ~13 and 11 ka cal. BP. These results suggest that these volcanic events had significant effects on the palaeoecological history of Flores and, presumably, nearby islands also. Our data also suggest that *H. floresiensis* and *S. florensis insularis*, along with giant marabou stork and vulture, were extinct by ~50 ka ago. This extinction event was coincident with, or followed immediately by, the arrival of modern humans on Flores at ~46 ka, as suggested by a significant shift in stone artefact raw material preference and the recovery of two isolated teeth that most likely represent *H. sapiens*. If our interpretation of this evidence is correct, then it marks the earliest cultural and biological evidence of modern humans in Indonesia and among the oldest in all of Island Southeast Asia. Whether late-surviving groups of *H. floresiensis* interacted with the first arrivals of *H. sapiens* on Flores is an open question that future research may help answer.

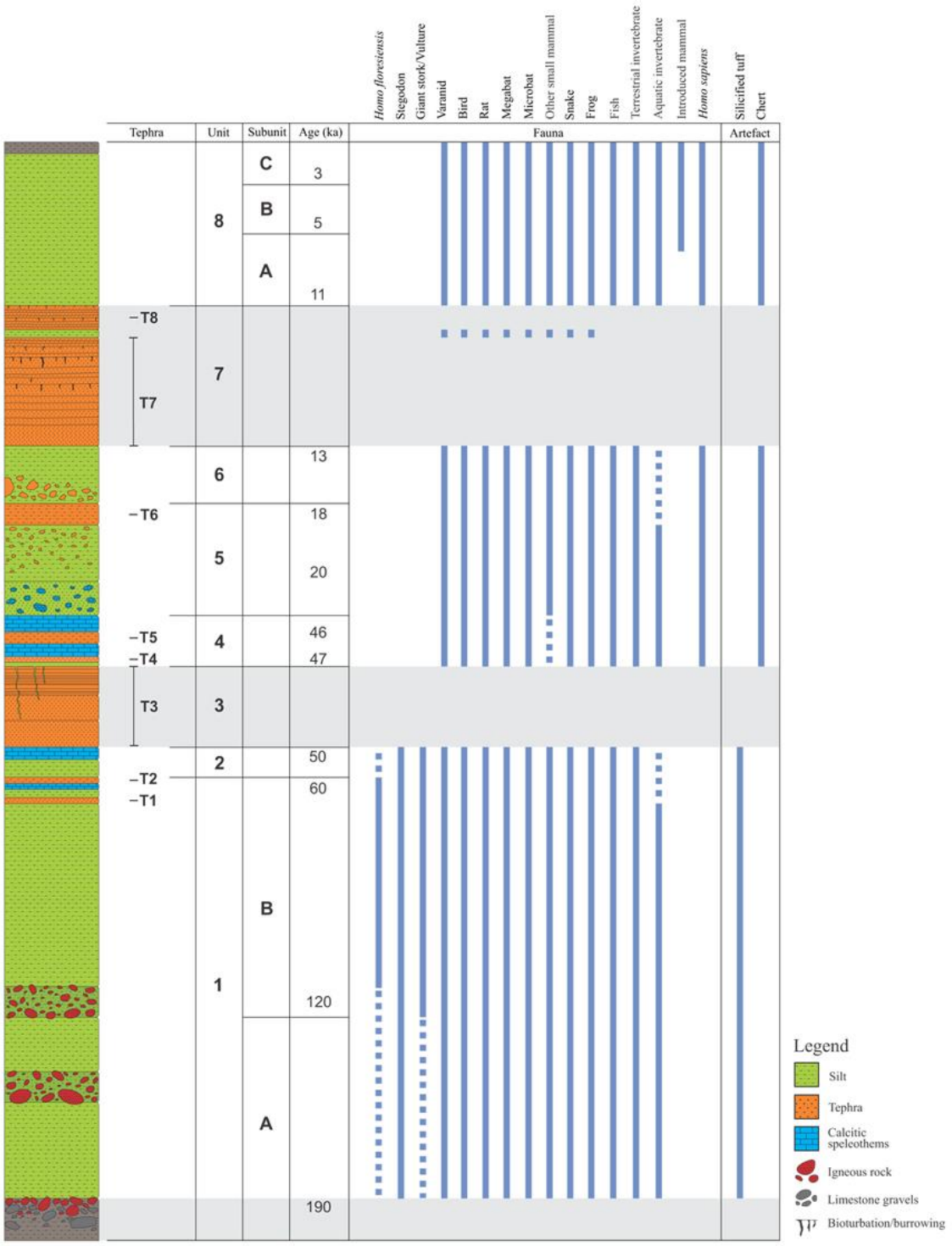

Figure 4.35 Composite stratigraphy at Liang Bua with approximate ages and units/subunits based on Sutikna *et al*. (2016). Same as Fig. 4.2, but updated with a summary of the results of this study. Note the many areas where significant questions have been answered. The dotted vertical lines indicate presumed presence of *H. floresiensis* based on stone artefacts, and possible extensions to the time ranges of some other fauna.

CHAPTER 5

Synthesis of findings, broader implications and directions for future research

5.1 Synthesis and implications of the new research at Liang Bua

As stated in Chapter 1, the overarching aim of this thesis was to contextually collect, describe and analyse information obtained from the Liang Bua excavations conducted between 2007 and 2014, and to integrate these findings with those done previously (2001–2004). The primary goal was to increase knowledge and understanding about the stratigraphy and chronology of the deposits, as well as the hominin skeletal and cultural remains (and other faunal elements) preserved within them. More specifically, the aims of this research were to: 1) test the validity of previous stratigraphic, chronological and archaeological claims for this important site, which is the type locality of *H. floresiensis*; 2) increase our knowledge of when *H. floresiensis* and modern humans used the cave and the nature of their respective activities; and 3) study the preserved faunal and cultural remains to inform on the past ecological and environmental conditions experienced by these two species. Each of these aims has been met, yielding important new insights into the history of Liang Bua and its human occupants, and casting new light on the antiquity and activities of modern humans in Island Southeast Asia. The remainder of this section summarises these collective findings and their broader implications.

The results of this study have revealed that the stratigraphic sequence of Liang Bua is more complex than previously interpreted (Morwood *et al*., 2004, 2005, 2009; Westaway *et al*., 2009b). Eight key volcanic tephras (T1–T8) are now recognised within the depositional sequence preserved at Liang Bua, whereas only three of these – T3 (formerly referred to as the "black tuff" or similar), T7 and T8 (formerly referred to as

the "white tuff" or similar) – featured prominently in previous reports (Morwood *et al*., 2004, 2005, 2009; Westaway *et al*., 2009b). These eight tephras serve as distinctive marker beds that clearly separate other sedimentary deposits within the site (e.g., the stratigraphic units and subunits used in Chapter 4; see Table 4.1 and Fig. 4.2). More importantly, documenting the complex spatial relationships between these tephras has been the key to recognising the existence of a major stratigraphic unconformity immediately above the sediments that contained the holotype (LB1) and other skeletal and cultural remains of *H. floresiensis* in the Sectors near the eastern wall of the cave. Ultimately, the presence of this unconformity has led to a fundamental reassessment and reinterpretation of the Liang Bua stratigraphy and its chronology (see Chapter 2).

This reevaluation has resulted in the following reconstruction of the history of sediment deposition and erosion at Liang Bua. The *H. floresiensis*-bearing deposits consist of multiple layers of fine-grained sediment, interspersed by layers of weathered limestone, speleothem and loose gravel. A ~2 m-thick sequence that includes five tephras (T1–T5) separated by clastic sediments and flowstones conformably overlies the *H. floresiensis*-bearing deposits. In combination, these deposits form a large remnant pedestal, the northern part of which has been truncated by one or more erosional events. These erosional event(s) created an undulating cave surface topography that sloped steeply down towards the cave mouth. Sediments, including three additional tephras (T6, T7 and T8), subsequently accumulated above and along this sloping erosional surface and eventually covered the entire remnant pedestal.

Several dating methods (luminescence, uranium-series and $^{40}Ar/^{39}Ar$) have been applied to the main stratigraphic units within the pedestal and to the skeletal remains of *H. floresiensis* and pygmy *Stegodon* recovered from these sediments. The results of this dating program do not support the ages inferred previously for the *H. floresiensis*

remains recovered in the Sectors near the eastern wall (~18 to 13–11 ka cal. BP). Instead, the skeletal remains of *H. floresiensis* and the deposits containing them are dated to between about 100 and 60 ka. Stone artefacts that can reasonably be attributed to this species (on the basis of raw material preference) range from approximately 190 to 50 ka in age, and extinct endemic fauna such as pygmy *Stegodon*, vulture and giant marabou stork (as well as Komodo dragon, which survives today on adjacent islands and the northern coast of Flores) disappeared from the Liang Bua sequence ~50 ka ago.

This revised stratigraphic and chronological interpretation of the Liang Bua sequence has resolved important questions about the last appearance date of *H. floresiensis* and its preceding temporal context, and has also shed new light on when modern humans first arrived on Flores. Previous research at Liang Bua suggested that the earliest evidence of modern humans at the site (and on the island) occurred no earlier than ~11 ka ago (Morwood *et al*., 2004, 2009). As a result of the research carried out at Liang Bua for this thesis, our understanding of the past 50 ka of depositional sequence has also been refined and expanded significantly (Chapter 3). In particular, deposits at the site dating to between ~41 and 25 ka were discovered between 2011 and 2014, and extended to ~46 ka in 2014 and 2015 with radiocarbon ages on charcoal recovered during the 2011 excavations. Thus, the post-50 ka stratigraphic sequence at Liang Bua is now reasonably complete and the interval from 46 to 12 ka presents a rare opportunity to address key questions regarding potentially late-surviving populations of *H. floresiensis* and/or an earlier presence of modern humans on the island.

Analyses of stone artefact assemblages from the 46–12 ka interval have revealed a significant shift in raw material preference for chert compared with silicified tuff in the *H. floresiensis*-bearing deposits, and this preference for chert mirrors that observed previously for modern humans in the Holocene sequence (Moore *et al*., 2009).

Moreover, the oldest artefacts from this interval are associated with two teeth that are most likely modern human, providing credible evidence that *H. sapiens* had arrived on Flores by ~46 ka (Chapter 4). Thus, Liang Bua preserves some of the earliest cultural and biological evidence of modern humans in Indonesia and, indeed, Island Southeast Asia. Given the dearth of archaeological sites in the region that are older than ~40 ka and contain skeletal remains or compelling behavioural evidence of modern humans (Barker *et al*., 2007; Higham *et al*., 2009; O'Connor *et al*., 2011; Storm *et al*., 2013; Aubert *et al*., 2014; O'Connor, 2015), Liang Bua – and potentially other sites on Flores – will likely play a critical role in future reconstructions of when and how modern humans dispersed across this region before ultimately reaching Australasia (Fig. 5.1). The results of this thesis provide additional support for hypotheses that favour a 'southern route' for modern human dispersal along the chain of Lesser Sunda Islands to Sahuland (Birdsell, 1977; Bird *et al*., 2005; O'Connor, 2007), but this long-standing debate will undoubtedly continue until evidence of modern humans in Wallacea is discovered that antedates the earliest sites in Australasia.

In addition to the results discussed above, the research conducted for this thesis has documented significant shifts in the abundance of faunal taxa during the Late Pleistocene and Holocene, with implications for palaeoenvironmental and palaeoecological reconstructions (see Chapter 4). The most conspicuous shift in faunal composition occurs immediately after deposition of tephra T3 ~50 ka ago. This marks the last appearance date for *H. floresiensis*, pygmy *Stegodon*, giant marabou stork and vulture, with the synchronous or subsequent arrival of modern humans signaling the onset of different hominin behaviours, such as the preference for chert and a more intensive use of fire (Moore *et al*., 2009; Morley *et al*., 2016), compared to those exhibited by *H. floresiensis*.

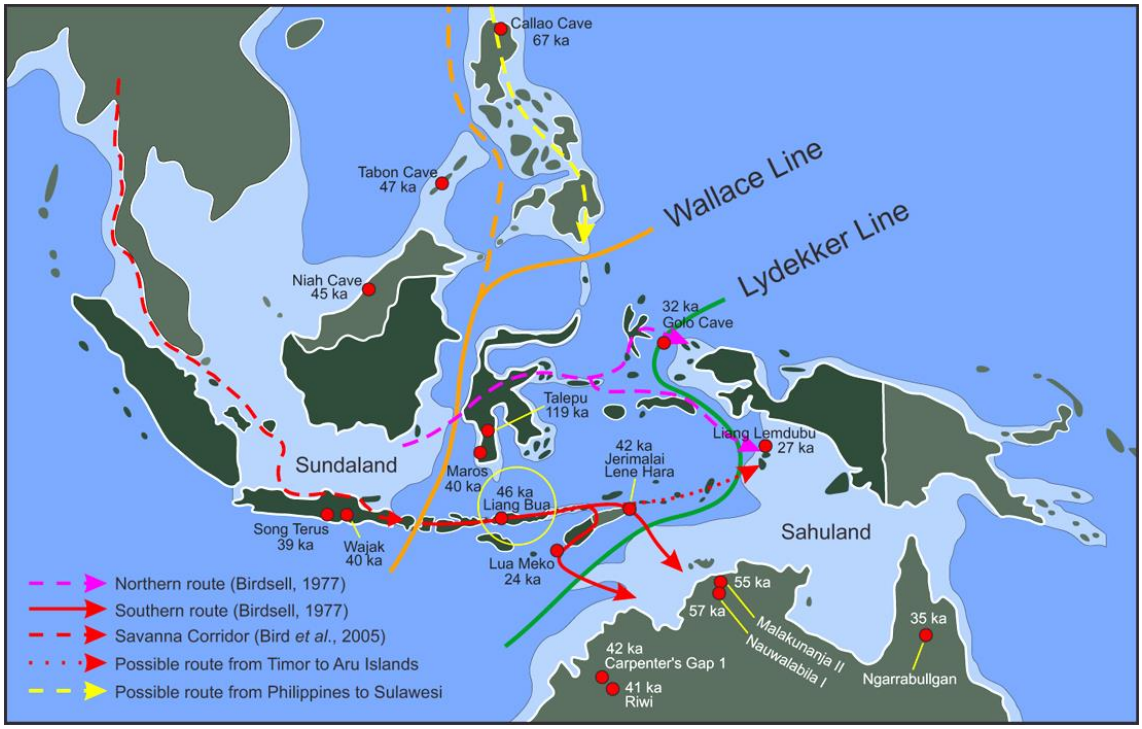

Figure 5.1 Map of Island Southeast Asia and Australasia showing Sundaland, Wallacea and Sahuland. Late Pleistocene archaeological sites and possible routes for modern human dispersal are also indicated. The yellow circle highlights the new evidence for modern humans at Liang Bua ~46 ka ago presented in this thesis (modified from Birdsell, 1977; Bird *et al*., 2005; O'Connor, 2007).

The next major faunal change took place at the transition between the Late Pleistocene and Holocene, following the volcanic eruptions that deposited T7 and T8 about 12 ka ago. There was also a significant climatic shift to wetter conditions at this time, as recorded in speleothems from two caves in the vicinity of Liang Bua (Westaway *et al*., 2007b). This shift is reflected in the faunal abundances, which are consistent with an expansion of moist rainforest during the early to middle Holocene.

The most recent shift occurred in the mid to late Holocene and was clearly the result of modern humans translocating animals (e.g., pigs, porcupine, macaque and civet cat) from other nearby islands to Flores. This marks the transition to a Neolithic lifestyle in the area surrounding Liang Bua and is associated with the appearance of pottery, which suggests that cooking and storing of resources was becoming increasingly

important and people more sedentary. These deposits contain a fully modern fauna (i.e., like exists on Flores today), including small and large introduced mammals, reptiles, avian fauna, terrestrial vertebrates and invertebrates, as well as aquatic vertebrates and invertebrates.

The palaeoecology of Flores – and, by extension, nearby islands also – has doubtless been impacted by successive volcanic events, at least locally and for short time periods after each eruption (e.g., Louys, 2012; Timmreck *et al*., 2012). Modern humans arrived at Liang Bua at the same time as, or soon after, the volcanic eruption than deposited T3, and climatic conditions have also changed considerably during the Late Pleistocene (Westaway *et al*., 2007b, 2009a, b). There are several possible agencies, therefore, that could have acted individually or in combination to affect the island's flora and fauna. At this stage, it would be premature to isolate one or other cause as the primary driver of faunal change and extinction on Flores, but some possible avenues for future research to help distinguish between these options are explored below.

The role of climatic changes, in particular, warrants further investigation. Flores is located on the southern edge of the Indo-Pacific Warm Pool (Visser *et al*., 2003; Dubois *et al*., 2014), which is a key driver of global climate (Gagan *et al*., 2004; Wurster *et al*., 2010; Russell *et al*., 2014) and regional rainfall (Dam *et al*., 2001; Russell *et al*., 2014; Konecky *et al*., 2016). Seasonal rainfall strongly influences ecosystem diversity (Feng *et al*., 2013), with modern vegetation on Flores and other islands in the Lesser Sunda dominated by grasslands and savannas, and monsoon rainforest restricted largely to mountainous areas (Dubois *et al*., 2014; Wicaksono *et al*., 2015).

Oxygen ($\delta^{18}O$) and carbon ($\delta^{13}C$) isotope analyses of stalagmites from Liang Luar and Liang Niki, the lower chambers of which are located close to Liang Bua, have

identified at least six significant isotopic shifts that represent palaeoclimate changes on Flores (Westaway *et al*., 2007b, 2009a). Western Flores was generally wet with a closed woodland environment from around 49 to 39 ka ago, after which rainfall decreased and C4 grasses increased from about 39 to 36 ka. Dry conditions then prevailed until ~17 ka, resulting in a savanna ecosystem. In central Sulawesi, carbon isotope analyses of lake sediments similarly suggest wet conditions and a rainforest ecosystem ~53 ka ago, with dry and more seasonal conditions between about 30 and 14 ka (Wicaksono *et al*., 2015). Wet conditions returned to western Flores from around 17 to 15 ka, resulting in an increase in vegetation taxa, and this was followed by sustained rainfall and a wide range of closed-canopy vegetation until ~11 ka. The Holocene climate in both western Flores and central Sulawesi was characterised by humid and wet conditions. Other palaeoenvironmental records from Sulawesi (Dam *et al*., 2001; Russell *et al*., 2014) and the Banda Sea (van der Kaars *et al*., 2000) show similar trends, but detailed and comparable datasets from across Island Southeast Asia are currently lacking.

For over a decade, *H. floresiensis* has attracted worldwide attention and ignited renewed debate about the recent history of human evolution. The fact that at least one premodern human species successfully crossed the Wallace Line long before modern humans reached Island Southeast Asia and Australasia demonstrates the need to adopt a more cautious approach to interpreting archaeological evidence from the broader region (Trinkaus, 2005; Barker *et al*., 2007; O'Connor, 2007). Without a direct association between stone artefact assemblages and hominin skeletal remains, it is not certain which species of hominin was the toolmaker. Modern humans, *H. floresienses*, Denisovans or possibly some other as yet unknown hominin species are all prospective candidates in Island Southeast Asia during the Late Pleistocene. The results of this research also raise another intriguing question: did *H. floresiensis* survive after 50 ka ago and perhaps

encounter modern humans on Flores or other hominins (such as the Denisovans) dispersing through Southeast Asia? The next section concludes this thesis with some suggestions for future research that would help answer some of these questions.

5.2 Future research directions

Modern archaeological research is an interdisciplinary undertaking and requires input from a wide variety of technical specialists to extract the maximum amount of information from any particular site and to test the reliability of the claims made using multiple, independent approaches. This study of the Liang Bua deposits illustrates the application of this strategy, with the deployment of several dating methods to provide a robust geochronological framework for the site, allied to the excavation of multiple Sectors to test the consistency of the stratigraphic interpretations. Such approaches have rarely been employed at sites in Southeast Asia and Australasia – Niah Cave being a notable exception (Barker *et al*., 2007). In addition, an important feature of the Liang Bua research is the sheer scale of the excavations: each Sector is commonly 2 m by 2 m in area and several metres in depth. Excavations on this scale are needed in complex cave settings to reliably reconstruct the sequence of events responsible for the deposition and erosion of sediments. It is only because of the information obtained from the additional large-scale excavations carried out at Liang Bua since 2007 that the original erroneous stratigraphic misinterpretation has come to light.

The technicalities of conducting ‘deep’ excavations are not trivial, however, and considerable care is required to ensure that safety standards are maintained at all times. The use of trench shoring techniques is now well established at Liang Bua, enabling Sectors to be dug safely to depths of almost 11 m (Morwood *et al*., 2009). The use of deep-excavation techniques has been applied to only three other sites in the region:

Song Terus (Sémah *et al*., 2004) and Song Gupuh (Morwood *et al*., 2008) in East Java – where the cave deposits were excavated to more than 15 m depth – and the open-air site of Talepu in Sulawesi (van den Bergh *et al*., 2016), which reached a depth of 12 m. In each case, important archaeological evidence was derived from the deeper deposits, just as LB1 was only discovered when Sector VII was extended beyond the upper ~3 m to a depth of ~6 m. These same large-scale, trench shoring techniques could be profitably applied to other archaeological sites in Island Southeast Asia and elsewhere to ensure that artefacts and fossils are recovered from the deepest deposits, and in a safe manner.

This latest study of Liang Bua has shed new light on the probable last appearance date of *H. floresiensis* and the likely arrival time of modern humans at the site. However, many issues remain unresolved, including the possibility of interaction between these two species. Any such encounter would most likely have occurred in the period between 60 and 45 ka ago, when modern humans are thought to have spread through Island Southeast Asia en route to Australia. Future research at Liang Bua will include concerted efforts to locate and excavate additional deposits of this age in the search for evidence of late-surviving *H. floresiensis* and pioneering modern humans, to address the question of whether these two species overlapped in time and space, and if and how they interacted.

If any inter-species encounter did take place, then this may be captured in the nuclear and mitochondrial genomes of the earliest *H. sapiens* at Liang Bua, in the same way that interbreeding between *H. sapiens*, *H. neanderthalensis* and Denisovans has been documented recently (e.g., Vattathil and Akey, 2015; Meyer *et al*., 2016; Vernot *et al*., 2016). However, to draw meaningful inferences about any admixture requires the extraction and sequencing of the DNA of *H. floresiensis*, and this poses a considerable technical challenge because of the poorer preservation of DNA in tropical

environments. Nonetheless, ancient DNA studies of *H. floresiensis* and early *H. sapiens* remains at Liang Bua represent an obvious avenue for future investigation, given the immense progress made in this field over the last few years.

Additional insights into the taphonomy and diagenesis of the organic and inorganic components of the deposit could also be gained by systematically applying micromorphology methods to the sediments and faunal remains (e.g., Goldberg and Sherwood, 2006; Goldberg and Berna, 2010; Stephens *et al*., 2016) and using archaeological chemistry techniques (e.g., vibrational spectroscopy and gas chromatography–mass spectrometry) to investigate issues such as bone preservation and the characterisation of residues attached to stone artefacts. These techniques could usefully be combined with zooarchaeological analyses and investigations of cave hydrology. Not only would such information refine our current knowledge of the processes of site formation and post-depositional modification, it would also provide complementary chemical data of relevance to questions of DNA preservation and the integrity of organic matter for ^{14}C dating. Such investigations are underway at Liang Bua (e.g., Morley *et al*., 2016) and micromorphology studies have been conducted at some other sites in Island Southeast Asia (e.g., Niah Cave), but they could usefully be applied more widely throughout the region.

One of the major remaining questions concerning *H. floresiensis* is the ultimate and proximal cause(s) of extinction. There are several confounding variables, including the environmental and ecological impacts of volcanic eruptions, changes in Late Pleistocene climates and the arrival of modern humans. This study and others (e.g., Morwood *et al*., 1998; Brumm *et al*., 2010) have shown that Flores experienced multiple volcanic eruptions over the last million years, but details of these volcanic events (e.g., size and spatial extent) are sketchy. The same applies to the climate history

of Flores: at present, there is a paucity of information on the prevailing climate for most of the Late Pleistocene, so it is not possible to rule in or out a climatic influence on the extinction of *H. floresiensis* (but see e.g., Scroxton *et al*., 2013). Systematic studies of the volcanic and climatic records in Flores for the 60–45 ka interval would assist considerably in establishing the importance or otherwise of these factors in the demise of *H. floresiensis*, while reconstructions extending from 200 ka to the present would illuminate the conditions under which this species and *H. sapiens* prospered.

Finally, a key objective of future research is to extend our knowledge of *H. floresiensis* beyond the type locality of Liang Bua to other parts of Flores and possibly other islands. At present, for example, the geographical distribution and variations in population size of this species over time are completely unknown. Yet, *H. floresiensis* or its ancestor somehow reached Flores (probably accidentally) and, thus, a record of these populations should be present on other adjacent islands (Dennell *et al*., 2014). There is clearly, therefore, a compelling need to explore other parts of Island Southeast Asia, including the chain of Lesser Sunda Islands to the west and Sulawesi to the north (Fig. 5.1) along which hominins must have dispersed in the past million years. Given this potential, future opportunities for groundbreaking archaeological and palaeoanthropological discoveries in this region are as great now as they were in 2003, when *H. floresiensis* was first discovered at Liang Bua.

References

Aitken, M.J., 1998. An Introduction to Optical Dating. Oxford University Press, Oxford.

Allen, J., O'Connell, J.F., 2014. Both half right: updating the evidence for dating first human arrivals in Sahul. Austr. Archaeol. 79, 86–108.

Alloway, B.V., Pribadi A., Westgate, J.A., Bird, M., Fifield, L.K., Hogg, A., Smith, I., 2004. Correspondence between glass-FT and ^{14}C ages of silicic pyroclastic flow deposits sourced from Maninjau caldera, west-central Sumatra. Earth Planet. Sci. Lett. 227, 121–133.

Argue, D., Donlon, D., Groves, C., Wright, R., 2006. *Homo floresiensis*: Microcephalic, pygmoid, *Australopithecus*, or *Homo*? J. Hum. Evol. 51, 360–374.

Aubert, M., Brumm, A., Ramli, M., Sutikna, T., Saptomo, E.W., Hakim, B., Morwood, M.J., van den Bergh, G.D., Kinsley, L., Dosseto, A., 2014. Pleistocene cave art from Sulawesi, Indonesia. Nature 514, 223–227.

Auclair, M., Lamothe, M., Huot, S., 2003. Measurement of anomalous fading for feldspar IRSL using SAR. Radiat. Meas. 37, 487–492.

Auffenberg, W., 1981. The Behavioral Ecology of the Komodo Monitor. University Presses of Florida, Gainesville.

Bae, C.J., Wang, W., Zhao, J., Huang, S., Tian, F., Shen, G., 2014. Modern human teeth from Late Pleistocene Luna cave (Guangxi, China). Quat. Int. 354, 169–183.

Barker, G. (Ed.), 2013. Rainforest foraging and farming in Island Southeast Asia. The Archaeology of the Niah Caves, Sarawak Vol. 1. McDonald Institute for Archaeological Research, University of Cambridge, UK.

Barker, G., Reynolds, T., Gilbertson, D., 2005. The human use of caves in peninsular and Island Southeast Asia: Research themes. Asian Perspect. 44, 1–15.

Barker, G., Barton, H., Bird, M., Daly, P., Datan, I., Dykes, A., Farr, L., Gilbertson, D., Harrisson, B., Hunt, C., Higham, T., Kealhofer, L., Krigbaum, J., Lewis, H., McLaren, S., Paz, V., Pike, A., Piper, P., Pyatt, B., Rabett, R., Reynolds, T., Rose, J., Rushworth, R., Stephens, M., Stringer, C., Thompson, J., Turney, C., 2007. The 'human revolution' in lowland tropical Southeast Asia: the antiquity and behavior of anatomically modern humans at Niah Cave (Sarawak, Borneo). J. Hum. Evol. 52, 243–261.

Barker, G., Barton, H., Cole, F., Doherty, C., Gilbertson, D., Hunt, C., Lloyd-Smith, L., Piper, J.P., Rabett, R.J., Reynolds, T., Szabó, K., 2013. The Niah Caves, the 'human revolution', and foraging/farming transitions in Island Southeast Asia. In: Barker, G. (Ed), Rainforest foraging and farming in Island Southeast Asia. The Archaeology of the Niah Caves, Sarawak Vol. 1. McDonald Institute for Archaeological Research, University of Cambridge, UK, pp. 341–366.

Barton, H., Barker, G., Gilbertson, D., Hunt, C., Kealhofer, L., Lewis, H., Paz, V., Piper, J.P., Rabett, R.J., Reynolds, T., Szabó, K., 2013. Late Pleistocene foragers, c. 35,000–11,500 years ago. In: Barker, G. (Ed), Rainforest foraging and farming in Island Southeast Asia. The Archaeology of the Niah Caves, Sarawak Vol. 1. McDonald Institute for Archaeological Research, University of Cambridge, UK, pp. 173–215.

Bellwood, P., Nitihaminoto, G., Irwin, G., Gunadi, Waluyo, A., Tanudirjo, D., 1998. 35,000 years of prehistory in the northern Moluccas. Mod. Quat. Res. SE Asia 15, 233–275.

Bergström, A., Nagle, N., Chen, Y., McCarthy, S. Pollard, M.O., Ayub, Q., Wilcox, S., Wilcox, L., van Oorschot, R.A.H., McAllister, P., Williams, L., Xue, Y., Mitchell, R.J., Tyler-Smith, C., 2016. Deep roots for Aboriginal Australian Y chromosomes. Curr. Biol. 26, 809–813.

Bird, M.I., Ayliffe, L.K., Fifield, L.K., Turney, C.S.M., Cresswell, R.G., Barrows, T.T., David, B., 1999. Radiocarbon dating of "old" charcoal using a wet oxidation, stepped-combustion procedure. Radiocarbon 41, 127–140.

Bird, M.I., Taylor, I.D., Hunt, C., 2005. Palaeoenvironments of insular Southeast Asia during the Last Glacial Period: a savannah corridor in Sundaland. Quat. Sci. Rev. 24, 2228–2242.

Birdsell, J.B., 1977. The calibration of a paradigm for the first peopling of greater Australia. In Allen, J., Golson, J., Jones, R. (Eds), Sunda and Sahul: Prehistoric studies in Southeast Asia, Melanesia and Australia. Academic Press, London. pp. 113–167.

Bøtter-Jensen, L., Andersen, C.E., Duller, G.A.T., Murray, A.S., 2003. Developments in radiation, stimulation and observation facilities in luminescence measurements. Radiat. Meas. 37, 535–541.

Bowler, J.M. Johnston, H., Olley, J.M., Prescott, J.R., Roberts, R.G., Shawcross, W., Spooner, N.A., 2003. New ages for human occupation and climatic change at Lake Mungo, Australia. Nature 421, 837–840.

Brock, F., Higham, T.F.G., Ditchfield, P., Bronk Ramsey, C., 2010. Current pretreatment methods for AMS radiocarbon dating at the Oxford Radiocarbon Accelerator Unit (ORAU). Radiocarbon 52, 103–112.

Brongersma, L.D., 1958. On an extinct species of the genus *Varanus* (Reptilia, Sauria) from the island of Flores. Zool. Meded. XXXVI, 113–130.

Brothwell, D.R., 1960. Upper Pleistocene human skull from Niah caves, Sarawak. Sarawak Mus. J. (new series) 15–16, 323–349.

Brown, P. 2016. Online database of modern human skeletal and dental measurements accessed at http://www.peterbrown-palaeoanthropology.net/resource.html

Brown, P. Sutikna, T., Morwood, M.J., Soejono, R.P., Jatmiko, Saptomo, E.W., Due, R.A., 2004. A new small-bodied hominin from the Late Pleistocene of Flores, Indonesia. Nature 431, 1055–1061.

Brumm, A., 2012. The 2011 excavations at Leang Burung 2 rockshelter in South Sulawesi, Indonesia. Centre for Archaeological Science, University of Wollongong. Unpublished report.

Brumm, A., Aziz, F., van den Bergh, G.D., Morwood, M.J., Moore, M.W., Kurniawan, I., Hobbs, D.R., Fullagar, R., 2006. Early stone technology on Flores and its implications for *Homo floresiensis*. Nature 441, 624–628.

Brumm, A., Jensen, G.M., van den Bergh, G.D., Morwood, M.J., Kurniawan, I., Aziz, F., Storey, M., 2010. Hominins on Flores, Indonesia, by one million years ago. Nature 464, 748–752.

Bulbeck, D., Sumantri, I., Hiscock, P., 2004. Leang Sakapao I, a second dated Pleistocene site from South Sulawesi, Indonesia. Mod. Quat. Res. SE Asia 18, 111-128.

Cannon, M.D., 2001. Archaeofaunal relative abundance, sample size, and statistical methods. J. Archaeol. Sci. 28, 185–195.

Cheng, H., Edwards, R.L., Hoff, J., Gallup, C.D., Richards, D.A., Asmerom, Y., 2000. The half-lives of uranium-234 and thorium-230. Chem. Geol. 169, 17–33.

Clark, T.R., Zhao, J.-x., Roff, G., Feng, Y.-x., Done, T.J., Nothdurft, L.D., Pandolfi, J.M., 2014. Discerning the timing and cause of historical mortality events in modern *Porites* from the Great Barrier Reef. Geochim. Cosmochim. Acta 138, 57–80.

Clarkson, C., Smith, M., Marwick, B., Fullagar, R., Wallis, L.A., Faulkner, P., Manne, T., Hayes, E., Roberts, R.G., Jacobs, Z., Carah, X., Lowe, K.M., Matthews, J., Florin, S.A., 2015. The archaeology, chronology and stratigraphy of Madjedbebe (Malakunanja II): a site in northern Australia with early occupation. J. Hum. Evol. 83, 46–64.

Curnoe, D., Ji, X., Shaojin, H., Taçon, P.S., Li, Y., 2016. Dental remains from Longtanshan cave 1 (Yunnan, China), and the intial presence of anatomically modern humans in East Asia. Quat. Int. 400, 180–186.

Dam, R.A.C, Fluin, J., Suparan, P., van der Kaars, S., 2001. Palaeoenvironmental developments in the Lake Tondano area (N. Sulawesi, Indonesia) since 33,000 yr B.P. Palaeogeogr. Palaeoclimatol. Palaeoecol. 171, 147–183.

Delta Bayu Murti, 2011. Beberapa patologi pada seri tengkorak dan gigi dari Situs Liang Bua, Lewoleba, dan Melolo: Suatu Tinjauan Bioarkeologis dan Rekomendasi Konservasinya. Unpublished Master Thesis. Gadjah Mada University, Jogjakarta.

Demeter, F., Shackelford, L.L., Bacon, A.-M., Duringere, P., Westaway, K., Sayavongkhamdy, T., Braga, J., Sichanthongtip, P., Khamdalavong, P., Ponche, J.-L., Wang, H., Lundstrom, C., Patole-Edoumba, E., Karpoff, A.M., 2012. Anatomically modern human in Southeast Asia (Laos) by 46 ka. Proc. Natl. Acad. Sci. USA 109, 14375–41380.

Dennell, R.W., Louys, J., O'Regan, H.J., Wilkinson, D.M., 2014. The origins and persistence of *Homo floresiensis* on Flores: biogeographical and ecological perspectives. Quat. Sci. Rev. 96, 98–107.

Dubois, N., Oppo, D.W., Galy, V.V, Mohtadi, M., van der Kaars, S., Tierney, J.E., Rosenthal, Y., Eglinton, T.I., Lückge, A., Linsley, B.K., 2014. Indonesian vegetation response to changes in rainfall seasonality over the past 25,000 years. Nat. Geosci. 7, 513–517.

Eggins, S.M., Grün, R., McCulloch, M.T., Pike, A.W.G., Chappell, J., Kinsley, L., Mortimer, G., Shelley, M., Murray-Wallace, C.V., Spötl, C., Taylor, L., 2005. In situ U-series dating by laser-ablation multi-collector ICPMS: new prospects for Quaternary geochronology. Quat. Sci. Rev. 24, 2523–2538.

Falk, D., Hildebolt, C., Smith, K., Morwood, M.J., Sutikna, T., Brown, P., Jatmiko, Saptomo, E.W., Brunsden, B., Prior, F., 2005. The brain of *Homo floresiensis*. Science 308, 242–245.

Feng. X., Porporato, A., Rodriguez-Iturbe, I., 2013. Changes in rainfall seasonality in the tropics. Nat. Clim. Change 3, 811–815.

Franklin, A.D., Prescott, J.R., Robertson, G.B., 2000. Comparison of blue and red TL from quartz. Radiat. Meas. 32, 633–639.

Fu, Q., Li, H., Moorjani, P., Jay, F., Slepchenko, S.M., Bondarev, A.A., Johnson, P.L.F., Aximu-Petri, A., Prüfer, K., Filippo, C., Meyer, M., Zwyns, N., Salazar-Garcia, D., Kuzmin, Y.V., Keates, S.G., Kosintsev, P., Razhev, D.I., Richards, M.P., Peristov, N.V., Lachmann, M., Douka, K., Higham, T.F.G., Slatkin, M., Hublin, J.J., Reich, D., Kelso, J., Viola, T.B., Pääbo, S., 2014. Genome sequence of a 45,000-year-old modern human from western Siberia. Nature 514, 445–450.

Gagan, M.K., Hendy, E.J., Haberle, S.G., Hantoro, W.S., 2004. Post-glacial evolution of the Indo-Pacific warm pool and El Nino-Southern Oscillation. Quat. Int. 118–119, 127–143.

Galbraith, R.F., Roberts, R.G., 2012. Statistical aspects of equivalent dose and error calculation and display in OSL dating: an overview and some recommendations. Quat. Geochronol. 11, 1–27.

Galbraith, R.F., Roberts, R.G., Laslett, G.M., Yoshida, H., Olley, J.M., 1999. Optical dating of single and multiple grains of quartz from Jinmium rock shelter, northern Australia: Part 1, experimental design and statistical models. Archaeometry 41, 339–364.

Gavin, D.G., Oswald, W.W., Wahlf, E.R., Williams, J.W., 2003. A statistical approach to evaluating distance metrics and analog assignments for pollen records. Quat. Res. 60, 356–367.

Glover, I.C., 1976. Ulu Leang Cave, Maros: A Preliminary Sequence of post-Pleistocene Cultural Development in South Sulawesi. Archipel. 11, 113–154.

Glover, I.C., 1977. The Late Stone Age in eastern Indonesia. World Archaeol. 9, 42–61.

Glover, I.C., 1981. Leang Burung 2: An upper palaeolithic rock shelter in South Sulawesi, Indonesia. Mod. Quat. Res. SE Asia 6, 1–38.

Goldberg. P., Sherwood, S.C., 2006. Deciphering human prehistory through the geoarcheological study of cave sediments. Evol. Anthropol. 15, 20–36.

Goldberg. P., Berna, F., 2010. Micromorphology and context. Quat. Int. 214, 56–62.

Gosden, C., Robertson, N., 1991. Models for Matenkupkum: interpreting a late Pleistocene site from southern New Ireland, Papua New Guinea. In: Allen, J., Gosden, C. (Eds), Report of the Lapita Homeland Project, Occasional Papers in Prehistory 20. Department of Prehistory, Research School of Pacific Studies, Australian National University, Canberra, pp. 20–45.

Grün, R., Huang, P.-H. , Huang, W., McDermott, F., Thorne, A., Stringer, C.B., Yan, G., 1998. ESR and U-series analyses of teeth from the palaeoanthropological site of Hexian, Anhui Province, China. J. Hum. Evol. 34, 555–564.

Grün, R., Eggins, S., Kinsley, L., Moseley, H., Sambridge, M., 2014. Laser ablation U-series analysis of fossil bones and teeth. Palaeogeogr. Palaeoclim. Palaeoecol. 416, 150–167.

Hammer, O., 2015. PAST: Paleontological Statistics Version 3.07. Reference Manual. University of Oslo, Oslo.

Harrisson, T., 1959. Radiocarbon datings from Niah: a note. Sarawak Mus. J. (new series) 13–14, 136–142.

Heinrich, K.F.J., 1991. Strategies of electron microprobe data reduction. In: Heinrich, K.F.J., Newbury, D.E. (Eds), Electron Probe Quantitation. Plenum, New York, pp. 9–18.

Hellstrom, J., Pickering, R., 2015. Recent advances and future prospects of the U–Th and U–Pb chronometers applicable to archaeology. J. Archaeol. Sci. 56, 32–40.

Higham, T.F.G., Barton, H., Turney, C.S.M., Barker, G., Ramsey, C.B., Brock, F., 2009. Radiocarbon dating of charcoal from tropical sequences: results from the Niah Great Cave, Sarawak, and their broader implications. J. Quat. Sci. 24, 189–197.

Hiscock, P., 2015. Cultural diversification and the global dispersion of *Homo sapiens*: lessons from Australia. In: Kaifu, Y., Izuho, M., Goebel, T., Sato, H., Ono, A. (Eds), Emergence and Diversity of Modern Human Behaviour in Paleolithic Asia. Texas A&M Univ. Press, College Station, pp. 225–236.

Hocknull, S.A., Piper, P.J., van den Bergh, G.D., Due, R.A., Morwood, M.J., Kurniawan, I., 2009. Dragon's paradise lost: palaeobiogeography, evolution and extinction of the largest-ever terrestrial lizards (Varanidae). PLoS One 4, e7241.

Hogg, A.G., McCormac, F.G., Higham, T.F.G., Reimer, P.J., Baillie, M.G.L., Palmer, J.G., 2002. High-precision radiocarbon measurements of contemporaneous tree-ring dated wood from the British Isles and New Zealand: AD 1850–950. Radiocarbon 44, 633–640.

Hogg, A.G., Hua, Q., Blackwell, P.G., Niu, M., Buck, C.E., Guilderson, T.P., Heaton, T.J., Palmer, J.G., Reimer, P.J., Reimer, R.W., Turney, C.S.M., Zimmerman, S.R.H., 2013. SHCal13 Southern Hemisphere calibration, 0–50,000 years cal BP. Radiocarbon 55, 1889–1903.

Huntley, D.J., Hancock, R.G.V., 2001. The Rb contents of the K-feldspars being measured in optical dating. Anc. TL 19, 43–46.

Huntley, D.J., Lamothe, M., 2001. Ubiquity of anomalous fading in K-feldspars and the measurement and correction for it in optical dating. Can. J. Earth Sci. 38, 1093–1106.

Jacobs, Z., Roberts, R.G., 2015. An improved single grain OSL chronology for the sedimentary deposits from Diepkloof Rockshelter, Western Cape, South Africa. J. Archaeol. Sci. 63, 175–192.

Jatmiko, 1989. Laporan Penelitian Arkeologi di Liang Bua Tahun 1989. Pusat Penelitian Arkeologi Nasional. Unpublished report.

Jochum, K.P., Stoll, B., Herwig, K., Willbold, M., Hofmann, A.W., Amini, M., Aarburg, S., Abouchami, W., Hellebrand, E., Mocek, B., Raczek, I., Stracke, A., Alard, O., Bouman, C., Becker, S., Dücking, M., Brätz, H., Klemd, R., De Bruin, D., Canil, D., Cornell, D., de Hoog, C.-J., Dalpé, C., Danyushevshy, L., Eisenhauer, A., Gao, Y., Snow, J.E., Groschopf, N., Günther, D., Latkoczy, C., Guillong, M., Hauri, E.H., Höfer, H.E., Lahaye, Y., Horz, K., Jacob, D.E., Kasemann, S.A., Kent, A.J.R., Ludwig, T., Zack, T., Mason, P.R.D., Meixner, A., Rosner, M., Misawa, K., Nash, B.P., Pfänder, J., Premo, W.R., Sun, W.D., Tiepolo, M., Vannucci, R., Vennemann, T., Wayne, D., Woodhead, J.D., 2006. MPI-DING reference glasses for in situ microanalysis: New reference values for element concentrations and isotope ratios. Geochem. Geophys. Geosyst. **7**, Q02008.

Jungers, W.L., Harcourt-Smith, W.E.H., Wunderlich, R.E., Tocheri, M.W., Larson, S.G., Sutikna, T., Rhokus Awe Due, Morwood, M.J., 2009a. The foot of *Homo floresiensis*. Nature 459, 81–84.

Jungers, W.L., Larson, S.G., Harcourt-Smith, W.E.H., Morwood, M.J., Sutikna, T., Rokhus Due Awe, Djubiantono, T., 2009b. Descriptions of the lower limb skeleton of *Homo floresiensis*. J. Hum. Evol. 57, 538–554.

Kaifu, Y., Baba, H., Sutikna, T., Morwood, M.J., Kubo, D., Saptomo, E.W., Jatmiko, Due Awe, R., Djubiantono, T., 2011. Craniofacial morphology of *Homo floresiensis*: description, taxonomic affinities, and evolutionary implication. J. Hum. Evol. 61, 644–682.

Konecky, B., Russell, J., Bijaksana, S., 2016. Glacial aridity in central Indonesia coeval with intensified monsoon circulation. Earth Planet. Sci. Lett. 437, 15–24.

Kosasih, S.A., 1985. Laporan Penelitian Arkeologi di Liang Bua Tahun 1985. Pusat Penelitian Arkeologi Nasional. Unpublished report.

Krause, J., Fu, Q., Good, J.M., Viola, B., Shunkov, M.V., Derevianko, A.P., Pääbo, S., 2010. The complete mitochondrial DNA genome of an unknown hominin from southern Siberia. Nature 464, 894–897.

Larson, S.G., Jungers, W.L., Morwood, M.J., Sutikna, T., Jatmiko, Saptomo, E.W., Rokus Awe Due, Djubiantono, T., 2007. *Homo floresiensis* and the evolution of the hominin shoulder. J. Hum. Evol. 53, 718–731.

Larson, S.G., Jungers, W.L., Tocheri, M.W., Orr, C.M., Morwood, M.J., Sutikna, T., Rokhus Due Awe, Djubiantono, T., 2009. Descriptions of the upper limb skeleton of *Homo floresiensis*. J. Hum. Evol. 57, 555–570.

Lee, J.-Y., Marti, K., Severinghaus, J.P., Kawamura, K., Yoo, H.-S., Lee, J.B., Kim, J.S., 2006. A redetermination of the isotopic abundances of atmospheric Ar. Geochim. Cosmochim. Acta **70**, 4507–4512.

Legendre, P., Legendre, L., 1998. Numerical Ecology (2nd English Edition). Developments in Environmental Modelling 20. Elsevier, Amsterdam.

Li, B., Li, S.-H., 2011. Luminescence dating of K-feldspar from sediments: a protocol without anomalous fading correction. Quat. Geochronol. 6, 468–479.

Li, B., Roberts, R.G., Jacobs, Z., 2013. On the dose dependency of the bleachable and non-bleachable components of IRSL from K-feldspar: improved procedures for luminescence dating of Quaternary sediments. Quat. Geochronol. 17, 1–13.

Li, B., Jacobs, Z., Roberts, R.G., Li, S.-H., 2014. Review and assessment of the potential of post-IR IRSL dating methods to circumvent the problem of anomalous fading in feldspar luminescence. Geochronometria 41, 178–201.

Liu, W., Martinón-Torres, M., Cai, Y.¬-j., Xing, S., Tong, H.-w., Pei, S.-w., Jan Sier, M., Wu., X.-h., Edwards, R.L., Cheng, H., Li, Y.-y., Yang, X.-x., Bermúdez de Castro., J.M., Wu, X.-j., 2015. The earliest unequivocally modern humans in southern China. Nature 526, 696–700.

Locatelli, E., Due, R.A., van den Bergh, G.D., van den Hoek Ostende, L.W., 2012. Pleistocene survivors and Holocene extinctions: the giant rats from Liang Bua (Flores, Indonesia). Quat. Int. 281, 47–57.

Locatelli, E., Due, R.A., Jatmiko, van den Hoek Ostende, L.W., 2015. Middle-sized murids from Liang Bua (Flores, Indonesia): insular endemics, human introductions and palaeoenvironment. Palaeobio. Palaeoenv. 95, 497–512.

Louys, J., 2012. Mammal community structure of Sundanese fossil assemblages from the Late Pleistocene, and a discussion on the ecological effects of the Toba eruption. Quat. Int. 258, 80–87.

Ludwig, A.J., Reynolds, J.F., 1988. Statistical Ecology: a Primer on Methods and Computing. Wiley, New York.

Ludwig, K.R., 2012. User's Manual for Isoplot 3.75: a Geochronological Toolkit for Microsoft Excel. Berkeley Geochronology Center, Berkeley.

Lyman, R.L., 2008. Quantitative Paleozoology. Cambridge University Press, Cambridge.

Magurran, A.E., 1988. Ecological Diversity and Its Measurement. Princeton University Press, Princeton.

Mahirta, 2009. Stone technology and the chronology of human occupation on Rote, Sawu and Timor, Nusa Tenggara Timur, Indonesia. Indo-Pacific Prehist. Assoc. Bull. 29, 101–108.

McDougall, I., Brown, F.H., Fleagle, J.G., 2005. Stratigraphic placement and age of modern humans from Kibish, Ethiopia. Nature 433, 733–736.

Meijer, H.J.M., Rokus Awe Due, 2010. A new species of giant marabou stork (Aves: Ciconiiformes) from the Pleistocene of Liang Bua, Flores (Indonesia). Zool. J. Linnean Soc. 160, 707–724.

Meijer, H.J.M., van den Hoek Ostende, L.W., van den Bergh, G.D., de Vos, J., 2010. The fellowship of the hobbit: the fauna surrounding *Homo floresiensis*. J. Biogeogr. 37, 995–1006.

Meijer, H.J.M., Sutikna, T., Saptomo, E.W., Rokhus Due Awe, Jatmiko, Wasisto, S., James, H.F., Morwood, M.J., Tocheri, M.W., 2013. Late Pleistocene–Holocene non-passerine avifauna of Liang Bua (Flores, Indonesia). J. Vert. Paleontol. 33, 877–894.

Meijer, H.J.M., Tocheri, M.W., Rokus Awe Due, Sutikna, T., Saptomo, E.W., James, H.F., 2015. Continental-style avian extinctions on an oceanic island. Palaeogeogr. Palaeoclimatol. Palaeoecol. 429, 163–170.

Meyer, M., Arsuaga, J.-L., de Filippo, C., Nagel1, S., Aximu-Petri1, A., Nickel1, B., Martínez, I., Gracia, A., Bermúdez de Castro, J.M., Carbonell, E., Viola, B., Kelso, J., Prüfer, K., Pääbo, S., 2016. Nuclear DNA sequences from the Middle Pleistocene Sima de los Huesos hominins. Nature 531, 504–507.

Mijares, A. S., Détroit, F., Piper, P., Grün, R., Bellwood, P., Aubert, M., Champion, G., Cuevas, N., De Leon, A., Dizon, E., 2010. New evidence for a 67,000-year-old human presence at Callao Cave, Luzon, Philippines. J. Hum. Evol. 59, 123–132.

Moore, M.W., 2005. The Design Space of Lithic Technology. PhD thesis, University of New England, Armidale.

Moore, M.W., 2007. Lithic design space modelling and cognition in *Homo floresiensis*. In: Shalley, A., Khlentzos, D. (Eds), Mental States: Nature, Function and Evolution. John Benjamins, Amsterdam, pp. 11–33.

Moore, M.W., Brumm, A., 2007. Stone artifacts and hominins in island Southeast Asia: new insights from Flores, eastern Indonesia. J. Hum. Evol. 52, 85–102.

Moore, M.W., Brumm, A., 2009. *Homo floresiensis* and the African Oldowan. In: Hovers, E., Braun, D.R. (Eds), Interdisciplinary Approaches to the Oldowan. Springer, New York, pp. 61–69.

Moore, M.W., Sutikna, T., Jatmiko, Morwood, M.J., Brumm, A., 2009. Continuities in stone flaking technology at Liang Bua, Flores, Indonesia. J. Hum. Evol. 57, 503–526.

Morley, M.W., Goldberg, P., Sutikna, T., Tocheri, M.W., Prinsloo, L.C., Jatmiko, Saptomo, E.W., Wasisto, S., Roberts, R.G., 2016. Initial micromorphological results from Liang Bua, Flores (Indonesia): site formation processes and hominin activities at the type locality of *Homo floresiensis*. J. Archaeol. Sci. (in press).

Morwood, M.J., O'Sullivan, P.B., Aziz, F., Raza, A., 1998. Fission-track ages of stone tools and fossils on the east Indonesian island of Flores. Nature 392, 173–176.

Morwood, M.J., Soejono, R.P., Roberts, R.G., Sutikna, T., Turney, C.S.M., Westaway, K.E., Rink, W.J., Zhao, J.- x., van den Bergh, G.D., Due, R.A., Hobbs, D.R., Moore, M.W., Bird, M.I., Fifield, L.K., 2004. Archaeology and age of a new hominin from Flores in eastern Indonesia. Nature 431, 1087–1091.

Morwood, M.J., Brown, P., Jatmiko, Sutikna, T., Saptomo, E.W., Westaway, K.E., Due, R.A., Roberts, R.G., Maeda, T., Wasisto, S., Djubiantono, T., 2005. Further evidence for small-bodied hominins from the Late Pleistocene of Flores, Indonesia. Nature **437**, 1012–1017.

Morwood, M.J., Sutikna, T., Saptomo, E.W., Westaway, K.E., Jatmiko, Awe Due, R., Moore, M.W., Dwi Yani Yuniawati, Hadid, P., Zhao, J.-x., Turney, C.S.M., Fifield, K., Allen, H., Soejono, R.P., 2008. Climate, people and faunal succession on Java, Indonesia: evidence from Song Gupuh. J. Archaeol. Sci. 35, 1776–1789.

Morwood, M.J., Jungers, W.L. (Eds), 2009. Paleoanthropological Research at Liang Bua, Flores, Indonesia. J. Hum. Evol. **57**, 437–648.

Morwood, M.J., Sutikna, T., Saptomo, E.W., Jatmiko, Hobbs, D.R., Westaway, K.E., 2009. Preface: research at Liang Bua, Flores, Indonesia. J. Hum. Evol. 57, 437–449.

Morwood, M.J., Jungers, W.L., 2009. Conclusions: implications of the Liang Bua finds for hominin evolution and biogeography. J. Hum. Evol. 57, 640–650.

Neter, J., Kutner, M., Nachtsheim, C., Wasserman, W., 1996. Applied Linear Statistical Models (4th edition). Richard D. Irwin, Chicago.

Neudorf, C.M., 2012. Luminescence Investigations into the Time of Final Deposition of Toba Volcanic Ash and Artefact-bearing Alluvial Sediments in the Middle Son Valley, Madhya Pradesh, India. PhD thesis, University of Wollongong.

Neudorf, C.M., Roberts, R.G., Jacobs, Z., 2012. Sources of overdispersion in a K-rich feldspar sample from north-central India: insights from D_e, K content and IRSL age distributions for individual grains. Radiat. Meas. 47, 696–702.

O'Connell, J.F., Allen, J., 2015. The process, biotic impact, and global implications of the human colonization of Sahul about 47,000 years ago. J. Archaeol. Sci. 56, 73–84.

O'Connor, S., 2007. New evidence from East Timor contributes to our understanding of earliest modern human colonisation east of the Sunda Shelf. Antiquity 81, 523–535.

O'Connor, S., 2015. Crossing the Wallace Line: the maritime skills of the earliest colonists in the Wallacean Archipelago. In: Kaifu, Y., Izuho, M., Goebel, T., Sato, H., Ono, A. (Eds), Emergence and Diversity of Modern Human Behaviour in Paleolithic Asia. Texas A&M Univ. Press, College Station, pp. 214–224.

O'Connor, S., Veth, P., 2005. Early Holocene shell fish hooks from Lene Hare cave, East Timor establish complex fishing technology was in use in Island Southeast Asia five thousand years before Austronesian settlement. Antiquity 79, 1–8.

O'Connor S., Aplin, K., 2007. A matter of balance: an overview of Pleistocene occupation history and the impact of the Last Glacial Phase in East Timor and the Aru Islands, eastern Indonesia. Archaeol. Oceania 42, 82–90.

O'Connor, S., Spriggs, M., Veth, P., 2002a. Excavation at Lene Hara Cave establishes occupation in East Timor at least 30,000–35,000 years ago. Antiquity 76, 45–50.

O'Connor, S., Spriggs, M., Veth, P., 2002b. Direct dating of shell beads from Lene Hara Cave, East Timor. Austr. Archaeol. 55, 18–21.

O'Connor, S., Aplin, K., Szabó, K., Pasveer, J., Veth, P., Spriggs, M., 2006. Liang Lemdubu: A Pleistocene cave site in the Aru Islands. In: O'Connor, S., Spriggs,

M., Veth, P. (Eds), The Archaeology of the Aru Islands, Eastern Indonesia. Terra Australis 22, ANU E Press, Canberra, pp. 171–204.

O'Connor, S., Barham, A., Spriggs, M., Veth, P., Aplin, K., St Pierre, E., 2010. Cave archaeology and sampling issues in the tropics: A case study from Lene Hara Cave, a 42,000 year old occupation site in East Timor, Island Southeast Asia. Aust. Archaeol. 71, 29–40.

O'Connor, S., Ono, R., Clarkson, C., 2011. Pelagic fishing at 42,000 years before the present and the maritime skills of modern humans. Science 334, 1117–1121.

Orr, C.M., Tocheri, M.W., Burnett, S.E., Rokus Due Awe, Saptomo, E.W., Sutikna, T., Jatmiko, Wasisto, S., Morwood, M.J., Jungers, W.L., 2013. New wrist bones of *Homo floresiensis* from Liang Bua (Flores, Indonesia). J. Hum. Evol. 64, 109–129.

Owen-Smith, R.N., 1988. Megaherbivores: the Influence of Very Large Body Size on Ecology. Cambridge University Press, Cambridge.

Pickrell, J.K., Reich, D., 2014. Toward a new history and geography of human genes informed by ancient DNA. Trends Genet. 30, 377–389.

Pike, A.W.G., Hoffmann, D.L., García-Diez, M., Pettitt, P.B., Alcolea, J., De Balbín, R., González-Sainz, C., de las Heras, C., Lasheras, J.A., Montes, R., Zilhão, J., 2012. U-series dating of Paleolithic art in 11 caves in Spain. Science 336, 1409–1413.

Prescott, J.R., Hutton, J.T., 1994. Cosmic ray contributions to dose rates for luminescence and ESR dating: large depths and long-term time variations. Radiat. Meas. 23, 497–500.

Rasmussen, M., Guo, X., Wang, Y., Lohmueller, K.E., Rasmussen, S., Albrechtsen, A., Skotte, L., Lindgreen, S., Metspalu, M., Jombart, T., Kivisild, T., Zhai, W., Eriksson, A., Manica, A., Orlando, L., De La Vega, F.M., Tridico, S., Metspalu, E., Nielsen, K., Ávila-Arcos, M.C., Moreno-Mayar, J.V., Muller, C., Dortch, J., Gilbert, M.T.P., Lund, O., Wesolowska, A., Karmin, M., Weinert, L.A., Wang, B., Li, J., Tai, S., Xiao, F., Hanihara, T., van Driem, G., Jha, A.R., Ricaut, F.X., de Knijff, P., Migliano, A.B., Romero, I.G., Kristiansen, K., Lambert, D.M., Brunak, S., Forster, P., Brinkmann, B., Nehlich, O., Bunce, M., Richards, M., Gupta, R., Bustamante, C.D., Krogh, A., Foley, R.A., Lahr, M.M., Balloux, F., Sicheritz-Pontén, T., Villems, R., Nielsen, R., Wang, J., Willerslev, E., 2011. An Aboriginal Australian genome reveals separate human dispersals into Asia. Science 334, 94–98.

Reich, D., Green, R.E., Kircher, M., Krause, J., Patterson, N., Durand, E.Y., Viola, B., Briggs, A.W., Stenzel, U., Johnson, P.L.F., Maricic, T., Good, J.M., Marques-Bonet, T., Alkan, C., Fu, Q., Mallick, S., Li, H., Meyer, M., Eichler, E.E., Stoneking, M., Richards, M., Talamo, S., Shunkov, M.V., Derevianko, A.P., Hublin, J-J., Kelso, J., Slatkin, M., Pääbo, S., 2010. Genetic history of an archaic hominin group from Denisova Cave in Siberia. Nature 468, 1053–1060.

Reich, D., Patterson, N., Kircher, M., Delfin, F., Nandineni, M.R., Pugach, I., Ko, Y.C., Jinam, T.A., Phipps, M.E., Saitou, N., Wollstein, A., Kayser, M., Pääbo, S., Stoneking, M., 2011. Denisova admixture and the first modern human dispersals into Southeast Asia and Oceania. Am. J. Hum. Genet. 89, 516–528.

Reimer, P.J., Baillie, M.G.L., Bard, E., Bayliss, A., Beck, J.W., Bertrand, C.J.H., Blackwell, P.G., Buck, C.E., Burr, G.S., Cutler, K.B., Damon, P.E., Edwards, R.L., Fairbanks, R.G., Friedrich, M., Guilderson, T.P., Hogg, A.G., Hughen, K.A., Kromer, B., McCormac, F.G., Manning, S.W., Ramsey, C.B., Reimer, R.W., Remmele, S., Southon, J.R., Stuiver, M., Talamo, S., Taylor, F.W., Van der Plicht, J., Weyhenmeyer, C.E., 2004. IntCal04 terrestrial radiocarbon age calibration, 0–26 cal kyr BP. Radiocarbon 46, 1029–1058.

Reynolds, T., Barker, G., Barton, H., Cranbrook, G., Farr, L., Hunt, C., Kealhofer, L., Paz, V., Pike, A., Piper, P.J., Rabett, R.J., Rushworth, G., Stimpson, C., Szabó, K., 2013. The first modern humans at Niah, c. 50,000–35,000 years ago. In: Barker, G. (Ed), Rainforest foraging and farming in Island Southeast Asia. The Archaeology of the Niah Caves, Sarawak Vol. 1. McDonald Institute for Archaeological Research, University of Cambridge, UK, pp. 135–172.

Rivera, T.A., Storey, M., Schmitz, M.D., Crowley, J.L., 2013. Age intercalibration of $^{40}Ar/^{39}Ar$ sanidine and chemically distinct U/Pb zircon populations from the Alder Creek Rhyolite Quaternary geochronology standard. Chem. Geol. 345, 87–98.

Roberts, R.G., Jones, R., 2001. Chronologies of carbon and of silica: evidence concerning the dating of the earliest human presence in northern Australia. In: Tobias, P.V., Raath, M.A., Moggi-Cecchi J., Doyle G.A. (Eds), Humanity from African Naissance to Coming Millennia: Colloquia in Human Biology and Palaeoanthropology. Firenze University Press, Firenze and Witwatersrand University Press, Johannesburg, pp. 239–248.

Roberts, R.G., Jones, R., Smith, M.A., 1990. Thermoluminescence dating of a 50,000-year-old human occupation site in northern Australia. Nature 345, 153–156.

Roberts, R.G., Jones, R., Spooner, N.A., Head, M.J., Murray, A.S., Smith, M.A., 1994. The human colonisation of Australia: optical dates of 53,000 and 60,000 years bracket human arrival at Deaf Adder Gorge, Northern Territory. Quat. Sci. Rev. 13, 575–583.

Roberts, R., Bird, M., Olley, J., Galbraith, R., Lawson, E., Laslett, G., Yoshida, H., Jones, R. Fullagar, R., Jacobsen, G., Hua, Q., 1998. Optical and radiocarbon dating at Jinmium rock shelter in northern Australia. Nature 393, 358–362.

Roberts, R.G., Yoshida, H., Galbraith, R., Lasteff, G., Jones, R., Smith, M.A., 1998. Single-aliquot and single-grain optical dating confirm thermoluminescence age estimates at Malakunanja II Rock Shelter in Northern Australia. Anc. TL, 16, 19-24.

Roberts, R.G., Westaway, K.E., Zhao, J-x., Turney, C.S.M., Bird, M.I., Rink, W.J., Fifield, L.K., 2009. Geochronology of cave deposits at Liang Bua and of adjacent river terraces in the Wae Racang valley, western Flores, Indonesia: a synthesis of age estimates for the type locality of *Homo floresiensis*. J. Hum. Evol. 57, 484–502.

Roberts, R.G., Jacobs, Z., Li, B., Jankowski, N.R., Cunningham, A.C., Rosenfeld, A.B., 2015. Optical dating in archaeology: thirty years in retrospect and grand challenges for the future. J. Archaeol. Sci. 56, 41–60.

Russell, J.M., Vogel, H., Konecky, B.L., Bijaksana, S., Huang, Y., Melles, M., Wattrus, N., Costa, K., King, J.W., 2014. Glacial forcing of central Indonesian hydroclimate since 60,000 y B.P. Proc. Natl. Acad. Sci. USA 111, 5100–5105.

Saltré, F., Rodríguez-Rey, M., Brook, B.W., Johnson, C.N., Turney, C.S.M., Alroy, J., Cooper, A., Beeton, N., Bird, M.I., Fordham, D.A., Gillespie, R., Herrando-Pérez, S., Jacobs, Z., Miller, G.H., Nogués-Bravo, D., Prideaux, G.J., Roberts, R.G., Bradshaw, C.J.A., 2016. Climate change not to blame for late Quaternary megafauna extinctions in Australia. Nat. Commun. 7, 10511.

Sambridge, M., Grün, R., Eggins, S., 2012. U-series dating of bone in an open system: the diffusion–adsorption–decay model. Quat. Geochronol. 9, 42–53.

SAS Institute I. 2002. Copyright © 2002-2003 SAS Institute Inc. SAS and all other SAS Institute Inc. product or service names are registered trademarks or trademarks of SAS Institute Inc., Cary, NC, USA.

Scroxton, N., Gagan, M.K., Ayliffe, L.K., Hellstrom, J., Cheng, H., Edwards, R., Zhao, J., Hantoro, W.S., Rifai, H., Scott-Gagan, H., Cowley, J.A., Suwargadi, B.W., 2013. Speleothem carbon isotopes in the tropics: a proxy for vegetation and what they reveal about the demise of *Homo floresiensis*. Am. Geophys. Union, Fall Meeting, abstract #PP33C-1935.

Sémah, F., Sémah, A-M., Falguères, C., Détroit, F., Gallet, X., Hameau, S., Moigne, A-M., Simanjuntak, T., 2004. The significance of the Punung karstic area (eastern Java) for the chronology of the Javanese Palaeolithic, with special reference to the Song Terus cave. Mod. Quat. Res. SE Asia 18, 45–62.

Soejono, R.P., 1978. Laporan Ekskavasi Arkeologi Liang Bua (Flores), Propinsi Nusa Tenggara Timur. Pusat Penelitian Arkeologi Nasional. Unpublished report.

Soejono, R.P., 1981. Laporan Singkat Penelitian Arkeologi Liang Bua Tahun 1981. Pusat Penelitian Purbakala dan Peninggalan Nasional. Unpublished report.

Stephens, M., Rose, J., Gilbertson, D.D., 2016. Post-depositional alteration of humid tropical cave sediments: Micromorphological research in the Great Cave of Niah, Sarawak, Borneo. J. Archaeol. Sci. (in press).

Storey, M., Roberts, R.G., Saidin, M., 2012. Astronomically calibrated $^{40}Ar/^{39}Ar$ age for the Toba supereruption and global synchronization of late Quaternary records. Proc. Natl Acad. Sci. USA 109, 18684–18688.

Storm, P., Wood, R., Stringer, C., Bartsiokas, A., de Vos, J., Aubert, M., Kinsley, L., Grün, R., 2013. U-series and radiocarbon analyses of human and faunal remains from Wajak, Indonesia. J. Hum. Evol. 64, 356–365.

Sutikna, T., Tocheri, M.W., Morwood, M.J., Saptomo, E.W., Jatmiko, Rokus Due Awe, Wasisto, S., Westaway, K.E., Aubert, M., Li, B., Zhao, J.-x., Storey, M., Alloway, B.V., Morley, M.W., Meijer, H.J.M., van den Bergh, G.D., Grün, R., Dosseto, A., Brumm, A., Jungers, W.L., Roberts, R.G., 2016. Revised stratigraphy and chronology for *Homo floresiensis* at Liang Bua in Indonesia. Nature 532, 366–369.

Szabó, K., Brumm, A., Bellwood, P., 2007. Shell artefact production at 32,000–28,000 BP in Island Southeast Asia. Thinking across media? Curr. Anthropol. 48, 701–723.

Thiel, C., Buylaert, J.-P., Murray, A., Terhorst, B., Hofer, I., Tsukamoto, S., Frechen, M., 2011. Luminescence dating of the Stratzing loess profile (Austria) – testing the potential of an elevated temperature post-IR IRSL protocol. Quat. Int. 234, 23–31.

Timmreck, C., Graf, H-F., Zanchettin, D., Hagemann, S., Kleinen, T., Krüger, K., 2012. Climate response to the Toba super-eruption: Regional changes. Quat. Int. 258, 30–44.

Tocheri, M.W., Orr, C.M., Larson, S.G., Sutikna, T., Jatmiko, Saptomo, E.W., Due, R.A., Djubiantono, T., Morwood, M.J., Jungers, W.L., 2007. The primitive wrist of *Homo floresiensis* and its implications for hominin evolution. Science 317, 1743–1745.

Trinkaus, E., 2005. Early modern humans. Annu. Rev. Anthropol. 34, 207–230.

Turney, C.S.M., Bird, M.I., Fifield, L.K., Roberts, R.G., Smith, M., Dortch, C.E., Grün, R., Lawson, E., Ayliffe, L.K., Miller, G.H., Dortch, J., Cresswell, R.G., 2001. Early human occupation at Devil's Lair, southwestern Australia 50,000 years ago. Quat. Res. 55, 3–13.

van den Bergh, G.D., Rokhus Due Awe, Morwood, M.J., Sutikna, T., Jatmiko, Saptomo, E.W., 2008. The youngest *Stegodon* remains in Southeast Asia from the Late Pleistocene archaeological site Liang Bua, Flores, Indonesia. Quat. Int. 182, 16–48.

van den Bergh, G.D., Meijer, H.J.M., Rokhus Due Awe, Morwood, M.J., Szabó, K.A., van den Hoek-Ostende, L.W., Sutikna, T., Saptomo, E.W., Piper, P.J., Dobney, K.M., 2009. The Liang Bua faunal remains: a 95 k.yr. sequence from Flores, East Indonesia. J. Hum. Evol. 57, 527–537.

van den Bergh, G.D., Li, B., Brumm, A., Grün, R., Yurnaldi, D., Moore, M.W., Kurniawan, I., Setiawan, R., Aziz, F., Roberts, R.G., Suyono, Storey, M., Setiabudi, E., Morwood, M.J., 2016. Earliest hominin occupation of Sulawesi, Indonesia. Nature 529, 208–211.

van der Kaars, S., Wang, X., Kershaw, P., Guichard, F., Setiabudi, D.A., 2000. A late Quaternary palaeoecological record from the Banda Sea, Indonesia: Patterns of vegetation, climate and biomass burning in Indonesia and northern Australia. Palaeogeogr. Palaeoclimatol. Palaeoecol. 155, 135–153.

Vattathil, S., Akey, J.M., 2015. Small amounts of archaic admixture provide big insights into human history. Cell 163, 281–284.

Verhoeven, T., 1952. Stenen werktuigen uit Flores (Indonésië). Anthropos 47, 95–98.

Vernot, B., Tucci, S., Kelso, J., Schraiber, J.G., Wolf, A.B., Gittelman, R.M., Dannemann, M., Grote, S., McCoy, R.C., Norton, H., Scheinfeldt, L.B., Merriwether, D.A., Koki, G., Friedlaender, J.S., Wakefield, J., Pääbo, S., Akey, J.M., 2016. Excavating Neandertal and Denisovan DNA from the genomes of Melanesian individuals. Science 352, 235–239.

Veth, P., Spriggs, M., O'Connor, S., 2005. The continuity of cave use in the tropics: examples from East Timor and the Aru Islands, Maluku. Asian Perspect. 44, 180–192.

Visser, K., Thunell, R., Stott, L., 2003. Magnitude and timing of temperature change in the Indo-Pacific warm pool during deglaciation. Nature 421, 152–155.

Voisin, J.-L., Condemi, S., Wolpoff, M.H., Frayer, D.W., 2012. A new online database (http://anthropologicaldata.free.fr) and a short reflection about the productive use of internet compiling data. PaleoAnthropology 2012, 241–244.

Westaway, K.E., 2009. The red, white and blue of quartz luminescence: a comparison of D_e values derived for sediments from Australia and Indonesia using TL and OSL emissions. Radiat. Meas. 44, 462–466.

Westaway, K.E., Roberts, R.G., 2006. A dual-aliquot regenerative-dose protocol (DAP) for thermoluminescence (TL) dating of quartz sediments using the light-sensitive and isothermally stimulated red emissions. Quat. Sci. Rev. **25**, 2513–2528.

Westaway, K.E., Morwood, M.J., Roberts, R.G., Zhao, J.-x., Sutikna, T., Saptomo, E.W., Rink, W.J., 2007a. Establishing the time of initial human occupation of Liang Bua, western Flores, Indonesia. Quat. Geochronol. 2, 337–343.

Westaway, K.E., Zhao, J.-x., Roberts, R.G., Chivas, A.R., Morwood, M.J., Sutikna, T., 2007b. Initial speleothem results from western Flores and eastern Java, Indonesia: were climate changes from 47 to 5 ka responsible for the extinction of *Homo floresiensis*? J. Quat. Sci. 22, 429–438.

Westaway, K.E., Roberts, R.G., Sutikna, T., Morwood, M.J., Drysdale, R., Zhao, J.-x., Chivas, A.R., 2009a. The evolving landscape and climate of western Flores: an environmental context for the archaeological site of Liang Bua. J. Hum. Evol. 57, 450–464.

Westaway, K.E., Sutikna, T., Saptomo, W.E., Jatmiko, Morwood, M.J., Roberts, R.G., Hobbs, D.R., 2009b. Reconstructing the geomorphic history of Liang Bua: a stratigraphic interpretation of the occupational environment. J. Hum. Evol. 57, 465–483.

Westaway, K.E. Morwood, M.J., Sutikna, T., Moore, M.W. Rokus, A.D., van den Bergh, G.D., Roberts, R.G., Saptomo, E.W., 2009c. *Homo floresiensis* and the Late Pleistocene environments of eastern Indonesia: defining the nature of the relationship. Quat. Sci. Rev. 28, 2897–2912.

White, T.D., Asfaw, B., DeGusta, D., Gilbert, H., Richards, G.D., Suwa, G., Howell, F.C., 2003. Pleistocene *Homo sapiens* from Middle Awash, Ethiopia. Nature 423, 742–747.

Wicaksono, S.A., Russell, J.M., Bijaksana, S., 2015. Compound-specific stable isotope records of vegetation and hydrologic change in central Sulawesi, Indonesia, since 53,000 yr BP. Palaeogeogr. Palaeoclimatol. Palaeoecol. 430, 47–56.

Wood, R., 2015. From revolution to convention: the past, present and future of radiocarbon dating. J. Archaeol. Sci. 56, 61–72.

Wurster, C.M., Bird, M.I., Bull, I.D., Creed, F., Bryant, C., Dungait, J.A.J., Paz, V., 2010. Forest contraction in north equatorial Southeast Asia during the Last Glacial Period. Proc. Natl. Acad. Sci. USA 107, 15508–15511.

Zhao, J.-x., Yu, K.-f., Feng, Y.-x., 2009. High-precision ^{238}U–^{234}U–^{230}Th disequilibrium dating of the recent past: a review. Quat. Geochronol. 4, 423–433.

Zhou, H.-y., Zhao, J.-x., Wang, Q., Feng, Y.-x., Tang, J., 2011. Speleothem-derived Asian summer monsoon variations in Central China, 54–46 ka. J. Quat. Sci. 26, 781–790.

APPENDIX A

Background to the excavation strategy at Liang Bua since 2001

The Sectors targeted for study between 2001 and 2003 were continuations of previous excavations that had obtained evidence of modern humans from ~11 ka cal. BP to the present (Soejono 1978–1989). The main aim was to reach beneath sediments previously interpreted as sterile cultural deposits in order to test whether there was earlier evidence of modern human activity at the site. In 2001, backfill was removed and excavations commenced in Sector IV, which is in the approximate middle of the cave (see Chapter 1, Fig. 1.3).

Our excavations of Sectors IV (2001) and III (2002) in the cave centre had encountered small blocks of consolidated dark volcanic ash below the distinctive layers of white tuffaceous silt (hereafter referred to as the 'white tuff'). Initially, it was not clear whether these small blocks were a significant feature of the Liang Bua stratigraphy and we were instead more focused on the white tuff. In 2003, after we once again encountered the white tuff in a new excavation near the eastern wall of the cave (Sector VII), we also found these same blocks of consolidated dark volcanic ash in the layers underneath it. However, this time these dark blocks of ash were more densely distributed and more varied in size (e.g., some of them were as large as ~27,000 cm^3) (Fig. A.1). I started to refer to these volcanic sediments as 'black tuff' and I was perplexed about how they came to be deposited in this way at Liang Bua. They were clearly reworked from somewhere else, but whether that was from within Liang Bua or outside of it was not clear.

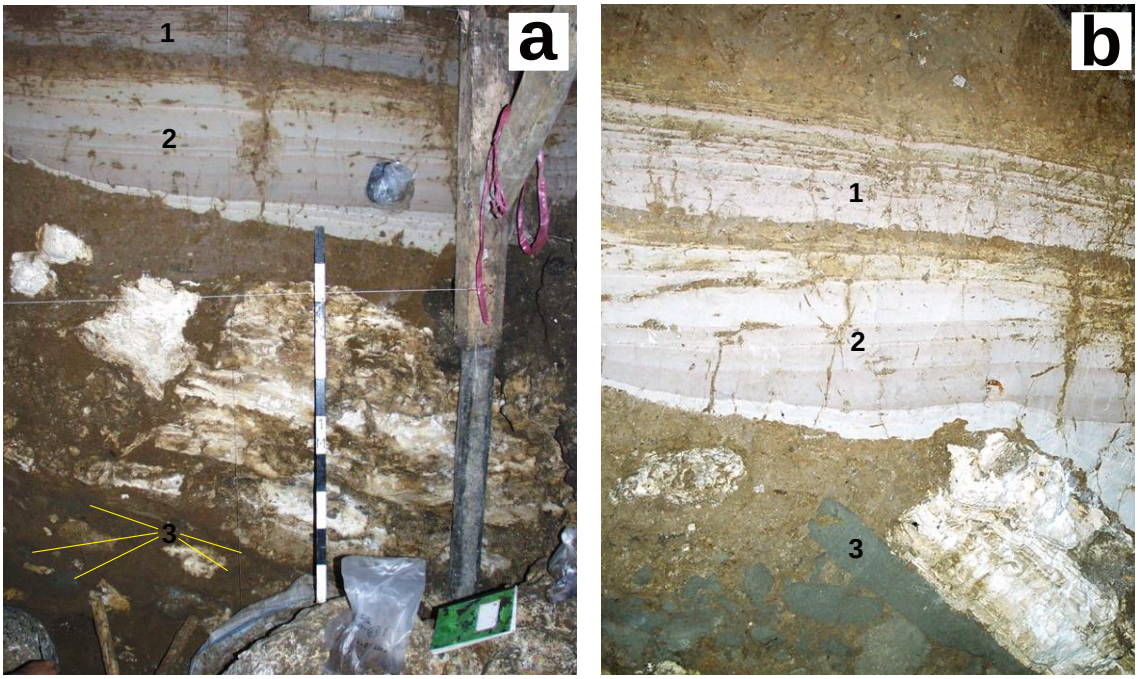

Figure A.1 Volcanic ashes recognised in the 2001–2003 excavations. **a.** North baulk of Sector IV. **b.** West baulk of Sector VII. Numbers denote the following: **1** = upper 'white tuff' (now Tephra 8 or T8), **2** = lower 'white tuff' (now Tephra 7 or T7), **3** = fragments 'black tuff' (with yellow lines in **a**, now Tephra 3 or T3). (Photos: © Liang Bua Team).

As our excavation of Sector VII continued, we discovered the partial skeleton near the southern baulk (Morwood *et al*., 2004) that was later designated as the holotype (LB1) of *H. floresiensis* (Brown *et al*., 2004) (Fig. A.2). Although the black tuff fragments were labelled and figured prominently in the stratigraphic drawing of Sector VII presented in Morwood *et al*. (2004), they were not mentioned at all in the article as their significance was not yet understood. When our team returned to Liang Bua in 2004, the aim was to try and recover additional skeletal elements of LB1 (e.g., the arm bones) that might be preserved in the area immediately adjacent to the south of Sector VII. Unlike Sectors I, III, IV and VII, which had all been partially excavated previously by Professor Soejono between 1978 and 1989, this newly targeted area (Sector XI) had to be excavated from the cave surface. Based on the excavations and dating results from Sectors IV and VII (Morwood *et al*., 2004), we expected that the first ~3.5 m of

deposits in Sector XI would be Holocene in age. This expectation, in hindsight, would lead to a major error in our initial interpretation of the site's stratigraphy.

Figure A.2 The discovery of *Homo floresiensis*. **a.** The moment when the partial skeleton of *Homo floresiensis* was unearthed in a fragile condition. **b.** Preparation for preserving the bones before they were lifted. Yellow arrow shows a small block of 'black tuff' ~1 m above the skeleton (see Fig. A.1b). (Photos: © Liang Bua Team).

After the excavation of Sector XI was underway, Mike Morwood and I had to travel back to ARKENAS in Jakarta to help facilitate filming of our research at Liang Bua by National Geographic. When I returned to Liang Bua, the excavation had already reached ~3 m depth. In the southern part of the square, the excavation had revealed a large concentration of black tuff (2 m wide, ~50 cm long and ~70 cm thick). However, in the southwest corner of the square, ~30 cm below this concentration, the top 'tail' of the upper white tuff (T8) extended southward ~55 cm underneath the black tuff material (Fig. A.3). The characteristics of this black tuff were similar to the fragments found in Sectors IV and VII, but because of its stratigraphic relationship to the white tuff in the southwest corner I thought that this concentration of black tuff represented another redeposition of the same volcanic ash (just a much larger block of it), subsequent to deposition of the white tuff ~13–11 ka cal BP.

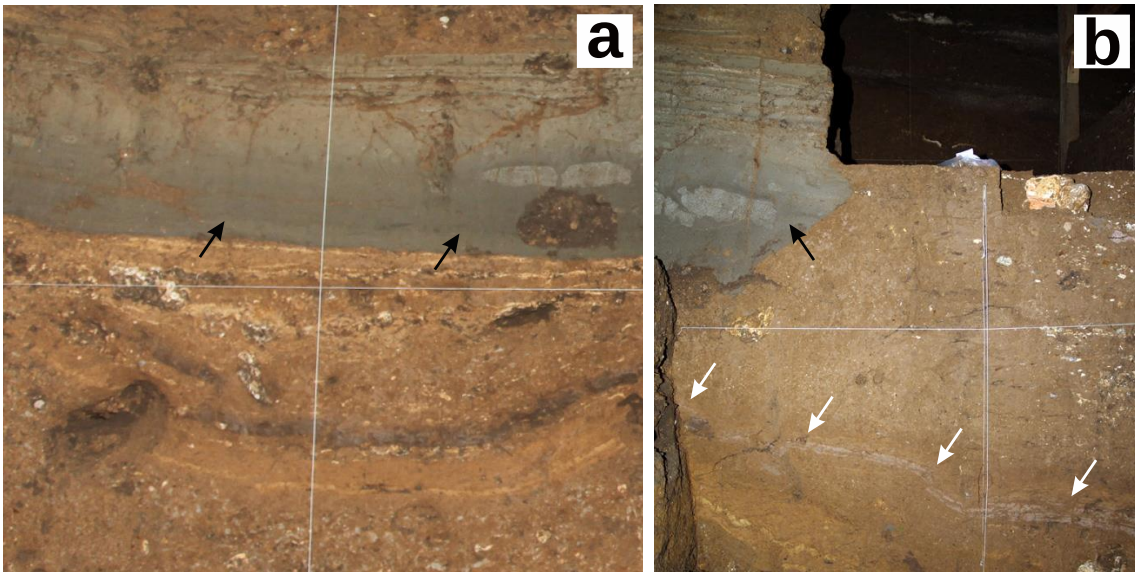

Figure A.3 Black tuff and white tuff in Sector XI. **a.** South baulk of Sector XI exposed black tuff (there is no white tuff in the south baulk). **b.** West baulk of Sector XI shows that the white tuff extended southward underneath the black tuff (this photo was taken in 2008 during excavation of Sector XV). White arrows indicate white tuff and black arrows indicate black tuff. (Photos: © Liang Bua Team).

In 2007, Sector XII was selected for excavation as it was roughly in the centre of the cave and we thought it would improve our understanding of the stratigraphic relationship between the Sectors we had excavated between 2001 and 2004. As we reached ~2 m depth and below, however, we were surprised to encounter the same depositional sequence as that in the southern part of Sector XI, except that in Sector XII it covered the entire 2 x 2 m square (Fig. A.4). I immediately suspected that we might have been wrong about the large concentration of black tuff in Sector XI. For the first time, I considered the possibility that this was the primary deposition of this material in Liang Bua and that it likely represented a pyroclastic flow event. Convincing my colleagues of this new hypothesis and its implications for our interpretation of the Liang Bua stratigraphy, however, was challenging.

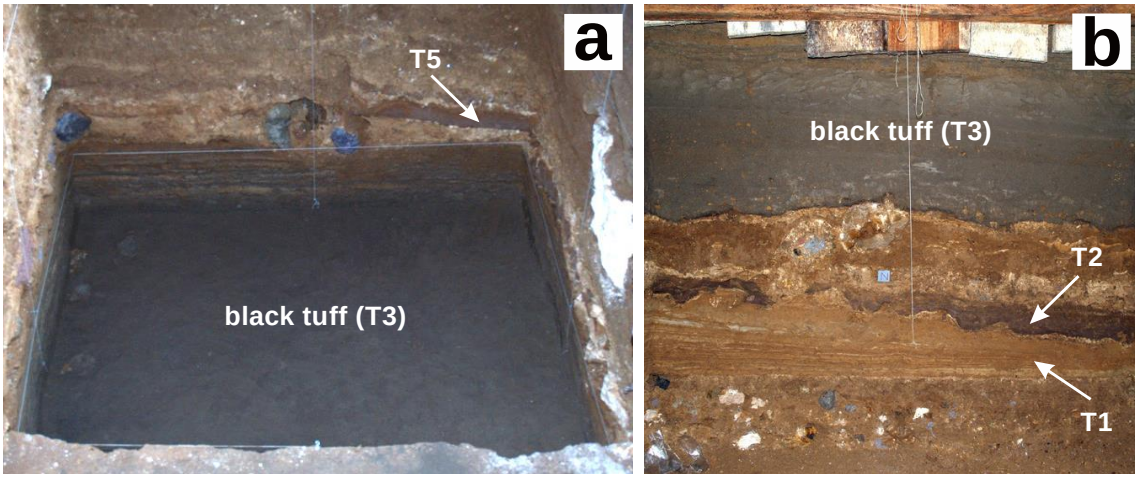

Figure A.4 Black tuff in Sector XII. **a.** The entire black tuff exposed at ~2 m depth in Sector XII (there is no white tuff in this Sector). **b.** North baulk of Sector XII, showing the black tuff is as thick as in Sector XI. (Photos: © Liang Bua Team).

Mike Morwood and I discussed intensely whether the black tuff was deposited before or after the white tuff – which we did not encounter at all in Sector XII – and whether its primary deposition extended from Sector XII in the cave centre to the south part of Sector XI along the eastern wall of the cave. The blocks of black tuff we had encountered previously at deeper levels and beneath the white tuff in Sectors III, IV, VII and the northern parts of XI could have been eroded from this primary position. If my hypothesis was correct, the implication was that the black tuff had to be older than the white tuff despite occurring at a higher elevation, but how much older was unclear. All of our team (including myself) were still uncertain, however, because we had observed that part of the large concentration of black tuff in the southwestern corner of Sector XI lay stratigraphically above the white tuff. There were also multiple ^{14}C ages from Sectors III, IV, VII and XI that suggested all of the sediments above and below the white tuff in these areas had been deposited over the past 20,000 years. Only the southwest corner of Sector IV appeared to contain older deposits (~74 ka in age) – based on coupled ESR and U-series dating of a *Stegodon* molar found within them – preserved beneath a thick layer of flowstone.

We decided that, when we returned to Liang Bua again in 2008, we would excavate the areas immediately adjacent to the west of Sectors VII and XI. This would serve two aims. First, it would satisfy Mike Morwood as there seemed to be good potential for finding additional remains of *H. floresiensis* as this was next to the area from which several specimens, including LB1, had been recovered. Second, I would be satisfied because I thought this area would provide the best opportunity to confirm the stratigraphic relationship between the black and white tuffs near the eastern wall.

By early 2008, Kira Westaway (then at Macquarie University) had received U-series dating results from Jian-xin Zhao (University of Queensland) from flowstones sampled from beneath the black tuff in Sector XII. The flowstone ages were ~50 ka and older, with the youngest age obtained from flowstone immediately underlying the black tuff. These results deepened my suspicion that the black tuff might be older than the white tuff, but Mike Morwood and others were still not convinced. We clearly needed more information about the spatial distribution of the black tuff in its primary deposition within the cave and, in particular, how it contacted with other sediments both immediately beneath and in front of it.

In 2008 and 2009, we followed our plan to excavate Sectors XV and XVI immediately to the west of Sectors XI and VII, respectively. We removed backfill from Sectors VII and XI to enable us to excavate the new sectors from above and from the side. This would allow us to observe the underlying stratigraphic layers in the western baulks of Sectors VII and XI and to follow their distribution in Sectors XV and XVI more precisely. At ~2 m depth in the southern part of Sector XV, I carefully exposed the very top of the black tuff and its immediately overlying sediments, including flowstone that capped a pinkish volcanic ash (now Tephra 5 or T5) which overlies the black tuff (Fig. A.5). The black tuff continued the east-west trajectory we had observed

in Sector XI, retreating further to the south as it proceeded westward. We now had a key opportunity to observe and confirm the contact boundary between the black tuff and the sediments directly in front of it, including the white tuff. We proceeded to excavate the sediments in front of the black tuff, but I kept about 25 cm thickness of unexcavated sediments in the boundary between the two Sectors to retain stratigraphic information from Sector XI as a reference. It soon became clear that the white tuff was deposited after the black tuff had already been emplaced in its primary position and after the black tuff (and surrounding sediments) had been truncated by erosion such that its northern face was exposed (Fig. A.6).

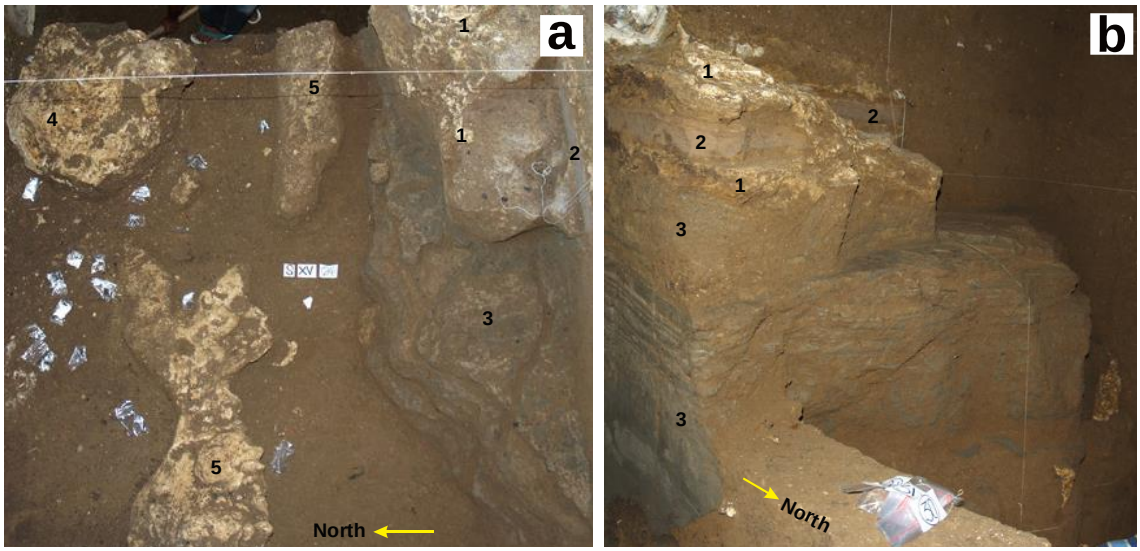

Figure A.5 Exposure of the black tuff in Sector XV. **a.** The upper part of the black tuff (T3) extends ~70 cm (in the middle) from the south baulk to the north (photo taken from the top). **b.** Black tuff overlain by pinkish volcanic ash (now Tephra 5 or T5) and flowstones. Numbers denote the following: **1** = flowstone, **2** = T5, **3** = T3, **4** = limestone block, **5** = broken fallen stalactites. (Photos: © Liang Bua Team).

In the western half of Sector XV, the black tuff rested on flowstone covering a huge limestone boulder, while the white tuff terminated well in front of the northern extent of this boulder (Fig. A.6). Due to the shape of this boulder, a small cavity had

been eroded underneath the black tuff in the southeastern part of Sector XV (and the southwestern part of Sector XI) and the white tuff and other younger sediments had subsequently filled this cavity (Fig. A.7).

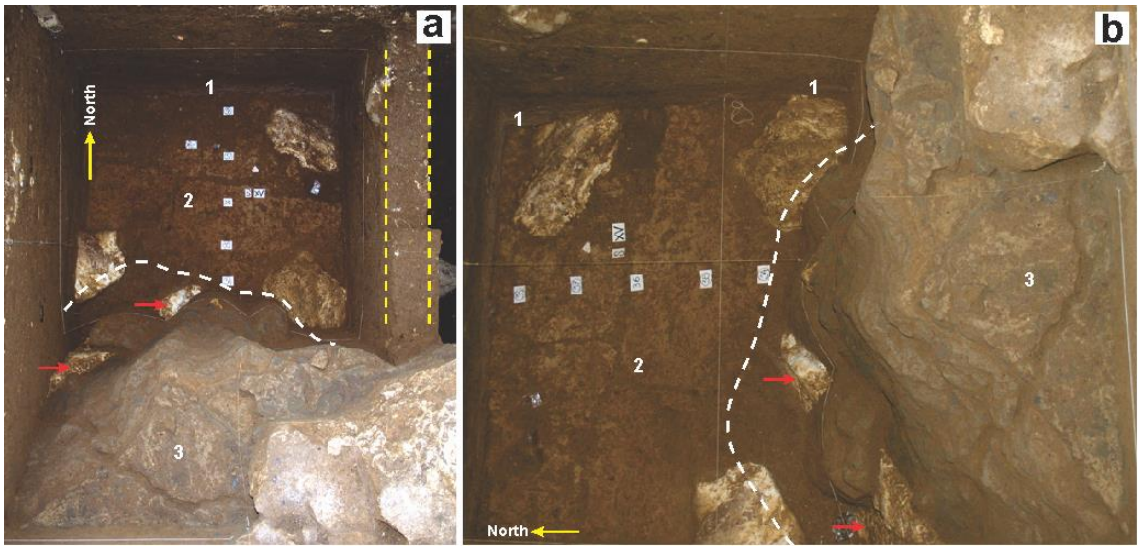

Figure A.6 Contact boundaries between the black and white tuffs in Sector XV. **a.** Photo taken from the top, south to north. **b.** Photo taken from the top, west to east. Numbers denote the following: **1** = upper white tuff (T8), **2** = lower white tuff (T7), **3** = black tuff (T3). White dashed lines indicate the termination of the white tuff and yellow dashed lines indicate the border between Sectors XI and XV. Red arrows indicate huge limestone boulder. (Photos: © Liang Bua Team).

Based on the orientation of the erosional surface of the black tuff in Sector XV, which seemed to continue to the cave centre, I suggested that we open a new area between Sectors XV and XII. This new excavation (Sector XVII) would be used to trace the erosional surface – which did not exist in Sector XII – and the contact boundaries between the black and white tuffs. While excavating Sector XVII, Mike Morwood and I had many intense discussions until we reached the black tuff in Sector XVII. My prediction had been correct and we were able to observe the erosional surface of the black tuff in the northernmost parts of the square (Fig. A.8).

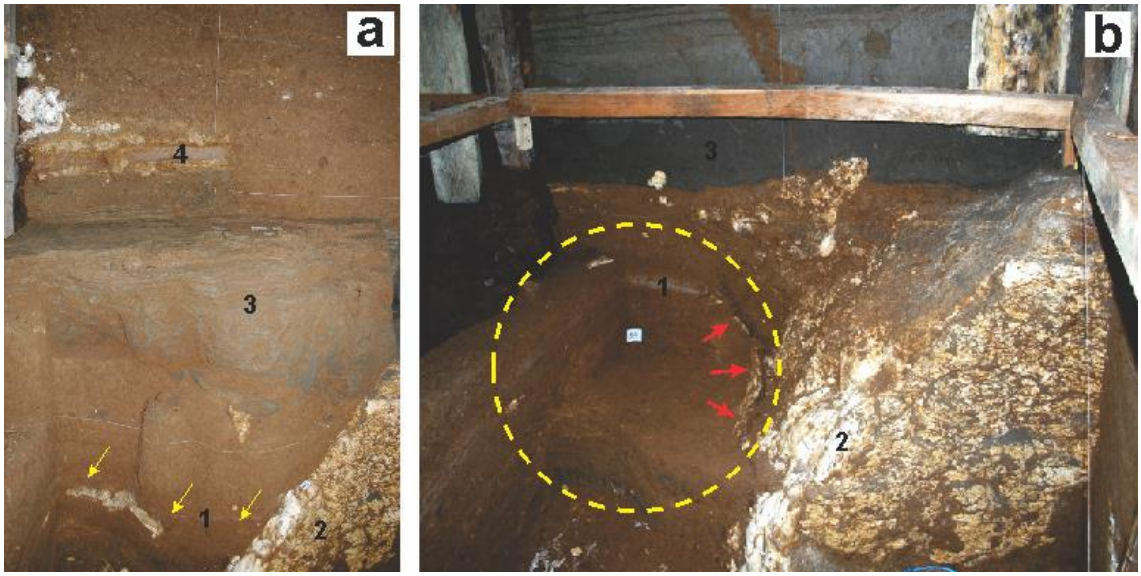

Figure A.7 White tuff in the small cavity beneath the black tuff. **a.** The black tuff rested on a huge limestone boulder in the south baulk of Sector XV. **b.** In the southeast corner of Sector XV, the distal 'tail' of white tuff and other younger sediments had filled the cavity beneath the black tuff (see also Fig. A.3b). Numbers denote the following: **1** = upper white tuff (T8), **2** = limestone block, **3** = black tuff (T3), **4** = pinkish volcanic ash (T5). The yellow dashed circle indicates the cavity and the red arrows indicate the thin flowstone covering it. Yellow arrows indicate the distal tail of white tuff. (Photos: © Liang Bua Team).

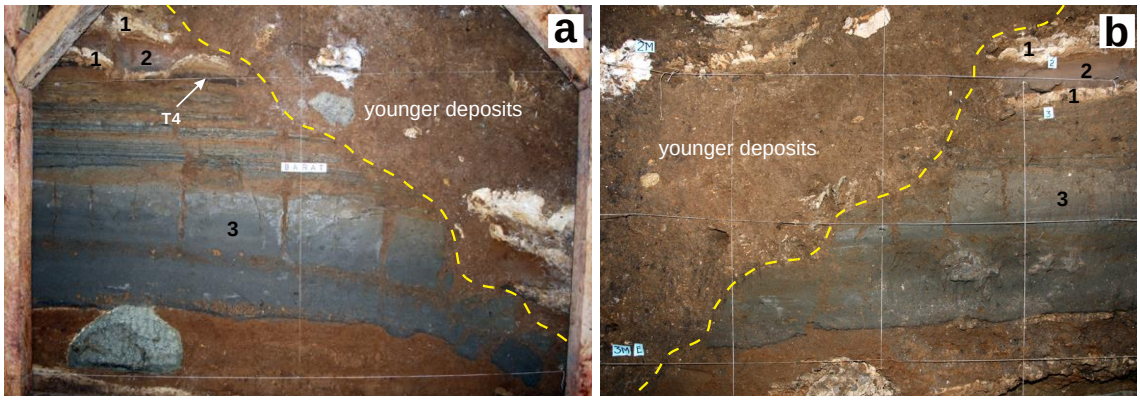

Figure A.8 Erosional surface of the black tuff. **a.** As exposed in the west baulk of Sector XVII. **b.** As exposed in the east baulk of Sector XIX. The yellow dashed lines indicate the erosional surface of the black tuff as well as the contact boundaries with much younger deposits. Numbers denote the following: **1** = flowstone, **2** = pinkish volcanic ash (T5), **3** = black tuff (T3). White arrow indicates T4. (Photos: © Liang Bua Team).

In 2010, we shifted to Sector XIX in order to further trace the erosional boundary of the black tuff to the cave centre and immediately south of Sector IV where this tuff

did not occur in its primary position. We were able to observe the erosional surface of the black tuff in the northernmost parts of Sector XIX (Fig. A.8b), similar to our observations in Sector XVII. By this time, the stratigraphic information was now pointing strongly to the fact that the *Homo floresiensis*-bearing deposits in Sector IV should be roughly contemporaneous with those in the eastern Sectors (VII, XI, XV and XVI).

With this new stratigraphic evidence, I was finally able to convince Mike Morwood and others in the field that the black tuff was stratigraphically older than the white tuff. He then suggested that the black tuff was probably ~17 ka old, only a few thousand years older than the white tuff (added as a footnote in Morwood *et al*., 2009), based on a ~17 ka cal. BP age for charcoal found mixed with eroded blocks of black tuff in Sector IV, just beneath the white tuff. I did not agree with this interpretation, however, and considered the flowstone ages (50 ka and older) from beneath the black tuff in Sector XII as more accurate indicators of its depositional age.

To resolve this issue once and for all required the excavation of additional Sectors and analysis of the excavated finds, as well as the application of further dating methods (including techniques that had not been developed at the time of the original study) and other indicators of relative age and environment (such as the preservation and composition of faunal remains). These activities formed the backbone of my PhD research, which was necessarily conducted in collaboration with other researchers owing to the range of technical specialisations involved. Between 2010 and 2014, seven new Sectors (XXI, XXII, XXIII, XXIV, XXV, XXVI and XXVII) have been excavated (see Chapter 1, Fig. 1.3) and the new stratigraphic interpretations, age determinations and analyses of the cultural and faunal remains are presented in Chapters 2, 3 and 4.